

**investigating the molecular and cellular basis of
pathogenesis in Huntington's disease**

Laura Kennedy

Thesis submitted for the degree of Doctor of Philosophy

University of Glasgow

**Division of Molecular Genetics
Faculty of Biomedical and Life Sciences**

June 2002

ProQuest Number: 13833917

All rights reserved

INFORMATION TO ALL USERS

The quality of this reproduction is dependent upon the quality of the copy submitted.

In the unlikely event that the author did not send a complete manuscript and there are missing pages, these will be noted. Also, if material had to be removed, a note will indicate the deletion.



ProQuest 13833917

Published by ProQuest LLC (2019). Copyright of the Dissertation is held by the Author.

All rights reserved.

This work is protected against unauthorized copying under Title 17, United States Code
Microform Edition © ProQuest LLC.

ProQuest LLC.
789 East Eisenhower Parkway
P.O. Box 1346
Ann Arbor, MI 48106 – 1346

GLASGOW
UNIVERSITY
LIBRARY:

THESIS 12747 - COPY 1

Abstract

Huntington's disease (HD) is a late onset, neurodegenerative disorder that typically progresses for 10-20 years, resulting in premature death. Symptoms include choreic movement disorder, cognitive deficits and psychiatric disturbances. The neurodegeneration associated with HD occurs most prominently in the striatum with the additional involvement of the cortex and other brain regions in later stages. Initial neuropathology within the striatum demonstrates the selective vulnerability of medium spiny neurons. HD is inherited in an autosomal dominant fashion and is caused by the expansion of a polymorphic trinucleotide (CAG) repeat within exon 1 of the ubiquitously expressed *HD* gene. The expansion mutation results in an elongated polyglutamine stretch within the protein product, called huntingtin. An inverse correlation between the repeat number and age at onset/extent of pathology has been observed with the longest repeats causing severe juvenile HD.

A knock-in HD mouse model has been created by homologous recombination, inserting a perfect CAG repeat tract (72-80 repeats) into exon 1 of the mouse *Hdh* gene (Shelbourne *et al.*, 1999), the mouse orthologue of the human *HD* gene. This HD knock-in mouse model provides an opportunity to explore the consequences of the HD mutation in its appropriate genomic and protein context.

Previous studies of the HD knock-in mice have demonstrated several alterations reminiscent of human HD, including behavioural changes (Shelbourne *et al.*, 1999) and synaptic dysfunction (Usdin *et al.*, 1999). Protein aggregates, a cellular hallmark of the HD disease process, have been detected within the nucleus and neuropil of neurons selectively vulnerable to HD (Li *et al.*, 2000). The presence of neuropil aggregates has also been associated with axonal degeneration (Li *et al.*, 2001). The alterations observed in HD knock-in mice occur in the absence of obvious cell loss, suggesting that this system maybe modelling the events involved in early HD pathogenesis.

Movement disorder is a prominent symptom associated with human HD. Behavioural studies using sensitive, quantitative methods to assess motor function have been carried out in the HD knock-in mice. Gait abnormalities, at 9 months of age, in the form of altered weight distribution were observed and appeared to be influenced by the sex of the mouse since significant alterations were restricted to male HD knock-in mice.

In an attempt to assess cognitive deficits that may result from hippocampal synaptic dysfunction previously observed in HD knock-in mice, spatial learning and memory was also investigated. Experimental design problems prevented the acquisition of robust data from these experiments and the cognitive abilities of the HD knock-in mice remain unknown.

To investigate the neuronal integrity in the HD knock-in mice, neurotransmitter receptor densities were determined by quantitative ligand binding autoradiography. By examining receptor density in the striatum and cortex of 18 month old HD knock-in mice a significant reduction in striatal dopamine D₂ receptors was detected, along with significant increases in striatal and cortical benzodiazepine receptor binding. Conversely, no changes were observed in dopamine D₁ and opioid receptor densities although a strong trend towards increased opioid receptor density was observed within the striatum. A comparison of neurotransmitter receptor densities in different congenic HD mouse lines demonstrated an influence of genetic background on neurotransmitter receptor levels in wild-type and HD knock-in mice, suggesting the presence of possible genetic modifiers of the disease process.

To investigate possible molecular mechanisms responsible for the selective pattern of HD neuropathology, mutation profiles in the somatic tissues of HD knock-in mice were investigated using a small pool PCR approach. Age-dependent, tissue-specific somatic repeat instability was observed, with the striatum, the brain region most affected by HD neuropathology, displaying the greatest level and magnitude of repeat size changes. Studies also suggested that the mechanism underlying brain repeat instability might not be replication-based. Finally, the tissue-specific mutation profiles observed appeared to be influenced by the presence or absence of amino acid residues downstream of the polyglutamine stretch within the huntingtin protein.

Investigations of human juvenile HD tissue confirm the presence of extensive brain region-specific repeat instability. The largest repeat size changes were observed in the cortex with lower levels of repeat instability in the striatum, perhaps reflecting the pattern of extensive cell loss noted at autopsy.

The work presented in this thesis contributes to the further phenotypic characterisation of the knock-in HD mouse model and identifies early molecular and cellular mechanisms underlying HD pathogenesis. These studies will inform future discussions of potential therapeutic targets and the utility of biomarkers to evaluate therapeutic efficacy.

Table of contents

Abstract	2
Table of contents	4
List of tables	9
List of figures	12
Acknowledgements	13
Abbreviations	15
1 INTRODUCTION	18
1.1 Huntington's disease	18
1.1.1 Clinical HD	18
1.1.1.1 Movement disorder in HD	18
1.1.1.2 Cognitive deficits in HD	18
1.1.1.3 Psychiatric disturbances in HD	19
1.1.2 Neuropathology of HD	19
1.1.2.1 Basal ganglia	20
1.1.2.2 Functional anatomy of the striatum	20
1.1.2.3 Pattern of neurodegeneration in HD	23
1.1.2.4 Neurodegeneration versus neuronal dysfunction in HD	24
1.2 Molecular basis of HD	25
1.2.1 Germline repeat instability in HD	28
1.2.2 Somatic repeat instability in HD	30
1.2.3 Homologues of the <i>HD</i> gene	31
1.2.4 Huntingtin	32
1.2.5 Huntingtin expression and selective vulnerability of neurons	33
1.2.6 Protein aggregation and HD pathogenesis	34
1.2.6.1 Nuclear localisation of huntingtin	35
1.2.7 Protein-protein interactions of huntingtin	38
1.2.7.1 Huntingtin protein partners	38
1.2.7.2 Transcriptional dysregulation and HD pathogenesis	40
1.2.8 Neurotransmitter receptor alterations in HD	43
1.3 Mechanisms underlying HD pathogenesis	46
1.3.1 Excitotoxicity	46
1.3.1.1 Glutamate-mediated excitotoxicity	46
1.3.1.2 Glutamate receptor expression pattern on different cell-types	47
1.3.1.3 Dopamine-mediated toxicity	48
1.3.1.4 Metabolic stress	50
1.3.1.5 Oxidative stress	52
1.4 Trinucleotide repeat diseases	54
1.5 Tools for investigating HD	58
1.5.1 HD model systems	58
1.5.1.1 Mammalian cell culture	59
1.5.1.2 Bacteria	59
1.5.1.3 Yeast	59
1.5.1.4 Fly	60
1.5.1.5 Nematode	60
1.5.1.6 Rodents	61
1.5.2 HD mouse models	62
1.5.2.1 HD 'knock-out' mice	62

1.5.2.2	Transgenics mouse models of HD	63
1.5.2.3	HD 'knock-in' mice	69
1.5.3	Knock-in HD mouse model <i>Hdh6/Q72</i> and <i>Hdh4/Q80</i>	71
1.5.3.1	Generation of <i>Hdh6/Q72</i> and <i>Hdh4/Q80</i>	71
1.5.3.2	Neuropathological studies of the HD mice	71
1.5.3.3	Nuclear and cytoplasmic aggregates in the HD mice	72
1.5.3.4	Phenotypic features of the HD mice	72
1.5.3.5	Synaptic dysfunction in the HD mice	72
1.5.3.6	Intergenerational mutation length variability in the HD mice	73
1.6	Mechanisms underlying trinucleotide repeat instability	74
1.6.1	Alternative DNA structures within TRS	74
1.6.2	Replication through TRS	76
1.6.3	DNA repair of TRS	80
1.6.3.1	Nucleotide excision repair (NER) and triplet repeat instability	80
1.6.3.2	Mismatch repair (MMR) in TRS	81
1.6.4	Transcription and Transcription-coupled repair	85
1.6.5	Recombination	86
1.6.5.1	Double-strand break repair	87
1.6.6	Factors contributing to locus-specific repeat instability	90
1.7	Aims	91
2	MATERIALS AND METHODS	93
2.1	Solutions	93
2.2	Mouse lines	95
2.3	General methods	95
2.3.1	Tissue collection	95
2.3.1.1	Post-mortem human tissue	95
2.3.1.2	Fresh-frozen mouse tissue	95
2.3.1.3	Mouse sperm	95
2.3.2	DNA extraction	96
2.3.2.1	Mouse DNA extraction	96
2.3.2.2	Sperm DNA extraction	96
2.3.2.3	Human DNA extraction	97
2.3.3	DNA quantification	97
2.3.4	Polymerase Chain Reaction (PCR)	97
2.3.4.1	PCR amplification of the CAG repeat region of the mouse <i>Hdh</i> locus	99
2.3.4.2	PCR amplification of the CAG repeat region of the human <i>HD</i> locus	99
2.3.5	Gel electrophoresis	99
2.3.6	Genescan analysis of the mouse <i>Hdh</i> locus	100
2.4	Small pool PCR (SP-PCR)	100
2.4.1	DNA digestion	100
2.4.2	DNA dilution	101
2.4.3	Polymerase Chain Reaction	101
2.4.3.1	SP-PCR of the CAG repeat within the mouse <i>Hdh</i> locus	102
2.4.3.2	SP-PCR of the CAG repeat within the human <i>HD</i> locus	102
2.4.4	Gel electrophoresis	102
2.4.5	Southern blotting	102
2.4.6	Visualisation of PCR products by radioactive hybridisation	103
2.4.6.1	Prehybridisation	103
2.4.6.2	Probe production	103
2.4.6.3	Hybridisation	105
2.4.6.4	Washing	105
2.4.6.5	Film Exposure, Development and Analysis	105

2.5	Quantitative ligand binding autoradiography	105
2.5.1	Tissue collection	105
2.5.2	Preparation and storage of brain tissue sections	106
2.5.3	Quantitative ligand binding autoradiography	106
2.5.4	Development of autoradiographic films	108
2.5.5	Data analysis	108
2.5.5.1	Image capture and analysis	108
2.5.5.2	Statistical analyses of data	110
2.6	Behavioural Paradigms	111
2.6.1	Gait analysis	111
2.6.1.1	Measurement of velocity and vertical reaction forces in mice	111
2.6.1.2	Data analysis	113
2.6.1.3	Cohorts	115
2.6.1.4	Acknowledgements	115
2.6.2	Spatial learning and memory	116
2.6.2.1	Rotating Holeboard Paradigm	116
2.6.2.2	Cohorts	118
3	INVESTIGATING PHENOTYPIC ALTERATIONS IN A KNOCK-IN MOUSE MODEL OF HUNTINGTON'S DISEASE	119
3.1	Aims of the study	119
3.2	Gait analysis in wild-type and HD^{+/-} mice	119
3.2.1	Aims of the study	119
3.2.2	Gait analysis in 4 month old wild-type and HD ^{+/-} mice	120
3.2.2.1	Investigating sex differences in gait of 4 month old mice	123
3.2.3	Gait analysis in 9 month old wild-type and HD ^{+/-} mice	127
3.2.3.1	Investigating sex differences in gait of 9 month old mice	130
3.2.4	Gait analysis in 12 month old wild-type and HD ^{+/-} mice	135
3.2.5	Velocity of 9 and 12 month old wild-type and HD ^{+/-} mice	137
3.2.6	Summary of Results	139
3.3	Investigating spatial learning and memory in wild-type and HD^{+/-} mice	140
3.3.1	Aims of the study	140
3.3.2	Results	140
3.3.3	Summary of findings	143
3.3.4	Future studies on HD knock-in mouse cognition	144
4	NEUROTRANSMITTER RECEPTOR PROFILES IN A KNOCK-IN MOUSE MODEL OF HUNTINGTON'S DISEASE	145
4.1	Aims of the study	145
4.2	Optimisation of binding protocols	146
4.2.1	Ligand concentration	146
4.2.2	Time of exposure	147
4.2.3	Autoradiographic Film	151
4.2.4	Summary of optimised binding conditions	153
4.2.5	Evaluation of optimised binding protocols	154
4.2.6	Non-specific binding	155
4.3	Neurotransmitter receptor profiles in the striatum of 18 month old wild-type and HD^{+/-} mice	157
4.4	Neurotransmitter receptor profiles in the cortex of 18 month old wild-type and HD^{+/-} mice	160

4.5	Investigating the influence of genetic background on neurotransmitter receptor profiles in mouse striatum and cortex	163
4.5.1	Investigating the influence of the HD mutation on neurotransmitter receptor densities in animals with the same genetic background	165
4.5.2	Investigating the influence of genetic background on neurotransmitter receptor densities in 18 month old HD ^{+/-} or wild-type mice	167
4.5.3	Investigating whether genetic background influences the consequences of the HD mutation	172
4.6	Investigating the influence of mouse age on neurotransmitter receptor profiles	173
4.7	Summary of Results	176
5	CHARACTERISATION OF SOMATIC REPEAT INSTABILITY IN A KNOCK-IN MOUSE MODEL OF HUNTINGTON'S DISEASE	177
5.1	Aims of the study	177
5.2	Investigating somatic repeat instability in 24 month old HD^{+/-} mice	178
5.3	Quantification of somatic repeat instability in 24 month old HD^{+/-} mice	185
5.3.1	Quantitative small pool PCR	185
5.3.2	Quantification of selected tissues from a 24 month old HD ^{+/-} mouse	186
5.3.3	Reproducibility of repeat instability profiles in 24 month old HD ^{+/-} mice	191
5.4	Investigating the progressive nature of somatic repeat instability within HD^{+/-} mice	197
5.5	Investigating somatic repeat instability in human HD	199
5.6	Investigating experimental techniques utilised to detect somatic repeat instability	202
5.6.1	Methods used to investigate somatic repeat instability	202
5.6.1.1	Radioactive PCR	202
5.6.1.2	Genescan Analysis	202
5.6.1.3	Small pool PCR	202
5.6.2	Comparison of somatic repeat instability analysed by SP-PCR and Genescan technology	203
5.7	Summary of results	205
6	INVESTIGATING THE UNDERLYING MECHANISMS OF SOMATIC REPEAT INSTABILITY IN HD MOUSE MODELS	207
6.1	Aims of the study	207
6.2	Investigating the possible involvement of replication in brain repeat instability in HD^{+/-} mice	208
6.3	Investigating somatic repeat instability in 24 month old homozygous HD mice	212
6.3.1	Quantification of somatic repeat instability in a 24 month old HD ^{-/-} mouse	212
6.3.2	Reproducibility of somatic repeat instability in 24 month old HD ^{-/-} mice	215
6.3.3	Comparing mutation profiles in HD ^{-/-} and HD ^{+/-} mice	220
6.4	Investigating somatic repeat instability in 24 month old HD^{trunc} mice	224
6.5	Summary of results	228

7	DISCUSSION	230
7.1	Investigating phenotypic alterations in a knock-in mouse model of Huntington's disease	230
7.1.1	Investigating gait abnormalities in HD knock-in mice	230
7.1.2	Investigating spatial learning and memory in HD knock-in mice	232
7.2	Investigating the cellular mechanisms underlying pathogenesis in HD knock-in mice by examining neurotransmitter receptor density	234
7.2.1	GABA _A /Benzodiazepine receptor density	235
7.2.2	Dopamine receptor density	236
7.2.3	Opioid receptor density	237
7.2.4	Receptor alterations and the effect on brain function	237
7.2.5	Future studies into neurotransmitter receptor densities in HD	239
7.2.6	Additional issues raised by the receptor density studies	241
7.3	Investigating molecular mechanisms underlying HD pathogenesis by characterising somatic repeat instability	242
7.3.1	Small pool PCR	243
7.3.2	Polyglutamine load and HD pathogenesis	244
7.3.3	Expression of full-length mutant huntingtin and HD pathogenesis	245
7.3.4	Somatic repeat instability and mechanisms of HD pathogenesis	246
7.3.5	Future studies into somatic repeat instability in HD	246
7.3.6	Underlying mechanisms of somatic repeat instability	247
	References	249
	Publication	273

List of tables

Table 1.1	Summary of the polyglutamine disorders	55
Table 1.2	Summary of triplet repeat disorders not associated with the expression of a polyglutamine tract	56
Table 1.3	Transgenic mouse models expressing truncated human mutant huntingtin	64
Table 1.4	Transgenic mouse models expressing full-length human mutant huntingtin	65
Table 1.5	Knock-in HD mouse models	70
Table 2.1	Summary of the different HD mouse lines utilised in the following studies	95
Table 2.2	The sequence, melting temperature (T_m) and orientation of all oligonucleotides used to amplify the CAG repeat sequence	98
Table 2.3	PCR programs	98
Table 2.4	Reaction mixture for amplification of the CAG repeat within the mouse <i>Hdh</i> locus	99
Table 2.5	Reaction mixture for amplification of the CAG repeat within the human <i>HD</i> locus	99
Table 2.6	SP-PCR DNA sample digestion	101
Table 2.7	Reaction mixture for SP-PCR of the CAG repeat region within the human <i>HD</i> locus	102
Table 2.8	Probe production	104
Table 2.9	Radiolabelled ligands and non-labelled displacers	106
Table 2.10	Ligand binding assays - Conditions for incubations and washes	107
Table 2.11	Ligand binding assays - X-ray films and exposure times	108
Table 3.1	Summary of mean body weight for 4 month old mice assessed for gait parameters	120
Table 3.2	Summary of the mean loads, as a percentage of body weight, exerted through all groups of limbs in 4 month old mice	122
Table 3.3	The median distribution of weight between the fore and hind limbs and the left and right limbs in all cohorts and the p values resulting from the Mann-Whitney U statistical test when comparing the median difference between loadings in wild-type and HD ^{+/-} mice	122
Table 3.4	Summary of mean body weight for 9 month old mice assessed for gait parameters	128
Table 3.5	Summary of the mean loads, as a percentage of body weight, exerted through all groups of limbs in 9 month old mice	128
Table 3.6	The median distribution of weight between the fore and hind limbs and the left and right limbs in all cohorts and the p values resulting from the Mann-Whitney U statistical test when comparing the median difference between loadings in wild-type and HD ^{+/-} mice	130
Table 3.7	Summary of mean body weight for 12 month old mice assessed for gait parameters	135
Table 3.8	Summary of the mean loads, as a percentage of body weight, exerted through all groups of limbs in 12 month old mice	137
Table 3.9	The median distribution of weight between the fore and hind limbs and the left and right limbs in all cohorts and the p values resulting from the Mann-Whitney U statistical test when comparing the median difference between the loadings in wild-type and HD ^{+/-} mice	137
Table 3.10	Summary of cohorts used and the mean velocities during locomotion in 9 and 12 month old wild-type and HD ^{+/-} mice	138
Table 3.11	Summary of cohorts used and the mean velocities during locomotion in mice of the same genotype at different ages	138
Table 3.12	Summary of the animals used and the results and conclusions from the practice sessions in the rotating holeboard paradigm	140
Table 3.13	Summary of rotating holeboard experiments using the modified apparatus	142
Table 3.14	Summary of the rotating holeboard carried out with animals known to respond to food	143
Table 4.1	The mean specific binding obtained from the brain sections bound with the optimised ligand concentration after the chosen exposure times	150
Table 4.2	The chosen ligand concentrations and exposure times used to detect neurotransmitter receptor densities of all four receptor types	153
Table 4.3	Average specific binding in nCi/mg for all ligands within the striatum and cortex and a comparison with the radioactive standard range	154
Table 4.4	Non-specific binding levels in the striatum and cortex for all binding protocols as a percentage of the total binding obtained	155
Table 4.5	The number of mice on three different genetic backgrounds used for striatal analysis of each receptor type	157

Table 4.6	The number of animals utilised and the neurotransmitter receptor density for each study investigating the receptor profiles within the striatum of 18 month old HD ^{+/-} and wild-type mice	158
Table 4.7	The number of mice on three different genetic backgrounds used for cortical analysis of each receptor type	160
Table 4.8	The number of animals utilised and the neurotransmitter receptor density for each study investigating the receptor profiles within the cortex of 18 month old HD ^{+/-} and wild-type mice	163
Table 4.9	Opioid neurotransmitter receptor densities in 18 month old wild-type and HD ^{+/-} mice on different genetic backgrounds	164
Table 4.10	Benzodiazepine neurotransmitter receptor densities in 18 month old wild-type and HD ^{+/-} mice on different genetic backgrounds	164
Table 4.11	Dopamine D ₁ neurotransmitter receptor densities in 18 month old wild-type and HD ^{+/-} mice on different genetic backgrounds	164
Table 4.12	Dopamine D ₂ neurotransmitter receptor densities in 18 month old wild-type and HD ^{+/-} mice on different genetic backgrounds	165
Table 4.13	Comparing neurotransmitter receptor densities in wild-type and HD ^{+/-} mice divided into cohorts of the same genetic background	166
Table 4.14	The results of the two-way ANOVA comparing wild-type or HD ^{+/-} mice on different genetic backgrounds	167
Table 4.15	The presence of any interaction between genetic background and the consequences of the HD mutation for the previously investigated neurotransmitter receptors	172
Table 4.16	Opioid neurotransmitter receptor densities in wild-type and HD ^{+/-} mice of different ages	173
Table 4.17	Benzodiazepine neurotransmitter receptor densities in wild-type and HD ^{+/-} mice of different ages	173
Table 4.18	Dopamine D ₁ neurotransmitter receptor densities in wild-type and HD ^{+/-} mice of different ages	174
Table 4.19	Dopamine D ₂ neurotransmitter receptor densities in wild-type and HD ^{+/-} mice of different ages	174
Table 4.20	The results of the Student's <i>t</i> -tests comparing wild-type or HD ^{+/-} mice of the same age	175
Table 4.21	The significance of the effect of the HD mutation and age on neurotransmitter receptor densities	175
Table 5.1	Semi-quantitative analysis of 1000-3000 mutant alleles for 16 different tissues in 24 month old HD ^{+/-} mice	182
Table 5.2	Mutation length profiles of 5 different tissues from a 24 month old HD ^{+/-} mouse with a progenitor allele of 77 CAG repeats (animal 1)	188
Table 5.3	Mutation length profiles of 5 different tissues from a 24 month old HD ^{+/-} mouse with a progenitor allele of 77 CAG repeats (animal 1)	188
Table 5.4	Statistical comparison of the mutation length distributions of five different tissues from one 24 month old HD ^{+/-} mouse (animal 1)	191
Table 5.5	Mutation length profiles of 5 different tissues from a 24 month old HD ^{+/-} mouse with a progenitor allele of 79 CAG repeats (animal 2)	193
Table 5.6	Mutation length profiles of 5 different tissues from a 24 month old HD ^{+/-} mouse with a progenitor allele of 79 CAG repeats (animal 2)	193
Table 5.7	Statistical comparison of the repeat size distributions of five different tissues from one 24 month old HD ^{+/-} mouse (animal 2)	194
Table 5.8	Statistical comparison of the repeat size distributions of the same tissues in different 24 month old HD ^{+/-} mice	195
Table 5.9	Statistical comparison of the repeat change distributions of the same tissues in different 24 month old HD ^{+/-} mice	196
Table 6.1	Mutation length profiles of 3 different tissues from a 24 month old HD ^{+/-} mouse with a progenitor allele size of 78 CAG repeats (animal 3)	212
Table 6.2	Mutation length profiles of 3 different tissues from a 24 month old HD ^{+/-} mouse with a progenitor allele of 78 CAG repeats (animal 3)	213
Table 6.3	Statistical comparison of the repeat size distributions of three different tissues from one 24 month old HD ^{+/-} mouse (animal 3)	215
Table 6.4	Mutation length profiles of 3 different tissues from a 24 month old HD ^{+/-} mouse with a progenitor allele size of 76 CAG repeats (animal 4)	216
Table 6.5	Mutation length profiles of 3 different tissues from a 24 month old HD ^{+/-} mouse with a progenitor allele of 76 CAG repeats (animal 4)	216

Table 6.6	Statistical comparison of the repeat size distributions of three different tissues from a second 24 month old HD ^{-/-} mouse (animal 4)	217
Table 6.7	Statistical comparison of the repeat size distributions from the same tissues in different 24 month old HD ^{-/-} mice	219
Table 6.8	Statistical comparison of the repeat change distributions of the same tissues in different 24 month old HD ^{-/-} mice	219
Table 6.9	Statistical comparison of the repeat size distributions of the same tissues in 24 month old mice of different genotypes	223
Table 6.10	Statistical comparison of the repeat change distributions of the same tissues in 24 month old mice of different genotypes	223
Table 6.11	Semi-quantitative analysis of 1000-2000 mutant alleles for 5 different tissues in 24 month old HD ^{+/-} and HD ^{trunc} mice	227

List of figures

Figure 1.1	The cortico-striato-thalamic circuit	21
Figure 1.2	The correlation between CAG repeat length and age of onset in HD	27
Figure 1.3	Alternative DNA structures that form in (CTG.CAG) _n repeat sequences	75
Figure 1.4	Replication slippage model of repeat instability	77
Figure 1.5	Expansion due to disrupted FEN-1 processing in repeat sequences	79
Figure 1.6	The effect of DNA repair on different length triplet repeat sequences	83
Figure 1.7	A model for mismatch repair induced expansions	84
Figure 1.8	Double-strand break repair through gene conversion mechanisms	89
Figure 2.1	Comparing the optical density of the tritium standards and the binding brain sections to establish a measure of bound radiation per mg of tissue	109
Figure 2.2	Gait analysis apparatus	112
Figure 2.3	Measuring vertical reaction forces in mice	114
Figure 2.4	Rotating holeboard apparatus	117
Figure 3.1	The mean load exerted through the limbs of 4 month old wild-type and HD ^{+/-} mice	121
Figure 3.2	The mean load exerted through the limbs of male 4 month old wild-type and HD ^{+/-} mice	124
Figure 3.3	The mean load exerted through the limbs of female 4 month old wild-type and HD ^{+/-} mice	126
Figure 3.4	The mean load exerted through the limbs of 9 month old wild-type and HD ^{+/-} mice	129
Figure 3.5	The mean load exerted through the limbs of male 9 month old wild-type and HD ^{+/-} mice	132
Figure 3.6	The mean load exerted through the limbs of female 9 month old wild-type and HD ^{+/-} mice	134
Figure 3.7	The mean load exerted through the limbs of 12 month old wild-type and HD ^{+/-} mice	136
Figure 4.1	The effect of radiolabelled ligand concentration on striatal and cortical receptor binding	148
Figure 4.2	The effect of radiolabelled ligand concentration on striatal and cortical receptor binding	149
Figure 4.3	Benzodiazepine receptor density in the striatum and cortex using Biomax-MR1 film and Hyperfilm	152
Figure 4.4	Specific and non-specific binding for all ligand binding protocols	156
Figure 4.5	Striatal neurotransmitter receptor densities	159
Figure 4.6	Cortical neurotransmitter receptor densities	162
Figure 4.7	Opioid receptor density in the striatum and cortex	168
Figure 4.8	Benzodiazepine receptor density in the striatum and cortex	170
Figure 4.9	Dopamine D ₁ and D ₂ receptor densities in the striatum	171
Figure 5.1	Serial dilutions of striatal DNA from a 24 month old HD ^{+/-} mouse analysed by small pool PCR (SP-PCR)	180
Figure 5.2	Somatic repeat instability of the CAG repeat mutation in 24 month old HD ^{+/-} mice	181
Figure 5.3	The CAG repeat length in 24 month old wild-type mice	184
Figure 5.4	The distribution of CAG repeat lengths carried by individual alleles within tissues of a 24 month old HD ^{+/-} mouse	187
Figure 5.5	Comparison of the mutation profiles in old HD ^{+/-} mice	192
Figure 5.6	The progressive nature of CAG repeat instability in the brain of HD ^{+/-} mice	198
Figure 5.7	Somatic repeat instability of the CAG repeat mutation in human juvenile HD brain tissue	200
Figure 5.8	Comparison of CAG repeat length variation detected in striatal tissue from a 24 month old HD ^{+/-} mouse using SP-PCR analyses and Genescan-based technology	204
Figure 6.1	Investigating the possible role of replication in somatic repeat instability	210
Figure 6.2	Mutation profiles in tissues from a 24 month old HD ^{+/-} mouse	214
Figure 6.3	Mutation profiles in 24 month old HD ^{+/-} mice	218
Figure 6.4	Comparison of repeat instability in selected tissues from HD ^{+/-} and HD ^{+/-} mice	221
Figure 6.5	Mutation profiles in tissues from 24 month old HD ^{+/-} and HD ^{+/-} mice	222
Figure 6.6	Comparison of somatic repeat instability in HD ^{+/-} mice and HD ^{trunc} mice	225

Acknowledgements

I must begin by thanking Peggy for all her wonderful support throughout my PhD. I much appreciated her enthusiasm and encouragement, which made my PhD an enjoyable and worthwhile experience. A big thank you to Peggy E, Heather and Liz for all their help, friendship and, of course, gossip. A special thank you to Mei for maintaining her laidback attitude as we learned the mysteries of the lab together.

For ensuring my safe passage through my PhD course and enticing me into reading more papers I thank my assessors Keith and Julian, whose honest and informative advice was greatly appreciated.

Everybody on level 5 has been a wonderful help through the years and has made the time spent working there an enjoyable one. Thank you all.

I would also like to thank the rest of the PhD students for going to the pub, lunch and coffee with me when we should all have been working and especially Mario for being a great friend, providing lots of laughs and embracing the Scottish drinking culture so enthusiastically.

I would like to thank Debbie and all the technical staff at the WSI for their guidance with the receptor binding. Thank you to the people in MBSU and the CRF for all the technical help. A big thank you to Ken Clarke and Linda Grant for teaching me how to handle all those numbers in such a short space of time.

Thank you to the Huntington's Disease Association of Great Britain and the Hereditary Disease Foundation for providing the opportunity and funding for me to carry out my PhD.

Lastly, I owe my biggest thank you to Mum, Dad, Claire and Tony for the never-ending supply of love, support and food that came my way, I could not have done it without you.

**The research in this thesis is my own original work,
except where otherwise stated and has not been
submitted for any other degree.**

Laura Kennedy

June 2002

Abbreviations

A	Adenine
Ach	Acetylcholine
AD	Autosomal Dominant
AMPA	α -amino-3-hydroxy-5-methylisoxazole-4-propionate
ANOVA	Analysis of variance
AOAA	Aminooxyacetic acid
BDNF	Brain derived neurotrophic factor
BER	Base excision repair
BNZ	Benzodiazepine
Bp	Base pair
BSA	Bovine serum albumin
BW	Body weight
C	Cytosine
Cb	Cerebellum
CBP	CREB-binding protein
cDNA	complementary DNA
<i>C.elegans</i>	<i>Caenorhabditis elegans</i>
Ci	Curie (unit of radioactivity)
CMV	Cytomegalovirus
cm	Centimetres
CNS	Central nervous system
Ctx	Cortex
°C	degrees Celsius
DA	Dopamine
DARPP-32	Dopamine- and cAMP-regulated phosphoprotein of M _r 32 kDa
dH₂O	deionised water
DM1	Myotonic Dystrophy Type 1
DM2	Myotonic Dystrophy Type 2
DMSO	Dimethyl sulfoxide
DMPK	Myotonic dystrophy protein kinase
DN	Dynorphin
DNA	Deoxyribonucleic acid
dNTPs	2'-deoxynucleoside 5'-triphosphates
DRPLA	Dentatorubral-pallidoluysian atrophy
DSBR	Double-strand break repair
<i>E.coli</i>	<i>Escherichia coli</i>
EDTA	Ethylenediaminetetra-acetic acid
EM	Electron Microscopy
ENK	Enkephalin
ES cells	Embryonic stem cells
F	Female
FA	Friedreich's ataxia
FRAXA	Fragile X syndrome type A
FRAXE	Fragile X syndrome type E
FRAXF	Fragile X syndrome type F
g	acceleration due to gravity
G	Guanine
GABA_A	γ -aminobutyric acid receptor type A
GAPDH	Glyceraldehyde-3-phosphate dehydrogenase
GFP	Green fluorescent protein
[³H]	Tritium
HAP-1	Huntingtin-associated protein 1
HDL2	Huntington's disease like-2
HD	Huntington's disease

HD^{+/-}	Knock-in HD mouse, heterozygous for full length mutant huntingtin
HD^{trunc}	Knock-in HD mouse, heterozygous for truncated mutant huntingtin
HD^{-/-}	Knock-in HD mouse, homozygous for full-length mutant huntingtin
HIP	Hippocampus
HIP-1	Huntingtin-interacting protein 1
Hprt	Hypoxanthine phosphoribosyltransferase
HNPCC	Hereditary non-polyposis colorectal cancer
Hz	Hertz
I_{Agp}	Intermediate allele, general population
I_{Anm}	Intermediate allele, new mutation
∞	Infinite
K	Kidney
kb	Kilo base pair
kDa	Kilodaltons
Kg	Kilogram
LTP	Long term potentiation
M	Male
μg	Microgram (10 ⁻⁶)
mg	Milligram (10 ⁻³)
mJ	MilliJules
MJD	Machado-Joseph Disease
mGluR	Metabotropic glutamate receptor
min	Minutes
μl	Microlitres (10 ⁻⁶)
ml	Millilitres (10 ⁻³)
μM	Micromolar (10 ⁻⁶)
mM	Millimolar (10 ⁻³)
MMR	Mismatch repair
mRNA	messenger RNA
MSN	Medium spiny neurons
N/A	Not applicable
NADPH	Nicotinamide adenine dinucleotide phosphate
N-CoR	Nuclear receptor co-repressor
neo	neomycin resistance cassette
NER	Nucleotide excision repair
ng	Nanogram (10 ⁻⁹)
NGF	Nerve growth factor
NI	Neuronal intranuclear inclusions
NLS	Nuclear localisation sequence
NMDA receptor	N-methyl-D-aspartate glutamate receptor
NO	Nitric oxide
NOS	Nitric oxide synthase
3NP	3-nitropropionic acid
N/R	Not reported
OD	Optical density
OLB	Oligonucleotide labelling buffer
PCR	Polymerase Chain Reaction
PET	Positron emission tomography
pg	Picogram (10 ⁻¹²)
pH	degrees of acidity or alkalinity of solutions
PSD-95	Postsynaptic density-95
PTP	Post-tetanic potentiation
PPF	Paired pulse facilitation
RNA	Ribonucleic acid
Rpm	Rotations per minute
RT	Room temperature
SBMA	Spinobulbar muscular atrophy

SCA	Spinocerebellar ataxia
S.D.	Standard deviation
SDS	Sodium dodecyl sulfate
SDSA	Synthesis-dependent strand annealing
S.E.	Standard error
sec	Seconds
SP	Substance P
SPET	Single-photon emission tomography
SP-PCR	Small Pool Polymerase Chain Reaction
St	Striatum
SVZ	Subventricular zone
T	Thymine
TAFs	TBP-associated factors
TBP	TATA-binding protein
TE	Tissue Equivalent
TRS	Trinucleotide repeat sequence
U	Units
UV	Ultraviolet
V	Volts
vs	versus
v/v	volume-to-volume ratio
W	Watts
Wks	Weeks
WT	Wild-type
X-ray	Electromagnetic ray
YAC	Yeast artificial chromosome

1 Introduction

1.1 Huntington's disease

Huntington's disease (HD) is an autosomal dominantly inherited neurological disorder affecting ~1 in 10000 individuals ((HDCRG), 1993). HD displays an adult-onset, typically during the 3rd-4th decade of life, and slowly progresses over a 10-20 year period to premature death (Harper, 1991). Approximately 7 % of HD patients suffer from the more severe juvenile form of the disease, which displays a faster decline in health (Foroud *et al.*, 1999; Harper, 1992) and variation in symptoms compared to typical adult-onset HD (Kirkwood *et al.*, 2001; Naarding *et al.*, 2001; Nance and Myers, 2001).

1.1.1 Clinical HD

HD is characterised by movement disorder, changes in behaviour and personality, and cognitive impairment (Harper, 1991; Hayden, 1981). The relationship between the symptoms is complex and significant variation between individuals in disease course and expression has been observed (Martin and Gusella, 1986).

1.1.1.1 Movement disorder in HD

The most common form of movement disorder associated with HD is chorea. Chorea, the Greek word for dance, refers to irregular, random, involuntary movements that occur in a rapid and flowing manner (Higgins, 2001). Initially writhing distal chorea can be mistaken for restlessness. However, disease progression leads to ballism, a term that describes severe proximal involuntary movements (Higgins, 2001). As HD progresses other movement disorders such as dystonia, athetosis and additional impairment of voluntary movement occur (Kirkwood *et al.*, 1999). Sensitive motor assessments have detected a subtle movement disorder in HD mutation carriers previously considered to be presymptomatic, suggesting that movement deficits manifest early in the disease course (de Boo *et al.*, 1997; Kirkwood *et al.*, 1999). In contrast, juvenile HD is commonly characterised by abnormalities in voluntary movement including bradykinesia, which progresses to Parkinsonian-like rigidity (Kirkwood *et al.*, 2001; Nance and Myers, 2001).

1.1.1.2 Cognitive deficits in HD

A variety of impairments in cognitive functioning have been reported in HD patients, including deficits in memory, executive functions, visuospatial abilities, cognitive speed, sensorimotor function and olfactory recognition (Brown and Marsden, 1988; Butters *et al.*, 1978; Caine *et al.*, 1978; Lawrence *et al.*, 1996; Moberg *et al.*, 1987). Brown and Marsden (1988) simplified the

description of HD-associated cognitive impairment by highlighting processing speed as a central component in many impaired functions, suggesting that a general reduction in 'mental tempo' that progresses to global sub-cortical dementia (Caine *et al.*, 1978).

A number of studies have attempted to dissect the complex nature of cognitive decline in HD and have suggested a differential onset for various types of cognitive deficits. Deficits in executive system functioning, short-term memory and visuospatial functioning present early in the disease process while language-based functions appear to remain intact (Kirkwood *et al.*, 2001; Lawrence *et al.*, 1996). Despite several studies claiming an absence of cognitive deficits prior to clinical onset (Campodonico *et al.*, 1996; de Boo *et al.*, 1997; Giordani *et al.*, 1995; Gomez-Tortosa *et al.*, 1996), evidence for subtle cognitive impairment in HD gene carriers before clinical onset is mounting (Foroud *et al.*, 1995; Hahn-Barma *et al.*, 1998; Jason *et al.*, 1997; Kirkwood *et al.*, 1999; Lawrence *et al.*, 1998a). The reasons for these discrepant findings may stem from the different population sizes, mean age, test sensitivity and clinical criteria used in various cognitive studies.

Juvenile HD cognitive ability is thought to differ from adult-onset HD, particularly in the severity of the visual and prefrontal deficits (Gomez-Tortosa *et al.*, 1998). In initial stages of juvenile HD cognitive ability is good (superior to that of adult-onset patients in initial stages) with this form of the disease predominantly characterised by psychiatric and movement symptoms (Gomez-Tortosa *et al.*, 1998; Kirkwood *et al.*, 2001).

1.1.1.3 Psychiatric disturbances in HD

Several studies have illustrated a high incidence (50-98 %) of psychiatric symptoms in HD (Anderson and Marder, 2001; Marder *et al.*, 2000; Paulsen *et al.*, 2001). Although the psychology of HD is complex, symptoms such as dysphoria, agitation, irritability, apathy and anxiety are all apparent in more than 50 % of HD patients (Paulsen *et al.*, 2001). Obsessive/compulsive disorders have also been observed, with 52 % of HD patients suffering from at least one obsessive disorder (Anderson and Marder, 2001). Despite the varied psychiatric phenotype displayed, the occurrence of serious psychoses in HD patients has rarely been observed (Bolt, 1970; Folstein *et al.*, 1983). It has been suggested that in most cases of HD psychiatric symptoms precede chorea and intellectual decline and in juvenile HD, psychiatric symptoms and dis-inhibition predominate (Paulsen *et al.*, 2001).

1.1.2 Neuropathology of HD

The neuropathology observed in HD is characterised by the selective neurodegeneration of the striatum (caudate nucleus and putamen) (Vonsattel *et al.*, 1985), with the additional loss of cortical layers (Rosas *et al.*, 2002; Vonsattel and DiFiglia, 1998). Although the striatum is most affected, a

general atrophy of the brain also occurs (Hedreen and DeLong, 1991; Vonsattel *et al.*, 1985). Initially neuropathology occurs in a cell-type specific manner affecting the medium spiny projection neurons (MSN) within the striatum selectively (Goto *et al.*, 1989; Graveland *et al.*, 1985).

1.1.2.1 Basal ganglia

The basal ganglia, comprised of the corpus striatum, subthalamic nucleus and substantia nigra, is thought to be involved in the integration of the cortico-striato-thalamic circuits concerned with the production of movement (Parent, 1990). The extensive connections of the basal ganglia with the temporal and anterior frontal cortex also indicate additional involvement in memory, emotion, and other cognitive functions (Brown *et al.*, 1997).

The major output structure of the basal ganglia is the inhibitory medial globus pallidus (named entopeduncular nucleus in rodents), part of the corpus striatum (Figure 1.1). Excitatory input to the medial globus pallidus comes from the subthalamic nucleus and inhibitory input is provided by the striatum. The major output tract from the medial globus pallidus innervates nuclei within the thalamus. The thalamic nuclei project to and excite the premotor, supplementary motor, prefrontal and temporal areas of the cerebral cortex. This creates a loop as cortical neurons project to the striatum, which can therefore modulate the activation of the thalamus (Mitchell *et al.*, 1999).

1.1.2.2 Functional anatomy of the striatum

The structures within the basal ganglia involved in HD pathology are the caudate nucleus and the putamen (striatum) within the corpus striatum (Vonsattel *et al.*, 1985). The corpus striatum is made up of the striatum (the caudate nucleus and the putamen are structurally distinct in primates but one integrated structure in rodents (Mitchell *et al.*, 1999)) and the pallidum (lateral and medial globus pallidus).

The major afferents to all areas within the striatum arise from the cerebral cortex (Goldman-Rakic and Selemon, 1990; Nauta, 1979). The fibres are topographically organised with each area preferentially receiving input from specific regions of the cerebral cortex (Goldman-Rakic and Selemon, 1990; McGeorge and Faull, 1989). The corticostriatal connections are excitatory glutamatergic fibres, which make direct synaptic contact with the medium spiny neurons (MSN), the main cell-type within the striatum (Bouyer *et al.*, 1984). The dopaminergic neurons of the midbrain (substantia nigra pars compacta) and the glutamatergic fibres from the thalamus also innervate all areas of the striatum (Parent, 1990; Pollack, 2001).

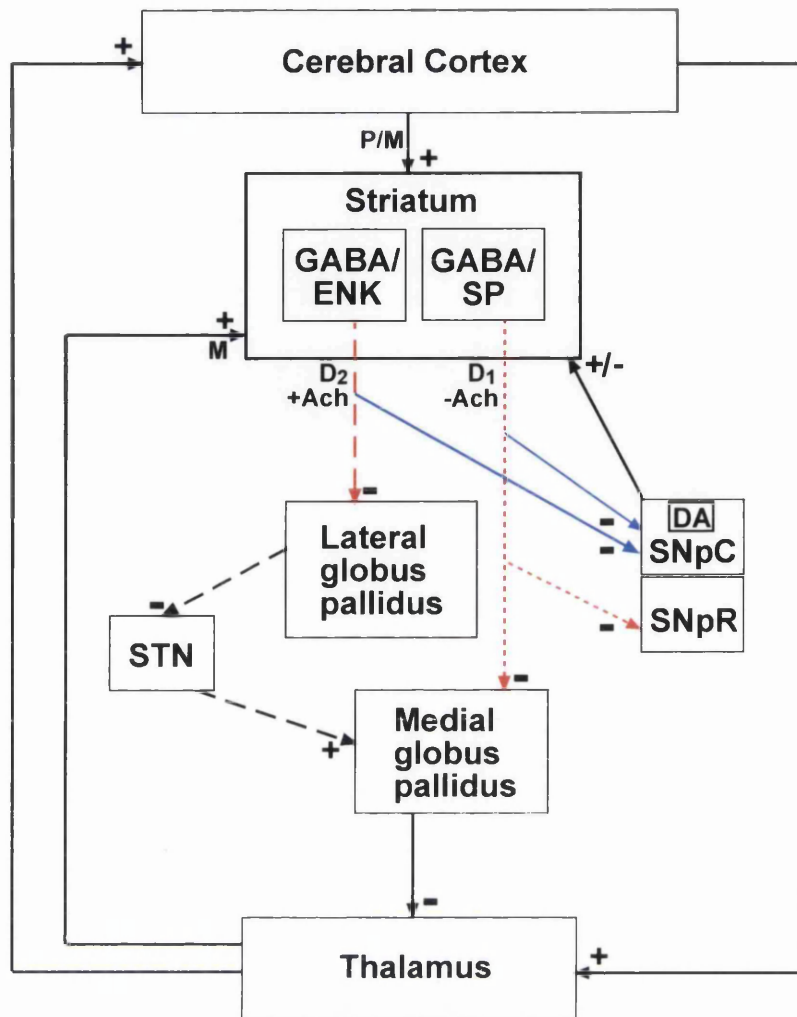


Figure 1.1 The cortico-striato-thalamic circuit

The striatum has an integral role in controlling the activity of the cortico-striato-thalamic circuit. The GABAergic MSN in the striatum are split into two groups by their neuropeptide content and route of projection to the medial globus pallidus (the output structure of the basal ganglia). The indirect pathway is made up of MSN expressing GABA and ENK, which project to the STN (---). The inhibitory effect of this pathway causes the STN to excite the medial globus pallidus and so inhibit the thalamus and therefore the cortex. The direct pathway consists of MSN expressing GABA and SP and/or DN, which project to the medial globus pallidus (-----). Their inhibitory effect releases the thalamus and therefore the cortex from the inhibitory effects of the medial globus pallidus. The output of the basal ganglia modulates the activity of the cortex and thalamus and is determined by the balance between the indirect and direct pathways. The activity of the pathways are controlled by differential responses to Ach and DA. The indirect pathway MSN express the inhibitory DA receptors D₂ and the direct pathway MSN express the excitatory DA receptors D₁. Ach has a excitatory effect of the indirect MSN and an inhibitory effect of the direct MSN. The striatum is split neurochemically into two compartments, the patch and matrix. MSN within both compartments receive excitatory glutaminergic input from the cortex. MSN within the matrix also receive excitatory input from the thalamus. The MSN within the matrix are those involved in the indirect and direct pathways (red), those in the patch project to the SNpC (blue). The HD-associated neurodegeneration is initially selective to the striatum. The MSN in the indirect pathway and all the patch MSN are more vulnerable to neurodegeneration than the direct pathway MSN. MSN = medium spiny neurons, STN = subthalamic nucleus, SNpR = substantia nigra pars reticulata, SNpC = substantia nigra pars compacta, P = patch, M = matrix, DA = dopamine, GABA = aminobutyric acid, Ach = Acetylcholine, SP = substance P, ENK = Enkephalin, DN = dynorphin, - = inhibitory projections, + = excitatory projections.

γ -aminobutyric acid (GABAergic) expressing medium spiny projection neurons (MSN) are the main cell-type within the striatum and constitute the output pathways of the structure. Although MSN show low levels of spontaneous discharge, they phasically respond to excitatory inputs from the cortex. In addition to the inhibitory neurotransmitter, GABA, MSN co-localise neuropeptides such as enkephalin (ENK) in those that project to the lateral globus pallidus (named globus pallidus in rodents) and substance P (SP) and/or dynorphin (DN) in neurons projecting to the medial globus pallidus and the substantia nigra pars reticulata (Figure 1.1) (Gerfen and Young, 1988; Parent *et al.*, 1984). Significant numbers of efferents from both groups of MSN synapse with the dopaminergic neurons of the substantia nigra pars compacta (Figure 1.1) (Gerfen, 1992; Somogyi and Smith, 1979). Although both kinds of MSN are distributed throughout the striatum, cells with common projections tend to be grouped in small clusters (Kawaguchi, 1997).

The MSN co-localising SP/DN make up the 'direct pathway', as they directly inhibit the output structure of the basal ganglia, the medial globus pallidus (Penney and Young, 1986). The ENK-containing MSN constitute the 'indirect pathway' as they indirectly stimulate the medial globus pallidus via inhibitory projections to the lateral globus pallidus and the subthalamic nucleus (Penney and Young, 1986). The direct pathway neurons principally express dopamine D₁ neurotransmitter receptors whereas indirect neurons express dopamine D₂ receptors (Albin, 1995; Hedreen and Folstein, 1995). The direct and indirect MSN also respond differently to cholinergic agonists, which stimulate indirect neurons but inhibit direct neurons (Harrison *et al.*, 1996). Indirect neurons also express the A2a adenosine receptor subtype, which are absent on the direct pathway neurons (Ferre *et al.*, 1993). The differential characteristics of the MSN populations provide the ability to control the output of the direct and indirect pathways, thereby, balancing the pattern and level of thalamic and cortical stimulation.

The neuronal population within the striatum is made up of ~95 % MSN and ~5 % interneurons (Kawaguchi, 1997). The main group of interneurons within the striatum are the cholinergic interneurons that possess large soma and widespread dendritic trees. They receive direct dopaminergic inputs from the midbrain and form synapses on MSN. Other interneurons present within the striatum stain positive for nicotinamide adenine dinucleotide phosphate (NADPH) diaphorase (a marker for nitric oxide synthase (NOS)), somatostatin, neuropeptide Y and the calcium binding protein, calbindin (Ferrante *et al.*, 1997) and a distinct population of medium-sized interneurons localise parvalbumin (Kawaguchi, 1997).

Different neurochemical compartments within the striatum have been observed, referred to as the patch (striosome) and matrix (Gerfen, 1992; Graybiel, 1990). Calbindin is expressed in MSN lying in the matrix whereas μ opiate receptors are found on neurons within the patch (Kawaguchi, 1997). Slightly different afferent connections to the compartments are observed, with innervation from

differing regions of the cortex. Efferent projections also vary, with patch MSN projecting to the dopaminergic cells of the substantia nigra pars compacta and matrix MSN directly to the lateral and medial globus pallidus and the substantia nigra pars reticulata (Gerfen, 1985). The dendrites of MSN tend to stay within their own compartment (Kawaguchi, 1997; Penny *et al.*, 1988) but interneurons are able to interact with all MSN as their dendritic trees extend into both compartments (Kubota and Kawaguchi, 1993).

1.1.2.3 Pattern of neurodegeneration in HD

Post-mortem investigation of HD brains has revealed that the caudate nucleus and putamen (striatum) are the brain regions predominantly involved in the neurodegeneration associated with HD (Vonsattel *et al.*, 1985). The additional loss of the large pyramidal neurons in layers III, V and VI of the cerebral cortex is also been seen in late stages of the disease process (Vonsattel and DiFiglia, 1998). The neurodegenerative changes within the striatum can be graded on macroscopic and light microscopic examination (Vonsattel *et al.*, 1985). Grade 0 indicates a patient with a clinical diagnosis of HD but no gross or microscopic abnormalities whereas grade 4 describes brain tissue with severe shrinking of the striatum and ~95 % neuronal loss. Subsequent quantitative analysis has revealed a reduced neuronal population in grade 0 HD brains compared to controls, in the absence of reactive gliosis, suggesting reduced numbers of cells due to abnormal brain development (Myers *et al.*, 1991). The striatum is generally thought to be involved in the control of movement. However, circuits connecting this region to other structures, such as the cortex and those involved in the limbic system also suggest involvement in functions including control of attention, executive function and motivated behaviours (McGeorge and Faull, 1989; Mogenson *et al.*, 1980; Saint-Cyr *et al.*, 1995). Therefore, the neuropathological findings from HD post-mortem brain tissue correlate with the clinical manifestations of the disease.

Whilst, neurodegeneration within the striatum is seen first in the caudate nucleus, it spreads to the putamen. The wave of degeneration spreads ventrally such that the nucleus accumbens (ventral striatum) is only affected in the late stages of the disease. A gradient of neuropathological change is seen in the striatum with the process beginning in a posterior, medial and dorsal location and moving along the antero-posterior, latero-medial and ventro-dorsal axes. This gradient is seen in grade 1 to 3 HD brains but severe degeneration is observed throughout the entire striatum in grade 4 brains (Vonsattel *et al.*, 1985).

Differential sensitivity of the MSN within the direct and indirect efferent pathways of the striatum has been observed, with the ENK/dopamine D₂ receptor-expressing MSN involved in the indirect pathway preferentially targeted by HD pathogenesis (Albin, 1995; Hedreen and Folstein, 1995; Richfield *et al.*, 1995). This sensitivity is illustrated by the early decrease in ENK immunoreactivity in the lateral globus pallidus but no alteration in SP immunoreactivity in the

medial globus pallidus in asymptomatic cases of HD (Albin, 1995). A reduction in preproenkephalin mRNA in the striatum early in HD is also observed but changes in preprotachykinin mRNA only become apparent in late stages of the disease (Richfield *et al.*, 1995). The circuitry within the cortico-striato-thalamic loop (Figure 1.1) would suggest that preferential degeneration or hypoactivity of the indirect pathway MSN causes an imbalance in the control of the cerebral cortex that leads to cortical excitation and involuntary movement. This suggestion is supported by the previous association of the indirect pathway with choreiform movements, the major movement disorder associated with HD (Crossman *et al.*, 1987).

The concentration of neuropeptides co-localising in NADPH diaphorase-positive interneurons increases in the striatum of HD patients, suggesting that these cells are retained as the MSN succumb to the disease process (Ellison *et al.*, 1987). Ferrante *et al.* (1987) similarly observed that large cholinergic interneurons remain relatively untouched in HD brains, illustrating the striking cell-selective vulnerability of MSN to the disease process.

In addition to the MSN-type specific neuropathology in HD, a compartment-specific pattern has also been reported. Neurodegeneration appears to affect MSN within the patch first before spreading to the matrix, since pathology in early stage HD correlates with calbindin-poor regions of the striatum (Hedreen and Folstein, 1995) and there is a preferential reduction in neuropeptide markers (ENK and SP mRNA) within the patch neurons (Augood *et al.*, 1996). Although it is unknown why cells within the patch are more vulnerable to HD pathology, the higher concentration of the calcium regulator, calbindin, in the matrix (Gerfen, 1985) may help prevent potential problems in calcium homeostasis that contribute to neurodegeneration (Gerlach *et al.*, 1996). The initial neurodegeneration in HD observed throughout the striatum within the patch compartment (Hedreen and Folstein, 1995) gradually spreads to the matrix progressing in a gradient fashion. MSN within the patch project mainly to the substantia nigra pars compacta where they synapse with dopaminergic neurons (Gerfen, 1985). Therefore, loss of patch MSN early in HD could lead to loss of GABAergic inhibition of dopaminergic cells and increased striatal dopamine levels. There is increasing evidence from studies that demonstrate intraparenchymal injections of dopamine produce dose-dependent striatal lesions (Hastings *et al.*, 1996) and toxicity in striatal cell culture, that this neurotransmitter can be neurotoxic (Cheng *et al.*, 1996). At this time, however, there is no evidence of increased dopamine levels in the striatum of HD brains (Pearson *et al.*, 1990) and no sign of cell loss in the substantia nigra pars compacta in HD brains (Albin, 1995; Ferrante *et al.*, 1997).

1.1.2.4 Neurodegeneration versus neuronal dysfunction in HD

Investigations into the relationship between anatomical and functional changes in HD brains have raised the possibility that functional deficits may be present prior to obvious anatomical alteration.

The first illustration of anatomical changes in clinical HD patients by brain imaging demonstrated a significant enlargement of the bi-caudate diameter, reflecting a reduction in caudate volume and dilation of the ventricles (Barr *et al.*, 1978). Further studies found a significant reduction of basal ganglia volume in asymptomatic HD gene carriers, indicating that anatomical changes may be present early in the disease process, before obvious symptoms (Aylward *et al.*, 1996). However, reports of HD patients suffering from overt symptoms in the absence of any obvious neuropathology (Vonsattel grade 0) have suggested that the development of gross anatomical changes within the striatum may lag behind clinical manifestations (Vonsattel *et al.*, 1985). The absence of a correlation between the rate of change in caudate size and reduced glucose metabolism in asymptomatic, at risk, subjects (Grafton *et al.*, 1992) suggests that metabolic decline and caudal atrophy can develop independently. In addition, significant hypometabolism with no evidence of caudate atrophy has been observed in at risk, HD gene carriers (Mazziotta *et al.*, 1987). No significant change in the bi-caudate ratio, despite significant caudate nucleus hypometabolism and a reduction in dopamine receptor binding, has also been demonstrated in asymptomatic HD gene carriers (Antonini *et al.*, 1996). These studies suggest that, at least in presymptomatic phases of HD, striatal dysfunctioning can occur without obvious striatal atrophy. A number of studies have now detected subtle phenotypic changes in HD gene carriers previously considered to be asymptomatic (de Boo *et al.*, 1997; Kirkwood *et al.*, 1999; Lawrence *et al.*, 1998a), suggesting that reduced striatal glucose metabolism and receptor binding alterations may contribute to early symptoms in HD without the requirement for overt cell loss. If a period of symptom-inducing neuronal dysfunction precedes neurodegeneration in HD, the effectiveness of treatment strategies purely aimed at preventing cell death is somewhat questionable, as they may not necessarily eliminate the entire HD phenotype.

1.2 Molecular basis of HD

Lengthening (expansion) of a repeated DNA sequence, most commonly a trinucleotide repeat, is the mutation associated with a growing number of human hereditary diseases. HD is caused by the expansion of the trinucleotide (CAG) repeat residing in exon 1 of the *HD (IT-15)* gene, which spans 210 kb of chromosome 4 ((HDCRG), 1993). The CAG repeat within the *HD* gene displays a non-pathogenic, polymorphic repeat range of between 10-41 repeats within the general population (Andrew *et al.*, 1993; Duyao *et al.*, 1993; (HDCRG), 1993; Snell *et al.*, 1993). The occurrence of HD has been noted in patients possessing between 36 and approximately 250 CAG repeats (Andrew *et al.*, 1993; Duyao *et al.*, 1993; (HDCRG), 1993; Nance *et al.*, 1999; Snell *et al.*, 1993). As long CAG repeat tracts tend to be unstable in the germline, pathogenic mutations may result from small, successive increases in repeats within the non-pathogenic range, eventually resulting in the inheritance of a disease-causing mutation (Leeflang *et al.*, 1999; Leeflang *et al.*, 1995). The alleles carrying the repeats that eventually give rise to HD mutations are designated intermediate

alleles (29-35 repeats) (Chong *et al.*, 1997; Goldberg *et al.*, 1993; Goldberg *et al.*, 1995). The normal and pathogenic repeat ranges overlap and HD patients possessing 36 to 41 repeats have been described expressing typical disease onset and course, while other individuals carrying repeats within this range have failed to display symptoms within a normal life-span (Brinkman *et al.*, 1997). These findings suggest that disease mutations may initially display reduced penetrance (36-41 repeats) (Brinkman *et al.*, 1997; McNeil *et al.*, 1997; Myers *et al.*, 1993; Rubinsztein *et al.*, 1996).

Repeat length also has an influence on the clinical manifestation of the disease. The length of the inherited repeat expansion displays an inverse correlation with age at onset (Figure 1.2A), disease severity and degree of pathology at death, suggesting increased toxicity of longer repeats (Andrew *et al.*, 1993; Duyao *et al.*, 1993; (HDCRG), 1993; Penney *et al.*, 1997; Snell *et al.*, 1993). A significant correlation has been observed between longer repeat lengths and a faster rate of clinical deterioration (Brandt *et al.*, 1996; Jason *et al.*, 1997). Several reports have established that the severity of cognitive deficits observed inversely correlates with the CAG repeat length (Foroud *et al.*, 1995; Lawrence *et al.*, 1998b; Snell *et al.*, 1993). The heterogeneity of neuropsychological symptoms observed within groups of HD mutation carriers is also related to the CAG repeat length (Hahn-Barma *et al.*, 1998). Analysis of subtle symptoms observed in preclinical HD gene carriers has shown that those who carry longer CAG repeats have greater cognitive impairment (Foroud *et al.*, 1995; Jason *et al.*, 1997) and motor deficits (Siemers *et al.*, 1996). However, no such correlation has been found with the psychiatric symptoms seen in preclinical HD gene carriers (Berrios *et al.*, 2001). The correlation between repeat length and cognitive deficits seen in preclinical HD patients appears to be lost when investigating cognitive deficits in clinically affected individuals (Jason *et al.*, 1997). Studies have suggested that cognitive functioning declines sharply prior to clinical onset and then levels out to a slow progressive decline. This sharp decline may be worse in patients with longer repeats, perhaps contributing to their earlier onset and explaining why there is a correlation with repeat length at this stage in the disease process (Jason *et al.*, 1997). The relationship between symptoms and repeat length is clearly complicated by the suggestion that only specific cognitive symptoms (language, memory, intelligence) have a significant correlation with repeat length when others may not (executive and spatial functioning) (Jason *et al.*, 1997).

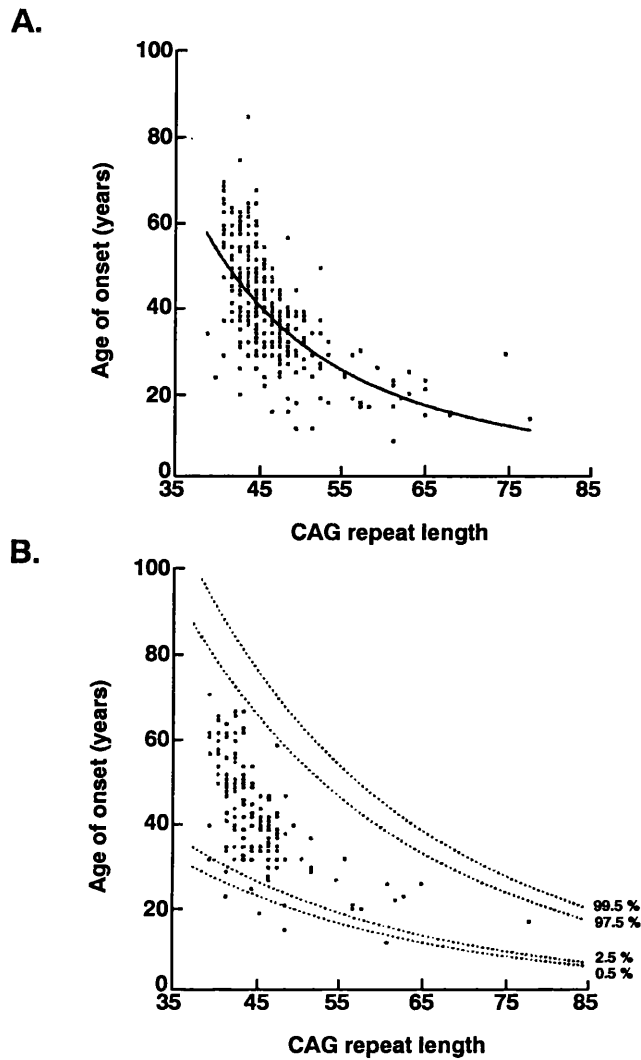


Figure 1.2 The correlation between CAG repeat length and age of onset in HD

A. A regression curve demonstrating the correlation between repeat length and age at onset of HD.
B. The confidence intervals for the predicted age at onset for a given repeat length. These data illustrate the large range of onset ages for the repeats within the 40-50 repeat range suggesting that other factors also influence age at onset. The graphs were generated with transformed data of the repeat length and age of onset from 360 HD sufferers.
 Figure modified from Andrew *et al.*, 1993.

The link between repeat length and disease manifestation is supported by the observation that HD patients carrying over 50 CAG repeats most commonly suffer from the severe juvenile form of HD (Nance and Myers, 2001). Whilst, the early age at onset observed in juvenile HD patients contributes significantly to the correlation between the age at onset and repeat length detected in HD (Figure 1.2A), the absolute repeat size for adult-onset HD is a relatively poor index for predicting the age at onset of symptoms (Figure 1.2B) (Andrew *et al.*, 1993; Barron *et al.*, 1993; Kremer *et al.*, 1995). Indeed, repeat length is thought to account for about 50 % of the variation in the age at onset for many adult-onset HD patients (Andrew *et al.*, 1993). The onset age of the parent, sex of affected parent and repeat size of the offspring are together thought to be responsible for ~69 % of the variance in age at onset for adult-onset HD cases (Ranen *et al.*, 1995), clearly indicating that other genetic or environmental factors can influence age at onset and severity of HD. Polymorphisms close to the CAG repeat tract have already been associated with a decreased age at onset when comparing alleles carrying the same repeat length (Vuillaume *et al.*, 1998), suggesting possible *cis*-acting genetic factors which may influence the course of HD pathogenesis.

1.2.1 Germline repeat instability in HD

By examining the inheritance of repeat sizes within HD families and identifying mutation sizes of individual germ cells, information can be obtained about the behaviour of the HD-associated CAG repeat tract within the germline. Inheritance studies have demonstrated that a high percentage of meioses (~70-85 %) result in a change of repeat size on the mutant HD chromosome (Duyao *et al.*, 1993; Kremer *et al.*, 1995; Leeflang *et al.*, 1995). This is in stark contrast to the ~1 % of meioses that produce a change in repeat size on normal chromosomes (Duyao *et al.*, 1993; Kremer *et al.*, 1995; Leeflang *et al.*, 1995). Repeat size spectra obtained from sperm cells show the mutation frequency and mean changes in allele size increase with higher somatic repeat number (Leeflang *et al.*, 1999). As longer repeats are more prone to expansion, repeats that have expanded on transmission are more likely to expand again, providing the genetic basis for the phenomenon of anticipation (Myers *et al.*, 1993; Telenius *et al.*, 1994; Zuhlke *et al.*, 1993). Anticipation is a term that describes a decrease of onset age in successive generations observed in HD families.

Evidence for a sex-of-origin effect influencing transmitted repeat sizes was provided by the observation that although small fluctuations are present in both maternal and paternal transmissions, there are overall differences in the behaviour of repeats within male and female germ lines. It is more likely that small contractions or no change in repeat size is transmitted through the maternal line (Kremer *et al.*, 1995) and dramatic increases in repeat number are most commonly observed on paternal transmission (Duyao *et al.*, 1993). Due to the correlation between repeat length and age at disease onset (Andrew *et al.*, 1993; Brinkman *et al.*, 1997; Ranen *et al.*, 1995) there is a preponderance (~80 %) for juvenile patients to inherit the HD mutation from their father (Brinkman *et al.*, 1997; Goldberg *et al.*, 1993; Kremer *et al.*, 1995; Ranen *et al.*, 1995).

Furthermore, inheritance studies indicate that ~14.5 % of affected fathers produce juvenile HD offspring but only 4.5 % of affected mothers (Duyao *et al.*, 1993). Offspring of affected mothers have similar onset ages to their mother whereas offspring of affected fathers have onset ages of ~8 years earlier than their father (= anticipation) (Kremer *et al.*, 1995). The differences in repeat instability observed in the male and female germlines remain unexplained. As DNA replication is a possible candidate for the underlying mechanism responsible for repeat instability, the high replication rate (~400 cell divisions per 30 year generation in humans (Drost and Lee, 1995)) of mature sperm cells compared to oocytes (~30 cell divisions per 30 year generation in humans), may in part explain the sex-of-origin effect observed in HD inheritance.

Studies have been carried out to investigate genomic factors that play a role in the germline repeat instability observed in HD patients. A comparison of single sperm containing intermediate alleles (29-35 repeats), which expanded into new mutations (IANm) and those that continued in the general population without change (IAGp), demonstrated that when IAGp and IANm have the same repeat length, IANm are significantly more unstable (Chong *et al.*, 1997). This study suggested that there are *cis*-acting factors involved in the propensity for repeat expansion. One common characteristic of the *HD* gene CAG tract is an interruption consisting of a penultimate CAA codon. Alleles with mutations in this codon, deleting the interruption and producing a perfect CAG repeat, have demonstrated significant increases in the spectrum of sperm repeat instability observed (Goldberg *et al.*, 1995; McNeil *et al.*, 1997). This illustrates the higher propensity of longer repeats to display instability and the stability conferred on a repeat sequence by interruptions in a perfect repeat tract. Indeed, investigations reporting the mutation responsible for SCA17 as a CAG repeat expansion within the TATA binding protein, demonstrated its complete germline stability and speculated that this was caused by the numerous CAA repeat interruptions present (Fujigasaki *et al.*, 2001). Investigations have also demonstrated that the CAG repeat size on the normal chromosome of either the affected parent or the affected offspring has no influence on the mutant CAG repeat instability (Kremer *et al.*, 1995).

Within the male germline, a 1:1 ratio of mutant to normal sperm suggests a lack of segregation distortion in male HD patients, with ~96 % of mutant sperm possessing a repeat length that differed from the somatic repeat length (Leefflang *et al.*, 1999). The variability of repeat length changes within the male germline was greater than previously estimated from inheritance studies and may reflect selection against sperm carrying longer CAG repeat tracts. This putative selection could reflect lower survival rates or an inability to carry out fertilisation of oocytes. However, if this negative selection is operating, it does not appear to reduce fertility in HD patients (Leefflang *et al.*, 1999). The mutation spectrum within the maternal germline has not been directly analysed due to the difficulty in obtaining oocytes. Although large expansions have rarely been transmitted through

the maternal line, it is thought that the low frequency of these transmissions may also be due to negative selection of oocytes containing larger repeats (Laccone and Christian, 2000).

1.2.2 Somatic repeat instability in HD

Although germline repeat instability is responsible for such interesting phenomenon as anticipation and sex-of-origin effects in HD, the behaviour of repeat sequences within somatic tissues could have important implications regarding the selective vulnerability of tissues to the disease process. Although the *HD* gene is widely expressed in all somatic tissues (Landwehrmeyer *et al.*, 1995a; Li *et al.*, 1993; Strong *et al.*, 1993), the pathology expressed is limited to specific brain regions. CAG repeat length in HD correlates with age of onset and clinical severity (Andrew *et al.*, 1993; Duyao *et al.*, 1993) and therefore, repeat length variation between somatic cells may present an explanation for why some tissues are less affected than others.

Radioactive PCR followed by separation of the products through polyacrylamide gels and densitometric analysis of the autoradiographic images has been used to investigate somatic repeat instability in HD. However, a number of studies have provided inconsistent results. MacDonald *et al.* (1993) investigated somatic repeat instability by PCR amplification, comparing the allele repeat size in blood and lymphoblastoid cell lines from HD patients at two time points. Additional bands detected did not alter with different samples or the progression of the disease and so were proposed to be due to PCR stutter, suggesting that there is no somatic instability of the mutation throughout the course of HD. Additional in depth studies of skeletal and heart muscle, liver, kidney, lymphocytes, cortex, thalamus, hippocampus, and the caudate nucleus were carried out and no significant somatic repeat instability was observed (Zuhlke *et al.*, 1993). The selection of tissues included at least one organ from all three regions of the embryo (endoderm, ectoderm and mesoderm) suggesting that the repeat is also stable throughout development.

Telenius *et al.* (1994) investigated DNA obtained from several somatic organs and central nervous system regions and found that the predominant mutant allele was invariably the same size in each tissue. However, the brain samples consistently showed extra bands above the major progenitor allele band. These additional bands previously dismissed as PCR artefacts by other investigators (MacDonald *et al.*, 1993; Zuhlke *et al.*, 1993), were interpreted as somatic repeat instability in this study. This stance was justified by the observation that no additional bands were detected when amplifying normal alleles or cloned mutant alleles. A densitometric index representing the ratio of intensity of the major band compared to the first band immediately above this was used as a measure of mosaicism when comparing individual tissues with the same major allele size from one patient. These studies produced a consistent tissue-specific pattern of CAG mosaicism. It was found that the mosaicism was always highest in the brain, specifically the cortex and striatum, intermediate in the blood and low in the liver and cerebellum. It was also reported that juvenile

cases of HD had higher degrees of instability than late-onset cases. Further analysis carried out on brain tissue from juvenile HD patients, demonstrated that the cerebellar cortex expressed a significantly lower repeat size (8-13 CAG repeats) compared to other brain regions. These findings were supported by the comparison of repeat size in severely affected, mildly and unaffected brain regions to other tissues (De Rooij *et al.*, 1995). Severely affected regions did not give rise to larger PCR products compared to mildly affected regions. However, alleles from all affected brain regions showed larger repeat lengths compared to cerebellum and blood.

1.2.3 Homologues of the *HD* gene

The human *HD* gene spans ~210 kb of genomic DNA and consists of 67 exons ((HDCRG), 1993). The protein sequence of human huntingtin has no significant similarity to any other known proteins. Nor have any proven functional domains or motifs been identified over any stretch of the large protein. One way of identifying potentially important functional domains within the protein is to isolate orthologues from other organisms. In the case of the HD protein, vertebrate homologues from mouse (Barnes *et al.*, 1994; Lin *et al.*, 1994), rat (Schmitt *et al.*, 1995), pufferfish (Baxendale *et al.*, 1995) and zebrafish (Karlovič *et al.*, 1998) have all been identified.

All vertebrate *HD* gene homologues identified have displayed high identity with the human *HD* gene sequence. The murine cDNA has 91 % peptide sequence identity with the human gene (Barnes *et al.*, 1994). DNA sequence analysis of the pufferfish and zebrafish *HD* genes have revealed 90 % and 70 % identity, respectively, at the amino acid level with the human sequence (Baxendale *et al.*, 1995; Karlovič *et al.*, 1998). When the human, mouse, pufferfish, and zebrafish huntingtin proteins are aligned, the overall amino acid identity is 64 %, and the homology spans the entire length of the protein. Despite the high level of conservation at the amino acid level, suggesting an important functional role, the HD protein family continues to exhibit no strong similarity to any known proteins or motifs currently held in the databases.

The polymorphic polyglutamine stretch within the human protein sequence has an average of 18 glutamines ((HDCRG), 1993). The rat *HD* gene sequence contains eight glutamines (Schmitt *et al.*, 1995) and the mouse has seven, with the third glutamine encoded by CAA rather than CAG (Barnes *et al.*, 1994; Lin *et al.*, 1994). The fish sequence displays four glutamines, encoded by (CAG)₃(CAA) in the pufferfish (Baxendale *et al.*, 1995) and (CAG)₂(CAA)₂ zebrafish (Karlovič *et al.*, 1998). The CAA interruption in the glutamine stretch in all vertebrates, other than humans, may account for the CAG repeat stability and why naturally occurring animal models of HD are unknown.

The high degree of amino acid sequence similarity between these vertebrate proteins has made it difficult to determine potential functional domains. Sequence comparison with more distantly related species, in particular that of an invertebrate, could be more informative.

Identification of the *Drosophila HD* gene homologue has shown three large, contiguous regions at the N-terminus, middle and C-terminus of the protein, in which there is an overall identity of 24 % with the human sequence (Li *et al.*, 1999b). Within this sequence, five relatively discrete regions are highly conserved with areas of the huntingtin protein family suggesting possible functional importance. However, at this time databases have failed to identify any known domains or motifs for these regions. The N-terminus was found to be the most highly conserved region between *Drosophila* and human although no polyglutamine is observed (Li *et al.*, 1999b).

1.2.4 Huntingtin

The *HD* gene encodes a ubiquitously expressed protein of unknown function, called huntingtin ((HDCRG), 1993). The huntingtin protein has a predicted size of ~350 kDa, and antibody studies have demonstrated that the CAG repeat tract within exon of 1 of the *HD* gene is translated into a polyglutamine stretch within the protein product (Jou and Myers, 1995). Huntingtin has been detected in the CNS and peripheral tissues (Gutekunst *et al.*, 1995; Li *et al.*, 1993; Strong *et al.*, 1993), with the highest expression levels observed within the brain and testis (Li *et al.*, 1993; Sharp *et al.*, 1995; Strong *et al.*, 1993). Expression throughout the brain is observed in all neurons and displays no sign of enrichment within the basal ganglia (Li *et al.*, 1993; Strong *et al.*, 1993).

The function of huntingtin is unknown and it displays no homology to other known genes ((HDCRG), 1993; Hoogeveen *et al.*, 1993; Lin *et al.*, 1993; Strong *et al.*, 1993). Expression is typically as a cytosolic protein associated with microtubules, vesicles and synaptic components, concentrated at the nerve endings, suggesting a role in cellular transport and neurotransmission (DiFiglia *et al.*, 1995; Gourfinkel-An *et al.*, 1997; (HDCRG), 1993; Li *et al.*, 2000; Li *et al.*, 1993; Sharp *et al.*, 1995; Strong *et al.*, 1993; Trottier *et al.*, 1995; Tukamoto *et al.*, 1997). Mice with reduced levels of wild-type huntingtin display aberrant brain development and pre-natal lethality (White *et al.*, 1997) or neuronal degeneration in the basal ganglia during adulthood (O'kusky *et al.*, 1999). *In vitro* studies have also suggested an anti-apoptotic property of wild-type huntingtin, as the expression of wild-type huntingtin has been shown to protect neurons from various apoptotic stimuli (Rigamonti *et al.*, 2000). The embryonic lethality, on day 8.5 of development (E8.5), of huntingtin knock-out mice demonstrated an essential role in embryonic development (Bhide *et al.*, 1996; Duyao *et al.*, 1995; Nasir *et al.*, 1995; Zeitlin *et al.*, 1995). Studies using transgenic HD mice have also illustrated that the expression of wild-type huntingtin reduces the toxicity of mutant huntingtin (Leavitt *et al.*, 2001). The production of a conditional knock-out mouse model has provided further evidence that normal huntingtin function is necessary to maintain viable and

properly functioning neurons in the adult brain (Dragatsis *et al.*, 2000) indicating, along with information derived from the other mouse models, that the role of normal huntingtin is essential for both embryogenesis and neuronal survival in the adult brain.

The mechanism of disease pathogenesis exerted by the extended polyglutamine stretch is largely unknown. However, several lines of evidence including the autosomal dominant inheritance pattern, a comparable phenotype in homozygous and heterozygous HD mutation carriers (Wexler *et al.*, 1987) and *HD* gene knockout mice lacking the appropriate disease phenotypes, suggest that the repeat expansion mutation exerts its toxicity through a gain-of-function mechanism. However, studies have also suggested that a loss of function effect due to the expansion mutation could also play a part in HD neuropathogenesis (O'kusky *et al.*, 1999; White *et al.*, 1997).

1.2.5 Huntingtin expression and selective vulnerability of neurons

Uncertainty remains concerning a possible correlation between the expression of huntingtin protein and the cell-selective vulnerability (section 1.1.2.3) observed in HD. It has been established that striatal neurons are not uniquely enriched in huntingtin compared with other parts of the brain (Li *et al.*, 1993; Strong *et al.*, 1993). Studies on post-mortem HD tissue have also showed that the regional and cellular expression levels of huntingtin or its mRNA are not significantly altered by the mutation or the disease process (Aronin *et al.*, 1995; Bhide *et al.*, 1996; Gourfinkel-An *et al.*, 1997; Landwehrmeyer *et al.*, 1995a; Sapp *et al.*, 1997; Schilling *et al.*, 1995; Sharp *et al.*, 1995; Trottier *et al.*, 1995). However, it remains unclear whether the initial cell-type specific pathology within the striatum is connected to differential expression levels in the mutant protein. Investigations have been carried out in an attempt to relate the distinct sensitivity observed in the patch and matrix compartments within the striatum to the expression of huntingtin but these have produced conflicting results. High levels of huntingtin within the matrix and lower levels within the patch have been reported (Ferrante *et al.*, 1997; Sapp *et al.*, 1997). However other studies have found the highest expression levels in the patch and the lowest in matrix (Kosinski *et al.*, 1997). In addition, differential expression in the striatal compartments has been questioned in several other studies, which failed to find any difference in expression levels (Bhide *et al.*, 1996; Fusco *et al.*, 1999; Landwehrmeyer *et al.*, 1995a).

Cholinergic interneurons that are resistant to pathology in HD, appear richer in huntingtin than the MSN, suggesting an inverse relationship between huntingtin expression levels and vulnerability (Kowall *et al.*, 1987). This theory is substantiated by the ENK, indirect, MSN, the most vulnerable cells in HD, expressing lower huntingtin mRNA levels than the less vulnerable SP, direct, MSN (Fusco *et al.*, 1999). The striatonigral projection neurons (ENK+ and SP+), which are as vulnerable as the ENK, indirect MSN also express low HD mRNA levels. The cortical pyramidal, pallidal, and basal forebrain cholinergic neurons are all relatively resistant to HD and all rich in huntingtin

(Sharp and Ross, 1996). In contrast, the aspiny NADPH-diaphorase, somatostatin striatal interneurons, which survive well in HD, are largely devoid of huntingtin (Ferrante *et al.*, 1997) and parvalbumin-positive striatal interneurons, which are as vulnerable as the projection neurons are often rich in huntingtin (Ferrer *et al.*, 1994). The cortical layer III and V neurons are uniformly rich in huntingtin and project to the striatum. However, they tend to be affected in later stages of the disease process.

In summary, at present there is no clear evidence to confirm that cells expressing higher levels of mutant huntingtin are more vulnerable, or indeed that cells with low levels are at increased risk of HD pathology. These findings do however suggest that factors other than huntingtin expression levels are probably involved in the cell-selective vulnerability observed in HD.

1.2.6 Protein aggregation and HD pathogenesis

The presence of neuronal intranuclear inclusions (NII) was reported in brain tissue of a HD transgenic mouse model, the R6/2 mice (Davies *et al.*, 1997). Further *in vitro* experiments confirmed that the mutant N-terminal huntingtin protein expressed from the human *HD* gene exon 1 construct present in R6/2 mice aggregates in ubiquitinated insoluble NII and that these structures have a fibrillar morphology (Scherzinger *et al.*, 1997). These findings suggest that mutant huntingtin protein is marked by the ubiquitination machinery but appears to be resistant to degradation. A pathogenic role for NII was suggested, as the inclusions were visible shortly before the animals developed behavioural abnormalities. These findings have since been supported with the observation of NII within brain regions involved in HD pathology in other HD mouse models (Li *et al.*, 1999a; Li *et al.*, 2000; Reddy *et al.*, 1998; Schilling *et al.*, 1999).

NII consisting of aggregated polyglutamine-containing protein were also detected in brain tissue of patients suffering from HD (Becher *et al.*, 1998; DiFiglia *et al.*, 1997; Gutekunst *et al.*, 1999) and other disorders caused by proteins expressing elongated stretches of polyglutamine, including, SCA1 (Skinner *et al.*, 1997), SCA3 (Paulson *et al.*, 1997), SCA7 (Holmberg *et al.*, 1998), SBMA (Li *et al.*, 1998b) and DRPLA (Becher *et al.*, 1998; Igarashi *et al.*, 1998).

Several forms of interactions have been proposed for proteins containing polyglutamine stretches. It has been noted that mutant huntingtin can self-polymerase *in vitro* in the absence of any enzymes (Scherzinger *et al.*, 1997). The formation of polar-zipper structures between proteins containing polyglutamine stretches, has been postulated (Perutz *et al.*, 1994). Transglutamination, with polyglutamine serving as a substrate for the enzyme transglutaminase (Green, 1993; Kahlem *et al.*, 1998) has also been discussed as a possible mechanism involved in aggregate formation.

1.2.6.1 Nuclear localisation of huntingtin

Studies of post-mortem human HD brain tissue have demonstrated the occurrence of NII within the neurons (striatal and cortical) specifically involved in HD pathogenesis. NII were not observed in control or presymptomatic HD brains, only in symptomatic brain tissue, suggesting a connection between aggregate formation and onset of symptoms (DiFiglia *et al.*, 1997). Aggregate formation occurs in a repeat length-dependent manner as juvenile HD brains display NII in 38-52 % of their cortical neurons whereas only 3-6 % of cortical neurons within adult onset HD brains contain NII (DiFiglia *et al.*, 1997). Immunohistochemistry analysis using an antibody raised to the first 17 N-terminal amino acids of huntingtin showed intense labelling of NII in the cortex and striatum but not within the globus pallidus or cerebellum. Studies using an antibody raised against an internal site downstream of the polyglutamine stretch labelled the cytoplasm in control and HD brains but showed no staining of the nuclei or NII. These results suggest that the NII are made up from N-terminal fragments of huntingtin. To substantiate these findings western blot analysis of control and juvenile HD brain protein extracts was carried (DiFiglia *et al.*, 1997). Total protein extracts from control cortical samples displayed huntingtin protein migrating at its expected 350 kDa, however, this band was absent in nuclear extracts. Juvenile HD brain samples displayed an additional band migrating at 40 kD suggesting the presence of huntingtin fragments (DiFiglia *et al.*, 1997). These findings support the toxic fragment hypothesis, which proposes the cleavage of full-length mutant huntingtin localised within the cytoplasm followed by nuclear translocation of the resultant truncated huntingtin fragment. Once in the nucleus it may disrupt cellular functioning by interacting with other polyglutamine rich proteins or sequester proteins during the formation of aggregates.

Ubiquitin appears to co-localise with huntingtin within NII in humans (DiFiglia *et al.*, 1997) and mice (Davies *et al.*, 1997), suggesting that huntingtin fragments may be targets for ubiquitin-dependent proteolysis. This may play a role in producing the toxic huntingtin fragments as huntingtin can be cleaved, in a repeat-dependent manner, at its N-terminus by apopain, a cysteine protease involved in ubiquitin-dependent proteolytic cleavage (Goldberg *et al.*, 1996). Full-length huntingtin could also undergo proteolytic cleavage by caspases before diffusing across the nuclear membrane (Kim *et al.*, 1999; Wellington *et al.*, 1998).

The toxic fragment hypothesis suggests that tissue-specific differences in protein proteolysis and ubiquitination could play a role in the selective vulnerability of HD pathology. Studies of huntingtin fragments in HD and control brains have demonstrated that the striatum of HD brains appears to contain more N-terminal fragments of huntingtin than controls (Mende-Mueller *et al.*, 2001), suggesting an enhanced production or inhibited degradation of the huntingtin fragments within the striatum in HD. In addition, different sized fragments of huntingtin and variation in

levels of ubiquitination were observed within different regions of HD brains also suggesting a role for differential huntingtin proteolysis in selective HD pathogenesis.

The processes leading to nuclear translocation of truncated huntingtin are still unclear but it has been demonstrated that the presence of a polyglutamine stretch is essential. Insertion of a polyglutamine coding sequence into the hypoxanthine phosphoribosyltransferase (Hprt) gene causes translocation of the normally cytoplasmic protein into the nucleus (Ordway *et al.*, 1997). Polyglutamine length also plays a role in translocation as many experimental systems have illustrated that longer polyglutamine stretches produce greater nuclear localisation within cells (Cooper *et al.*, 1998; Hackam *et al.*, 1998; Hackam *et al.*, 1999b; Li and Li, 1998; Martindale *et al.*, 1998; Wheeler *et al.*, 2000). Another factor that influences translocation is the length of the huntingtin molecule. Studies have indicated that translocation is more efficient for shorter huntingtin fragments with longer fragments tending to remain in the cytoplasm (Lunkes and Mandel, 1998; Martindale *et al.*, 1998). Transgenic mouse models expressing truncated forms of mutant huntingtin (Mangiarini *et al.*, 1996; Schilling *et al.*, 1999), display more NII formation and greater phenotypic alterations than mice expressing full-length mutant huntingtin (Hodgson *et al.*, 1999; Li *et al.*, 2000; Reddy *et al.*, 1998; Shelbourne *et al.*, 1999; Wheeler *et al.*, 2000). Similar results have been obtained in cell culture-based (Davies *et al.*, 1999; Li and Li, 1998; Scherzinger *et al.*, 1997) and *Drosophila* models (Marsh *et al.*, 2000) of HD. These findings suggest that the expression of a truncated form of the mutant huntingtin protein may bypass a rate limiting cleavage step and allow faster accumulation of toxic truncated fragments within the nucleus.

However, protein truncation may not be the only mechanism involved as nuclear extracts from juvenile HD patients contain detectable levels of apparently full-length huntingtin (DiFiglia *et al.*, 1997). This suggests that a conformational change due to the elongated polyglutamine may unmask a nuclear localisation sequence (NLS) or a protein association domain that allows huntingtin to be transported to the nucleus, perhaps by binding other proteins (e.g. chaperones) destined for the nucleus.

Studies have shown that nuclear localisation of mutant huntingtin increases cellular toxicity (Kim *et al.*, 1999; Peters *et al.*, 1999; Saudou *et al.*, 1998). However, further *in vitro* experiments have suggested that nuclear localisation of mutant huntingtin is crucial for toxicity, whereas aggregate formation is not (Klement *et al.*, 1998; Saudou *et al.*, 1998).

To investigate whether nuclear localisation of the polyglutamine stretches is required for cytotoxicity in mice carrying mutant ataxin-1, a mutant NLS was used to prevent nuclear localisation (Klement *et al.*, 1998). The resulting mice displayed no ataxia, NII or obvious histopathological alterations in their Purkinje cells, the usual site of pathology. In contrast, animals

expressing the same mutant ataxin-1 protein with an intact NLS displayed cellular alterations, NII and ataxia (Klement *et al.*, 1998), suggesting that nuclear localisation is a necessary step in the pathogenic process. When mutant ataxin-1 with a disrupted self-association domain was transiently expressed in transfected cells, it appeared to enter the nucleus but did not form aggregates. Mice expressing this protein developed Purkinje cell pathology that was similar to that of mice expressing intact mutant ataxin-1, capable of association (Klement *et al.*, 1998). Thus, it appears that the formation of nuclear aggregates is not required for the initiation of mutant ataxin-1-mediated pathogenesis in transgenic mice (Klement *et al.*, 1998).

Saudou *et al.* (1998) utilised cultured striatal neurons transfected with cDNAs encoding wild-type or mutant versions of huntingtin and scored cell survival. Expression of a truncated huntingtin peptide containing an expanded polyglutamine stretch led to the accumulation of large nuclear aggregates and ultimately cell death. Co-expression of a mutant huntingtin fragment and a dominant negative mutant of the ubiquitin conjugating enzyme (Kalchman *et al.*, 1996) caused a significant decrease in the number of NII and markedly increased the rate of cell death compared to cultures expressing mutant huntingtin fragments alone. These findings suggest that the formation of NII might be a cellular strategy to inactivate toxic nuclear forms of mutant huntingtin. In support of this idea, aggregates have been shown to increase in size in advanced pathological grades, suggesting that they may persist in neurons that are more likely to survive (Gutekunst *et al.*, 1999). It is also noteworthy that in adult-onset HD the striatum only displays NII in ~ 4 % of neurons, in all grades of HD pathology (DiFiglia *et al.*, 1997; Gutekunst *et al.*, 1999).

The protective role of NII has been questioned by the findings of aggregates in peripheral tissues. For example, they have been observed in the pancreatic islets of R6/2 mice, which often suffer from diabetes (Hurlbert *et al.*, 1999). However, no association with cell death was observed when investigating NII found in the peripheral tissues in SBMA patients (Li *et al.*, 1998a).

In addition to NII, electron microscopy studies of human post-mortem tissue have detected numerous neuropil aggregates (DiFiglia *et al.*, 1997; Gutekunst *et al.*, 1999; Maat-Schieman *et al.*, 1999). Neuropil aggregates were frequently observed in the brain of asymptomatic HD patients suggesting that they play a role in early neuronal dysfunction (DiFiglia *et al.*, 1997; Gutekunst *et al.*, 1999). Aggregates are also present in the neuronal processes of HD mouse models (Li *et al.*, 1999a; Li *et al.*, 2001). The formation of neuropil aggregates is highly correlated with the development of symptoms in HD mice expressing exon 1 of a mutant human *HD* gene. Neuropil aggregates are more common in the cortex than in the striatum, perhaps acting to impair axonal transport or associate with synaptic vesicles, thereby affecting corticostriatal transmission (Gutekunst *et al.*, 1999). Neuropil aggregates occur more frequently within the dendrites and dendritic spines and could play a role in the known dendritic pathology that occurs in HD

(Gutekunst *et al.*, 1999; Li *et al.*, 2001; Petersen *et al.*, 2001). These cytoplasmic aggregates differ from nuclear aggregates in that they are usually smaller and are not ubiquitinated.

The phenomenon of aggregation could be involved in HD pathogenesis in many ways. Aggregate formation may cause the sequestration of other polyglutamine proteins within the nucleus or neuropil, thereby, disrupting neuronal gene and protein expression. The neuropil aggregates may also disrupt axonal trafficking and neuronal signalling, perhaps by altering the machinery involved in neurotransmission.

1.2.7 Protein-protein interactions of huntingtin

By studying huntingtin's protein partners, insights into the cellular pathways which huntingtin contributes may be provided. These findings will help determine huntingtin's wild-type function and suggest pathways involved in HD pathogenesis. Elongation of the polyglutamine stretch within huntingtin may alter binding to customary protein partners or cause novel protein interactions. These aberrant interactions may disrupt cellular function by altering the function of the protein partners and/or huntingtin. As HD pathology occurs in a cell-selective manner but huntingtin is a ubiquitously expressed protein, the expression pattern of protein partners may be a factor involved in determining selective HD pathology. In addition to soluble huntingtin protein interactions, huntingtin protein partners could also be sequestered due to the formation of aggregates, reducing the amount of protein available within the cell.

1.2.7.1 Huntingtin protein partners

Huntingtin has been found to interact with a novel protein called huntingtin-associated protein 1 (HAP-1) (Li *et al.*, 1995). HAP-1 binds to huntingtin in a repeat-dependent manner, with longer polyglutamine stretches enhancing interaction. The expression pattern of HAP-1 shows that it is specifically expressed in neurons, and is absent from glia cells and the periphery. However, HAP-1 is not enriched within the striatum and cortex, the brain regions specifically involved in HD pathogenesis. The function of HAP-1 is unknown, however, cellular localisation studies have illustrated a pattern of distribution similar to that of huntingtin. Both proteins have been associated with synaptic vesicles within axon terminals and postsynaptic dendritic spines. An association with microtubule and dynactin P150^{Glucd}, an accessory protein for the microtubule motor, dynein, suggests a role in microtubule-dependent retrograde transport of membrane organelles (Li *et al.*, 1998c). The increased binding between mutant huntingtin and HAP-1 could therefore disrupt vesicle transport within neurons and cause cellular dysfunction through signalling deficits. On the other hand, it has been shown that HAP-1 does not bind to the huntingtin exon 1 fragment expressed in a transgenic mouse of HD, suggesting that cellular dysfunction reminiscent of HD can be produced in the absence of huntingtin and HAP-1 interactions (Bertaux *et al.*, 1998). HAP-1

knock-out mice have demonstrated a vital role for HAP-1 in postnatal feeding behaviour with homozygous mutant mice dying at day P2 (Chan *et al.*, 2002). No alterations in huntingtin or dynactin P150^{Glued} expression were detected and abnormalities in vesicle transport were not reported. Abnormal brain morphology in these animals is probably due to the significant malnutrition suffered because of the abnormal feeding behaviour. There is no significant connection between this phenotype and that of HD, suggesting that inhibition of HAP-1 by enhanced huntingtin binding may not play a significant role in HD pathogenesis.

Immunofluorescence microscopy and subcellular fractionation studies have demonstrated that huntingtin co-localises with the membranes of the trans-Golgi-network and with clathrin-coated vesicles in the cytoplasm (Velier *et al.*, 1998). Huntingtin-interacting protein 1 (HIP-1) is also enriched in the membrane-containing fractions suggesting that this protein also plays a functional role in vesicle transport *in vivo*. HIP-1, a clathrin and α -adaptin-binding protein involved in receptor-mediated endocytosis, binds to huntingtin in a repeat length-dependent manner (Wanker *et al.*, 1997). Abnormal binding between HIP-1 and huntingtin may impair the formation and/or the transport of clathrin-coated vesicles *in vivo*. HIP-1 and HAP-1 also bind to each other suggesting that a general dysfunction in vesicle transport may result from mutant huntingtin disrupting several proteins involved in this pathway (Waelter *et al.*, 2001). Although HAP-1 and HIP-1 may be involved in HD pathogenesis, both are expressed in many neuronal cells type and can not be entirely responsible for the selective pathology observed in HD.

Huntingtin also binds to the ubiquitously expressed, key glycolytic enzyme, glyceraldehyde-3-phosphate dehydrogenase (GAPDH) in a repeat dependent-manner (Burke *et al.*, 1996). The enhanced binding of mutant huntingtin to GAPDH could lead to its sequestration or inhibition and subsequent depletion of cellular energy stores. These events could contribute to the impairment of energy metabolism that has been demonstrated in HD brains (section 1.3.1.4) and suggest a possible mechanism responsible for HD pathogenesis.

SH3GL3 is a novel SH3-containing protein, which binds the exon 1 fragment of huntingtin in a repeat length-dependent manner (Sittler *et al.*, 1998). The enhanced binding of mutant huntingtin was found to promote the formation of insoluble aggregates *in vivo*. Furthermore, mutant huntingtin and SH3GL3 can be co-immunoprecipitated from human HD brain tissue (Sittler *et al.*, 1998). The selective expression pattern of SH3GL3 mirrors that of huntingtin with the highest levels found in the brain and testis (Sittler *et al.*, 1998).

PSD-95 is a scaffold protein that binds to the NMDA receptor NR2 subunit and kainate receptor GluR6 subunit (Garcia *et al.*, 1998; Kim *et al.*, 1996). The binding of PSD-95 to NMDA or kainate receptors causes the clustering of the receptors in the postsynaptic membrane and regulates

processes such as long term potentiation (LTP) (Garcia *et al.*, 1998). PSD-95 knock-out mice have severely impaired spatial learning due to alterations in NMDA-dependent long-term potentiation and depression (Migaud *et al.*, 1998). PSD-95 mediates these processes by also binding to cytoplasmic signalling proteins, linking the receptors to cellular signalling cascades (Tezuka *et al.*, 1999). Reduced PSD-95 expression inhibits NMDA receptor-mediated activation of NOS and excitotoxicity (Sattler *et al.*, 1999). Normal huntingtin binds to PSD-95 and is therefore associated with NMDA and kainite receptors (Sun *et al.*, 2001). The expanded polyglutamine within mutant huntingtin interferes with its ability to interact with PSD-95 and the expression of mutant huntingtin has been shown to cause sensitisation of NMDA receptors and promote glutamate-induced neuronal apoptosis (Sun *et al.*, 2001). These findings suggest that normal huntingtin binds to PSD-95, sequestering the scaffold protein in order to inhibit NMDA receptor activity and/or clustering. Over-expression of normal N-terminal huntingtin significantly attenuates neuronal toxicity by both NMDA receptors and the mutated huntingtin and over-expression of PSD-95 reverses this neuroprotection (Sun *et al.*, 2001). PSD-95 has been shown to mediate the neuronal toxicity induced by NMDA receptors and mutant huntingtin has been shown to disrupt this ability. Evidence to support these findings has been provided by protein lysates from human HD brains demonstrating that the expression of mutant huntingtin impairs the ability of normal huntingtin to bind PSD-95 (Sun *et al.*, 2001). This aberrant binding of mutant huntingtin to PSD-95 could be the underlying mechanism responsible for the suggested NMDA-mediated excitotoxicity associated with HD (section 1.3.1.1).

1.2.7.2 Transcriptional dysregulation and HD pathogenesis

It has been postulated that mutant huntingtin could cause neuronal dysfunction by disrupting transcription (Cha *et al.*, 1999). Many transcription factors contain polyglutamine stretches and so could be prone to interacting with mutant huntingtin. Aberrant protein binding functions of mutant huntingtin could disrupt the pattern or level of transcription in HD brains in several ways. Firstly, the elongated polyglutamine stretch could provide mutant huntingtin with the ability to directly bind to DNA. It could cause aberrant binding and inactivation of specific transcription factor proteins, thereby repressing transcription. Alternatively it could form complexes with co-repressor proteins and therefore de-repress transcription of normally silent genes. Finally it could sequester transcription factors, depleting the levels of required factors within the cells. It is still unknown whether pathological protein interactions occur in the cytoplasm or nucleus, or whether they occur during the formation of aggregates or are mediated by soluble mutant huntingtin.

An important study using a HD mouse model (R6/2) investigated alterations in gene expression, by DNA microarray, at different stages of the disease (Luthi-Carter *et al.*, 2000). Numerous changes were apparent at early stages (6 weeks) when mice showed minimal motor anomalies. The affected genes appear to be limited to several key molecular systems including neurotransmitter receptors,

intracellular signalling mechanisms, retinoic acid receptor machinery and calcium homeostasis systems. Overall, only 1.2 % of the genes examined were altered. Gene expression changes that occurred at the presymptomatic time-point were still affected at later symptomatic stages. This finding suggests that detectable alterations in gene expression occur prior to cell loss, supporting the idea that neuronal dysfunction precedes cell loss in human HD patients (section 1.1.2.4). Interestingly there was no change in the expression levels of cytoskeletal proteins, enzymes of intermediary metabolism, caspases or mitochondrial proteins, which might have been postulated from several theories of HD-associated pathogenesis. It is only at the latest time-point (12 weeks) tested, that alterations in genes relating to inflammation were noted, indicating that these changes are probably secondary to the events that initiate neuronal dysfunction. Thus, the selective pattern of pathology in HD might not be due to the level or pattern of huntingtin expression, but the individual set of genes transcribed in a particular cell-type and the importance of those that are altered by mutant huntingtin.

Recruitment of TATA-binding protein (TBP) and the transcriptional co-activator, CREB binding protein (CBP), into aggregates has been shown *in vitro* and in human HD post-mortem brains (Huang *et al.*, 1998; Kazantsev *et al.*, 1999; McCampbell and Fischbeck, 2001). CBP is also depleted from its normal nuclear location and CBP-activated gene transcription is altered within a cell culture HD model (Nucifora *et al.*, 2001). Over-expression of CBP rescued the polyglutamine-induced cytotoxicity observed in this system. In support, recent studies have demonstrated that postnatal disruption of CREB transcription factor expression, in a conditional knock-out mouse, leads to progressive neurodegeneration restricted to the dorsolateral striatum and the CA1 and dentate gyrus regions of the hippocampus (Mantamadiotis *et al.*, 2002). Mutant huntingtin could produce transcriptional dysregulation by sequestering proteasomal subunits, as the activation of NF- κ B and p53 transcription factors is dependent upon proteasomal processing (Ciechanover, 1994).

Yeast-two hybrid experiments have also shown that mutant huntingtin binds to transcriptional repressors including nuclear receptor co-repressor (N-CoR) (Boutell *et al.*, 1999). N-CoR and mSin3A proteins link specific DNA-binding proteins to proteins with histone deacetylase activity and both have shown altered immunohistochemical staining patterns in the brains of patients with HD (Boutell *et al.*, 1999). In control human brains, neurons demonstrate N-CoR and mSin3A immunoreactivity in both the nucleus and the cytoplasm. However, HD brains demonstrate N-CoR and mSin3A immunoreactivity solely in the cytoplasm, suggesting that binding of mutant huntingtin may cause redistribution of transcriptional repressors. The lack of mSin3A within the nucleus may be related to the observation that a subset of NII in HD brains displays mSin3A immunoreactivity (Boutell *et al.*, 1999). These interactions support the possibility that huntingtin

might affect cellular functioning by disrupting gene expression through abnormal protein interactions, redistribution and/or sequestration.

Sp1 is a ubiquitous transcriptional activator whose major function is recruitment of the general transcription factor TFIID to DNA. TFIID is a multi-subunit complex made up of the TBP and multiple TBP associated factors (TAFs). Yeast two hybrid studies have shown that Sp1 and TAFII130 bind to full-length huntingtin (Dunah *et al.*, 2002). Interactions between Sp1 and huntingtin are repeat length dependent and binding to the soluble form of N-terminal mutant huntingtin is tighter than to the aggregated form (Li *et al.*, 2002). TAFII130 binds equally well to normal or mutant huntingtin in the soluble form. Recently Sp1, TAFII130 and huntingtin have been shown to co-immunoprecipitate in extracts from human HD brain samples (Dunah *et al.*, 2002). Primary striatal neurons transfected with the dopamine D₂ promoter gene constructs along with mutant or normal huntingtin displayed decreased Sp1 binding to the dopamine D₂ receptor promoter in extracts expressing mutant huntingtin, compared to those expressing wild-type huntingtin. Sp1 DNA binding is reduced by ~20 % in the presence of normal huntingtin and ~70 % in the presence of mutant huntingtin. Suppression of transcriptional activity by mutant huntingtin and Sp1 interaction is not restricted to the dopamine D₂ receptor promoter, as reduced transcription from the nerve growth factor (NGF) receptor promoter has also been demonstrated (Li *et al.*, 2002). Over-expression of Sp1 and TAFII130 in cultured striatal cells reverses the transcriptional inhibition of the dopamine D₂ receptor and NGF genes caused by mutant huntingtin and protects the neurons from huntingtin-induced cellular toxicity (Dunah *et al.*, 2002; Li *et al.*, 2002). Decreased DNA binding activity of Sp1 has been reported in presymptomatic HD human brain samples (Dunah *et al.*, 2002). The resulting transcriptional inhibition is not seen when other transcription factors (e.g. MEF2C) or other TAFs (TAFII105 and TAFII150), are co-expressed with mutant huntingtin suggesting that specific transcriptional changes are mediated by mutant huntingtin. Levels of Sp1 and TAFII130 proteins are increased selectively in the caudate nucleus of HD brains, perhaps illustrating a compensatory mechanism that attempts to maintain normal transcription levels. Since TAFII130 expression appears to be specific to different regions of CNS (Metsis *et al.*, 2001) and displays a role in transcribing a specific set of genes (Albright and Tjian, 2000), the disruption of TAFII130-regulated transcription may play a role in the selective pathology in HD. A prominent feature of the genes shown to have altered transcription in a transgenic mouse model of HD is that most contain Sp1 binding sites in their promoters (Dunah *et al.*, 2002).

Brain-derived neurotrophic factor (BDNF) has an important role in the survival of striatal neurons. It is produced by cortical and nigral neurons and released onto striatal neurons by anterograde transport (Altar *et al.*, 1997). BDNF mRNA and protein are decreased in the cortex of HD patients and HD transgenic mice expressing human mutant huntingtin (Zuccato *et al.*, 2001). In transgenic

HD mice, a decrease in cortical BDNF correlated with a decrease in striatal BDNF, suggesting that the integrity of striatal cells may be compromised by a reduction in cortical BDNF. In an excitotoxic rat model of HD, BDNF prevented the death of striatal neurons (Perez-Navarro *et al.*, 2000). A reporter-gene assay has demonstrated that mutant huntingtin reduces transcription of the BDNF gene driven by 3 of its 4 promoters (Zuccato *et al.*, 2001). In addition, BDNF gene transcription is regulated by CBP (Shieh *et al.*, 1998; Tao *et al.*, 1998), which is sequestered into aggregates during HD. In cultured neurons and the brains of transgenic mice, BDNF depletion can be reversed by the over-expression of wild-type human huntingtin since this stimulates expression of BDNF mRNA (Zuccato *et al.*, 2001). The mechanism by which wild-type huntingtin reverses the reduction of BDNF transcription is not known, as wild-type huntingtin is predominantly a cytoplasmic protein. However, transcription factors can have a cytoplasmic distribution, as demonstrated by HYPB, which interacts with both wild-type and mutant huntingtin (Passani *et al.*, 2000). These findings suggest that a disruption of BDNF transcription by mutant huntingtin, perhaps through its aberrant binding to CBP or its interference with wild-type huntingtin function, causes a reduction in the levels of the vital neurotrophic factor in the corticostriatal projection neurons. This leads to insufficient trophic support for the striatal neurons, perhaps rendering them more vulnerable to insults such as excitotoxicity. It remains unknown whether the reduction in BDNF transcription is due to loss of wild-type huntingtin function, as this has not been reported in HD (Cattaneo *et al.*, 2001). As wild-type huntingtin is required for efficient vesicle trafficking, it is also possible that mutant huntingtin causes disturbances in the anterograde transport of cortical BDNF, contributing to BDNF depletion in the striatum.

1.2.8 Neurotransmitter receptor alterations in HD

One group of proteins that may be affected by transcriptional dysregulation or aberrant protein interactions with mutant huntingtin are the neurotransmitter receptors. Numerous studies have suggested that expression of neurotransmitter receptors are altered in HD and that this may play an important role in phenotypic changes and mechanisms of pathogenesis in HD.

Efficient communication between neurons and therefore normal brain functioning, is reliant on the correct expression of functional neurotransmitter receptors. Studies on human HD post-mortem tissue have indicated a progressive reduction in the levels of a number of neurotransmitter receptors within the striatum including dopamine, acetylcholine, GABA_A-benzodiazepine, glutamate, histamine, adenosine and cannabinoid receptors, suggesting that a disruption in neuronal circuitry and function occurs in HD (Dure *et al.*, 1991; Faull *et al.*, 1993; Glass *et al.*, 2000; Goodchild *et al.*, 1999; Penney and Young, 1982; Richfield *et al.*, 1991). These post-mortem studies have been supported by brain imaging studies in HD patients investigating dopamine, opioid and GABA_A-benzodiazepine receptor types (Andrews *et al.*, 1999; Ginovart *et al.*, 1997; Holthoff *et al.*, 1993; Kunig *et al.*, 2000; Pinborg *et al.*, 2001; Turjanski *et al.*, 1995; Weeks *et al.*, 1997). Severe loss of

striatal dopamine D₁ and D₂ receptor binding in HD has been demonstrated *in vivo* using positron emission tomography (PET) and single-photon emission tomography (SPET), which have revealed a 60 % reduction in dopamine receptor binding potentials in the striatum of clinically affected HD patients compared to controls (Turjanski *et al.*, 1995). Benzodiazepine receptor binding within the caudate nucleus is also reduced by 26-31 % in early HD (Holthoff *et al.*, 1993; Pinborg *et al.*, 2001). Several of these studies have also established that the extent of receptor binding loss correlates with the duration of the disease (Ginovart *et al.*, 1997; Pinborg *et al.*, 2001). The levels of reduction depends on receptor type, with striatal opioid receptor binding less severely compromised than dopamine receptor binding measurements at equivalent stages of the disease (Weeks *et al.*, 1997).

As substantial cell loss has generally occurred in HD post-mortem tissue the exact nature of neurotransmitter receptor changes is sometimes difficult to establish. However, support for early alterations in the expression of neurotransmitter receptors in HD without obvious neuropathology, has been provided by autoradiographic studies carried out on grade 0 HD brains. Significant reductions in dopamine D₂ (~60 %) and cannabinoid CB₁ receptors (~50 %) with no change in dopamine D₁ receptors, were observed within HD caudate putamen compared to control tissue (Glass *et al.*, 2000). A dramatic loss of adenosine A_{2a} receptors (~65 %) in the caudate putamen along with complete loss of adenosine A_{2a} receptors in the lateral globus pallidus was observed in grade 0 HD brains (Glass *et al.*, 2000). This observation supports the suggestion that the adenosine A_{2a} receptor-expressing MSN within the indirect pathway projecting specifically to the lateral globus pallidus, are preferentially vulnerable in HD (section 1.1.2.3). *In situ* hybridisation studies of HD brain tissue displaying no overt striatal pathology demonstrated significantly reduced levels of D₁ and D₂ dopamine receptor mRNAs and that the level continued to drop with increasing pathology (Augood *et al.*, 1997). Two factors are thought to contribute to this reduction in dopamine receptors; a reduction in the number of dopamine receptor expressing cells and/or reduced mRNA expression in the remaining cells. The abundance of dopamine D₂ mRNA in the remaining cells also reduced as the disease progressed. Although dopamine D₁ transcript levels in individual cells were also reduced with increasing pathology, at end stage HD the level of dopamine D₁ receptor mRNA in the remaining cells appears to revert back to control levels, reflecting the selective pathology and the survival of dopamine D₁ receptor expressing interneurons (Augood *et al.*, 1997).

To establish the role of receptor change in early HD pathogenesis and minimise the confounding effects of cell loss, studies utilising brain-imaging techniques on asymptomatic HD gene carriers have been carried out. Changes in dopamine receptor binding have been demonstrated in asymptomatic HD gene carriers (Andrews *et al.*, 1999; Antonini *et al.*, 1996; Lawrence *et al.*, 1998b; Weeks *et al.*, 1996). PET has demonstrated ~50 % of asymptomatic mutation carriers have

reduced striatal dopamine D₁ and D₂ receptor binding. These healthy, at risk subjects were found to have binding potentials that were 20-30 % below the population mean (Antonini *et al.*, 1996; Weeks *et al.*, 1996). Abnormalities were more commonly found in gene carriers nearer the typical age of onset for HD, rather than in younger subjects. Subtle cognitive deficits were also detected and correlated with the extent of receptor binding in asymptomatic gene carriers (Lawrence *et al.*, 1998b). These studies suggest that receptor alterations may cause changes to the functional integrity of the MSN early in the disease process.

In vivo studies have also illustrated that HD is not solely associated with dysfunction of the striatum, but alterations in signalling may occur throughout the entire brain. For example, reductions in dopamine D₁ receptor binding have been reported in the cortical regions of HD patients (Antonini *et al.*, 1996; Ginovart *et al.*, 1997). In addition, widespread reduction in opioid receptor binding within the caudate nucleus, putamen, globus pallidus, midbrain, cingulate and medial temporal cortex and increased binding in the thalamus and prefrontal areas in patients with early HD has also been demonstrated (Weeks *et al.*, 1997).

Imaging studies have indicated that it is not only receptor loss that is associated with HD. For example, a reduction in dopamine D₂ receptors in the caudate nucleus and putamen of HD brains reflecting reduced glucose metabolism in both areas, suggest cell loss within these brain regions (Kunig *et al.*, 2000). However, although a loss of benzodiazepine receptors was also observed in the caudate nucleus there was no parallel change within the putamen (Holthoff *et al.*, 1993; Kunig *et al.*, 2000). Previous post-mortem studies of GABA binding have also observed an increase in GABA_A binding in the globus pallidus, despite cell loss with increasing grades of neuropathology (Glass *et al.*, 2000; Penney and Young, 1982). These findings suggest receptor activation may compensate for cell loss in the caudate nucleus as the globus pallidus loses its primary inhibitory input i.e. the MSN. These studies illustrate that not all receptor changes are reductions and there may be active modification by the cell to compensate for HD-induced dysfunction.

Many of these changes have been confirmed in transgenic mouse models of HD (Cha *et al.*, 1998). In R6/2 transgenic mice, neurotransmitter receptors appear to be affected selectively and down-regulation of specific receptor types argues against a generalised problem with receptor production. Decreases in receptor binding reflect decreases in receptor mRNA levels, suggesting that affected receptors decrease in number, rather than changing their binding characteristics. Because receptor down-regulation occurs before the onset of symptoms or observable cell loss in this mouse model, receptor decreases do not appear to be a result of disease progression, supporting the notion that neuronal dysfunction as well as cell loss may contribute to the manifestation of HD symptoms. The fact that a single mutant gene can affect the expression of multiple neurotransmitter receptors,

increases the likelihood that mutant huntingtin acts by affecting a crucial central mechanism. One such mechanism could be transcriptional regulation as discussed in section 1.2.7.2.

1.3 Mechanisms underlying HD pathogenesis

1.3.1 Excitotoxicity

1.3.1.1 Glutamate-mediated excitotoxicity

A role for glutamate excitotoxicity has long been proposed to contribute to striatal cell death in HD (McGeer and McGeer, 1976; McGeer and McGeer, 1978). The striatum receives abundant glutamatergic excitatory input from the corticostriatal and thalamostriatal projections (Figure 1.1). Excitotoxic lesions of the striatum have been produced in animals by infusion of glutamate or ionotropic glutamate receptor agonists (Beal *et al.*, 1991; Beal *et al.*, 1986). These lesions have been found to reproduce many of the neuropathological changes seen in HD. The NMDA receptor (an ionotropic glutamate receptor) agonist, quinolinic acid, produces lesions which most closely replicate HD striatal pathology with selective loss of MSN, relative sparing of large NADPH diaphorase, somatostatin, neuropeptide Y and cholinergic interneurons and gliosis in rats (Beal, 1992a; Beal *et al.*, 1991; Beal *et al.*, 1986; Dunnett *et al.*, 1998; Figueredo-Cardenas *et al.*, 1997; Malcon *et al.*, 1997; Young *et al.*, 1988) and primates (Ferrante *et al.*, 1993). Medium spiny neurons in the striata of quinolinic acid-lesioned rats also show changes in neurite morphology and calbindin immunoreactivity that resembles those seen in HD brains (Huang *et al.*, 1995). These findings have led to the suggestion that neurodegeneration in HD may result from an NMDA receptor-mediated excitotoxic process (Beal *et al.*, 1991). Excess glutamate over-stimulation of NMDA receptors causes a toxic increase in intracellular calcium. The exact pathogenic targets for this calcium are unknown but biochemical pathways including the phospholipases, proteases, kinases and calmodulin-regulated enzymes such as NOS probably play a prominent role (Brouillet *et al.*, 1999). The initial alteration could be an influx of calcium into the mitochondrion resulting in a blockade of the respiratory chain, thus disrupting cellular metabolism (Budd and Nicholls, 1996). An alteration in metabolic stress appears to increase the potential for glutamate excitotoxicity since prior decortication can attenuate, the mitochondrial inhibitor, 3-nitropropionic acid (3-NP)-induced lesions (Beal *et al.*, 1993). Excitotoxic striatal lesions in rodents are also associated with behavioural deficits including hyperactivity but not chorea (Sanberg *et al.*, 1989). The slow progression of pathology in HD does not correspond to the complete neuronal depletion observed within hours of experimental excitotoxic lesion studies. However, prolonged intra-striatal infusion of low levels of glutamate (McBean and Roberts, 1984), or long term exposure of cultured striatal/cortical cells to low concentrations of quinolinic acid (Whetsell *et al.*, 1989) still produces the same selective pattern of cell death. In contrast, the selective vulnerability of quinolinic acid lesions is lost at higher concentrations of excitotoxin (Davies and Roberts, 1987; Malcon *et al.*,

1997) and even optimal concentrations can cause extra-striatal receptor changes and degeneration. To date, excitotoxic striatal lesions have also failed to reproduce the preferential degeneration of the striatal patch compartment and the pattern of selective degeneration of ENK MSN seen in early HD (section 1.1.2.3). Despite this, the suggestion that glutamate excitotoxicity plays a part in HD pathology has also been supported by brain imaging studies demonstrating disordered glutamate metabolism in HD patients (Taylor-Robinson *et al.*, 1996).

1.3.1.2 Glutamate receptor expression pattern on different cell-types

Excitotoxicity relies on the activation of glutamate receptors and so selective vulnerability in HD could be determined by the glutamate receptor profiles expressed by different cell-types. The neurotransmitter glutamate activates three major families of ionotropic receptors (NMDA, AMPA, kainate) and one family of metabotropic glutamate receptors (mGluR). NMDA agonists appear to produce excitotoxic lesions that most closely reflect the pathology seen in HD (Beal, 1992a; Beal *et al.*, 1991).

A direct link between mutant huntingtin and sensitivity to NMDA agonists has been illustrated by the binding of huntingtin to PSD-95, a scaffold protein that binds to the NMDA receptor NR2 and kainate receptor GluR6 subunits, inducing receptor clustering and mediating receptor signalling (section 1.2.7.1). Mutant huntingtin has been shown to disrupt this protein interaction, increasing receptor clustering and render cultured cells more sensitive to glutamate-induced apoptosis.

Native NMDA glutamate receptors exist mostly in heteromeric forms composed of NR1 and NR2 (A-D) subunits. The NR1 subunit is required for NMDA receptors to function but heteromeric expression with NR2s increase channel permeability and determine other channel properties, such as the extent of the voltage dependent Mg^{2+} block, glycine sensitivity and deactivation time (Sucher *et al.*, 1996). At the single cell level, all striatal neurons possess functioning NMDA receptors, i.e. express NR1 subunits (Ghasemzadeh *et al.*, 1996). However, there is a different pattern of NR2 subunits expressed in MSN and interneurons. Most MSN express high levels of NR2B but cholinergic interneurons tend to express less NR2B/A mRNA and protein. NADPH diaphorase, somatostatin interneurons lack the NR2B/A protein altogether and generally express receptors with subunit combinations that have a lower agonist binding affinity compared to those expressed on MSN (Chen *et al.*, 1999; Landwehrmeyer *et al.*, 1995b). This differential expression of NMDA receptor subunits may make interneurons less sensitive to over-excitation by glutamate. Supporting this idea, it has been demonstrated that cultured cells co-expressing mutant huntingtin and NMDA receptors display increased ionic flow through the NR1/NR2 NMDA receptor types, which predominate on MSN and are less abundant on interneurons (Chen *et al.*, 1999). These findings were replicated during NMDA-induced stimulation of MSN expressing mutant huntingtin (Zeron *et al.*, 2002). In addition, it has been demonstrated that MSN and cholinergic interneurons do show

different responses to glutamate receptor activation (Calabresi *et al.*, 1998). NR2B subtype-specific antagonists abolish the NMDA-induced cell death in neuronal cultures from a HD mouse model (Zeron *et al.*, 2002). Further evidence that NMDA receptors may have an important role in HD pathogenesis is the observation that NMDA receptors are selectively reduced in the striata of presymptomatic HD brains and NMDA receptor-expressing cells are preferentially lost in HD brains (Albin *et al.*, 1990; Arzberger *et al.*, 1997).

Non-NMDA glutamate receptors could also contribute to cell-selective pathology as mutant huntingtin can disrupt the number and distribution of AMPA receptors, the expression of GluR2 subunits and render AMPA receptors impermeable to Ca^{2+} in cortical cell-types (Pellegrini-Giampietro *et al.*, 1997; Weiss and Sensi, 2000). Studies using *in situ* hybridisation and immunocytochemical techniques have shown that various subtypes of mGluRs and AMPA receptors, depending on their preferred activation substances and effects, are differentially expressed in striatal neuronal populations (Calabresi *et al.*, 1999). The MSN and pyramidal cells of the striatum and cortex express high levels of GluR2/GluR3 subunits, which are absent or present at low levels on interneurons (Bernard *et al.*, 1997; Tallaksen-Greene and Albin, 1996). Differential receptor binding in the striatal compartments is also apparent with normal human striatum showing NMDA and AMPA receptor binding moderately enriched in the matrix compartment (by 17 % and 32 % respectively) but kainate binding 35 % higher in the patch (Dure *et al.*, 1992).

1.3.1.3 Dopamine-mediated toxicity

The mechanisms by which glutamate and glutamate analogues can induce excitotoxic lesions of the striatum are complicated by the action of dopamine. Dopamine acts at proximal synapses on MSN dendritic spines and regulates the action of glutamate at more distal synapses (Smith and Bolam, 1990). In addition, the existence of dopamine receptors on glutamatergic corticostriatal terminals has also been demonstrated (Calabresi *et al.*, 1996). In contrast, glutamate acting at presynaptic glutamate receptors on dopaminergic nigrostriatal neurons can regulate the release of striatal dopamine (Kulagina *et al.*, 2001; Martinez-Fong *et al.*, 1992). Dopamine levels in normal brain are higher in the dorsal striatum and become lower more ventrally, a gradient which corresponds to the pattern of the neuropathology seen in HD (Cass, 1997). Dopamine levels also appear to increase in the striatum after excitatory amino acid-induced striatal lesions (Buisson *et al.*, 1991; Chapman *et al.*, 1989). The potential for dopamine toxicity has been demonstrated in a study where excitotoxic striatal damage, induced by transient ischemia, was attenuated by lesioning the nigrostriatal pathway to reduce the striatal dopamine levels (Hashimoto *et al.*, 1994). Cell culture systems derived from HD transgenic mouse models have demonstrated that transgenic cells are far more susceptible to cell death induced by a single exposure to toxic level of dopamine (Petersen *et al.*, 2001). This cell death involves production of oxyradicals and the induction of neuronal autophagy.

It was also shown that translocation of the huntingtin fragment to the nucleus only occurs after dopamine exposure. This toxicity was not attenuated through inhibiting dopamine receptors, suggesting the toxic action is mediated through the oxidation of dopamine and the production of free radicals, causing increased oxidative stress in the neurons. This potential has been further illustrated by the finding that dopamine metabolites themselves can be neurotoxic. In rodents, dopamine is metabolised via monoamine oxidase to 3,4-dihydroxy-phenylacetaldehyde and hydrogen peroxide (Spina and Cohen, 1989). Hydrogen peroxide can react with iron or other transition metals and generate highly toxic hydroxyl radicals. Dopamine can also undergo oxidation with molecular oxygen to form radical semi-ubiquinones and superoxide radicals (Graham *et al.*, 1978). Indeed, administering antioxidants have provided neuroprotection against dopamine-induced cell death in striatal cell culture (McLaughlin *et al.*, 1998). Depletion of striatal dopamine, with either the neurotoxin 6-hydroxydopamine or inhibition of monoamine oxidase, was neuroprotective against lesions induced by 3-NP (Maragos *et al.*, 1998; Reynolds *et al.*, 1998).

These findings raise the possibility that the dense striatal dopaminergic innervation, originating from the substantia nigra, and the distribution of the dopamine receptors within the striatum may play a role in the selective pathology in HD.

Dopamine receptors modulate the responsiveness of neurons to excitatory neurotransmitters within the striatum. In the striatum, glutamate mediates fast excitatory synaptic transmission from cortical afferents through ion channels on MSN (Kita, 1996) (Kita 1996), whereas dopamine, from the substantia nigra, modulates intracellular cyclic-AMP levels by activating G-protein coupled receptors (Grandy and Civelli, 1992). One pathway by which dopamine may modulate glutamatergic input from the cortex onto MSN is through activation of the inhibitory presynaptic dopamine D₂ receptors present on cortical glutamatergic terminals. This action may reduce the excitation of striatal MSN (Hsu *et al.*, 1995). In support of this idea, dopamine D₂ receptor activation appears to reduce both NMDA and kainate-induced neuronal swelling (Cepeda *et al.*, 1998). A reduction of dopamine D₂ receptors in HD may compromise this influence on glutamate stimulation of the MSN and may lead to excess glutamate release. Preferential loss of dopamine D₂ receptors early in HD has been observed (Augood *et al.*, 1997; Glass *et al.*, 2000). In contrast, dopamine D₁ receptor agonists potentiate MSN activation by enhancing postsynaptic glutamate receptor responsiveness (Cepeda *et al.*, 1993) and could therefore enhance NMDA receptor mediated toxicity.

As membrane potential dictates the responsiveness of neurons, the modulatory effects of dopamine receptor activation may vary in different activity states. Although tolerated under normal physiological conditions, it is conceivable that endogenous levels of dopamine might potentiate cell death in neurons with bioenergetic defects or subjected to glutamate excitotoxicity. In support of

this suggestion, it has been reported that over a third of asymptomatic relatives of HD patients developed dyskinesias after being challenged with administration of the dopamine analogue, L-DOPA (Klawans, 1970).

1.3.1.4 Metabolic stress

There have been several observations indicating metabolic stress may play a role in HD. HD patients often experience chronic weight loss despite an increased fat intake and several imaging studies have demonstrated reduced glucose metabolism within the striatum, prior to any cell loss (section 1.1.2.4). Evidence of anaerobic respiration has also been provided by the observation that the lactate concentration within the striatum of HD patients is increased (Jenkins *et al.*, 1993; Koroshetz *et al.*, 1997). It is not only HD that may display selective striatal vulnerability as a result of metabolic stress. It has been demonstrated that damage to basal ganglia structures occurs in humans who attempt suicide by ingestion of cyanide or carbon monoxide inhalation, both of which block complex IV of the mitochondrial respiratory chain (Klawans *et al.*, 1982; Uitti *et al.*, 1985). In addition, mitochondrial disorders such as Leigh's disease, idiopathic dystonia and Leber's hereditary optic neuropathy, also display striatal lesions (Beal *et al.*, 1993).

The discovery that HD pathology can be mimicked in experimental animals by using mitochondrial inhibitors, has substantiated the role of metabolic stress in HD and argued for its further investigation (Beal, 1992a). Mitochondrial inhibitors such as 3-NP, aminooxyacetic acid (AOAA) and malonate have been used, all of which act to inhibit succinate dehydrogenase activity, a key component of the mitochondrial respiratory chain. Administration of both 3-NP and AOAA has been reported to induce neuronal death, which is primarily confined to the striatum (Chang and Jang, 1995; Martinou *et al.*, 1994). Systemic injection of 3-NP in rats produces selective loss of MSN in the striatum whilst sparing the dopaminergic fibres and NADPH diaphorase-positive interneurons (Beal *et al.*, 1993; Brouillet *et al.*, 1993; Guyot *et al.*, 1997; Ludolph *et al.*, 1991). Other dosing regimes have induced preferential damage to dorsal aspects of the striatum with relative sparing of NADPH-diaphorase positive interneurons (Palfi *et al.*, 1996). Ingestion of 3-NP via contaminated food can also produce selective lesions of the basal ganglia in humans (Ludolph *et al.*, 1991).

Studies have been carried out to establish if the striatal lesions induced by mitochondrial inhibitors produce deficits commonly observed in HD. Administration of 3-NP in rats and primates can induce either a hyperactive or hypoactive syndrome depending on the dosing regime (Borlongan *et al.*, 1995b; Guyot *et al.*, 1997). Both of these states could resemble HD, as the movement disorder is initially hyperactive (chorea), but progresses into a hypoactive, dystonic state. Following 3-NP treatment animals also display cognitive deficits reminiscent of fronto-striatal problems shown in HD (Borlongan *et al.*, 1995a; Palfi *et al.*, 1996). The common hypoactive symptoms produced by

3-NP are normally associated with the late stages or juvenile forms of HD and are probably the consequences of significant degeneration of MSN in both the direct and indirect pathways (Penney and Young, 1986). This suggests that the cellular toxicity of 3-NP lesions does not produce the cell-type and compartment-specific neuropathology required to model the early stages of HD.

In order to maintain normal functioning, neurons must sustain their transmembrane ion gradients by a high energy-dependent process mediated by Na^+/K^+ ATPase. Any compromise in cellular energy metabolism, and therefore the activity of this enzyme, will result in the collapse of the transmembrane gradients (Lees, 1991). This causes elevation of intracellular calcium, which is strongly implicated in the mechanisms involved in excitotoxic cell death, whether through loss of the transmembrane gradient or excessive receptor activation (Beal, 1992a; Beal, 1992b). The application of ouabain (an inhibitor of the Na^+/K^+ ATPase) on identified MSN results in an irreversible inward current with increased conductance, leading to cell deterioration (Calabresi *et al.*, 1997a; Calabresi *et al.*, 1995). A lower dose of Na^+/K^+ ATPase inhibitor dramatically increases the membrane depolarisation and inward current produced by excitatory amino acids and increases the response to repetitive cortical activation of MSN. This suggests that impairment of Na^+/K^+ ATPase will render MSN more sensitive to the action of glutamate and produce a lower threshold for excitotoxicity (Henneberry, 1989).

The ability to produce excitotoxic damage at normal concentrations of excitatory amino acids is termed 'weak excitotoxicity' (Albin and Greenamyre, 1992; Beal, 1994). Cerebellar granule cells in culture are normally resistant to the excitotoxic effects of glutamate but if deprived of glucose, these neurons become sensitive to the excitotoxic effects of glutamate acting via NMDA receptors (Henneberry, 1989). Presumably, impaired cellular energy metabolism leads to failure of the Na^+/K^+ ATPase that normally maintains the membrane potential. The following membrane depolarisation leads to a reduction in the magnesium blockage and easy activation of NMDA receptors. In summary, the process of cell death could be initiated by impairment of cellular metabolism or membrane potential but excitotoxicity would be the final common pathway leading to neuronal death.

It is possible that the differential distribution of various calcium-binding proteins could contribute to the selective vulnerability of striatal neurons. Intracellular calcium levels are normally tightly regulated by a series of calcium-binding proteins including calbindin, parvalbumin and calretinin. Calbindin is present at high concentrations within many striatal cells and comprises one of the criteria for distinguishing matrix from patch (section 1.1.2.3). The medium sized interneurons spared in HD are calbindin positive and probably account for the increased levels observed in the matrix compartment of the striatum in end-stage disease (Cicchetti and Parent, 1996). The profile of calcium-binding proteins cannot be the sole explanation for selective vulnerability since discrete

populations of both calbindin-positive and parvalbumin-positive striatal interneurons do degenerate in HD (Ferrer *et al.*, 1994). However, stimulation of NMDA receptors can lead to neurotoxic effects through mechanisms that are not directly dependent upon calcium influx, such as the activation of nitric oxide synthase (NOS) (Sato *et al.*, 1995).

Evidence has also been reported suggesting a role for the free radical nitric oxide (NO) in the striatal degeneration induced by inhibitors of mitochondrial respiration. NO is known to irreversibly inhibit mitochondrial complexes II-III and IV and succinate dehydrogenase, which could lead to further toxic impairment of metabolism and production of radical oxygen species (Bolanos *et al.*, 1997; Connop *et al.*, 1996). It has been reported that 3-NP-induced lesions in the rat striatum are accompanied by activation of nitric oxide synthase (NOS) (Nishino *et al.*, 1996). The potential toxic effects of NO production could also arise during excitotoxicity as NO formation can be induced by activation of NMDA receptors on NOS-containing neurons (Connop *et al.*, 1996). The resultant release of NO within the striatum could lead to damage of surrounding neurons, irrespective of their calcium-binding protein content. Indeed, in culture, NMDA activation-induced toxicity appears to be mediated by NO (Dawson *et al.*, 1993) and neurons from mice with deletions of the neuronal NOS gene appear to be resistant to excitotoxicity (Dawson, 1995). In addition, treatment with NOS inhibitors ameliorates several forms of excitotoxicity in animal models (Schulz *et al.*, 1995).

The selective vulnerability of striatal cells after mitochondrial inhibition may be due to the different metabolic rates of different cell-types. Cells with higher metabolic demands are probably more susceptible to toxicity (Bossi *et al.*, 1993). This notion is supported by the observation that increased metabolic demands caused by glucose deprivation produces depolarisation of MSN but hyperpolarisation of cholinergic interneurons (Calabresi *et al.*, 1997a).

Early reports of a reduction in mitochondrial complex II and IV activities in the caudate of individuals with HD first provided the clue that defects in energy metabolism may be pathologically relevant in HD (Brennan *et al.*, 1985). Mitochondrial complexes II-III and IV were later shown to have reduced activity within the striatum but not the cortex or cerebellum of HD patients (Bossi *et al.*, 1993; Brown *et al.*, 1997; Gu *et al.*, 1996; Tabrizi *et al.*, 1999). In addition, huntingtin has been shown to bind, in repeat length-dependent manner, to GAPDH, a key enzyme in energy metabolism (Guyot *et al.*, 1997). This altered protein interaction could inhibit GAPDH activity and cause depleted energy stores, contributing to deficits in energy metabolism.

1.3.1.5 Oxidative stress

Compounds such as superoxide and hydroxyl radicals, are endogenously formed, highly reactive molecules that can oxidise lipids, proteins and DNA, thereby altering neuronal structure and

function (Halliwell, 1992). The oxidative stress that results from excessive excitatory amino acid receptor stimulation or metabolic stress is a candidate for contributing to neuronal cell death in HD.

It has been demonstrated that following the administration of 3-NP and glutamate agonists there is an increased production of striatal reactive oxygen species in rats (Schulz *et al.*, 1995; Schulz *et al.*, 1996). The pathology caused can be attenuated by antioxidants (Beal, 1995; Schulz *et al.*, 1996), confirming the role of oxidative stress in mediating metabolic impairment-induced cell death.

Several pathways may be involved in the production of increased levels of reactive oxygen species and their toxicity (Coyle and Puttfarcken, 1993). For example, NMDA receptor-mediated intracellular calcium increases can activate phospholipase A2, resulting in the release of arachidonic acid (Miller *et al.*, 1992). The subsequent metabolism of arachidonic acid can produce free radicals. Elevated calcium levels can also activate calcium-dependent proteases leading to the cleavage of xanthine dehydrogenase, converting it to xanthine oxidase. The subsequent conversion of xanthine and hypoxanthine to uric acid produces superoxide radical and hydrogen peroxide (Greene and Paller, 1992; Sanhueza *et al.*, 1992). Hydrogen peroxide, especially in the presence of Fe^{2+} , decomposes to toxic hydroxyl radicals. Similarly, NMDA receptor activation can produce increased levels of free radical NO (Dawson, 1995; Sato *et al.*, 1995). Disruption of mitochondrial electron transport and subsequent energy deficiency can also lead to the increased production of toxic oxidants, including free radicals (Coyle and Puttfarcken, 1993; Schulz *et al.*, 1995). Activation of microglia in response to neurodegeneration could exacerbate the situation since they release a variety of toxins including glutamate, NO, hydrogen peroxide and superoxide (Bal-Price and Brown, 2001).

Several reports support the occurrence of increased oxidative stress in HD patients. Levels of oxidised glutathione (Sian *et al.*, 1994) and 8-hydroxydeoxy-guanosine (Browne *et al.*, 1997), which are markers of oxidative stress, are significantly increased in the striatum in HD patients. The inactivation of mitochondrial aconitase is considered an indirect indicator of reactive oxygen species production (Hausladen and Fridovich, 1994). Aconitase activity is decreased by more than 90 % in the caudate and 70 % in the putamen of HD sufferers whereas normal levels are detected in cerebellar and fibroblast tissue (Tabrizi *et al.*, 1999). It has also been suggested that the natural decline in oxidative brain metabolism and mitochondrial metabolism that occurs with increasing age could contribute to the onset age of the HD phenotype (Bossi *et al.*, 1993), supported by the observation that the severity of mitochondrial inhibitor-induced lesions increases with age (Bossi *et al.*, 1993).

1.4 Trinucleotide repeat diseases

An increasing number of human hereditary diseases are associated with the lengthening (expansion) of repeated DNA sequences (Tables 1.1 and 1.2). The repeat sequences responsible are either trinucleotide, tetranucleotide or pentanucleotide repeat units and are typically polymorphic in length within the general population. However, expansion of the repeat sequence to above a threshold number of repeat units initiates a pathogenic process.

To date, it is the trinucleotide repeat sequences that are most commonly associated with disease. This group can be divided into two general categories. Firstly, various untranslated trinucleotide repeat sequences responsible for diseases such as Fragile XA (CGG repeat), myotonic dystrophy type 1 (CTG), spinocerebellar ataxia 8 (CAG) and Friedreich's ataxia (GAA). Secondly, translated CAG repeat sequences that manifest as elongated polyglutamine stretches within the gene product and cause the polyglutamine disorders.

There are currently nine different disorders that have been associated with elongated polyglutamine stretches: Huntington's disease (HD), spinobulbar muscular atrophy (SBMA), dentatorubral pallidolusian atrophy (DRPLA) and several spinocerebellar ataxias (SCA), 1, 2, 3, 6, 7 & 17 (David *et al.*, 1996; Fujigasaki *et al.*, 2001; (HDCRG), 1993; Kawaguchi *et al.*, 1994; La Spada *et al.*, 1991; Nagafuchi *et al.*, 1994; Orr *et al.*, 1993; Sanpei *et al.*, 1996; Zhuchenko *et al.*, 1997). Polyglutamine disorders typically have a non-pathogenic repeat range of below 40 repeats and pathogenic expansions of between 36 and ~250 repeats. Most of the expanded CAG repeat tracts responsible for polyglutamine disorders reside in genes, which encode proteins of unknown function, with the exceptions of SBMA (androgen receptor), SCA 6 (α_{1A} voltage-dependent Ca^{2+} channel) and SCA 17 (TATA-binding protein).

Although the mechanism of disease pathogenesis in the polyglutamine disorders is largely unknown, several lines of evidence suggest that the repeat expansion mutations exert their toxicity through a gain-of-function mechanism. These include autosomal dominant inheritance patterns (except in SBMA), similar phenotypes of homozygous and heterozygous gene carriers and gene knockout mice lacking the appropriate disease phenotypes. The fact that the disorders share features such as late onset clinical picture, slow progression and specific patterns of pathology induced by ubiquitous mutant proteins, intergenerational anticipation and a common disease threshold-expansion length (~36 CAG repeats) suggests the common mutation type may act through similar pathogenic mechanisms.

Disease	Inheritance	Repeat on coding strand	Chromosomal location of gene	Protein	Repeat location in gene	Reference
HD	AD	CAG	4p16.3	Huntingtin	Exon 1	HDCRG 1993
SBMA	x-linked recessive	CAG	Xq11-12	Androgen receptor	Exon 1	La Spada <i>et al</i> 1991
DRPLA	AD	CAG	12p13.31	Atrophin 1	Exon 5	Koide <i>et al</i> 1994 Nagafuchi <i>et al</i> 1994
SCA1	AD	CAG	6p22-23	Ataxin 1	Exon 8	Orr <i>et al</i> 1993
SCA2	AD	CAG	12q24.1	Ataxin 2	Exon 1	Sanpei <i>et al</i> 1996 Puist <i>et al</i> 1996 Imbert <i>et al</i> 1996
SCA3/MJD	AD	CAG	14q32.1	Ataxin 3	Exon 9	Kawaguchi <i>et al</i> 1994
SCA6	AD	CAG	19p13	alpha1A voltage -dependent Ca ²⁺ channel	Exon 47	Zhuchenko <i>et al</i> 1997
SCA7	AD	CAG	3p12-13	Ataxin 7	Exon 3	David <i>et al</i> 1997
SCA17	AD	CAG/CAA	6q27	TATA binding protein	N-terminal coding region	Fujigasaki <i>et al</i> 2001 Nakamura <i>et al</i> 2001

Table 1.1 Summary of the polyglutamine disorders
 HD = Huntington's disease, SBMA = spinobulbar muscular atrophy, DRPLA = dentatorubral pallidoluysian atrophy, SCA = spinocerebellar ataxia, MJD = Machado-Joseph disease, AD = Autosomal dominant.

Disease	Inheritance	Repeat on coding strand	Chromosomal location of gene	Protein	Repeat location in gene	Reference
HDL2	AD	CTG	16q23	Junctophilin-3	Exon 2A differentially spliced	Holmes et al 2001 Stevanin et al/ 2002
DM1	AD	CTG	19q13.3	Myotonic dystrophy protein kinase	3'UTR	Brook et al/ 1992
FA	AR	GAA	9q13	Frataxin	Intron 1	Campuzano et al/ 1996
SCA8	AD	CTG	13q21	SCA8	3'UTR	Koob et al/ 1999
SCA10	AD	ATTCT	22q13	SCA10	Intron 9	Matsuura et al/ 2000
SCA12	AD	CAG	5q31-33	PPP2R2B	5'UTR	Holmes et al 1999 Holmes et al/ 2001
FRAXA	x-linked Dominant reduced penetrance	CGG	Xq27.3	FMR-1 protein	5'UTR	Fu et al/ 1991 Verkerk et al/ 1991
FRAXE	x-linked Dominant	CGG	Xq28	FMR-2 protein	5'UTR	Flynn et al/ 1993 Knight et al/ 1993
FRAXF	x-linked Dominant	CGG?	Xq28	unknown	5'UTR	Hirst et al/ 1993
DM2	AD	CCTG	3q21	Zinc finger protein 9	Intron 1	Liquori et al/ 2001

Table 1.2 Summary of triplet repeat disorders not associated with the expression of a polyglutamine tract
HDL2 = HD like-2, DM = myotonic dystrophy, FA = Friedreich's ataxia, FRAX = Fragile X, UTR = Untranslated region.

A common pathological feature observed in the polyglutamine disorders is the occurrence of NII in post-mortem brain tissue, reported in patients suffering from HD (Becher *et al.*, 1998; DiFiglia *et al.*, 1997; Gutekunst *et al.*, 1999), SCA1 (Skinner *et al.*, 1997), SCA3 (Paulson *et al.*, 1997), SCA7 (Holmberg *et al.*, 1998), SBMA (Li *et al.*, 1998b) and DRPLA (Becher *et al.*, 1998; Igarashi *et al.*, 1998), substantiating the suggestion of a common underlying mechanism of pathogenesis (Ross *et al.*, 1999).

However, each polyglutamine disorder shows a specific, characteristically distinct pattern of neurodegeneration (Ross *et al.*, 1999), suggesting that the protein context of the repeat and protein-specific interactions may also play a role in the pathology observed. Although the mutant genes responsible for the polyglutamine disorders are widely expressed in all somatic tissues (Banfi *et al.*, 1996; Doyu *et al.*, 1994; Landwehrmeyer *et al.*, 1995a; Li *et al.*, 1993; Strong *et al.*, 1993; Yazawa *et al.*, 1995) each disorder displays selective neurodegeneration. As a significant correlation between pathology and somatic repeat length is well established in the tissue-specific pathology observed in other triplet repeat diseases such as DM1 (Joseph *et al.*, 1997; Lavedan *et al.*, 1993; Monckton *et al.*, 1995), somatic mutation instability is a possible explanation for the tissue-specific pathology in polyglutamine disorders. Studies on post-mortem tissues from polyglutamine disorders have shown variable levels of somatic repeat instability (Cancel *et al.*, 1998; Chong *et al.*, 1995; Koefoed *et al.*, 1998; MacDonald *et al.*, 1993; Spiegel *et al.*, 1996; Takano *et al.*, 1996; Tanaka *et al.*, 1996; Telenius *et al.*, 1994). However, several of these studies have produced conflicting results, reporting the appearance or absence of somatic repeat instability in the same polyglutamine disorders (MacDonald *et al.*, 1993; Telenius *et al.*, 1994). The general pattern of somatic repeat instability reported (Cancel *et al.*, 1998; Chong *et al.*, 1995; Takano *et al.*, 1996) is similar to that previously reported for HD (Telenius *et al.*, 1995) but does not obviously correlate with the tissue-specific pattern of pathology. A common observation is that shorter CAG repeats are present within the cerebellum compared to other CNS tissues. In HD the cerebellar cortex is rarely involved in neuropathology and displays low levels of CAG repeat instability (Telenius *et al.*, 1995). However, the cerebellum is involved in the pathology associated with DRPLA, SCA1 and SCA3 but also displays a shorter repeat length and less repeat length variability than other areas of the brain (Cancel *et al.*, 1998; Chong *et al.*, 1995; Takano *et al.*, 1996). Moreover, regions showing the most obvious neuropathology, such as the dentate nucleus, red nucleus and cerebellar white matter in DRPLA and the spinal and bulbar motor neurons and dorsal root sensory ganglia in SBMA, do not show higher levels of CAG instability (Takano *et al.*, 1996). Although these findings do suggest similarities between the behaviour of CAG repeats in somatic tissues, the corresponding patterns do not appear to support a role for somatic repeat instability in the tissue-specific pathology of the polyglutamine disorders.

It has been suggested that genomic *cis*-acting factors may play a role in repeat instability observed in the germline (section 1.2.1). When comparing the magnitude of paternal expansion of the CAG repeat units in different polyglutamine disorders, an average increase of 9 repeat units is observed in HD (Duyao *et al.*, 1993), 4.2 repeat units in DRPLA (Koide *et al.*, 1994), 3.1 repeat units in SCA3 (Maruyama *et al.*, 1995) and 1.4 repeat units in SBMA (La Spada *et al.*, 1992; Shimada *et al.*, 1995). These findings suggest that factors other than the absolute repeat length can affect repeat instability, perhaps including the surrounding genomic sequence, which differs for each polyglutamine mutation. For example, the GC content of the DNA flanking the expanded repeats has been implicated in influencing their tendency to expand (Brock *et al.*, 1999). As CAG repeat length correlates with age of onset and clinical severity in several polyglutamine disorders, anticipation is observed (Andrew *et al.*, 1993; Doyu *et al.*, 1994; Duyao *et al.*, 1993; La Spada *et al.*, 1994). However, the differing extents of germline repeat instability means that variations in the clinical presentation are observed such as less apparent anticipation and fewer juvenile cases.

The polyglutamine disorders display similarities suggesting that the CAG repeat expansion and subsequent expression of elongated polyglutamine initiates a common sequence of pathogenic events resulting in the same cellular hallmarks of pathology (NII) and causing similar disease characteristics, i.e. inheritance patterns, tissue-specific vulnerability, late-onset symptoms. It is clear that this common mechanism of pathogenesis must be modified in some way to generate the distinct behaviour of the repeat in the germline and the unique pattern of disease-associated neurodegeneration. This modifying influence may be due to the differing genomic and protein context of each repeat sequence.

1.5 Tools for investigating HD

1.5.1 HD model systems

Investigations into HD using human post-mortem tissue are hampered by the limited availability of this tissue and the extensive neurodegeneration that occurs prior to death. To elucidate the events involved in HD pathogenesis it is essential to develop model systems to investigate the early pathological, cellular and molecular alterations caused by the HD mutation, which cannot be measured within HD patients *in vivo*. HD model systems may also provide high throughput systems to assess the efficacy of potential treatments. Generating HD models is simplified by the discovery that a single mutation is responsible for the disease ((HDCRG), 1993). The strategies undertaken to produce HD model systems generally entail either mutating the particular *HD* gene orthologue within another species or expressing a mutant version of the human *HD* gene in a transgenic system.

1.5.1.1 Mammalian cell culture

Mammalian cell culture allows investigations into the consequences of elongated polyglutamine stretches in a simple and flexible system. Many mammalian cell lines have been used to produce models of HD by stably transfecting cells with constructs expressing different sized fragments of mutant huntingtin, containing repeat tracts of differing lengths. For example, cell culture systems have been commonly used to investigate the factors involved in the formation of aggregates (Cooper *et al.*, 1998; Hackam *et al.*, 1999a; Li and Li, 1998; Ravikumar *et al.*, 2002), the potential toxicity of aggregates in HD (Carmichael *et al.*, 2000; Chun *et al.*, 2002; Kim *et al.*, 1999; Saudou *et al.*, 1998) and the cellular alterations observed due to aggregate formation (Li *et al.*, 1999a; Nucifora *et al.*, 2001). However, the investigations carried out in cell culture can be broadened to include studies into the role of receptor subunit expression in cell-selective vulnerability in HD (Zeron *et al.*, 2002) and the pathways of cell death observed in HD (Kegel *et al.*, 2000).

1.5.1.2 Bacteria

The bacterial species, *Escherichia coli* (*E.coli*) is commonly used to examine the behaviour of triplet repeat sequences and factors that influence repeat length changes. This system allows rapid investigation into the stability of repeat sequences of different lengths, different compositions and under different conditions (i.e. mutant strains of *E.coli*). Triplet repeat sequences appear to be unstable in *E.coli* (Kang *et al.*, 1995), however, they exhibit preponderance for deletions, a behaviour not replicated in organisms such as mice and humans. This repeat behaviour has made the maintenance of long triplet repeat sequences within plasmids in bacterial systems difficult. Despite these problems studies have revealed factors involved in the generation of varying repeat lengths, which have been supported by studies in other systems. Studies in *E.coli* have suggested that mechanisms such as DNA replication (Bacolla *et al.*, 1997; Bowater *et al.*, 1997; Bowater *et al.*, 1996; Kang *et al.*, 1995; Kang *et al.*, 1996; Schumacher *et al.*, 1998), methyl-directed mismatch repair (Jaworski *et al.*, 1995), transcription (Bowater *et al.*, 1997; Schumacher *et al.*, 2001) and nucleotide excision repair (Parniewski *et al.*, 1999) may contribute to triplet repeat instability.

1.5.1.3 Yeast

Yeast (mostly *Saccharomyces cerevisiae*) have also been used to analyse the behaviour of repeat tracts under different conditions. Like *E.coli*, yeast cells have failed to exhibit the dramatic and frequent expansions observed in human disease (Freudenreich *et al.*, 1997; Kang *et al.*, 1995). Indeed, long triplet repeat sequences in yeast are predisposed to undergoing origin of replication orientation-dependent expansions and frequent, large deletions (Freudenreich *et al.*, 1997; Maurer *et al.*, 1996; Miret *et al.*, 1997). An advantage of using a yeast model system is that mutant strains are widely available. Many strains affecting aspects of DNA replication, repair and recombination

have allowed investigations into their role in CAG tract stability (Freudenreich *et al.*, 1997; Jankowski *et al.*, 2000; Maurer *et al.*, 1996; Richard *et al.*, 1999; Schweitzer and Livingston, 1997).

Aberrant protein interactions that lead to transcriptional dysregulation and aggregate formation may represent an underlying mechanism for cellular disruption in HD (section 1.2.7). The yeast-two hybrid system has commonly been utilised to determine protein interactions with wild-type or mutant huntingtin. To date this use of yeast cells has revealed many huntingtin-interacting protein partners (Boutell *et al.*, 1999; Boutell *et al.*, 1998; Holbert *et al.*, 2001; Li *et al.*, 1998c; Li *et al.*, 1995; Sittler *et al.*, 1998).

1.5.1.4 Fly

The strategy of manipulating the genome to express a copy of the mutant human *HD* gene has been carried out in *Drosophila melanogaster*. The first *Drosophila* HD model expressed an N-terminal truncated mutant (75 or 150 glutamine residues) human huntingtin cDNA within the *Drosophila* eye by using the eye-specific P element expression vector pGMR (Jackson *et al.*, 1998). Cell loss within the *Drosophila* photoreceptor neurons expressing truncated huntingtin occurred in a repeat length dependent, progressive manner. It was noted that nuclear accumulation of the mutant huntingtin fragment preceded cell death; an event previously identified in cell culture models as a vital step in pathogenesis (section 1.2.6.1). In studies using other transgenic *Drosophila* lines, widespread expression of elongated polyglutamine tracts induced degeneration in many cell-types. Reduced toxicity and specificity was conferred by the addition of varying protein contexts (Marsh *et al.*, 2000). Studies suppressing aggregation and polyglutamine binding within a *Drosophila* HD model increased survival rates and decreased neuropathology (Kazantsev *et al.*, 2002). Over-expression of the chaperone heat-shock proteins Hsp40 and Hsp70 also reduced pathology in *Drosophila* expressing polyglutamine peptides (Kazemi-Esfarjani and Benzer, 2000). *Drosophila* studies have also illustrated that aberrant protein binding plays an essential role in initiating pathogenesis, suggesting that peptides designed to interfere with aberrant protein interactions may be of therapeutic benefit (Kazantsev *et al.*, 2002).

1.5.1.5 Nematode

A transgenic *Caenorhabditis elegans* (*C.elegans*) model of HD has been produced by expressing the N-terminal (171 amino acids) region of human huntingtin with polyglutamine tracts of 2, 23, 95 and ~150 residues (Faber *et al.*, 1999). To assess the effect of the polyglutamine tracts, the structure and function of sensory neurons were studied. Expression of a huntingtin fragment containing 150 glutamine residues led to progressive neuronal dysfunction. However, the co-expression of a sub-threshold level of a second toxic protein (OSM-10::GFP) in the 95

polyglutamine expressing line lead to neuronal dysfunction and in the 150 polyglutamine line resulted in progressive neuronal dysfunction leading to neurodegeneration. Under these circumstances, the huntingtin (150Q) protein forms cytoplasmic aggregates within the neurons and the number of neurons containing aggregates increases with age. Similar results were obtained by expressing the 57 N-terminal amino acids of human huntingtin with an expanded polyglutamine stretch (Q128) (Parker *et al.*, 2001). Mechanosensory defects and the appearance of cytoplasmic aggregates and morphological abnormalities in the neuronal processes indicates that cellular dysfunction in these animals does not correlate with the formation of nuclear aggregates but with aggregation and morphological changes in the axons (Parker *et al.*, 2001).

Polyglutamine stretches of the length previously responsible for producing significant phenotypic alterations in humans and mice have been shown to cause cellular dysfunction in *C.elegans*. However, cell death only occurs if challenged with additional cellular insults. Investigations of this cellular dysfunction may reveal insights into early HD pathogenesis but the short lifespan of this organism may restrict the modelling of the entire course of the disease process.

1.5.1.6 Rodents

HD rodent models have been produced by the administration of neurotoxins. It has been established that several chemicals produce selective patterns of cell death reminiscent of HD and that these result in similar phenotypic alterations (section 1.3) (Beal *et al.*, 1993; Beal *et al.*, 1991; Coyle and Schwarcz, 1976). By investigating the mechanisms governing this cell-type selective neuropathology important factors influencing the production of the selective HD-associated neuropathology may be elucidated.

A genetic HD rat model has been generated through lentiviral-mediated delivery of mutant huntingtin into the striatum (de Almeida *et al.*, 2002). Lentiviral vectors expressing the first 171, 853, 1520 amino acids of huntingtin, with either 19, 44, 66 or 82 CAG glutamines, driven by either the phosphoglycerate kinase 1 or CMV promoters were injected into the rat striatum. When constructs expressing mutant (82Q) huntingtin infected cells, NII formation occurred within one week followed by cell death associated with astrogliosis at 6 months. The cell death occurs selectively in the MSN, leaving the infected, striatal interneurons relatively untouched. Following NII formation but preceding cell death, DARPP-32, a regulator of dopamine receptor signalling, was depleted in the MSN 4 weeks after injection, suggesting neuronal dysfunction. Earlier onset and more severe pathology is observed with shorter protein fragments, longer repeats and higher expression levels. It was also shown that cells expressing longer protein fragments or lower expression levels displayed fewer NII but had a higher frequency of neuritic aggregates, suggesting a switch in the site of pathology. Injection of mutant constructs directly into the striatum has allowed quick analysis of the effects that many different mutations have on cells within the

striatum and has also demonstrated the variations produced by differing expression levels and huntingtin protein fragment sizes.

Modelling aspects of HD pathogenesis has been achieved in many different organisms ranging from bacteria to primates. The ability to replicate aspects of HD pathogenesis in a single cellular environment provides the opportunity to investigate the behaviour of CAG repeats and the possible modes of polyglutamine toxicity in simple and easily manipulated organisms. Many observations made in cellular models have been replicated in higher organisms, illustrating how these model systems can be relevant to HD research. Investigations using *Drosophila* and *C.elegans* transgenic models have allowed the consequences of the HD mutation to be determined in a more complex environment. However, it has been suggested that the late-onset, slowly progressive nature of HD pathogenesis may not be fully modelled in organisms with such short life spans. Whilst, the rodent and primate brain may provide a more appropriate environment to model HD pathogenesis, there are limitations associated with the use of these organisms due to the complexity of this environment. It is clear that all HD model systems have the potential to provide useful information concerning the mechanism of HD pathogenesis each with its own advantages and disadvantages.

1.5.2 HD mouse models

To date, it is the mouse genome that has been the most successfully manipulated to generate models of HD. Several gene-targeted and transgenic models have been produced to help elucidate the phenotypic, cellular and molecular consequences of the HD expansion mutation. In addition, mouse models can also be cross-bred with other genetically altered mice to further dissect the molecular mechanisms involved in HD (Manley *et al.*, 1999) and specific alterations within the cells of HD mouse models can be investigated using cell cultures derived from these animals (Manley *et al.*, 1998; Petersen *et al.*, 2001; Trettel *et al.*, 2000; Zeron *et al.*, 2002).

1.5.2.1 HD 'knock-out' mice

The HD mutation is widely considered to generate the pathogenesis of HD through a gain-of-function mechanism. However, the initial genetic manipulation of the mouse genome involved generating a null allele for the *HD* locus. These studies were primarily designed to help determine the wild-type function of the huntingtin protein associated with HD. In addition, these HD knock-out mice have also been used to establish if any aspects of HD pathogenesis can be attributed to a loss of protein function (section 1.2.4).

It was observed that homozygous HD knockout animals died during embryogenesis at day E8.5 (Duyao *et al.*, 1995; Nasir *et al.*, 1995; Zeitlin *et al.*, 1995). This embryonic lethality can be rescued by mutant huntingtin, suggesting that the expansion mutation does not result in a significant loss of

protein function and therefore may work through a gain-of-function mechanism (White *et al.*, 1997). However, in-depth analysis of mice that are heterozygous for the *Hdh* knock-out allele did reveal neuronal degeneration within the basal ganglia during adulthood (Nasir *et al.*, 1995; Okusky *et al.*, 1999). In addition, a conditional knock-out HD mouse, in which huntingtin is selectively depleted in the brain and testis during adult life, showed phenotypic alterations reminiscent of HD, suggesting that loss of huntingtin function could contribute, in part, to the disease process (Dragatsis *et al.*, 2000). Studies into the function of normal huntingtin have demonstrated that normal huntingtin but not mutant huntingtin possesses functions that if lost might contribute to the disease process. One such example is the involvement of huntingtin in the expression of BDNF, a trophic factor for striatal neurons (Zuccato *et al.*, 2001). Although the knock-out models have revealed an essential role for huntingtin in embryonic development and neuronal maintenance in adult life, they are not generally considered good models of the HD disease process.

Two further kinds of mouse models have been generated to model the gain-of-function mechanism suggested for the HD mutation. Firstly, transgenic mice in which the mutant gene, or part of it, is inserted randomly into the mouse genome, leading to the expression of a mutant protein in addition to normal levels of endogenous huntingtin. Secondly, knock-in mice, in which the mutation is inserted into the endogenous mouse *Hdh* gene. Typically, knock-in mice express the mutant gene under the control of its natural promoter within the appropriate genomic and protein context.

Many of the HD transgenic and knock-in mouse models display some form of cellular alteration and/or phenotypic change prior to cell death, substantiating the previous suggestions from human studies (section 1.1.2.4) that the HD mutation can produce a lengthy period of cellular dysfunction, capable of inducing phenotypic alterations, prior to cell death. Evidence from HD mouse models has also supported the observation that longer CAG repeats cause an earlier age at onset and greater severity of disease phenotype (Hodgson *et al.*, 1999; Levine *et al.*, 1999; Lin *et al.*, 2001; Mangiarini *et al.*, 1996; Wheeler *et al.*, 1999).

1.5.2.2 Transgenics mouse models of HD

Comparisons between the transgenic HD mouse models can provide information concerning the influence of the protein context of the mutation on the disease process, as several models have been generated expressing the HD mutation within a truncated (Table 1.3) (Mangiarini *et al.*, 1996; Schilling *et al.*, 1999) or full-length (Table 1.4) (Hodgson *et al.*, 1999; Reddy *et al.*, 1998) version of the human *HD* gene.

Model	Transgene Promoter/Repeat number /Expression level	Background	Lifespan	Phenotype	Cellular changes	Neuropathology	NII /neuropil aggregates
R6/2 Mangiarini <i>et al</i> 1996*	HD 144 75% ^A	CBA x C57BL/6J	10-14 wks ^B	Learning impairment (3-4 wks) Motor deficits (5-6 wks) Overt abnormalities (8 wks) Weight loss (8 wks) Diabetes	Electrophysiological changes (5 wks) Gene expression changes (4 wks) Increased oxidative damage (12-14 wks)	Delayed cell death (14 wks) No apoptosis No gliosis Brain atrophy (12 wks)	Huntingtin nuclear localisation (3.5-4.5 wks) NII (widespread) (4 wks) Neuropil aggregates (widespread) (4 wks)
N171/82Q Schilling <i>et al</i> 1999+	Mouse prion protein 82 10-20 % ^C	C3H/HEJ x C57BL/6J	24-30 wks	Motor deficits, clapping limb weakness, ataxia (12 wks) No weight gain (>8wks) Hypokinesia (>18 wks)	N/R	Progressive atrophy of striatal neurons (>4 mo) Brain atrophy (>3 mo) No gliosis	NII (widespread) (6.5 mo) Neuropil aggregates (widespread) (8 mo)
HD94 Yamamoto <i>et al</i> 2000	tet-regulated CAMKII-tTA x BitetO CMV minimal Gene off at 18 wks assessment after 16 wks	CBA x C57BL/6J	Normal	Clasping (4 wks) Overt progressive movement disorder (>20 wks) Clasping reversed to near control levels	Progressive reduction of DA D ₁ receptors (18 wks) Progressive reduction of DA D ₁ receptors halted	No cell loss ^D No TUNEL staining ^E Reactive gliosis Brain atrophy Shrunken striatum (4.5 mo)	Huntingtin nuclear localisation, NII, Neuropil aggregates (8 wks)

Table 1.3 Transgenic mouse models expressing truncated human mutant huntingtin

A. Measured using RT-PCR and compared to endogenous huntingtin levels. B. Sudden death of unknown cause. C. Measured by western blot and compared to endogenous huntingtin levels. D. Cell shrinkage or atrophy of the extracellular matrix. E. TUNEL staining detects DNA damage and may suggest apoptosis. NII = neuronal intranuclear inclusions, N/R = not reported, mo = months and Wks = weeks, representing age deficits reported. Additional references * Lione *et al.*, 1999; Carter *et al.*, 1999; Murphy *et al.*, 2000; Cha *et al.*, 1998; Luthi-Carter *et al.*, 2000. + Andreassen *et al.*, 2001.

Model	Transgene Promoter/Repeat number /Expression level	Background	Lifespan	Phenotype	Cellular changes	Neuropathology	NII /neuropil aggregates
HD48/ HD89 Reddy <i>et al</i> 1999	CMV 48F 100- 89 500% G	FVB/N	18-20 mo	Clasping (8 wks) No weight gain Hyperactive (20 wks)	N/R	Cell death and gliosis (6 mo) Prominent in striatum, also in Ctx, Hip and thalamus	NII in St, Ctx, Hip & Cb 1 % of St neurons contain NII
YAC48/ YAC72 Hodgson <i>et al</i> 1999*	HD 48 30-50 % ^H 72 (2511) 72 (2498) 200 %	FVB/N	>20 mo	Hyperkinetic movement disorder (7 mo) Obvious behavioural deficits (10 mo)	Electrophysiology alterations (6 mo) Increased sensitivity to QA and altered NMDA receptor function (6 mo)	Apoptotic striatal neurons (12 mo) Brain atrophy (12 mo) (line 2498)	St and Ctx huntingtin nuclear staining (12 mo) (widespread in line 2498) No NII

Table 1.4 Transgenic mouse models expressing full-length human mutant huntingtin

F. HD48 mice express 4 times the endogenous levels of huntingtin, which may account for extent of phenotype and pathology in mice carrying 48 repeats. G. Levels depend on line, measured by western blot and compared to endogenous huntingtin. H. Measured by western blot and compared to endogenous huntingtin levels. St = striatum, Ctx = cortex, Hip = hippocampus, Cb = cerebellum, NII = Neuronal intranuclear inclusions, QA = Quinolinic acid, N/R = not reported, mo = months and wks = weeks, representing time deficits reported. Additional references * Cepeda *et al.*, 2001; Zeron *et al.*, 2002.

The R6 mice are a well characterised transgenic HD mouse model (Mangiarini *et al.*, 1996). They were generated by random insertion of a ~1 kb fragment encompassing the 5' UTR sequences, exon 1 containing an expanded CAG repeat of ~130 units and the first 262 bp of intron 1 of the human *HD* gene and express an N-terminal fragment of human mutant huntingtin. Several lines were generated carrying transgenes with different length repeat tracts on a hybrid genetic background. The most frequently used line is the R6/2 line and carries a construct that originally contained ~144 CAG repeat units and expresses the mutant protein at ~75 % of the endogenous huntingtin level.

Another transgenic model expresses an N-terminal truncated human huntingtin cDNA encoding 82 glutamine residues and the first 171 amino acids of the huntingtin protein (N171-82Q) (Schilling *et al.*, 1999). Transgene expression in these mice is directed by the mouse prion protein promotor, which typically drives the expression of foreign genes in virtually every CNS neuron. Levels of mutant HD-N171 polypeptide appear to be lower than endogenous full-length huntingtin protein (~10-20 %).

Transgenic mice expressing full-length mutant huntingtin protein carry 2-22 copies of a construct containing the entire human huntingtin cDNA with different repeat lengths (16, 48, 89), under the control of the CMV promoter (Reddy *et al.*, 1998). Further lines of transgenic mice expressing the HD mutation within the context of the full-length huntingtin protein have been generated using a yeast artificial chromosome (YAC) containing human genomic DNA spanning the full-length *HD* gene. This sequence is thought to include all HD regulatory elements, including the endogenous human promoter and has been manipulated to contain 18, 42 and 72 CAG repeats (Hodgson *et al.*, 1999). Although, one line of YAC72 (2498) mice expressed mutant huntingtin at twice the endogenous level of normal huntingtin, the other lines (YAC18, YAC46 and YAC72 (2511)) expressed mutant huntingtin at 30-50 % of endogenous huntingtin levels.

Investigations of these HD transgenic mice have demonstrated that animals expressing truncated forms of mutant human huntingtin display the earliest and most severe phenotype. Despite this severe phenotype none of these animals display any significant cell death until late in life. Conversely, mice expressing full-length human huntingtin express phenotypes that are less severe and progress more slowly. In addition, neuropathological observations indicate that the expression of a truncated form of mutant huntingtin protein produces early nuclear staining and subsequently high numbers of NII and neuropil aggregates, with a distribution pattern that does not correlate well with patterns of selective pathology in HD. These findings indicate that cells containing aggregates can continue for long periods of time without experiencing cell death. Conversely, in transgenic models expressing full-length mutant huntingtin specific patterns of striatal cell loss are accompanied by rare NII formation suggesting that the aggregates may not necessarily induce cell

death. Indeed, even in animals that over-express full-length mutant huntingtin (Reddy *et al* 1999, line HD48) low levels of NII formation are observed.

If proteolysis of the mutant huntingtin protein and subsequent translocation of the cleaved peptide to the nucleus are vital steps in HD pathogenesis (section 1.2.6.1) then the severe phenotype exhibited in transgenic mice expressing a truncated form of mutant huntingtin may be due to the by-passing of the proteolytic processing step required early in the disease process. The large influx of truncated mutant huntingtin may explain the high levels of aggregate formation in animals expressing truncated forms of the protein. The widespread distribution of aggregates in these animals may also indicate that a cell-specific mechanism may be involved in the processing of mutant huntingtin and that striatal specific neurodegeneration may only occur in animals expressing full-length mutant huntingtin.

Comparison of the HD mouse models has also indicated that levels of transgene expression can influence the disease process. The R6/1 line differs from the R6/2 line in that it carries a slightly shorter repeat expansion (115 repeats) and its transgene is expressed at 10-20 % of endogenous levels (compared to 75 % in the R6/2 line). The R6/1 animals display a more slowly evolving neurological phenotype (Mangiarini *et al.*, 1996) and protein aggregation late in the disease course (Davies *et al.*, 1997). The other transgenic mouse model expressing a truncated fragment of huntingtin at 10-20 % of normal levels, also displays a protracted disease course (Schilling *et al.*, 1999). The YAC72 (2498) mouse line expresses 4 times the amount of full-length mutant huntingtin expressed by line YAC72 (2511) mice. Whilst both lines display phenotypic alterations only YAC72 (2498) mice display brain atrophy and widespread nuclear huntingtin immunostaining at 12 months of age. At the same age YAC72 (2511) mice display nuclear huntingtin immunostaining, but specifically within striatal MSN and cortical neurons.

Recently a conditional transgenic mouse model of HD has been created, taking advantage of the tetracycline-responsive gene system (Yamamoto *et al.*, 2000). In this system, the expression of a transgene is turned off by oral administration of tetracycline analogues. This is possible because the tetracycline-regulated transactivator (tTA) protein induces transcription of the transgene when it specifically binds to the tetO operator (tetO). However, tetracycline can bind to tTA, preventing its interaction with tetO and consequently switching off transcription of the transgene. Mice carrying a transgene containing a chimeric HD mouse/human exon 1 with a CAG repeat expansion of 94 repeats under the control of a minimal CMV promoter and a tetO response promoter, were produced (BiTetO mice). Mice that carry a transgene encoding the tTA transactivator under the control of a calcium/calmodulin kinase II α promoter, were also generated (CamKii α -tTA mice). When these mouse lines were crossed, progeny expressing both transgenes were under-represented because of perinatal lethality. It was postulated that this was due to the expression of the

polyglutamine and to ensure that the expression of polyglutamine did not interfere with development, transcription of the transgene was switched off by administering doxycycline (an analogue of tetracycline) to the pregnant mothers. Administration of the doxycycline was withdrawn after birth and transgene expression switched on. Mutant huntingtin expression was seen in the striatum, septum, cortex, and hippocampus and to a lesser extent the amygdala and hypothalamus but no expression was detected within the cerebellum. The animals displayed a clasping phenotype, which began at 4 weeks and progressed throughout life until death after a normal life span. Immunoreactivity for the polyglutamine stretch was observed in the nuclei of the majority of striatal cells. Both NII and neuropil aggregates were found within the striatum and cortex. At 4.5 months general brain atrophy was displayed with a further decrease in striatal size along with reactive gliosis and reduction in dopamine D₁ receptor levels. There was no TUNEL staining and no reduction in cell number observed, suggesting brain atrophy may result from shrinkage of the cells or extracellular matrix.

Once the phenotypic and cellular alterations produced by the expression of the mutant huntingtin fragment had been established transcription of the transgene was switched off in order to determine if the phenotypic and pathological alterations in the HD mice were irreversible or required the continued expression of the transgene.

Doxycycline treatment was commenced at 18 weeks to completely abolish the expression of the mutant polyglutamine-containing huntingtin peptide for a 16 week period. Limb clasping and the NII and neuropil aggregates were all apparent at this time. At 18 weeks, 40 % of striatal neurons had nuclear huntingtin immuno-staining. In the 'gene-off' animals only 1 % of striatal neurons had nuclear staining at 34 weeks in contrast to the 60 % observed in gene-on animals of this age. Both NII and neuropil aggregates disappeared from the striatum in gene-off animals at 34 weeks of age. The reduction in striatal size, astrogliosis and reduction in dopamine D₁ receptor levels all continued in gene-on mice but halted in gene-off animals. Gene-off animals also demonstrated a recovery of the clasping phenotype to levels approaching controls.

These studies indicate that neurons can disperse NII and cytoplasmic aggregates, suggesting that the proteasome is capable of accessing the NII and the proteolytic pathways needed to clear aggregated material are not irreversibly compromised, even in animals displaying cellular dysfunction and phenotypic alterations. They also demonstrate that the continuous expression of mutant huntingtin is required for the progression of pathology.

1.5.2.3 HD 'knock-in' mice

Knock-in mouse models allow the study of the behavioural and functional consequences of the HD expansion mutation in its appropriate genomic and protein context. Although, knock-in HD mice tend to display a subtler phenotype than some of the transgenic HD models, studies have revealed subtle changes that are reminiscent of clinical HD (Lin *et al.*, 2001; Shelbourne *et al.*, 1999; Wheeler *et al.*, 1999). Knock-in mice have been generated by two different strategies. One results in wild-type and mutant *Hdh* alleles that differ only in the length of the repeat sequence (Lin *et al.*, 2001; Shelbourne *et al.*, 1999). The second generates a chimeric mouse/human sequence within exon 1 of the mutant *Hdh* allele (Ishiguro *et al.*, 2001; Levine *et al.*, 1999; Wheeler *et al.*, 1999).

A consistent feature of most HD knock-in mice is the presence of nuclear staining and micro-aggregates of huntingtin in the brain. These appear between 2-6 months of age, relatively early in the course of the disease (Ishiguro *et al.*, 2001; Levine *et al.*, 1999; Li *et al.*, 2000; Wheeler *et al.*, 1999). In contrast, NII are only observed when the mice are older (>10 months) (Ishiguro *et al.*, 2001; Levine *et al.*, 1999; Li *et al.*, 2000; Wheeler *et al.*, 1999). No significant cell death is observed in knock-in HD mouse models however, most display reactive gliosis within the striatum late in life (Ishiguro *et al.*, 2001; Lin *et al.*, 2001; Wheeler *et al.*, 1999; Wheeler *et al.*, 2002). Knock-in mice, including those with no dramatic phenotypic alterations, exhibit altered gene expression, changes in membrane properties and increased sensitivity to glutamate receptor agonists, all suggesting that these animals may be modelling early time points in HD pathogenesis (Levine *et al.*, 1999; Shelbourne *et al.*, 1999). It is possible that HD mutations expressed at the appropriate level, within the correct genomic and protein context are only capable of modelling the early stages of the disease process within the ~2 year life span of this organism. However, this situation has benefits in studies designed to determine the initial events responsible for triggering HD pathogenesis.

Model	Transgene Promoter/Repeat number /Expression levels	Background	Lifespan	Phenotype	Cellular changes	Neuropathology	NII /neuropil aggregates
Hdh71/ Hdh94 Levine et al 1999*	Hdh 71 ~100 % ⁱ 94	129Sv x C57BL/6J	Normal	N/R	Neuronal resting membrane potential depolarised (3 mo) Gene expression changes (4 mo)(Hdh94 only) Sensitivity to NMDA receptor agonist (3 mo)	No cell loss No gliosis (8 mo)	Huntingtin nuclear staining and microaggregates (>6 mo) (Hdh94)
Hdh80/ Hdh150 Lin et al 2000	Hdh 80 ~100 % ⁱ 150	129/Ola x C57BL/6J	> 1 years	Inactivity, Clasping, Motor deficits, Seizures, Abnormal gait (40 wks) (Hdh150). Reduced body weight (Hdh80 & Hdh150) (>25 wks)	N/R	No cell loss or gliosis (>90 wks) (Hdh80) No cell loss, St gliosis (Hdh150) (>52 wks)	Rare NII (<90 wks) (Hdh80) St NII but no neuropil aggregates (Hdh150) (>40 wks) Huntingtin nuclear staining (31 wks) (Hdh150)
Hdh77 Ishiguro et al 2001	Hdh 77 N/R	C57BL/6J x ICR	Normal	N/R	N/R	No cell loss No TUNEL staining Reactive gliosis St, GP & SN (10 mo)	Huntingtin nuclear staining (17 mo) No NII
HdhQ92/Hdh+ HdhQ111/Hdh+ Wheeler et al 1999+	Hdh 90 N/R 109	CD1 x 129Sv	Normal	Gait abnormality (24 mo)	N/R	Cell loss (24 mo) No TUNEL staining Reactive gliosis (24 mo) (HdhQ111)	St huntingtin nuclear staining (6 wks) (HdhQ111) (2.5 mo) (HdhQ92) St NII (10 mo) (HdhQ111) (12 mo)(HdhQ92) St neuropil aggregates (17 mo) (HdhQ111)
Hdh6/Q72 Hdh4/Q80 Shelbourne et al 1999**	Hdh 72 ~45 % ⁱ 80 ~55% ⁱ	FVBN DBA/2 C57BL/6J	Normal	Hyper-aggressive (3 mo)	Electrophysiological changes (8-14 mo)	No cell loss No gliosis St neuron axonal degeneration (>17 mo)	St huntingtin nuclear staining (4 mo) Nuclear micro- aggregate (>11 mo) St NII (>20 mo) St neuropil aggregates (>7 mo)

Table 1.5 Knock-in HD mouse models

i. Levels of mutant huntingtin compared to levels of huntingtin in wild-type mice. j. Levels of mutant huntingtin expressed as % of total huntingtin. St = striatum, GP = globus pallidus, SN = substantia nigra, NII = Neuronal intranuclear inclusions. Additional references * Menalled *et al.*, 2000. + Wheller *et al.*, 2000; Wheller *et al.*, 2002.

** Li *et al.*, 2001; Usdin *et al.*, 1999; Li *et al.*, 2001.

1.5.3 Knock-in HD mouse model *Hdh6/Q72* and *Hdh4/Q80*

The work presented in this thesis was carried out on an HD knock-in mouse model designated *Hdh6/Q72* and *Hdh4/Q80* (Shelbourne *et al.*, 1999). A brief summary of their generation and preliminary characterisation follows.

1.5.3.1 Generation of *Hdh6/Q72* and *Hdh4/Q80*

This mouse model was generated using a gene targeting strategy to modify the *Hdh* allele by homologous recombination in mouse embryonic stem (ES) cells. A targeting vector was produced that contained part of the *Hdh* gene but with the normal polyglutamine-encoding sequence within exon 1 replaced with a 72 or 80 CAG repeat tract. A neomycin resistance expression cassette (*loxPneo*) flanked by 34 bp *loxP* sites was also inserted ~200 bp downstream of the CAG mutation and 60 bp into intron 1. Although correctly targeted ES cell lines carrying the CAG mutation were identified, they did not express full-length mutant huntingtin protein until Cre-mediated deletion of the *loxPneo* sequences within the modified *Hdh* locus had occurred. Recombinant ES cell lines were used to generate mouse lines carrying the modified *Hdh* allele with the CAG expansion and the *loxPneo* sequences. Heterozygous mutant males were then crossed with Cre-expressing females to facilitate *in vivo* deletion of the *loxPneo* sequences in developing embryos. The resultant founder animals of two successful lines were designated *Hdh4/Q80* and *Hdh6/Q72* and bred to establish the HD knock-in mouse lines used in this study.

Western blotting confirmed the expression of full-length mutant huntingtin protein in several tissues and that the mutant form of the protein contained an elongated polyglutamine stretch. Optical densitometry of the immunoblots indicated that the mutant protein in heterozygous animals was expressed at ~ 45 % (*Hdh6/Q72*) and ~ 55 % (*Hdh4/Q80*) of wild-type levels. Reduced levels of mutant huntingtin expression have been suggested by studies on human HD tissue (Persichetti *et al.*, 1996; Trottier *et al.*, 1995). However, the modified mutant *Hdh* allele does contain a single 34 bp *loxP* sequence within intron 1 and it remains a formal possibility that this could exert a residual influence on the expression of the mutant *Hdh* gene.

1.5.3.2 Neuropathological studies of the HD mice

Brain atrophy (10-15 % smaller than wild-type) from 4 months of age was present although no other obvious gross abnormalities were observed. Brains from 4-6 and 16-17 month old mice exhibited no gliosis, ventricular enlargement or neuronal loss in any brain area. The neuronal-specific degeneration in HD was investigated by examining the immunoreactivity of leucine-enkephalin and substance P (markers of the striatal projection neurons), calbindin (marker of the matrix compartment), NADPH-diaphorase (NOS expressing interneuron marker) and cytochrome

oxidase activity, reflecting neuronal activity. No differences were detected in HD knock-in mice and wild-type littermates.

1.5.3.3 Nuclear and cytoplasmic aggregates in the HD mice

The formation of nuclear aggregates (NII) has been detected in the striatum of 27 month old HD mice (Li *et al.*, 2000). Double labelling experiments using calbindin-D and the EM48 antibody, which detects long polyglutamine stretches suggested that almost all neurons containing NII were MSN. Labelling studies detecting NOS and parvalbumin within the interneurons showed no co-localisation with NII. Nuclear immuno-staining of mutant huntingtin occurs in the striatum as early as 4 months of age, increasing in intensity until 11 months, when small puncta can be seen. By 21-27 months many neuronal nuclei contain a single, large aggregate. The striatum also contains neuropil aggregates which appear later than NII, from ~11 months of age. Using antibodies raised against different epitopes of mutant huntingtin, it was established that the NII and neuropil aggregates were made up of huntingtin fragments smaller than the first N-terminal 549 amino acids. The neuropil aggregates reside in the processes and axonal terminals of the MSN within the lateral globus pallidus and the substantia nigra pars reticulata. These neuropil aggregates have been associated with degenerating MSN axons containing dark, swollen organelles that resemble degenerated mitochondria (Li *et al.*, 2001).

1.5.3.4 Phenotypic features of the HD mice

General observations suggest that the HD mice displayed heightened aggressive behaviour from about 3 months of age. This was confirmed using the resident-intruder test, which demonstrated an increased incidence of isolation-induced aggression in a HD mouse cohort of 9 months of age (Shelbourne *et al.*, 1999). This abnormal social behaviour appears to occur in the absence of overt neurodegeneration and prior to aggregate formation. These findings have led to the conclusion that this model, as well as other knock-in HD mice, may be modelling features of early HD pathogenesis and that neuronal dysfunction, rather than cell death may be responsible for some of the clinical features of HD.

1.5.3.5 Synaptic dysfunction in the HD mice

Synaptic function has been examined by the input-output relationship of Schaffer collateral-CA1 synapses, in response to single electrical stimuli (Usdin *et al.*, 1999). Differences in synaptic density or altered strength of individual synapses within the population would cause input-output variation. No difference between 8-14 month old HD and wild-type mice was observed, indicating the correct density of functioning synapses within the hippocampus of HD mice.

LTP, a synaptic mechanism that is thought to be involved in some forms of learning and memory, is an increase in synaptic strength induced by a high-frequency stimulus. HD mice showed significantly less potentiation than their wild-type littermates. The threshold stimulation needed to induce LTP seemed to be raised in HD mice. Post-tetanic potentiation (PTP) immediately following stimulation was impaired in mutant mice after both standard and enhanced stimulation. PTP arises from changes within the presynaptic terminal, indicating the possibility of altered presynaptic function in HD mice. Paired pulse facilitation (PPF) occurs if two stimuli are delivered to synapses in rapid succession and the synaptic response to the second stimulus is facilitated by the cumulative calcium influx into the presynaptic terminal. A depression of PPF is observed in the HD mice, particularly after longer inter-pulse intervals. The observed decrease could be due to a reduced capacity for facilitation itself or an increase in synaptic inhibition. However, as HD and wild-type mice need the same stimulation to generate a postsynaptic action potential, an increase in synaptic inhibition appears less likely. The impairment of both PPF and PTP suggest that presynaptic terminals in HD mice can respond to normal single stimuli but are unable to sustain neurotransmitter release with repetitive stimulation. These studies indicate that the HD mutation results in an impaired ability of excitatory synapses to respond fully to activation rates as low as 1 Hz, which is well within the range of normal physiological synaptic activation. As huntingtin protein is normally present within synapses and surrounding vesicles, a dysfunction in presynaptic activity may be due to deficits in vesicle release or recycling mediated by mutant huntingtin. If this was the case then diminished neurotransmitter release and therefore weaker LTP induction, PPF and PTP may result. This notion is supported by studies that have shown a reduction in the amount of glutamate released from hippocampal synapses during high frequency activation in these HD mice (Usdin *et al.*, 1999).

1.5.3.6 Intergenerational mutation length variability in the HD mice

Intercrossing of heterozygous HD mice produced progeny genotypes that showed no obvious deviation from the expected Mendelian ratio (Shelbourne *et al.*, 1999). Further backcrossing of heterozygous HD mice was carried out and the intergenerational stability of the CAG repeat mutation was investigated. The germline mutation rate in both males and females was ~25 %, lower than that (70-85 %) described in human HD (Duyao *et al.*, 1993; Kremer *et al.*, 1995; Leeflang *et al.*, 1995). However, there was a strong sex-of-origin effect observed, mirroring that described in human HD (Myers *et al.*, 1993; Telenius *et al.*, 1994; Zuhlke *et al.*, 1993). Transmission of the mutation through the female germline tended to be associated with small contractions of up to four repeats in length. In contrast, only increases in the repeat length were observed during transmission of the mutation through the male germline. Most of the repeat expansions were 1-4 repeats in length with the largest observed exhibiting an increase of 8 repeats.

1.6 Mechanisms underlying trinucleotide repeat instability

Repeat instability within the germline is responsible for clinical anticipation of the disease phenotype in HD families and within somatic tissues can further contribute to the onset and progression of disease pathogenesis. By determining the mechanisms, which underlie repeat instability, it may be possible to manipulate these processes and therefore alter pathogenesis. Studies into triplet repeat sequences (TRS) suggest that they are more prone to forming secondary structures than random DNA sequence and that these formations may play a central role in repeat instability. These structures may disrupt DNA processes, such as replication or transcription and may even be generated due to the unwinding of the DNA helix associated with these events. It has also been established that these structures can act as activating substrates for DNA repair mechanisms. It has been suggested that repair can either prevent repeat size changes or increase the likelihood that they will occur, depending on the length of the TRS (Sinden and Wells, 1992). Several DNA repair pathways have been implicated in generating triplet repeat instability. These include nucleotide excision repair (NER), mismatch repair (MMR) and recombinational mechanisms. Many studies have been carried out to investigate the occurrence of secondary structures in TRS and the mechanisms by which DNA repeat instability can occur.

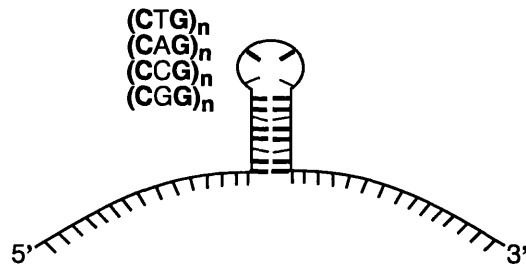
1.6.1 Alternative DNA structures within TRS

Several *in vitro* studies have illustrated that repetitive sequences within DNA can form many different thermodynamically stable secondary structures such as hairpins, slipped DNA structures, triplexes, and quadruplexes (Gacy *et al.*, 1995; Kang *et al.*, 1995; Pearson and Sinden, 1996; Sinden and Wells, 1992; Wells, 1996) (Figure 1.3). The type and stability of the structures appear to vary depending on the base composition of the repeat units (Gacy *et al.*, 1995; Sinden, 1999), perhaps influencing the differential patterns of repeat instability displayed by various TRS. Biochemical and genetic analyses have also indicated the formation of hairpin structures within (CTG.CAG) repeats in bacteria (Sarkar *et al.*, 1998) and yeast (Moore *et al.*, 1999).

The instability of a triplet repeat stretch is proportional to its length, with longer repeat stretches more prone to alterations (Leefflang *et al.*, 1999). The length of the TRS is also proportional to the likelihood of alternative structure formation, suggesting these structures may play a role in generating repeat instability (Pearson and Sinden, 1998; Wells, 1996). In addition, it has been shown that interruptions within TRS decrease their propensity to form alternative DNA structures (Pearson and Sinden, 1998; Sinden, 1999) and to expand (section 1.2.1).

It has been shown that TRS can form alternative structures and that this characteristic may mediate their propensity for instability. However, the mechanisms by which these structures may contribute to repeat lengths changes remain uncertain.

A.



B.

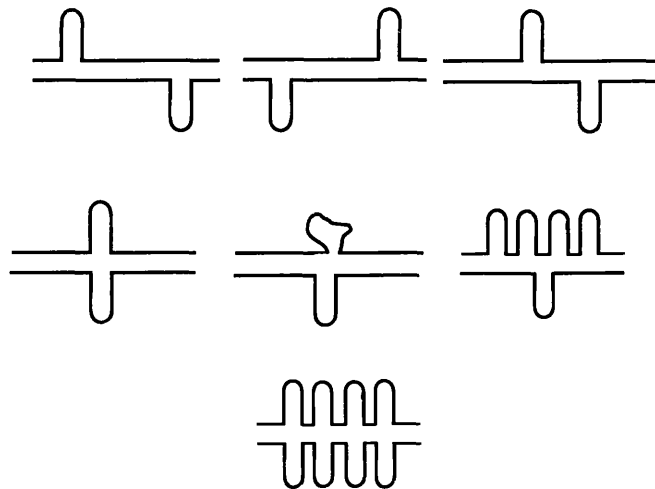


Figure 1.3 Alternative DNA structures that form in $(CTG.CAG)_n$ repeat sequences

A. Hairpin structures can form within $(CTG)_n$, $(CAG)_n$, $(CGG)_n$ and $(CCG)_n$ repeat sequences. In the hairpin two stable CG base pair bonds are followed by a T.T, A.A, C.C or G.G mispair. These hairpins have varying degrees of thermal stability. Figure modified from Sinden, 1999.
B. Due to the repetitive nature of triplet repeat sequences a variety of slipped strand structures could form with varying positions and sizes. Figure modified from Pearson and Sinden, 1996.

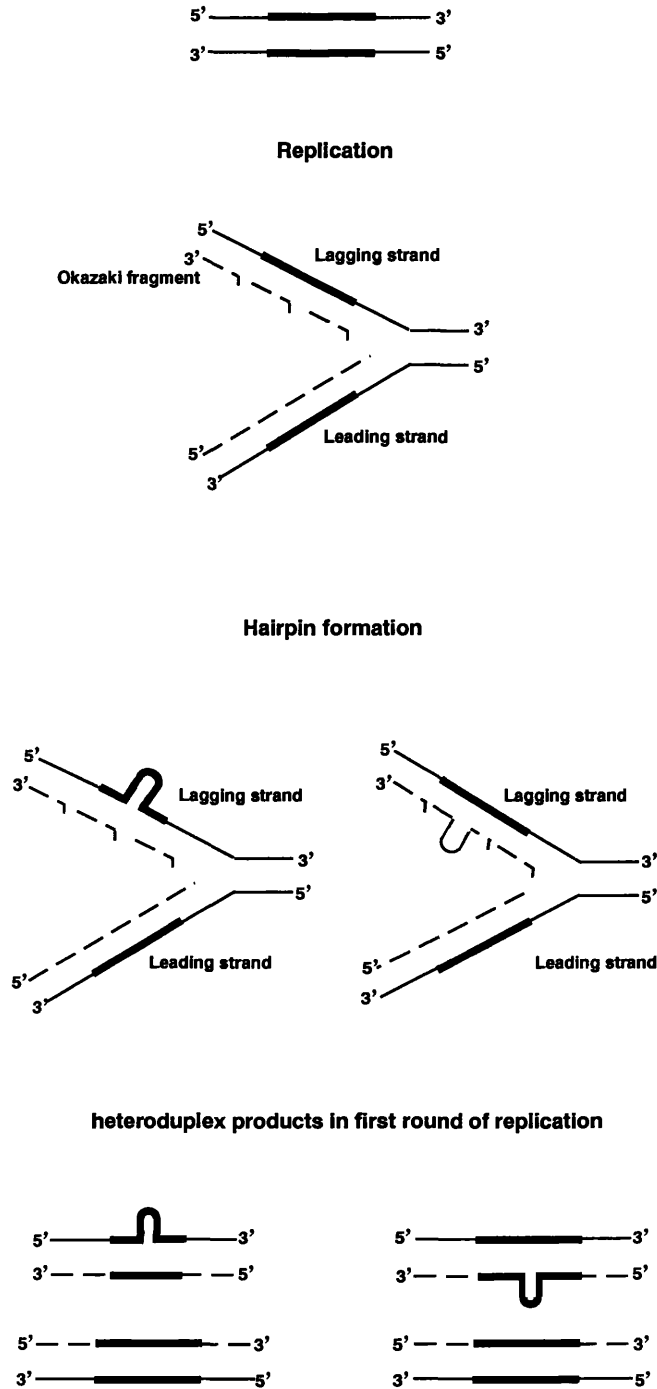
1.6.2 Replication through TRS

Studies have confirmed that alternative structures within triplet repeat sequences can influence the fidelity of DNA polymerases *in vitro* (Kang *et al.*, 1995; Ohshima *et al.*, 1996) and *in vivo* (Samadashwily *et al.*, 1997) suggesting increased disruption of replication through TRS. It has been proposed that during replication of long TRS it is easier for the newly synthesised and template DNA strands to become misaligned when DNA enzymes pause and separate from the template. Enzyme pausing may be mediated by the replication fork meeting an alternative DNA structure within the TRS. This misalignment (replication slippage) can itself cause hairpin loop formation and would cause deletions or expansions in the sequence once the replication machinery has reformed (Pearson and Sinden, 1998; Wells, 1996) (Figure 1.4).

Several studies have reported findings supportive of the replication slippage mechanism. Studies with (CTG.CAG) repeats have demonstrated that stalling of the DNA polymerase promotes hairpin formation and primer realignment within the repeat sequence (Ohshima and Wells, 1997). *In vitro* analysis of DNA synthesis using a single-stranded template of CAG repeats, also demonstrated that human DNA polymerase β and T7 DNA polymerase both introduce frequent deletions into the TRS (Kroutil and Kunkel, 1999). Indeed, *in vitro* studies have indicated that slippage-generated expansions occur during DNA synthesis in (CTG.CAG) and (GGC.CCG) TRS with several different DNA polymerases (Ji *et al.*, 1996; Petruska *et al.*, 1998). Deletions in (CTG.CAG) repeat sequences were dramatically reduced when bacteria were grown at slower rates (Bowater *et al.*, 1996), perhaps due to the slowing of replication fork progression.

Furthermore, mutations in proteins involved in DNA replication such as the DNA polymerase proofreading proteins within *E.coli*, also affect repeat instability (Iyer *et al.*, 2000). Mutant strains that result in destabilising of the replication fork have also been shown to produce substantial deletions in the (CTG.CAG) tract, perhaps due to the increased opportunity to generate slipped structures (Iyer *et al.*, 2000).

Many studies have now established that the process of replication through a TRS can mediate changes in repeat length. However, further studies have demonstrated several factors, which play a role in determining the bias toward expansions or deletions.



Second round of replication to produce unchanged alleles, deleted alleles and expanded alleles

Figure 1.4 Replication slippage model of repeat instability

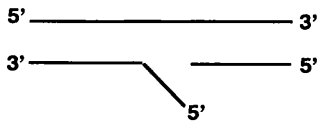
A representation of replication through triplet repeat DNA sequence. During replication hairpins form when the DNA helix unwinds either on the template or nascent strand. If the structures form on the template strand they result in deletions and if they occur on the nascent strand a expansion is generated. Hairpin formation can occur on either the lagging strand or the leading strand, however, is more likely on the lagging strand due to the increased proportion of single stranded DNA. In addition, CTG sequences form more stable hairpin structures than those with CAG repeat units. (————) template DNA. (-----) nascent DNA. (————) repeat sequence.

The orientation of the repeat sequences, with respect to the direction of replication, has been shown to affect the stability of TRS. This effect has been observed in plasmids within *E.coli* (Bowater *et al.*, 1996; Kang *et al.*, 1995) and in chromosomal locations in *Saccharomyces cerevisiae* (Balakumaran *et al.*, 2000; Freudenreich *et al.*, 1997; Maurer *et al.*, 1996). For example, studies in yeast and bacteria have shown that hairpin formation is favoured on the lagging strand since a greater proportion of it is single-stranded during replication. It has been suggested that repeat expansions and deletions occur when an alternative DNA structure, such as a hairpin, occurs within the newly synthesised DNA strand or on the template DNA, respectively (Figure 1.4). In addition, CTG sequences are thought to form more stable hairpin structures than CAG sequences. If this is the case, more hairpins may occur on a lagging strand template comprising of CTG repeats thereby leading to deletions (Gacy *et al.*, 1995; Pearson and Sinden, 1996). When the lagging strand template is made up of CAG repeats the probability of a hairpin is lower and deletions are less likely. However, stable CTG hairpins could still form on the leading strand template and cause a deletion or alternatively a CTG hairpin could form on the nascent lagging strand and result in an expansion.

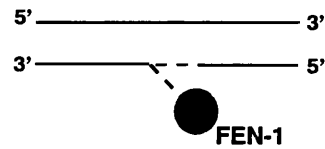
One mechanism that could enhance the formation of structures on the lagging strand is the processing of the Okazaki fragments. Rad27 is the yeast homologue of the mammalian protein FEN-1; a flap endonuclease that processes Okazaki fragments during replication (Hosfield *et al.*, 1998). *Rad27* mutant yeast strains display an increased frequency of TRS changes and although length changes in wild-type yeast are predominantly deletions, approximately half of all changes seen in *Rad27* mutant were expansions in (CTG.CAG) (Freudenreich *et al.*, 1998; Schweitzer and Livingston, 1998) and (CGG.CCG) sequences (White *et al.*, 1999) (Figure 1.5A). However, a trans-acting factor role for altered or insufficient levels of FEN-1 protein in HD repeat instability is unlikely as no mutations in the FEN-1 gene were observed in HD families (Otto *et al.*, 2001). Moreover, defective FEN-1 functioning would cause mutations throughout the genome and triplet repeat instability is associated with specific loci. It was suggested that secondary structure within the displaced flap might prevent normal FEN-1 processing (Gordenin *et al.*, 1997). This hypothesis was tested in yeast and secondary structure formation was found to inhibit FEN-1 binding (by reducing exposure of the 5' end of the flap) at TRS leading to expansion (Spiro *et al.*, 1999) (Figure 1.5B). These findings demonstrate that normal FEN-1 functioning may be involved in repeat instability due to TRS specific secondary structure formation.

A.

Flap of random sequence on Okazaki fragment

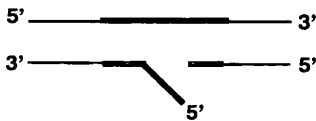


Flap cleavage by FEN-1 followed by gap processing

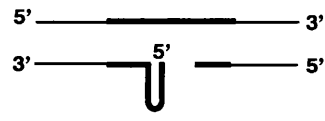


B.

Flap of repeat sequence on Okazaki fragment



Hairpin formation preventing FEN-1 cleavage



Hairpin incorporation by gap processing

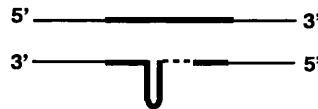


Figure 1.5 Expansion due to disrupted FEN-1 processing in repeat sequences

A. During replication the newly synthesised lagging strand is composed of Okazaki fragments which generate flaps of DNA which must be cleaved before the gap can be processed and the new strand completed. FEN-1 binds to the 5' ends of the Okazaki fragment flaps and its endonuclease activity removes the excess DNA allowing completion of replication. **B.** Okazaki fragments composed of repeat sequence may form secondary structures disguising the 5' end of the flap and inhibiting cleavage. The additional DNA will be incorporated into the genome by gap filling DNA synthesis and subsequent replication. (—) repeated sequence, (——) random sequence.

Studies manipulating the conditions under which replication takes place have produced largely consistent patterns of deletions and expansions, which have substantiated the replication slippage model. However, replication is not the only time that secondary structures form and DNA synthesis occurs. Many proteins involved in replication also mediate DNA synthesis during such mechanisms as DNA repair. Therefore, many studies have investigated the potential role of DNA repair mechanisms in generating repeat instability.

1.6.3 DNA repair of TRS

DNA repair could contribute in many ways to generating repeat length changes. The excision of DNA lesions produces a single-stranded region of TRS, which would presumably be highly prone to secondary structure formation and result in the wrong number of repeat units being synthesised during gap repair. Excision might also generate DNA flaps, which, as in replication, must be processed by exonuclease proteins to ensure faithful repair. It has been demonstrated that small hairpin structures can activate repair mechanisms such as mismatch repair. DNA repair proteins could also bind to and stabilise these structures, thereby promoting their incorporation during replication and causing changes in the repeat length. In addition, replication and polymerase stalling have been shown to cause strand breaks within TRS and the repair of these lesions might involve recombinational repair mechanisms.

1.6.3.1 Nucleotide excision repair (NER) and triplet repeat instability

The NER system recognises DNA damage that distorts the DNA helix and removes a wide range of lesions by excising the stretch of DNA surrounding the lesion and promoting resynthesis of the DNA molecule. In humans, a multisubunit ATP-dependent nuclease makes dual incisions, one on either side of the lesion, and excises a ~24-29 base oligonucleotide carrying the damage. Approximately 16 polypeptides are required to carry out this excision (including the XPA-E and ERCC proteins) and proteins such as DNA polymerases and ligases then carry out gap repair (Wood, 1996).

Inactivation of the NER system causes instability of dinucleotide repeats (Modrich and Lahue, 1996; Petes *et al.*, 1997). Parniewski *et al.* (1999) demonstrated that deficiency of some NER functions dramatically affected the stability of a long (CTG.CAG)₁₇₅ plasmid insert within *E.coli*. The UvrA protein plays an integral role in the NER process within bacteria (Braun and Grossman, 1974) and the absence of the *uvrA* gene product greatly enhances the instability of the TRS (increased number of deletions). These findings suggest that UvrA normally destabilises hairpins within the TRS and initiates repair. In its absence the hairpin will not be removed from the DNA template and DNA synthesis will bypass the structure, creating a deletion. Deletions were only observed when the lagging strand comprised of the CTG repeat sequence (Parniewski *et al.*, 1999).

These findings support those seen in replication studies and again suggest that the formation of stable secondary structures on the CTG strand is a primary event involved in repeat instability and that the NER system is able to recognise these structures.

The effects of deficient NER were shown to be repeat sequence-specific as no effect was demonstrated with (CGG.CCG) or (GAA.TTC) tracts (Parniewski *et al.*, 1999). The repeat tract specificity many indicate that different protein isoforms are involved in lesion recognition (due to different properties of the secondary structures formed by different repeats, (Ohshima *et al.*, 1996; Wang *et al.*, 1994)) or excision in NER. Differential tissue expression patterns of these proteins might help explain the tissue-specific pattern of repeat instability observed with disease-associated TRS.

1.6.3.2 Mismatch repair (MMR) in TRS

The mismatch repair (MMR) system not only corrects mismatched base pairs but also alternative DNA structures such as small loops and unpaired regions (up to 4 bp in *E.coli* and 16 bp in humans) (Modrich and Lahue, 1996). The bacterial protein MutS recognises and binds to the lesions and together with MutL, in the presence of ATP, activates a third MMR protein, MutH, an endonuclease, that cleaves the strand containing the error (Yang, 2000). In humans the MutS function is carried out by two heterodimers, MSH2/MSH3 and MSH2/MSH6 (Kolodner and Marsischky, 1999). These heterodimers appear to target distinct mismatches. MSH2/MSH6 complexes preferentially target pair mismatches and slipped structures that are 1-2 nucleotides long whereas MSH2/MSH3 complexes preferentially target slipped structures that are larger than 2 nucleotides (Kolodner and Marsischky, 1999). MutL human homologues have been identified and designated MLH1, MLH2, MLH3 and PMS2 (Lipkin *et al.*, 2000; Prolla *et al.*, 1994). MLH1 associates with each of the other three MutL homologues, producing three different heterodimers with distinct functions in MMR. The heterodimer with the most prominent role in MMR is MLH1/PMS2 (Tomer *et al.*, 2002). Although a MutH homologue is yet to be discovered in eukaryotes, a polymerase with proofreading activity would be a good candidate. As MMR recognises slipped-strand structures and has DNA nicking activity that would produce single-stranded regions within TRS during repair, it is implicated in repeat instability.

Most studies into the effect of MMR on the stability of TRS have been carried out with MMR mutant bacterial and yeast strains. These studies had illustrated the contrasting effects of MMR on different lengths of TRS. MMR defective bacteria and yeast displayed a reduced occurrence of large deletions (>8 repeats) with (CTG.CAG)₁₆₀₋₁₇₅ tracts (Iyer *et al.*, 2000; Jaworski *et al.*, 1995). However, mutations in MMR proteins also generated an increased frequency of small changes (<8 repeats) in short (CTG.CAG)₆₄₋₉₂ repeat tracts in *E.coli* (Schumacher *et al.*, 1998; Wells *et al.*, 1998) and yeast (Schweitzer and Livingston, 1997). Further studies have attempted to clarify these

conflicting results using a variety of (CTG.CAG)₄₅₋₁₇₅ tracts to determine the effects of MMR on repeat tract stability in *E.coli*. These have confirmed that functional MMR appears to promote large deletions (>8 repeats) in long (CTG.CAG) tracts, but prevents length changes (expansions and deletions) of less than eight repeats (Parniewski *et al.*, 1999; Schmidt *et al.*, 2000).

The suggested mechanism responsible for these results proposes that slipped structures are produced during replication of TRS and in MMR-deficient cells, these unrepaired structures cause small expansions and contractions. On the other hand if repair of these slipped structures is carried out there is the opportunity for hairpins to form in the single-stranded DNA, and this creates a deletion (Figure 1.6). This is only observed in long TRS as the single-stranded regions within smaller TRS are less able to form stable hairpin structures. As in replication and NER-based hypotheses, repeat instability appears to occur in a replication origin orientation-dependent manner when the CTG is on the lagging strand. This suggests that the more stable CTG slipped structures are involved in repeat instability and that the structures are recognised by the MMR system (Schmidt *et al.*, 2000).

Several *in vivo* studies have also demonstrated a role for MMR proteins in the production of repeat expansions. Direct evidence that MSH2 has a role in somatic repeat instability in HD was produced by a study that crossed HD transgenic mice (R6/2) onto a MSH2-deficient background. The resulting HD mice displayed a significant reduction in the age-dependent, tissue-specific somatic repeat instability previously observed (Manley *et al.*, 1999). It has been suggested that MSH2 would generate repeat instability (expansions) by binding to a slipped structure, stabilising or protecting it from repair, and subsequently incorporating the structure during replication and producing an expansion (Pearson *et al.*, 1997). Somatic repeat instability in DM1 knock-in mice display differing patterns when crossed onto either MSH3- or MSH6-deficient backgrounds (van den Broek *et al.*, 2002). Somatic repeat instability was completely abolished in DM1 animals on a MSH3-deficient background, but on a MSH6-deficient background greater repeat instability was observed that varied in a tissue-specific manner. MSH3 and MSH6 both form functional complexes with MSH2 but the MSH2/MSH3 complex recognises slipped structures whereas MSH2/MSH6 is involved in mismatch repair (Acharya *et al.*, 1996) (Figure 1.7). The loss of MSH6 would still allow MSH2/MSH3 to recognise and stabilise the looped structures thought to be responsible for expansions. In addition, absence of MSH6 might increase the amount of MSH2 protein able to bind to MSH3 to carry out this role, thereby increasing the frequency of expansions. Although the lack of repeat instability observed in DM1 mice on a MSH3-deficient background would suggest that the looped structures are resolved it is unknown how this occurs.

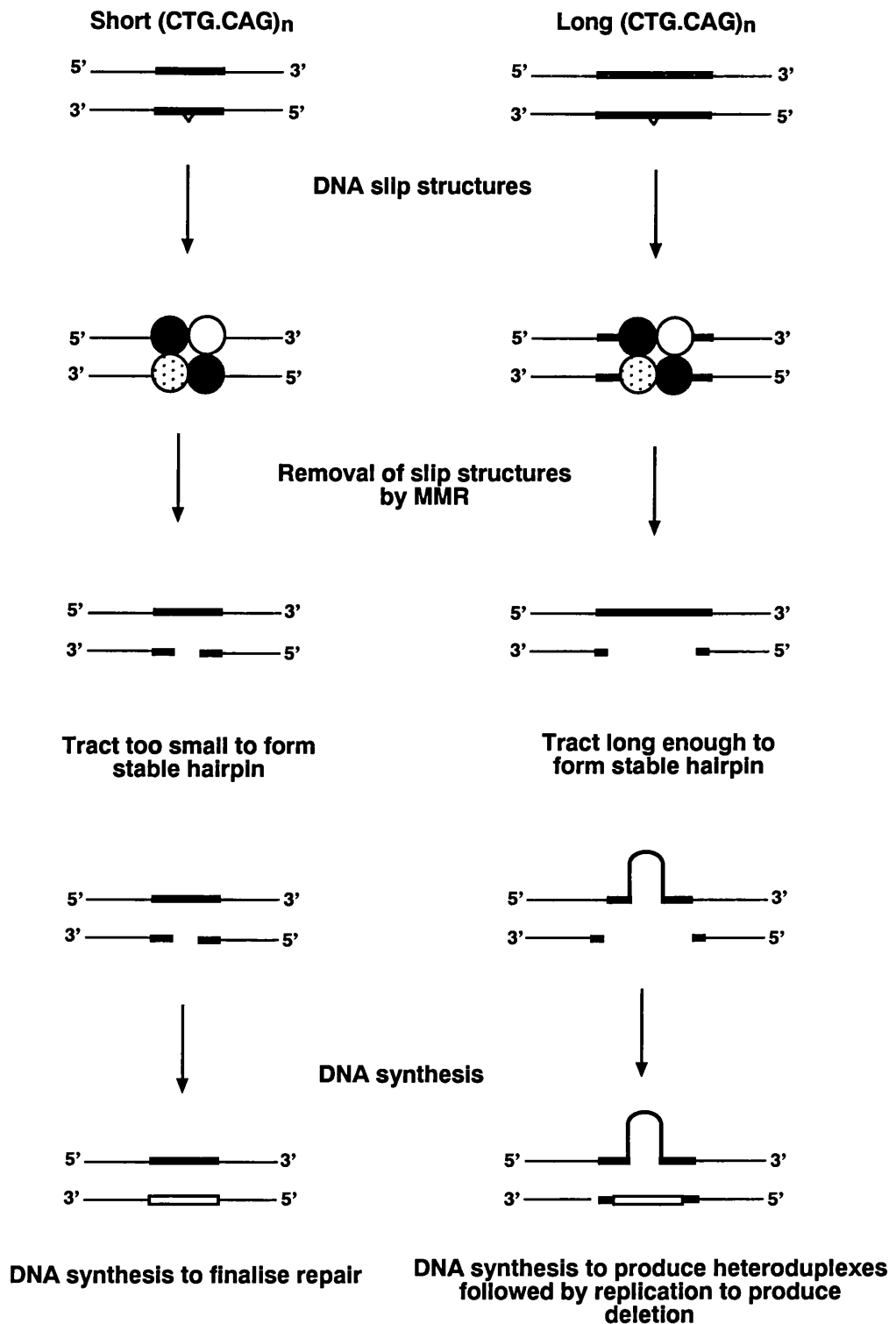


Figure 1.6 The effect of DNA repair on different length triplet repeat sequences

Small slippage events are recognised by the mismatch repair machinery. Recognition of the lesion and excision of the loop generates single-stranded DNA and presents an opportunity for hairpin structure formation. Hairpin structures would only be formed if the single-stranded repeat sequence is long enough to generate stable secondary structures. Subsequent DNA synthesis would therefore either leave alleles unchanged in length or create large deletions.

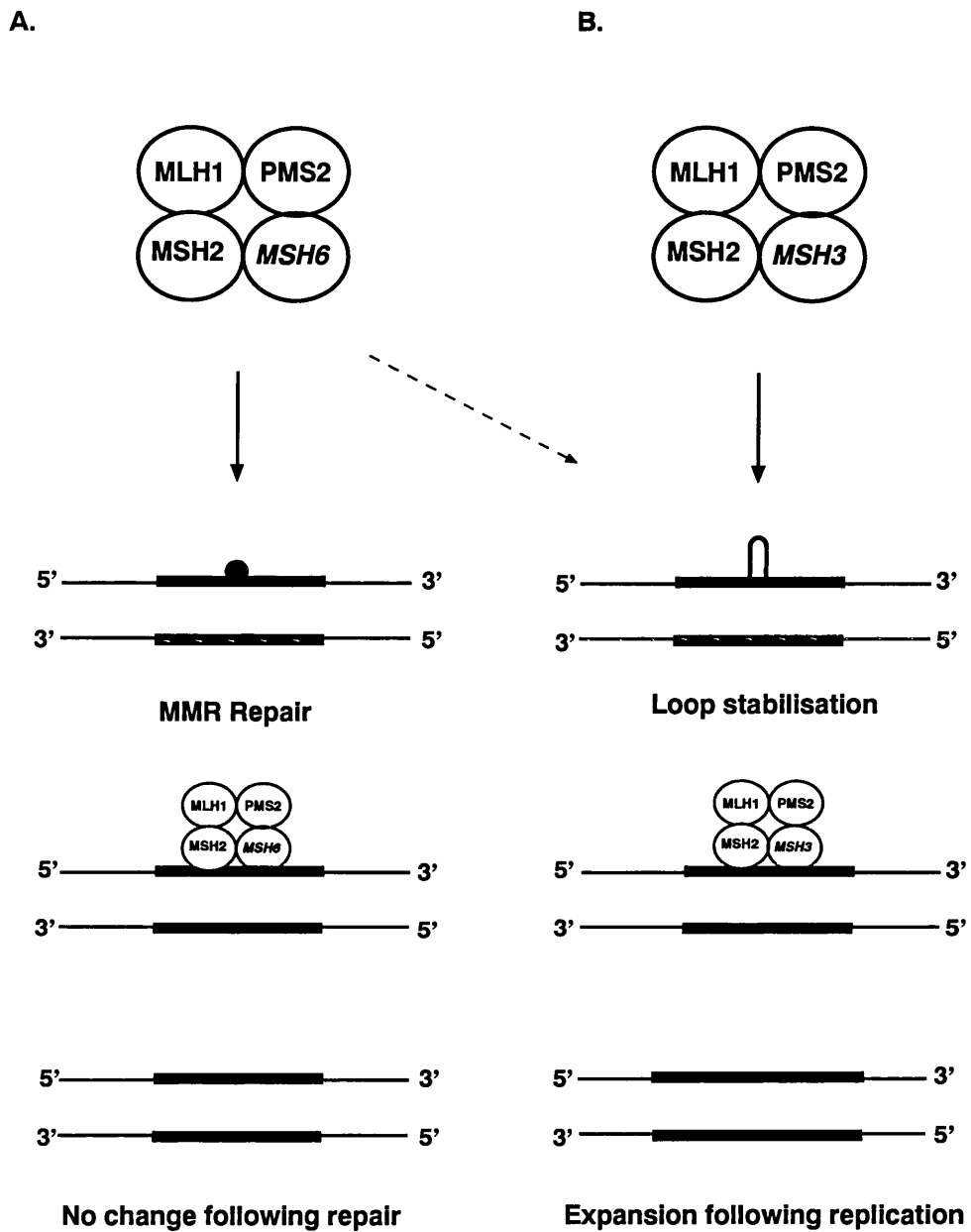


Figure 1.7 A model for mismatch repair induced expansions

MSH2 forms recognition complexes with either MSH6 and MSH3. These complexes have preferential recognition for mismatch base pairs (MSH6) and looped structures (MSH3). **A.** MSH6 will successfully repair the mismatched base pairs. **B.** It is postulated that MSH3 binds and stabilises the looped structures which results in their incorporation into the genome after replication, generating an expansion. In MSH6-deficient mice the expansions will still be generated and may even occur more frequently as there will be an excess of MSH2 available to complex with MSH3 and stabilise looped structures. Deficiency in MSH3 will result in a loss of expansions and this role will not be taken on by MSH6 due to its selective recognition of mismatched base pairs. The loops which are not stabilised may resolve at the next round of helix unwinding (e.g transcription etc).

● = mismatched base pair. ∩ = looped structure. (■) = repeat sequence.

Stabilisation of looped structures within an elongated CAG repeat by MSH2 has also been implicated in repairing strand breaks in haploid germ cells, which do not perform replication or recombination, from HD transgenic mice (R6/1). MSH2 is proposed to bind to and stabilise looped structures which form at DNA breaks and initiate MMR-mediated DNA synthesis and ligation (gap repair), incorporating the looped structures into the genome (Kovtun and McMurray, 2001).

In an attempt to investigate whether the MMR machinery could play a role in human repeat instability, investigations have been carried out to determine if the main component of the human MMR system, MSH2, can bind to human (CTG.CAG) tracts *in vitro* (Pearson *et al.*, 1997). It appears that MSH2 can bind to both slipped-strand structures (S-DNA) and slipped-intermediate structures (SI-DNA). Slipped-strand structures have an equal number of repeats and slipped-intermediate structures have an excess of either CTG or CAG repeats. MSH2 was also shown to have a greater affinity for CAG hairpin loops. The undefined structural difference between CAG and CTG hairpin loops that make CAG structures less stable may render them more prone to recognition by MSH2.

These studies have shown that to generate the expansion-biased small repeat size changes, commonly observed in human HD, a proficient MMR system is required. This is in contrast to earlier findings from bacteria and yeast studies, which suggested that a deficient MMR system was needed to generate small fluctuations in repeat length (Parniewski *et al.*, 1999; Schmidt *et al.*, 2000). These results demonstrate that the model systems of bacteria and yeast, although easily manipulatable, may not be the best systems to investigate the mechanisms underlying repeat instability in humans.

1.6.4 Transcription and Transcription-coupled repair

Another DNA process that has been implicated in triplet repeat instability is transcription. *In vitro* transcription of a wide variety of (CTG.CAG)_n and (CGG.CCG)_n tracts has been performed using human RNA polymerase II (Pearson and Sinden, 1998) and in general, transcription rates through TRS are slower than through random DNA sequence. The RNA polymerase also appears to adopt a transient elongation-incompetent configuration at the start of the repeat stretches (Pearson and Sinden, 1998). In primate cell culture the (GAA.TTG) repeat sequence also suppresses transcription rates in a length and orientation-dependent fashion (Ohshima *et al.*, 1998). These studies have shown that TRS can affect transcription and several factors involved in this disruption have also been shown to influence repeat instability.

It is possible that transcription could destabilise repeat tracts by promoting the formation of alternative DNA structures as the RNA polymerase complex opens the DNA helix and generates single-stranded DNA (Pearson and Sinden, 1996). Transcription could also produce repeat

instability by interfering with the replication process. DNA replication and transcription can occur simultaneously on the same DNA molecule. As the rate of replication is much faster than transcription, collisions of the RNA polymerases with the replication fork will eventually occur, perhaps resulting in a brief stalling of the replication fork and replication slippage. In addition, transcription is a vital component of some DNA repair pathways such as transcription coupled NER and MMR, as many proteins involved in transcription are also involved in recognition of DNA damage and repair (Hanawalt, 1994; Lindahl *et al.*, 1997; Sancar, 1999). Transcription through the TRS has been found to be important for mediating the effect on repeat instability by NER (Parniewski *et al.*, 1999) and MMR (Bowater and Wells, 2001).

Transcription of long (CTG.CAG) TRS in *E.coli* displaying extended growth times, appears to increase the frequency of deletions within the repeat stretch (Bowater *et al.*, 1997; Parniewski *et al.*, 1999). This is also found to occur in an orientation-dependent manner with the (CTG.CAG)₁₇₅ tract more stable when the CTG strand is transcribed than when the CAG strand is transcribed (Parniewski *et al.*, 1999). It is postulated that the transcription of the CAG strand may allow the remaining single-stranded CTG sequence to form secondary structures. These findings have also been replicated when examining the behaviour of dinucleotide sequences in yeast (Wierdl *et al.*, 1996).

1.6.5 Recombination

Repetitive sequences have been shown to be substrates for recombinational mechanisms such as homologous recombination, gene conversion, and sister chromatid exchange (Bi and Liu, 1996; Lupski, 1998). During these processes strand slippage or unequal crossing over have the potential to generate repeat instability. Blocked or stalled replication could promote classical RecA-dependent recombinational repair of chromosomes and result in the loss or gain of repeat units. RecA-independent recombinational mechanisms, which require less homology and have been shown to induce rearrangements in direct repeats, include sister-strand or chromosome exchange (Bi and Liu, 1994; Morag *et al.*, 1999). It is postulated that such mechanisms could play a role when very large expansions (>100s repeats) of TRS occur in FRAXA or DM1. Human genetic studies have illustrated through haplotype analyses that types of recombination could be involved in some repeat length changes in DM1 and FRAXA (Brown *et al.*, 1996; O'Hoy *et al.*, 1993). However, as the flanking DNA sequences are generally unaltered after the majority of TRS mutations (Sinden and Wells, 1992) it is thought unlikely that these recombinational events occur frequently. Several studies investigating repeat instability in *E.coli* have demonstrated that the frequency of deletions in TRS is independent of RecA proficiency, suggesting that recombinational mechanisms may not play a role in the repeat instability observed in *E.coli* (Bowater *et al.*, 1996; Jaworski *et al.*, 1995).

However, demonstrations of recombination-based changes in TRS have been achieved when using (CTG.CAG) sequences in a two-plasmid system in recombination-proficient *E.coli* cells (Jakupciak and Wells, 1999). Recombination is indicated by the presence of both antibiotic resistance genes (originally on different plasmids) in the recombinant products, the formation of long cointegrant DNAs, the expansion of (CTG.CAG) tracts and the transfer of a G-to-A polymorphism from the TRS in one plasmid to that on the other. Previous studies of repeat instability have been carried out in recombination-deficient *E.coli* and yeast and have shown deletions and expansions at a ratio of 100:1 (Freudenreich *et al.*, 1997; Kang *et al.*, 1995; Kang *et al.*, 1996; Maurer *et al.*, 1996; Ohshima *et al.*, 1996). In the study using recombination-proficient cells, the ratio of expansions to deletions was as high as 100:1 (Jakupciak and Wells, 1999). These findings are of interest since expansion-biased repeat instability predominates in human HD. The extent of the expansions observed in the bacterial system were several fold the original length of ~80 repeats.

In summary, it is thought that replication slippage and repair may be responsible for smaller repeat changes, perhaps responsible for repeats expanding from the intermediate range in the germline, but recombination may contribute to the larger changes observed in already expanded repeat sequences.

The point of recombination initiation appears to lie within the (CTG.CAG) repeat sequence since recombination did not occur in other regions of the plasmids (Jakupciak and Wells, 1999). As previous studies have not reported this level of expansion in cells proficient in replication and repair, it is thought that these additional expansions must occur due to the recombination proficiency. They suggest that most realistic way for these large expansions to occur with no crossing over of flanking regions would be by double-stranded break repair (DSBR) within the TRS.

1.6.5.1 Double-strand break repair

Studies have shown that the DNA replication fork stalls when it encounters (CTG.CAG) sequences (Ohshima and Wells, 1997; Samadashwily *et al.*, 1997) and this may result in double-stranded breaks (Freudenreich *et al.*, 1998; Tishkoff *et al.*, 1997).

The expansion of (CTG.CAG) tracts by recombination without the exchange of flanking sequence can be explained by the double-strand break repair (DSBR) model based on gene conversion (Figure 1.8A) (Jakupciak and Wells, 1999). Similar mechanisms have been used to explain polymorphisms at minisatellites (Jeffreys *et al.*, 1994). The DNA break may cause the broken strands to be paired with a homologous template, followed by strand invasion and DNA synthesis. Resolution of the two Holliday-like junctions will be carried out in a way that leaves the flanking sequences unaltered. Due to the repetitive nature of the sequence, slippage during DNA synthesis

or misalignment during strand invasion could occur and generate repeat length changes (Jakupciak and Wells, 1999) (Figure 1.8B).

Others studies have suggested variations on this model of DSBR. In addition to the gene conversion model already described, a model called synthesis-dependent strand annealing (SDSA) has also been proposed (Richard *et al.*, 1999).

SDSA does not require resolution of Holliday junctions, just strand invasion and DNA synthesis, as the new strands could unwind from the template before ligation and the two free 3' ends surrounding the double-stranded break could then anneal (Figure 1.8C) (Paques *et al.*, 1998). The distinctive feature of this model is that the recipient strand receives two newly synthesised strands and the donor template remains unchanged. This model is supported by experiments in yeast in which 375 bp repeats shared frequent expansions and contractions in a system in which the donor strand and template strand could be recovered and identified after repair of a double-stranded break. Approximately half of all recombinants contained expansions or deletions and the template was never modified (Richard *et al.*, 1999). The magnitude of expansions could exceed more than 4 kb. For the replication slippage model to generate changes of this magnitude, it would need to extensively unwind the DNA helix and perhaps generate very large unstable alternative structures. In the SDSA gene conversion model the creation of hairpin structures would be likely during DNA synthesis and may cause polymerase pausing. This would favour dissociation of the elongated strand from its template and repair would require strand reinvasion. This could take place many times during a single repair event and therefore would be capable of generating very large amplifications during repair of one double-stranded break (Paques *et al.*, 1998).

A further mechanism has been suggested for DSBR, based on the finding that MSH2-dependent repair of double or single-stranded breaks during maturation of sperm cells caused expansion in haploid cells displaying no replication or recombination (Kovtun and McMurray, 2001). It is postulated that MSH2 binds to the alternative structures formed at the strand breaks, stabilising them and initiates DNA synthesis and ligation to perform gap repair. This locks the looped structures into the genome and produces germ cells containing DNA with heteroduplex structures within the TRS.

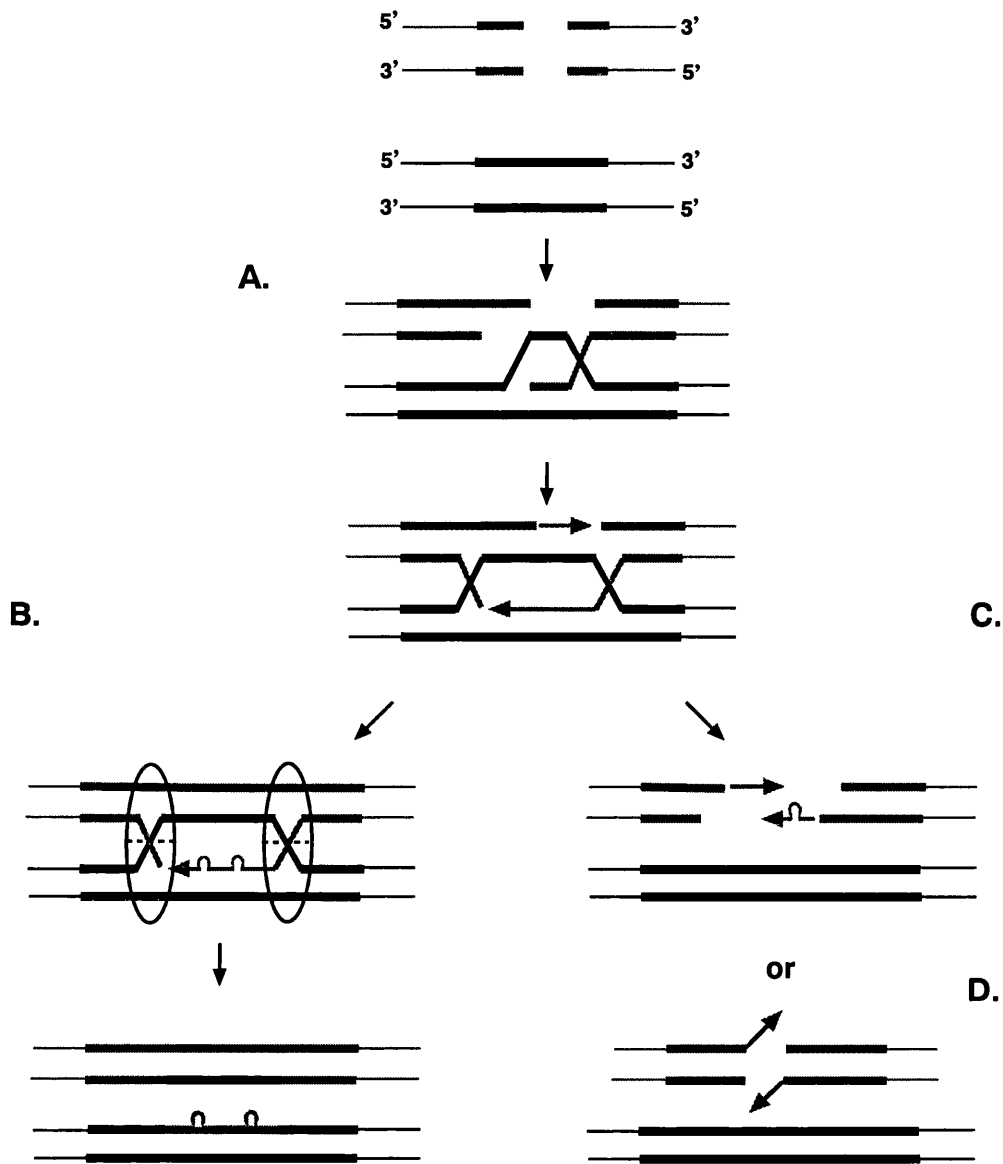


Figure 1.8 Double-strand break repair through gene conversion mechanisms

Two alternative models for double-strand break repair have been proposed.

A. The 3' ends produced by exonucleolytic processing of the strand break invade a homologous template and initiate DNA synthesis.

B. The basic gene conversion model proposes that after synthesis and ligation resolution of the two Holliday junctions within the repeat sequence produces rearrangements of the donor and recipient molecules. Repeat instability could be due to slippage events during DNA synthesis (e.g. an expansion as shown) or misalignment at invasion (A.).

C. The synthesis-dependent strand annealing (SDSA) model proposes that the 3' ends do not ligate and form Holliday junctions but disassociate from the template and reanneal. This mechanism allows for the donor strand to remain unchanged. Repeat instability could be due to slippage during DNA synthesis (e.g. an expansion as shown) or misalignment at invasion (A.). Disassociation due to slippage may initiate cycles of strand reinvasion incorporating more repeats each time, resulting in large changes in repeat length.

D. Repeat instability (e.g. deletion as shown) could also occur due to the unequal annealing of the two nascent strands.

1.6.6 Factors contributing to locus-specific repeat instability

Many studies have generated information concerning mechanisms underlying repeat instability. However, all of the mechanisms proposed are capable of generating repeat instability at all TRS within the genome. The MMR system is one such mechanism as mutations within the MMR genes are responsible for the high frequency of genome wide microsatellite instability associated with hereditary nonpolyposis colon cancer (HNPCC) (Modrich and Lahue, 1996; Prolla *et al.*, 1996). Unlike HNPCC, the trinucleotide repeat disorders are associated with the genetic instability of specific loci. Repeat instability of a different locus is responsible for each repeat disorder and each repeat sequence displays variations in the relative levels of instability and the size and direction of repeat length changes. These observations suggest that there must be *cis*-acting factors unique to each locus, dictating its propensity to expand.

A simple illustration of the importance of *cis*-acting factors on the repeat sequence within the HD locus was provided by a study comparing single sperm containing intermediate alleles (29-35 repeats), which expanded into new mutations (IANm) and those that continued in the general population without change (IAGp) (Chong *et al.*, 1997). It was demonstrated that while IAGp and IANm may have the same repeat length tract, IANm are significantly more unstable than IAGp, suggesting that *cis*-acting factors may be involved in the propensity for repeat expansion.

Several different lines of transgenic mice generated using the 3'-untranslated region of the myotonic dystrophy protein kinase (*DMPK*) gene carrying a (CTG.CAG)₁₆₂ tract from a DM1 patient have been investigated to determine the factors involved in repeat instability (Monckton *et al.*, 1997). The Dmt-D and Dmt-E mouse lines carry one copy of this transgene on the same genetic background with different integration sites. Differential frequencies of somatic and germline repeat instability have been observed in these animals, with Dmt-D mice displaying higher mutation rates and magnitude of repeat size changes compared to the relatively stable Dmt-E mice (Fortune *et al.*, 2000; Zhang *et al.*, 2002). These findings suggest that the sites of transgene integration and therefore the surrounding genome may contribute to the mutation frequency.

The most obvious *cis*-acting factor influencing repeat instability is the length of the repeat sequence itself. It has been shown that longer repeats have a greater propensity for instability. For example, repeat size spectra obtained from sperm cells in HD patients show the mutation frequency and mean changes in allele size increase with higher somatic repeat number (Leefflang *et al.*, 1999). The integrity of the repeat sequence is also likely to be a crucial influence on instability as pure repeat sequences are much more prone to expansion than those possessing interruptions (Fujigasaki *et al.*, 2001; Goldberg *et al.*, 1995; McNeil *et al.*, 1997). The GC content of the DNA flanking TRS has been implicated in influencing their tendency to expand. It has been established that the extent of

expansion associated with a TRS was correlated to their location within CpG islands (Brock *et al.*, 1999).

Cleary *et al.* (2002) have recently established a primate cell model of repeat instability in which they observed a repeat-length dependent, expansion-biased pattern of repeat instability in one line. In this system the repeat length, direction of replication and the site of replication initiation all demonstrated an influence on repeat instability. The direction of replication influenced repeat instability in the expected way; the CTG tract on the lagging strand induced a bias towards deletions. However, unlike bacteria and yeast, reversing the direction of replication does not influence the frequency of deletions but alters the type of mutation as there is a bias towards expansions if CAG is on the lagging strand. Identical transgenes at different distances from the replication origin demonstrated differences in mutation frequency and mutation type. One transgene demonstrated a propensity towards expansion, three predominantly displayed deletions, one generated both expansions and deletions and two did not display repeat instability (Cleary *et al.*, 2002). These findings suggest that the location of replication origin may be important in dictating the extent and direction of repeat instability.

These studies have illustrated that *cis*-acting factors do influence locus-specific repeat instability and have presented various candidates for this role. Further studies will be required to determine if the same *cis*-acting factors influence each specific triplet repeat disease locus and to establish if manipulating these factors affects repeat instability.

1.7 Aims

Investigations into the molecular and cellular basis of HD were undertaken by utilising a knock-in HD mouse model. These mice have displayed a variety of behavioural and cellular alterations in the absence of significant cell death, indicating that they are modelling early stages of the disease process. This model system therefore presents the opportunity to investigate the initial events involved in HD pathogenesis and possible targets for early therapeutic intervention.

Firstly, this project aimed to contribute to the phenotypic characterisation of the HD knock-in mice. Detailed observations of the phenotypic consequences of the HD mutation are required to assess the appropriateness of this system as a model of HD and to identify suitable disease markers for assessing potential therapies. Characterisation of phenotypic alterations may also provide clues to the possible molecular and cellular abnormalities underlying the HD phenotype.

Phenotypic characterisation of HD knock-in mice was undertaken by:

- Investigating motor function in HD knock-in mice by examining mouse gait.

- Examining the cognitive abilities of HD knock-in mice by assessing spatial learning and memory.

Secondly, this study aimed to investigate early cellular mechanisms involved in HD pathogenesis by determining the nature and progression of molecular events underlying dysfunction in HD knock-in mice

This issue was addressed by:

- Examining the density of specific neurotransmitter receptors within the striatum and cortex of HD knock-in mice using quantitative ligand binding autoradiography.
- Investigating somatic mutation instability in HD knock-in mice by small pool PCR analysis.

These studies aimed to integrate the molecular and cellular changes involved in HD pathogenesis to the phenotypic manifestations observed in HD knock-in mice. By incorporating additional studies on somatic mutation instability on human juvenile HD tissue it was aimed to decipher the molecular changes involved in human HD pathogenesis and to assess the validity of the findings in HD knock-in mice.

2 Materials and Methods

All chemicals and reagents used were analytical or molecular biology grade. Materials were generally purchased from Sigma Chemical Company Ltd or Merck Ltd and other sources are mentioned where appropriate.

2.1 Solutions

Benzodiazepine receptor binding buffer	10 mM Tris-HCl, 1 mM EDTA, pH 7.4
Chloroform:Octanol	24:1 (v/v) Chloroform (Fisher Chemicals) and Octan-1-ol
Denaturing Solution	0.4 M NaOH, 0.5 M NaCl
Depurinating Solution	0.25 M HCl
Dilution Buffer	0.1 μ M MHD-16 oligonucleotide, 1 x TE
DNA marker (1 kb plus)	40 ng/ μ l 1 kb plus DNA marker (GibcoBRL)
Dopamine receptor binding buffer	25 mM Tris-HCl, pH 7.5, 100 mM NaCl, 1 mM MgCl ₂ , 10 mg/l Ascorbic acid, and 1 μ M Pargyline
0.5 M EDTA	0.5 M EDTA with NaOH to pH 8
70 % Ethanol	70:30 (v/v) 100 % Ethanol (Banford Laboratories) and dH ₂ O
Ethidium Bromide	25 mM Ethidium Bromide
Hybridisation Solution	7 % SDS, 1 mM EDTA, 0.5 M NaPO ₄ pH 7.2
Loading Dye (x 5)	15 % Ficoll, 0.05 % Orange G, 5 mM EDTA

Lysis Buffer	100 mM Tris-HCl, pH 8.5, 200 mM NaCl, 0.2 % SDS, 5 mM EDTA, pH 8, 0.1 mg/μl Proteinase K
Neutralising Solution	0.5 M Tris-HCl, 3 M NaCl, pH 7.5
OLB	2:5:3 (v/v) solutions A, B and C Solution A: 1.2 M Tris pH 8, 121 mM MgCl ₂ , 0.48 mM dATP, dGTP and dTTP, 18 μl of 2-mercaptoethanol in a final volume of 1033 μl. Solution B: 2 M Hepes, pH 6.6 Solution C: Ultrapure dNTP set (Pharmacia Biotech) suspended in 0.2 mM EDTA, pH 7 to an optical density of 90 OD units ml ⁻¹
Opioid receptor binding buffer	0.17 M Tris-HCl, pH 7.4
Phenol:Chloroform	50:50 (v/v) Phenol and Chloroform (Fisher Chemicals)
10 % SDS	100 g of SDS in 1 litre of dH ₂ O
20 x SSC	6 M NaCl, 0.6 M Na ₃ C ₆ H ₅ O ₇ ·2H ₂ O
Subbed slide coating	6 g Gelatin in 600 mls of 3 mM K ₂ SO ₄
10 x TBE	1 M Tris-Base, 1 M Boric Acid, 20 mM EDTA, pH 8
1 x TE	10 mM Tris-HCl, 1 mM EDTA, pH 7.5
Wash Solution	0.2 % SSC, 0.2 % SDS

2.2 Mouse lines

Table 2.1 Summary of the different HD mouse lines utilised in the following studies

Name	Construct (Shelbourne <i>et al</i> 1999)	CAG repeat number	Genetic background	Mice used in each experiment (Chapter or section)
6C9 Δ neo	<i>Hdh6/Q72</i>	72	C57BL/6	3.3, 5, 6.2 & 6.3
4A11 Δ neo	<i>Hdh4/Q80</i>	80	C57BL/6	4
4A11 Δ neo	<i>Hdh4/Q80</i>	80	FVB/N	3.2, 4
4A11 Δ neo	<i>Hdh4/Q80</i>	80	DBA/2	4
6C9neo	<i>Hdh6/neo</i>	72	C57BL/6	6.4

The generation of the HD mice used is described in (Shelbourne *et al.*, 1999). All mice used were congenic to a statistical minimum of 97 % of the stated genetic background.

Animals that were heterozygous for the HD mutation are referred to as HD^{+/-} mice in the text. HD^{-/-} mice denote animals homozygous for the HD mutation. Mice that were heterozygous for the HD mutation from the 6C9neo line are denoted as HD^{trunc} mice. Full details of the mutations carried by the different mouse lines are provided in section 1.5.3.1.

2.3 General methods

2.3.1 Tissue collection

2.3.1.1 Post-mortem human tissue

Post-mortem tissue samples from a known HD case (time from death to autopsy = 10 hours) were provided by Dr ER Nairn at Crosshouse Hospital, Kilmarnock, in 1996 after appropriate permissions were obtained. All samples were stored at -70°C until use.

2.3.1.2 Fresh-frozen mouse tissue

Mice were culled by dislocation of the neck followed by prompt dissection of several somatic tissues and regions of the central nervous system. Tissue samples were frozen immediately on dry ice and stored at -70°C until use.

2.3.1.3 Mouse sperm

Mice were culled by dislocation of the neck and subsequent dissection of the testes, epididymides and vas deferens' was swiftly carried out. The vas deferens' were detached from the epididymides and immersed in 1 ml of 1 x SSC. Each vas deferens was held at one end with fine-nosed tweezers while simultaneously squeezed along the length of its structure, extruding sperm into the solution. The solution was transferred to an eppendorf tube and frozen until DNA extraction. The testes and

epididymides were separated and each immersed in 1 ml of 1 x SSC. The structures were cut into small pieces and transferred, along with the 1 x SSC, into eppendorf tubes and frozen awaiting DNA extraction.

2.3.2 DNA extraction

2.3.2.1 Mouse DNA extraction

Tissue digestion was performed at 50 °C overnight by agitation of a 1.5 ml eppendorf tube containing the tissue sample and 700 µl of lysis buffer. The digested tissue was further dissociated by vigorous vortexing and then centrifuged at 16,000 x g for 10 minutes.

The tissue digestion supernatant was transferred to a clean eppendorf tube and a phenol:chloroform extraction performed to eliminate any protein and fat. An equal volume of phenol:chloroform solution was added and the solution emulsified by vortexing. The aqueous and organic phases were then separated by centrifugation at 16,000 x g. The aqueous layer was transferred to another clean eppendorf tube for repetition of the above phenol:chloroform extraction.

The same technique was then used to ensure the full removal of all phenol by extraction with chloroform:octanol solution.

DNA precipitation was achieved by adding 0.1 volume of cold 3 M CH_3COONa , pH 4.8 followed by 2 volumes of cold absolute ethanol to the aqueous layer. The mixture was inverted several times and stored at -20 °C overnight. The DNA pellet was recovered by centrifugation for 10 minutes at 16,000 x g. To wash excess salt from the pellet the precipitation liquid was removed and replaced with 300 µl of 70 % ethanol. Following vortexing the DNA pellet was again recovered by centrifugation and the wash repeated. The pellet was finally allowed to air dry for 30 minutes at room temperature.

Once all ethanol had evaporated the pellet was resuspended for 4 hours at 37 °C in an appropriate volume of 1 x TE (typically, 30-50 µl).

2.3.2.2 Sperm DNA extraction

To obtain the sperm cells from within the dissected testes and epididymides (section 2.3.1.3), the samples were vortexed and the pieces of tissue allowed to settle for 5 minutes. After repeating this agitation the cell suspension was removed avoiding any large pieces of tissue. These samples, along with the tubes containing the extruded sperm from the vas deferens' (section 2.3.1.3), were then centrifuged at 1,000 x g for 5 minutes to pellet the cells.

The supernatant was decanted and the cell pellet resuspended in 100 μl of 1 x SSC. To lyse non-sperm cells, the volume was made up to 900 μl with 1 x SSC followed by 100 μl 10 % SDS. The mixture was vortexed and the unlysed sperm cells pelleted as before.

Resuspension of the sperm cells and SDS lysis of non-sperm cells was repeated with the final pellet of sperm cells resuspended in 80 μl of 1 x SSC.

To lyse sperm cells 10 μl of 2-mercaptoethanol was added and the solution incubated at room temperature for 5 minutes. 10 μl of 10 % SDS was then added and the solution vortexed vigorously and incubated for a further 15 minutes. To precipitate any proteins 450 μl of 1 x SSC and 220 μl of 5 M NaCl were added. The mixture was vortexed and the cellular debris and proteins pelleted at 16,000 x g for 15 minutes.

DNA precipitation was achieved when the supernatant was transferred to a clean eppendorf tube containing 750 μl of cold isopropanol and mixed well. The recovery, washing and resuspension of the DNA were carried out as described in section 2.3.1.2 for all mouse DNA samples.

2.3.2.3 Human DNA extraction

DNA was extracted and purified following the protocol outlined in the NucleonST™ Soft Tissue Kit (Nucleon Biosciences).

2.3.3 DNA quantification

The concentration of a DNA solution was determined by diluting 5 μl of the solution in 695 μl 1 x TE. A clear quartz glass 1 ml cuvette containing the solution was placed in a spectrophotometer (Shimadzu UV-1201) and readings obtained at $\lambda 260 \text{ nm}$. An OD of 1 corresponds to approximately 50 $\mu\text{g/ml}$ of double-stranded DNA.

$$\text{OD}_{260 \text{ nm}} \times \text{dilution factor} \times 50 = ? \text{ ng}/\mu\text{l}$$

2.3.4 Polymerase Chain Reaction (PCR)

Sequences for all primer oligonucleotides used in mouse and human PCR can be found in Table 2.2. The PCR programs referred to in the text have been outlined in Table 2.3.

Table 2.2 The sequence, melting temperature (T_m) and orientation of all oligonucleotides used to amplify the CAG repeat sequence.

Name	Target sequence	Direction	T_m	Sequences
MHD-16	Mouse <i>HD</i> gene	Forward	80.3	5'-CCCATTCATTGCCTTGCTGCTAA G-3'
MHD-18	Mouse <i>HD</i> gene	Reverse	71.0	5'-GACTCACGGTCGGTGCAGCGG TTCC-3'
LK-1	Human <i>HD</i> gene	Forward	77.7	5'-CCCATTCATTGCCCGGTGC TG-3'
LKH-5	Human <i>HD</i> gene	Reverse	70.8	5'-TGGGTTGCTGGGTCACCTCTG C-3'
MHD-5	Mouse <i>HD</i> gene	Forward	82.7	5'-GAAAAGCTGATGAAGGCTTTC GAGTCGCTCAAGTGGTT-3'
MHD-4	Mouse <i>HD</i> gene	Reverse	95.1	5'-GCGTGGCGGCGCCTGCGGC GGTGGCTG-3'

Table 2.3 PCR programs

Name	Cycles	Temperature ($^{\circ}$ C)	Duration
Touchdown	1	94	5 min
	20	94	30 sec
		71- 61	30 sec (ramping - 0.5 $^{\circ}$ C per cycle)
		72	30 sec
	10	94	30 sec
		60	30 sec
		72	30 sec
1	72	7 min	
	4	∞	
DGM	30	94	45 sec
		68	45 sec
		70	3 min
	1	68	1 min
	1	70	10 min
		4	∞

PCR was performed in a Perkin Elmer Applied Biosystems GeneAmp PCR system 9700.

2.3.4.1 PCR amplification of the CAG repeat region of the mouse *Hdh* locus

Amplification was carried out in a volume of 10 μ l using the Touchdown PCR program.

Table 2.4 Reaction mixture for amplification of the CAG repeat within the mouse *Hdh* locus

Reagent	Final concentration
10 x PCR buffer	1 x PCR buffer (10 mM Tris-HCl, pH 8.3, 50 mM KCl)
DMSO	10 %
dNTPs (2 mM) (Amersham)	200 μ M
MHD-16 (24 μ M)	1.2 μ M
MHD-18 (24 μ M)	1.2 μ M
Taq polymerase (5 U/ μ l)	1 U
MgCl ₂ (25 mM)	1 mM
dH ₂ O	as required
DNA	as required

2.3.4.2 PCR amplification of the CAG repeat region of the human *HD* locus

Amplification was carried out in a volume of 10 μ l using the DGM PCR program.

Table 2.5 Reaction mixture for amplification of the CAG repeat within the human *HD* locus

Reagent	Final concentration
10 x custom PCR buffer (ABgene)	1 x custom PCR master mix (6.4 mM Tris-HCl, pH 8.8, 1.6 mM (NH ₄) ₂ SO ₄ , 0.6 mM MgCl ₂ , 0.016 mg/ml BSA, 0.6 μ M EDTA, 143 μ M each of dATP, dCTP, dGTP and dTTP, 6.7 mM 2-mercaptoethanol)
DMSO	10 %
LK-1 (24 μ M)	1 μ M
LKH-5 (24 μ M)	1 μ M
Taq polymerase (5 U/ μ l)	0.5 U
dH ₂ O	as required
DNA	as required

2.3.5 Gel electrophoresis

Visualisation of PCR products was achieved by running the PCR reaction through an agarose gel providing separation of the DNA fragments by size. Typically a 1 % agarose gel in 1 x TBE was used. The 1 % agarose gel was made by adding 1 g of agarose MP (Roche) to 100 mls of the appropriate buffer. This mixture was then heated until the agarose completely dissolved. Once cooled, EtBr was added to a final concentration of 0.25 μ M. The mixture was then poured into a gel cast containing the appropriate comb and left to set on an even surface. Once set the comb was

removed and the gel was placed in a tank (Biorad) completely immersed in the same buffer used to dissolve the agarose. The PCR reactions were mixed with loading dye (to prevent dispersal into the buffer) and loaded into the wells. One lane on each gel was loaded with DNA marker to help size and identify the PCR products. The gel was then electrophoresised at between 40 and 120 V at room temperature for the time required to achieve appropriate separation of the PCR products.

To visualize the PCR products the gel was removed from the tank and placed on the transilluminator (UVP) at λ 260 nm. The UV-light illuminates the EtBr intercalated within the DNA. A gel documentation system (UVP 7500) was then used to photograph the gel and produce an image on thermal paper K65HM-CE (Mitsubishi).

2.3.6 Genescan analysis of the mouse *Hdh* locus

Amplification of the CAG repeat region of the mouse *Hdh* gene was carried out as previously described in section 2.3.4.1 with the exception that the reverse primer, MHD-16, was replaced by an identical primer modified to carry a 3' fluorescent tag (Oswell). 1 μ l of the resultant fluorescent PCR product was mixed with 1 μ l of the Genescan standard mix and the samples denatured for 2 minutes. The Genescan standard mix contains 40 μ l of Formamide (Kodak), 10 μ l of Genescan dye (Perkin Elmer) and 13 μ l of Rox 1000 internal standard (Perkin Elmer). The samples were then electrophoresed through a 4.75 % urea polyacrylamide gel in a 373XL automated sequencing machine for 12 hours. A laser accurately detects the fluorescent PCR products, and by utilising the internal standards in each sample lane, provides precise sizing of the DNA fragments. The resultant gel file was analysed with the Genescan software version 3.1.

2.4 Small pool PCR (SP-PCR)

2.4.1 DNA digestion

2 μ g of DNA was digested with the restriction enzyme *HindIII* (GibcoBRL) in a 200 μ l volume (Table 2.6). The mixture was incubated at 37 °C for 2 hours followed by enzyme inactivation at 65 °C for 10 minutes and storage at -20 °C.

Table 2.6 SP-PCR DNA sample digestion**Final concentration**

2 µg DNA	}	1 x restriction enzyme React 2 buffer (GibcoBRL)
40 µg BSA		
50 mM Tris-HCl, pH 8.0		
10 mM MgCl ₂		
50 mM NaCl		
20 U <i>Hind</i> III		

2.4.2 DNA dilution

SP-PCR reveals the CAG trinucleotide repeat lengths present on individual alleles by amplification of a small number of DNA templates followed by sensitive visualisation techniques. This technique requires DNA stability in very dilute solutions and dilutions of uniform DNA quantities. To facilitate these requirements, DNA dilutions were made on the day of the experiment to reduce the chance of DNA degradation. Dilutions were made using dilution buffer (1 x TE containing 1 µM MHD-16 oligonucleotide). Dilution buffer increased the DNA concentration of the dilution thus assisting in DNA dispersal by reducing the electrostatic forces between the DNA molecules and the eppendorf tubes and also helping to prevent DNA degradation.

The final concentration of DNA in the digest (section 2.4.1) was 10 ng/µl. To achieve the highest dilution (1.2 ng/ul) used for SP-PCR, 20 µl of digest was added to 147 µl of dilution buffer. Serial dilutions were generally performed to obtain the following concentrations: 600 pg/µl, 300 pg/µl, 60 pg/µl, 30 pg/µl, 12 pg/µl and 6 pg/µl. It is assumed that approximately 6 pg of DNA is the equivalent of 1 cells worth of DNA, i.e. one genome is ~ 3 pg of DNA.

2.4.3 Polymerase Chain Reaction

Due to the sensitivity of SP-PCR a common technical problem was contamination. The sensitive visualisation techniques used could detect extremely small amounts of contaminating DNA and this was of particular significance when analysing the products of a small number of DNA templates. To combat this problem all SP-PCR reactions were carried out in designated laminar flow hoods using pipettes and filter tips specified for SP-PCR use only.

2.4.3.1 SP-PCR of the CAG repeat within the mouse *Hdh* locus

SP-PCR amplification of the mouse *Hdh* locus was carried out exactly as described in section 2.3.4.1.

2.4.3.2 SP-PCR of the CAG repeat within the human *HD* locus

SP-PCR amplification of the human *HD* locus was carried out in a volume of 7 μ l (Table 2.7) using the DGM PCR program (Table 2.3).

Table 2.7 Reaction mixture for SP-PCR of the CAG repeat region within the human *HD* locus

Reagents	Final concentration
10 x custom PCR buffer (ABgene)	1 x custom PCR master mix (6.4 mM Tris-HCl, pH 8.8, 1.6 mM (NH ₄) ₂ SO ₄ , 0.6 mM MgCl ₂ , 0.016 mg/ml BSA, 0.6 μ M EDTA, 143 μ M each of dATP, dCTP, dGTP and dTTP, 6.7 mM 2-mercaptoethanol)
DMSO	10 %
LK-1 (24 μ M)	200 nM
LKH-5 (24 μ M)	200 nM
Taq polymerase (5 U/ μ l)	0.35 U
dH ₂ O	as required
DNA	as required

2.4.4 Gel electrophoresis

SP-PCR agarose gels were cast in gel trays measuring 20 cm x 40 cm with a 35 well comb. 400 ml of 1.5 % agarose in 0.5 x TBE was used to prepare each gel. EtBr was added to give a final concentration of 0.25 μ M to visualise the DNA markers when exposed to UV light. Set gels were equilibrated by immersion in 0.5 x TBE buffer for 15 - 30 minutes at 4 °C.

Gels were removed from the buffer and loaded at the bench. 120 ng of 1 kb plus DNA marker (GibcoBRL) was added to the middle and end lanes of each SP-PCR agarose gel. An entire PCR reaction, mixed with 5 x loading dye, was added to each of the other lanes. The loaded gel was run initially at 300 V for 15-30 minutes and then at 180 V for a further 16-18 hours at 4 °C.

2.4.5 Southern blotting

Once the gel had run sufficient distance the markers were visualised under UV light and the excess gel cut off and discarded. The gel was flipped so the underside was face-up and rinsed in dH₂O. Depurinating solution was added to cover the surface of each gel and they were shaken on a platform (100 rpm) for 10 minutes. The depurinating solution was poured off and the gels again rinsed in dH₂O. Denaturing solution was added after removal of the dH₂O and the gels were left shaking for 30 minutes. The gels were rinsed with dH₂O once more and neutralising solution was added for a minimum of 30 minutes of shaking. Hybond-N nylon membrane (Amersham) and 4

pieces of 3 MM chromatography paper (Whatman) were cut to the appropriate size of the gel (typically, 20 cm x 20 cm). 2 pieces of 3 MM paper were soaked in neutralising solution and placed on the bench protected by Saran wrap film (Dow). The gel was placed on top of the 3 MM paper followed by the Hybond-N nylon membrane. The Hybond-N nylon membrane was first soaked in dH₂O and then in neutralising solution before being placed carefully on the gel. Air bubbles were removed by applying slight pressure over the membrane. This technique was repeated a further two times with the addition of neutralising solution-soaked pieces of 3 MM paper. A thick pile of paper towels was added to the top of the assembly, followed by a glass plate and a weight of approximately 1.5 Kg. This construction was then left for 2 hours 30 minutes. After dismantling the 'Squash blot' the membrane was placed on a dry piece of 3 MM paper, DNA side face up, and transferred to the 80 °C oven for > 20 minutes. To ensure the DNA was fixed to the membrane it was placed in a Stratalinker instrument (Stratagene) and exposed to 120 mJ of UV light.

2.4.6 Visualisation of PCR products by radioactive hybridisation

2.4.6.1 Prehybridisation

Prehybridisation of the Hybond-N nylon membranes was carried out in rotating hybridisation tubes (Biometra) at 65 °C. 10 ml of hybridisation solution was added to each tube containing a maximum of 3 rolled membranes and incubated for 30 minutes. This solution was then discarded and replaced with fresh hybridisation solution and the prehybridisation repeated.

2.4.6.2 Probe production

The probe template was the PCR product obtained under the conditions described in section 2.3.4.1. The PCR template was a cloned human CAG trinucleotide repeat stretch and requires the primer pair MHD-4 and MHD-5 as replacements for MHD-16 and MHD-18. The 300 bp sized PCR product was detected by gel electrophoresis through a low melting point agarose (NuSieve GTG agarose) gel and the PCR product obtained by cutting out the resultant band. The DNA in the gel fragments was then purified using a QIAquick™ gel extraction kit (Qiagen).

To allow simultaneous detection of the DNA marker and the PCR products on the autoradiograms, 2.5 ng of the DNA marker run through the agarose gels was also added to each labelling reaction.

Several methods were used to produce the radio-labelled probe used for hybridisation.

Method 1

Table 2.8 Probe production

Labelling reaction

15.8 μ l dH₂O
~25 - 50 ng DNA template
2.5 ng of marker template
mix, spin and denature for 3 minutes at 100 °C. Transfer onto ice and add
6 μ l OLB
24 μ g BSA
5 μ Ci ³²P- α -dCTP
~2.5 - 5 U Klenow (Boehringer)
incubate at 37 °C for at least one hour.

The probe volume was then made up to 150 μ l with dH₂O and unincorporated radio-nucleotides removed by passing through a Sephadex G50 (Amersham Pharmacia) column. Readings from the scintillation counter (Bioscan/QC 2000) were obtained before and after probe clean up to check for adequate radiolabel incorporation.

Method 2

Probe production was achieved by following the protocol outlined in Ready-To-Go™ DNA Labelling Beads (-dCTP) (Amersham Pharmacia Biotech)

Method 3

Probe production was achieved by following the protocol outlined in the Ready-To-Go™ DNA Labelling Kit (-dCTP) (Amersham Pharmacia Biotech)

A final denaturing step was undertaken in all three methods by placing the probe at 100 °C for 5 minutes before adding the probe to the hybridisation tubes.

2.4.6.3 Hybridisation

Hybridisation of the Hybond-N nylon membranes was carried out in rotating hybridisation tubes at 65 °C overnight. 4 mls of hybridisation solution was used to dilute the denatured probe and provide sufficient coverage of the membranes.

2.4.6.4 Washing

The probe and hybridisation solution were removed and the membranes rinsed in wash solution. 10 mls of wash solution was then added and the tubes returned to the ovens (65 °C) and left rotating for 30 minutes. The wash solution was then removed and the rinse and wash repeated. Membranes were then removed from the hybridisation tubes and flat washed at room temperature for 15-20 minutes. This wash was carried out in a tray shaking at 100 rpm with wash solution preheated to 65 °C. Washed membranes were either dried in the 80 °C oven for 15 minutes or left to air-dry for 15 minutes and then covered in cling-film.

2.4.6.5 Film Exposure, Development and Analysis

Membranes were exposed to X-ray film (Konica) and developed using a X-Ograph Compact X2 (X-Ograph Ltd).

Initially images were obtained by overnight exposure at room temperature. An enhanced image could be produced by exposure with intensifier sheets at -70 °C overnight. Intensifier sheets, made of calcium tungstate, produce an enhanced image due to the reaction between the radioactive particles and the silver halide crystals in the X-ray film emulsion being enhanced five fold by the emission of photons from the sheets when they are hit by β particles from the radioactive membrane. Exposure with intensifier sheets is carried out at low temperatures because the silver atoms and ions formed on the X-ray film are stabilised at this temperature.

Accurate sizing of bands on SP-PCR autoradiograms was carried out using Kodak digital science 1D volume 3.5 computer software.

2.5 Quantitative ligand binding autoradiography

2.5.1 Tissue collection

Following dislocation of the neck, dissection of whole mouse brains was carried out swiftly and brains quick-frozen by lowering into dry ice-cooled iso-pentane. Brains were then wrapped in Parafilm (American National) and stored at -70 °C until use.

2.5.2 Preparation and storage of brain tissue sections

Frozen brains were mounted onto chucks using frozen specimen embedding medium (Shandon cryomatrix) and the surface of the brains covered in embedding matrix (Lipshaw) for frozen sectioning. Cryostat coronal sections of 20 μ M thickness were cut at -15 °C and thaw mounted onto subbed microscope slides. Slides were then stored at -70 °C until use.

2.5.3 Quantitative ligand binding autoradiography

Localisation of radioactive molecules bound to receptor binding sites by autoradiography produces an image in which optical density varies in accordance with the amount of bound radiolabelled ligand. Quantitative ligand binding autoradiography, therefore, allows the measurement of receptor density throughout the brain with a high level of spatial resolution.

Brain sections were incubated with 'total binding solution', comprising binding buffer containing a previously optimised amount of a radiolabelled reversible antagonist to the chosen receptor. Receptor ligands can however, interact with numerous sites on biological membranes and to account for this possibility non-specific binding was determined in a concurrent experiment utilising the 'total binding solution' containing a non-labelled displacer which preferentially binds to the chosen receptor (Table 2.9).

Table 2.9 Radiolabelled ligands and non-labelled displacers

Receptor	Ligand (conc) (reference)	Specific activity	Displacer (conc)
Opioid	[³ H]-Diprenorphine (2 nM) (Biscoe <i>et al.</i> , 1972)	50 Cimmol ⁻¹	Naloxone Hydrochloride (10 μM)
Benzodiazepine	[³ H]-Ro15-1788 (1.5 nM) (Hunkeler <i>et al.</i> , 1981)	70.8 Cimmol ⁻¹	Flunitrazepam (10 μM)
Dopamine D ₁	[³ H]-SCH23390 (0.5 nM) (Hytel, 1983)	75.5 Cimmol ⁻¹	Cis-flupenthixol (1 μM)
Dopamine D ₂	[³ H]-YM09151-2 (240 pM) (Grewe <i>et al.</i> , 1982)	85.5 Cimmol ⁻¹	Dopamine (50 μM)

conc = concentration used in main study (section 4.2)

Five brain sections were used from each animal examined. Three alternate sections were used to analyse total binding and the intervening two sections were used to assess non-specific binding. The coronal brain sections used for the studies were cut at the level with the approximate stereotaxic co-ordinates of interaural 4.48 mm and bregma 0.98 mm (Franklin and Paxinos, 1997). These sections contained the striatum and motor and somatosensory cortical brain regions.

The precise binding conditions used for each ligand were based on those found in previously published work (Cha *et al.*, 1998; Sur *et al.*, 1999; Young and Kuhar, 1979) and further optimisation of the protocols is described in section 4.2.

All brain sections were thawed to room temperature before initiation of receptor binding assays. Investigations into opioid and benzodiazepine neurotransmitter receptor densities required an initial pre-incubation step with the appropriate binding buffer to wash away any endogenous ligand still bound to the neurotransmitter receptors (Table 2.10). Following pre-incubation the binding buffer was discarded and all brain sections allowed to dry. Incubation with the appropriate total or non-specific binding solution was carried out, at the correct temperature, for the predetermined time (Table 2.10). After incubation the total or non-specific binding solution was poured off and excess ligand and displacer washed off by racking the microscope slides and washing in binding buffer (Table 2.10). All protocols were completed with a rinse in ice-cold dH₂O.

Table 2.10 Ligand binding assays - Conditions for incubations and washes

Receptor	Preincubation with binding buffer	Incubation with total or non-specific binding solution	Washes* with binding buffer
Opioid	15 min/RT	1 h/RT	2 x 5 min/RT
Benzodiazepine	3 x 10 min/4 °C	2 h/4°C	2 x 1 min/4 °C
Dopamine D ₁	N/A	150 min/RT	2 x 10 min/RT
Dopamine D ₂	N/A	3 h/RT	2 x 10 min/RT

N/A = not applicable, RT = room temperature. *All washes were followed by a rinse in ice-cold dH₂O.

Washed slides were dried rapidly in front of a fan for approximately 1 hour and then left overnight at room temperature. The microscope slides, with the appropriate animals I.D. numbers clearly displayed, were attached firmly to card along with a set of autoradiographic [³H]-microscale tritium standards (High 1.4 - 33.3 nCi/mg TE) (Amersham). The cards were then exposed to tritium sensitive film, HyperfilmTM-³H (Amersham) or BioMax MR-1 film (Kodak Scientific Imaging) for a predetermined period to provide images of the appropriate intensity (Table 2.11).

Table 2.11 Ligand binding assays - X-ray films and exposure times

Receptor	Film	Exposure (Duration and temperature)
Opioid	Hyperfilm	3 wks RT
	Biomax MR-1	4 wks RT
Benzodiazepine	Hyperfilm	3 wks RT
	Biomax MR-1	4 wks RT
Dopamine D ₁	Hyperfilm	2 wks RT
	Biomax MR-1	3 wks RT
Dopamine D ₂	Hyperfilm	2 wks RT
	Biomax MR-1	3 wks RT

wks = weeks, RT = room temperature

2.5.4 Development of autoradiographic films

Exposed films were developed with intermittent shaking for 5 minutes using X19 liquid developer (Kodak) followed by incubation in liquid fix (Kodak) for 10 minutes. Films were then rinsed in continuously flowing water for 30 minutes and dried.

2.5.5 Data analysis

2.5.5.1 Image capture and analysis

Autoradiogram images were captured by the MCID M4 image analyser and analysed using the MCID volume 4.3 imaging software (Imaging research Inc).

Image analysis compares the optical density on the film provided by the tritium standards, representing eight different values of the tissue equivalent (TE) tritium concentration (Figure 2.1A and B), to the optical density produced by the brain sections processed through the receptor binding assays (Figure 2.1C).

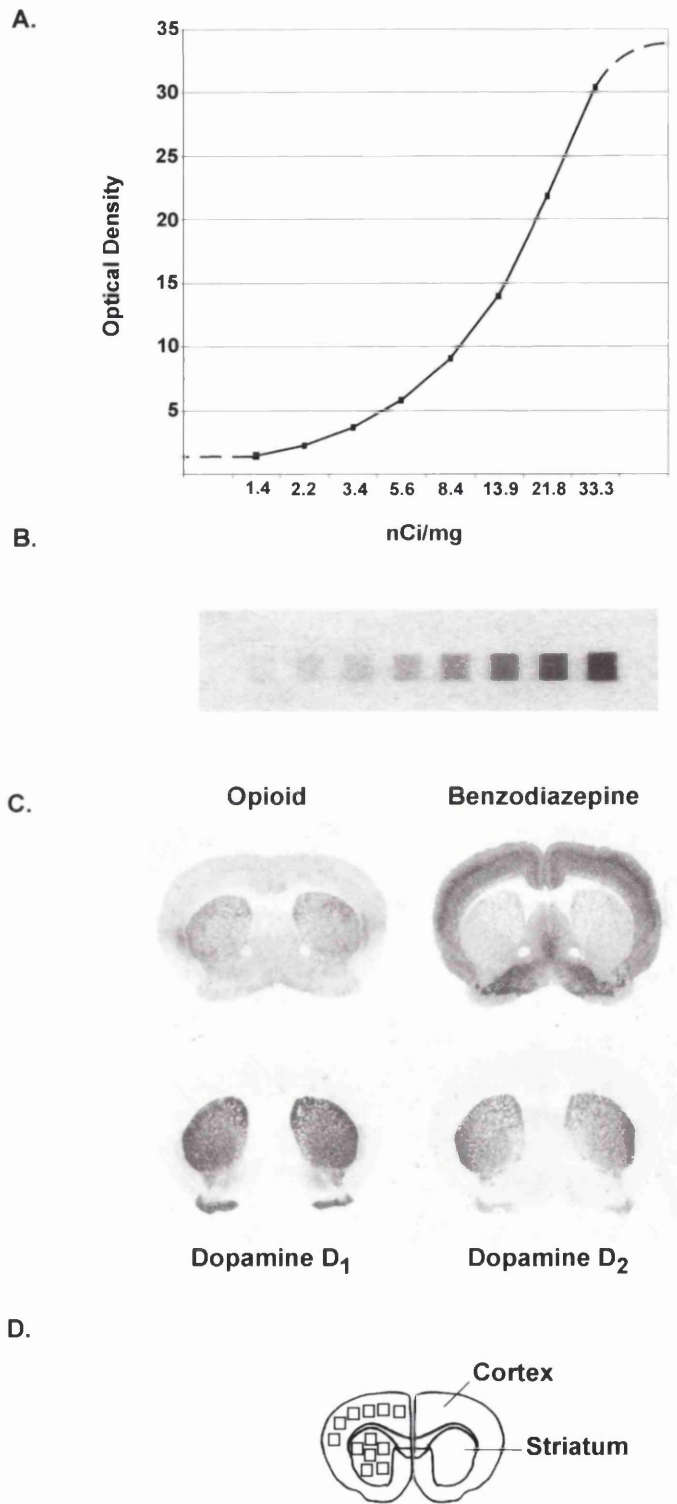


Figure 2.1 Comparing the optical density of the tritium standards and the binding brain sections to establish a measure of bound radiation per mg of tissue

A. The standard curve produced by the eight values obtained from the autoradiographic microscale tritium standards. The optical density of the standards (**B.**) was converted to a measure of radiation per mg of tissue (nCi/mg) using the manufacturer's values of tissue equivalent radiation. Using this standard curve the optical density produced by the brain sections (**C.**) was converted into a value of radiation per mg of tissue. **D.** A diagram of a coronal brain section at the stereotaxic co-ordinates of interaural 4.48 mm and bregna 0.98 mm illustrating the two brain regions (striatum and cortex) investigated in these studies. The left hemisphere of the brain illustrates the areas used and the number of optical density readings taken in the image capture and analysis (section 2.5.5.1).

Twelve readings for the cortex and striatum (Figure 2.1D) were taken for each total binding brain section, resulting in 36 data points per animal per brain region. Optical density of the standards was converted to a measure of radiation per mg of tissue (nCi/mg) using the manufacturer's values of tissue equivalent radiation, calibrated for the auto-absorptive features of intact brain grey matter. Using these standard values, the optical density data points were converted to 'specific binding', a measure representative of the total radiation associated with a particular mass of tissue. Specific binding, (that is non-specific binding subtracted from total binding) was automatically calculated by taking one reading for a specific area of each brain region. This was possible because the image of the non-specific brain section was superimposed onto the captured image of the total binding brain section. The mean of the 36 specific binding values was then calculated resulting in 1 data point for each animal per brain region. Since each ligand has a specific activity value (a measure of the amount of radioactivity in a molar solution of the ligand (Ci mol^{-1})) the data point was finally converted to a measure of ligand concentration per weight of tissue (typically, fmol/mg tissue). This value is thought to be representative of the number of receptor binding sites in that weight of tissue and is referred to in the text by 'neurotransmitter receptor density'.

2.5.5.2 Statistical analyses of data

All data (neurotransmitter receptor density) was analysed primarily by comparing wild-type and HD^{+/-} mice with the unpaired, two-tailed, Student's *t*-test. Further analysis of data obtained was carried out by two-way ANOVA. All neurotransmitter receptor densities in this text are expressed in fmol/mg tissue equivalent as a mean \pm one S.D.

2.6 Behavioural Paradigms

2.6.1 Gait analysis

2.6.1.1 Measurement of velocity and vertical reaction forces in mice

To obtain quantitative gait parameters from mice during spontaneous locomotion the apparatus shown in Figure 2.2A was used. This general set-up can be used to gather two different kinds of locomotor data; spatiotemporal data, including velocity and vertical reaction forces, i.e. the force transmitted by a paw (load).

All experiments were carried out in a soundproofed laboratory to which all mice had been habituated for 24 hours in a 12:12 light:dark cycle. All observations were made between 1000 and 1300 hours to minimise possible effects of diurnal variability. Each mouse was weighed before the beginning of the procedure as body weight is taken into account when analysing vertical reaction forces.

Velocity was assessed in an inverted U-shaped Plexiglas tunnel 98 cm (L) x 4 cm (W) x 6.5 cm (H) located over a glass floor. Light was shone into the long edge of the 30 cm central section of the floor using an 8-W fluorescent tube. The tube was shielded to prevent light escaping anywhere except into the glass causing it to be internally reflected between the top and bottom surfaces. This internal light means when a paw touches the surface of the glass floor the contact points show up as brightly illuminated areas (Figure 2.2B and C). Images of the moving mice were recorded from below using Panasonic wv-BP310 cameras. For high quality image resolution the camera must be close to the glass floor and therefore two cameras were needed to film the entire central area. The cameras were deployed with a JVC TK-C50E video effector to provide a split-screen image with information from both cameras (Figure 2.2B). The images from the cameras were recorded onto tape (Fuji 180) using a Panasonic AG 7350 video cassette recorder.

The apparatus to measure vertical reaction forces was a variant on that described in the previous paragraph. Another glass-floored Plexiglas chamber 120 cm (L) x 12 cm (W) x 12 cm (H) was used with the 30 cm central floor section divided into 6, 10 x 8 cm pieces of high quality 5 mm thick glass plates (Avimo Ltd). Four of the plates were internally illuminated as described above to allow the visualisation of the paw contact points. Another 4 plates, 2 common with the internally illuminated 4, form pressure sensitive load cell platforms (Uniweigh FSO cell, Maywood Instruments).

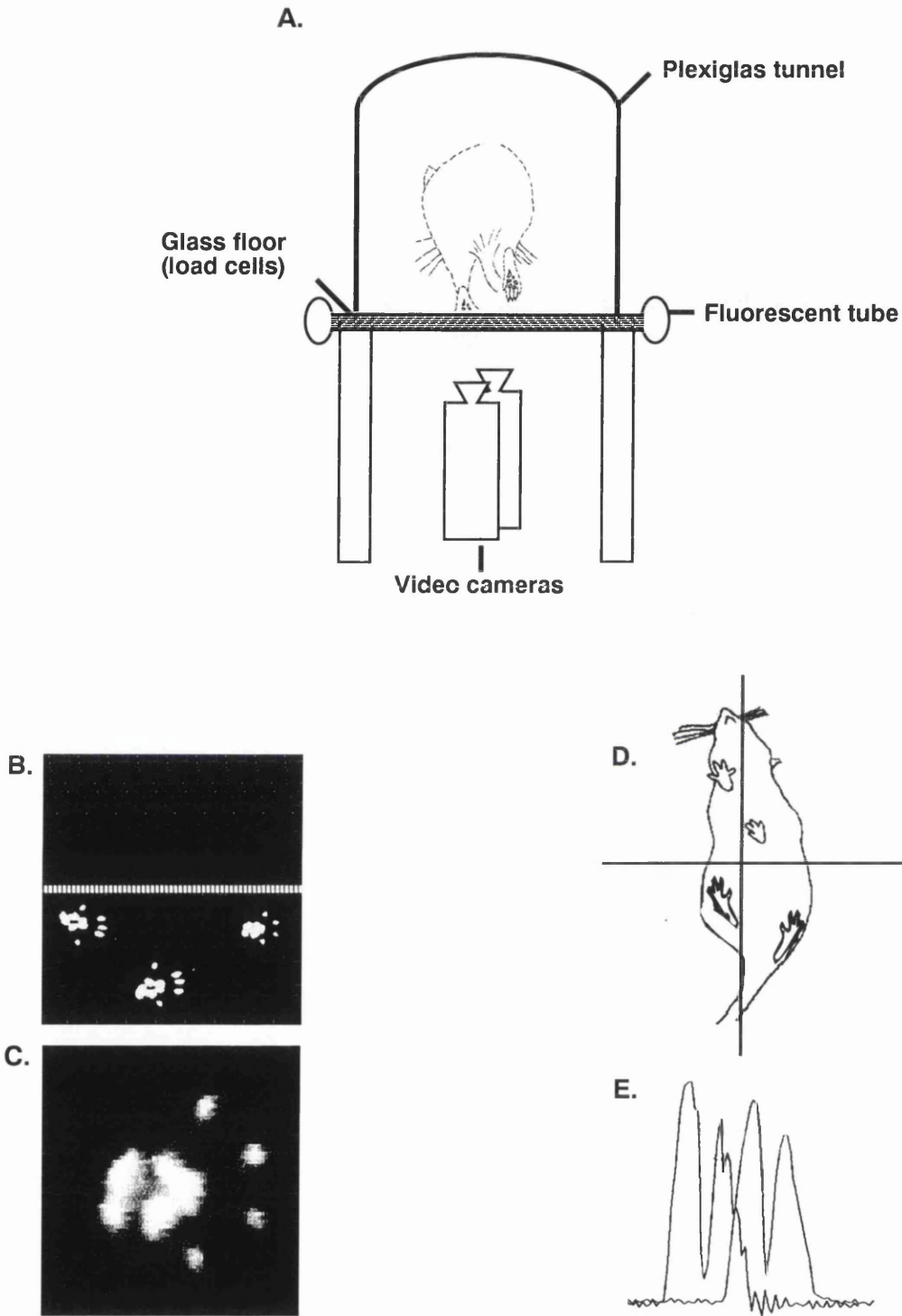


Figure 2.2 Gait analysis apparatus

A. A diagrammatic cross section of the general testing chamber to assess velocity and vertical reaction forces in mice. **B.** and **C.** Representative images of mouse paw prints. Contact points are illuminated due to internally reflected light within the glass floor. Illuminated paw contact points help visualisation of paw placement by the mouse. **D.** A diagrammatic underside image of a mouse in locomotion crossing the four load cells. **E.** A representative trace detected from the load cells, illustrating the vertical reaction forces transmitted by each paw (see figure 2.3). (Diagram modified from Clarke and Still, 1999)

The output from these load cells was captured by a data acquisition system sampling at 200 Hz (Powerlab 400 series) and analysed in an Acer PC running Chart on Windows software shown in Figure 2.2E (AD Instruments Ltd). Data collection was restricted to when the mouse was moving across the load cells by the incorporation of a trigger threshold switch that began recording only when a load cell was triggered by a weight > 5 g. This trigger also activated a 500 ms pre-trigger recording period to ensure full data collection. The cameras positioned below the central part of the chamber recorded the underview of the mouse walking (Figure 2.2D). This meant that detailed analysis could be performed on the data stored in the Chart files by assigning particular load profiles to the limbs transmitting them (Figure 2.3).

2.6.1.2 Data analysis

Typically, normal mouse gait is symmetrical in the left/right axis with limbs on both sides of the body transmitting the same force. The distribution of weight however is not symmetrical when examining the fore/hind axis. A normal mouse gait shows that the fore limbs exert greater load than the hind limbs by approximately 4 % of the animal's body weight (Clarke and Still, 1999)

A mean load for each limb was calculated by assigning each peak on the trace (Figure 2.3) to each paw print captured on video. By measuring the force exerted onto the load cell by the paw and taking into account the body weight of the animal a measure of load for that limb, expressed as a percentage of body weight, was produced. This was carried out for 8-15 peaks for each limb from each animal and a mean load for each limb was then calculated.

At the 4 and 12 month old time points each animal was put through the apparatus 3 times, once a week for three consecutive weeks. Each experiment was terminated after 5 minutes and the mean load for each limb calculated from 8-15 runs over the load cell apparatus. A final mean value for each limb, for each mouse was calculated from the three means from the experiments. The 9 month old animals were, due to time constraints, put through the apparatus once and the mean from 8-15 runs used as the overall mean for each limb.

All figures show the mean vertical reaction forces (load) as a percentage of body weight \pm one S.E. These data were obtained for fore, hind, left or right limbs by calculating the mean load between both limbs of each category.

When assessing if cohorts exert significantly more load through a particular group of limbs (fore or hind or right or left) compared to the load exerted through the same group of limbs in the other cohort, the mean loads of a particular group of limbs were compared between cohorts using the Mann-Whitney U statistical test.

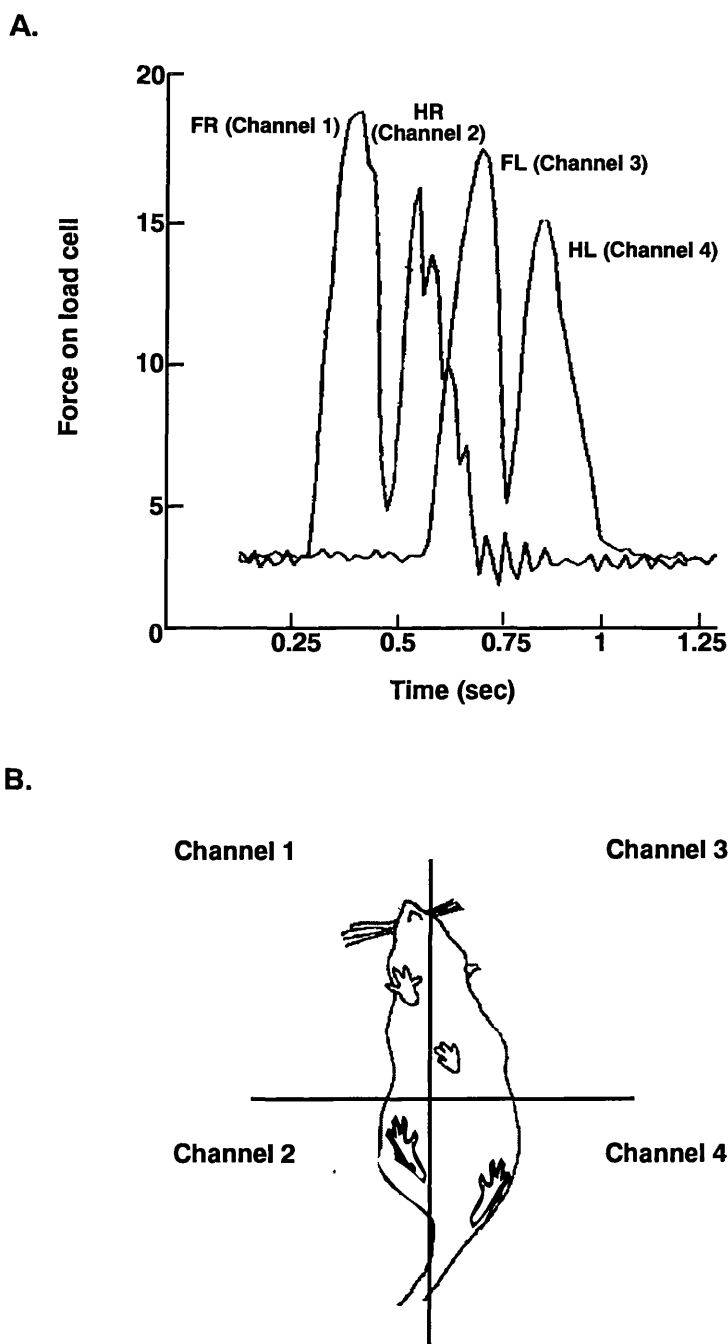


Figure 2.3 Measuring vertical reaction forces in mice

A. A representative example of the trace obtained when a mouse has traversed the four load cells. Each peak on the trace indicates vertical reaction force against time (seconds). **B.** The image captured from below the load cells enables limb assignment to the corresponding loads on the trace. FR = Fore right limb, HR = Hind right limb, FL = Fore left limb, HL = Hind left limb.

To examine the distribution of weight during locomotion the mean hind limb load was subtracted from the mean fore limb load and the mean left limb load from the mean right limb load. Gait was therefore assessed in two planes, side to side and front to back. The resulting difference between the mean loads was analysed using a Mann-Whitney U statistical test to determine if weight distribution of HD^{+/-} and wild-type mice was significantly different.

The velocity at which the mouse was travelling at each peak was calculated so that measures of gait were only obtained when animals were travelling between 10-45 cms⁻¹. This ensured that gait was analysed during walking.

Velocity of the mice was measured in cms⁻¹ by calculating the number of video frames needed for the mouse to walk over 4 load cells, 10 cm in length. A mean velocity for each mouse was determined and the wild-type and HD^{+/-} mice cohorts then compared using the unpaired, one-tailed, Student's *t* test.

2.6.1.3 Cohorts

The initial study to assess gait of HD^{+/-} mice was performed on a cohort of HD^{+/-} mice and their wild-type littermates at 12 months of age (group 1). Further studies to investigate the temporal nature and onset of gait abnormalities utilised a cohort of mice assessed twice, once at age 4 months and again at 9 months (group 2). Group 1 consisted of 6 HD^{+/-} mice (3 males and 3 females) and 6 wild-type littermates (3 males and 3 females). Group 2 contained 10 HD^{+/-} mice (5 female, 5 male) and 10 wild-type littermates (5 female and 5 male). All mice used in these studies are described in Table 2.1. One male wild-type mouse from group 2 died in the intervening time between test points and is therefore missing from the 9 month cohort. Group 2 allowed comparisons to be made between male and female mice, however, the numbers in group 1 were too few to allow comparison of the sexes.

2.6.1.4 Acknowledgements

Data collection for mouse groups at the 4 and 12 month time points was carried out by Jackie Still and Linda Grant in Dr Ken. A. Clarke's laboratory at the University of Sheffield where the gait analysis instrumentation is housed. All experiments with the intermediate, 9 month old, mouse group were carried out and analysed by Laura Kennedy. The data obtained from all time points was prepared and statistically analysed by Laura Kennedy.

2.6.2 Spatial learning and memory

2.6.2.1 Rotating Holeboard Paradigm

To investigate possible cognitive deficits in HD mice, spatial learning and memory was assessed using the cognitive behavioural paradigm, the rotating holeboard (Brosnan-Watters and Wozniak, 1997).

Mice used in this paradigm had been handled by the experimenter three times weekly from weaning and all animals went through a process of apparatus habituation for 4 weeks prior to testing, in an attempt to minimise the stress response. Habituation involved handling by the experimenter and placement into the start box and release into the rotating holeboard apparatus. As the design of the start box was altered all animals were re-habituated to the release procedure. Mice were placed in the new start box 3 times weekly and released into the apparatus a minimum of 5 times in each habituation session. The apparatus was assembled in the same configuration as in the future tests, but each hole contained inaccessible and accessible food baits. Animals were housed in the testing room from weaning and all experiments were carried out between 0930 and 1130 hours to reduce the influence of any diurnal effects.

The rotating holeboard was made up from several components (Figure 2.4A): 1. a square Perspex board with 16 holes cut into the floor in a 4 x 4 matrix (Figure 2.4A(a)), 2. clear Perspex sides to enclose the board and allow uninterrupted views around the room (Figure 2.4A(b)), 3. an opaque plastic insert placed on the board covering all but four corner holes (Figure 2.4A(c)), 4. punctuated screens that cover the holes but allow odour to be released (Figure 2.4A(d)), 5. a turntable for the entire apparatus, making rotation easy (Figure 2.4A(e)).

Once assembled (Figure 2.4B) the apparatus was placed in the centre of a testing room and the visual cues set up. The visual cues were conspicuous and constant: 1. green cloth covering home cages (Figure 2.4C(i)), 2. black video camera and recorder (Figure 2.4C(ii)), 3. red Perspex sheet in front of home cages (Figure 2.4C(iii)) and 4. experimenter wearing blue laboratory coat (Figure 2.4C(iv)).

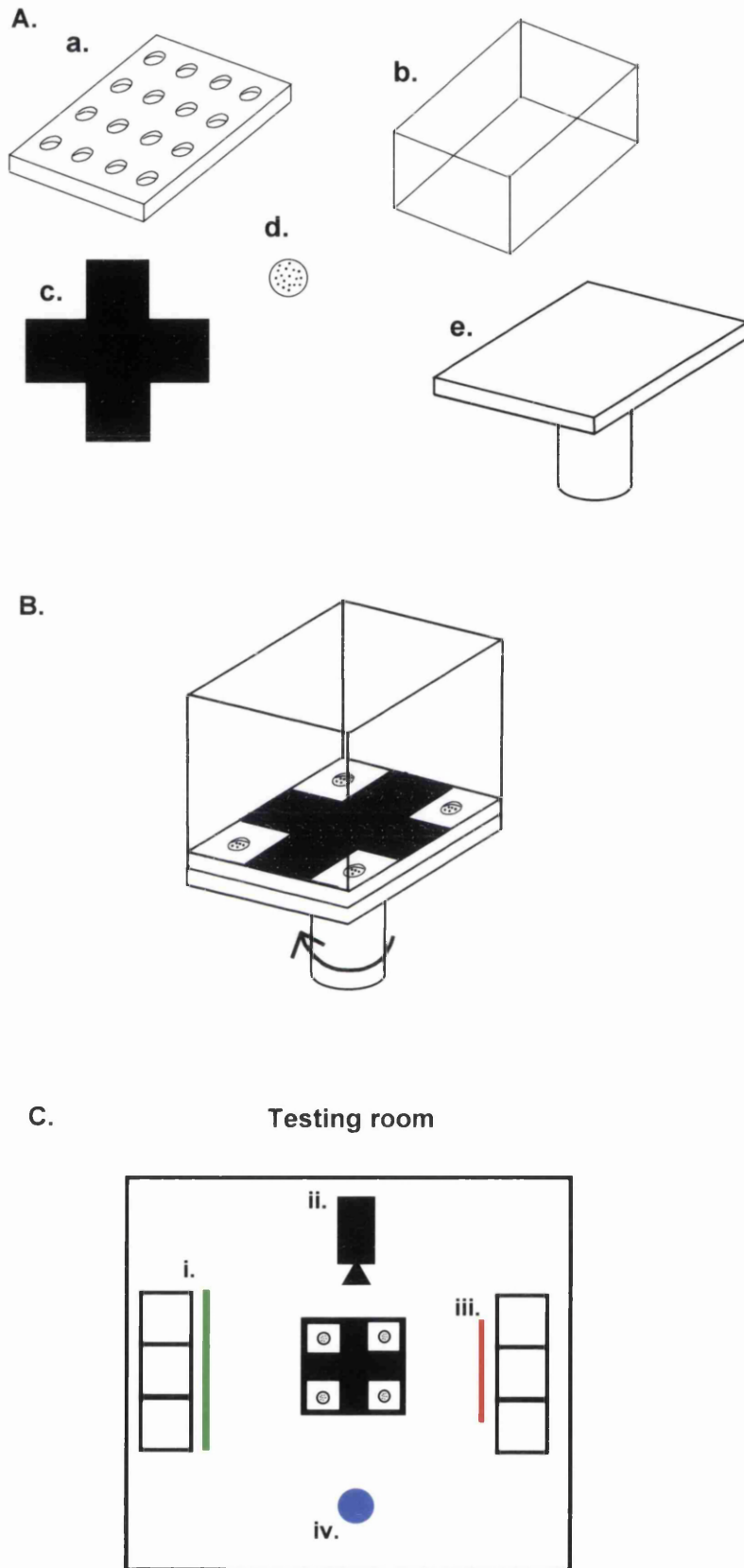


Figure 2.4 Rotating holeboard apparatus

A. Diagrammatic representations of the individual pieces which make up the rotating holeboard apparatus.
B. The rotating holeboard apparatus when assembled and placed on the rotating stand.
C. An overhead view of the testing room with the rotating holeboard apparatus in the centre and the constant visual cues around the room.

In order to test spatial learning and memory the aim of the paradigm was to locate the bait, a small piece of cereal, whose relative position was maintained with respect to the visual cues. To ensure that spatial learning and memory were investigated olfactory and tactile cues were eliminated. To negate olfactory cues a constant and general food odour was achieved by placing a large piece of cereal under the punctuated screens covering the four corner holes. In addition to this constant inaccessible bait, the small accessible bait was placed on top of the screen in one of the holes. Following each trial the apparatus was dismantled and cleaned with detergent (TriGene II, MediChem International). To protect against possible tactile cues provided by the apparatus the entire construction was rotated after every trial in a pseudo-random manner. The mouse was released into the apparatus from a start box, this ensured that the animal was always placed in the centre of the apparatus and did not receive any information about the apparatus set-up prior to the initiation of the experiment.

To encourage the animals to find the bait, food was withdrawn overnight prior to testing. A trial was terminated when the mouse had found the bait or when 3 minutes had elapsed. During the trial data collection involved scoring the number of times the animal poked its nose into an incorrect hole. A successful trial was deemed as one where the mouse found the bait prior to any incorrect nose pokes. The entire experiment was terminated when 8 out of 9 consecutive trials were successful. The experimenter carried out data collection during the trial as well as simultaneous recording of the experiment on videotape. This allowed the scores to be double checked and verified by a second experimenter. Food was withdrawn from the mice overnight again and the experiment repeated using the same criteria the next day to assess if learning had been retained.

2.6.2.2 Cohorts

All mice used in the experiments are described in Table 2.1. HD^{+/-} and wild-type mice of both sexes were investigated and all mice were 6 months of age.

3 Investigating phenotypic alterations in a knock-in mouse model of Huntington's disease

3.1 Aims of the study

The following studies were designed to further investigate possible phenotypic alterations in this HD mouse model. It is necessary to determine the nature, onset and progression of phenotypic changes to establish if the phenotypic consequences of the HD mutation are reminiscent of symptoms seen in human HD patients. Investigations into different aspects of phenotypic alteration such as movement disorder and cognitive decline would provide further understanding into the relationship between several different aspects of phenotypic change. Understanding phenotypic alterations may offer insights into the possible molecular and cellular consequences of the HD mutation and their downstream effects. In depth investigations may establish whether the same underlying mechanisms are responsible for all phenotypic alterations. In addition, quantification of any phenotypic consequences of the HD mutation will provide markers of the disease process, allowing the effectiveness of future HD therapies to be assessed.

3.2 Gait analysis in wild-type and HD^{+/-} mice

3.2.1 Aims of the study

The aim of the following study was to ascertain if HD mice display alterations in gait, during spontaneous locomotion. Gait abnormalities such as lack of movement control and co-ordination are prominent symptoms associated with human HD (see section 1.1.1.1). Using gait analysis apparatus and associated data acquisition equipment described in section 2.6.1.1, load exerted through limbs, weight distribution and velocity were assessed to establish if HD^{+/-} mice possess an altered gait compared to their wild-type littermates. Wild-type and HD^{+/-} mice of various ages were investigated to determine the progressive nature of any alterations in gait. Previous studies investigating co-ordination and balance within these HD^{+/-} mice have illustrated significant differences between males and females (C-M Chen, unpublished data). Although there is no evidence in the literature that the course or severity of HD is significantly different in male and female HD patients, phenotype can be highly variable between human patients and no detailed studies on sex differences in human HD have been carried out. To investigate differences in the phenotype of male and female HD^{+/-} mice animals of both sexes were used in the studies. These investigations will also illustrate whether mixed cohorts could be used in subsequent behavioural studies.

3.2.2 Gait analysis in 4 month old wild-type and HD^{+/-} mice

Gait analysis was performed as described in section 2.6.1. The mean load transmitted through the limbs, the difference between the loads for different groups of limbs and body weight have been investigated for 4 month old wild-type and HD^{+/-} mice. The mean body weights for wild-type and HD^{+/-} mice are presented in Table 3.1. The data representing the load transmitted through each group of limbs (fore, hind, left and right) is expressed as a percentage of body weight and is presented in Table 3.2.

The body weights of wild-type (26.6 ± 0.9 g) and HD^{+/-} (25.3 ± 1.3 g) mice were not significantly different at 4 months of age (Table 3.1, $p=0.2$).

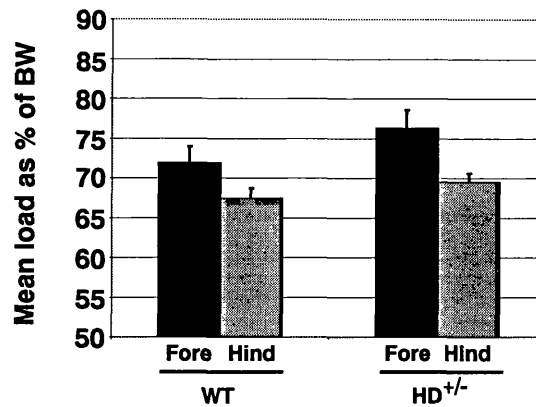
Table 3.1 Summary of mean body weight for 4 month old mice assessed for gait parameters

Genotype /Sex	Number of mice	Mean body weight (grams \pm S.E.)	*p value
WT	10	26.6 ± 0.9	0.2
HD ^{+/-}	10	25.3 ± 1.3	
Male WT	5	28.1 ± 1.4	0.5
Male HD ^{+/-}	5	28.3 ± 1.5	
Female WT	5	25.1 ± 0.86	0.03
Female HD ^{+/-}	5	22.2 ± 0.9	

* comparing mean body weight between wild-type and HD^{+/-} mice using the unpaired, one-tailed, Student's *t*-test.

The mean load transmitted through the fore limbs of wild-type mice was 71.9 ± 2.04 percent of their body weight (%) and the mean load transmitted through the hind limbs was 67.5 ± 1.20 %. Wild-type mice appeared to be transmitting a greater force through their fore limbs than their hind limbs (Figure 3.1A and Table 3.2). This is in accordance with previously published data stating that normal mouse gait is asymmetrical across the fore/hind axis, with approximately 4 % greater load exerted through the fore limbs (Clarke and Still, 1999). The HD^{+/-} mice displayed the same asymmetrical distribution of weight across the fore/hind axis. The mean load transmitted through the fore limbs was 76.3 ± 2.29 % and 69.5 ± 1.1 % through the hind limbs (Figure 3.1A and Table 3.2).

A.



B.

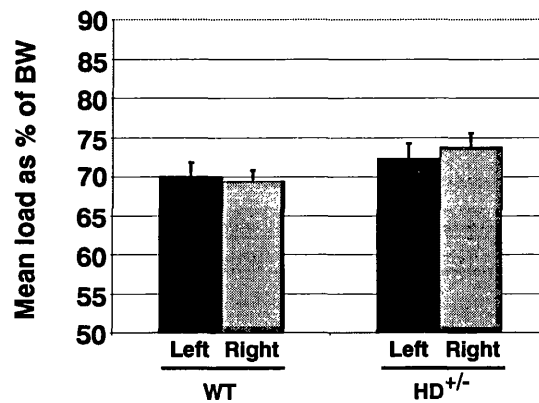


Figure 3.1 The mean load exerted through the limbs of 4 month old wild-type and HD^{+/-} mice

The bar graphs show the mean load, expressed as a percentage of body weight (BW) \pm one standard error, transmitted through all four groups of limbs (fore, hind, left and right) in 4 month old wild-type and HD^{+/-} mice. **A.** A normal mouse gait displays asymmetry across the fore/hind axis with the fore limb transmitting greater load than the hind limb. The median difference between the fore and hind limb loads in wild-type (n=10) and HD^{+/-} mice (n=10) were compared using the Mann-Whitney U statistical test and no significant difference in weight distribution was detected (p=0.2). **B.** A normal mouse gait displays symmetry across the left/right axis. The median difference between the left and right limb loads in wild-type (n=10) and HD^{+/-} mice (n=10) were compared using the Mann-Whitney U statistical test and no significant difference in weight distribution was detected (p=0.1).

Table 3.2 Summary of the mean loads, as a percentage of body weight, exerted through all groups of limbs in 4 month old mice

Genotype/ Sex	Number of mice	Mean load (% BW \pm S.E.)			
		Fore	Hind	Left	Right
WT	10	71.9 \pm 2.04	67.5 \pm 1.2	70.03 \pm 1.82	69.4 \pm 1.43
HD ^{+/-}	10	76.3 \pm 2.29	69.5 \pm 1.1	72.3 \pm 1.92	73.8 \pm 1.80
Male WT	5	69.6 \pm 3.73	65.16 \pm 1.81	68.1 \pm 3.31	66.71 \pm 2.26
Male HD ^{+/-}	5	81.2 \pm 3.05	71.2 \pm 1.61	75.4 \pm 2.78	77.6 \pm 2.4
Female WT	5	74.2 \pm 1.42	69.8 \pm 0.78	71.9 \pm 1.48	72.05 \pm 0.75
Female HD ^{+/-}	5	71.3 \pm 1.46	67.9 \pm 1.21	69.3 \pm 2.06	69.92 \pm 1.21

To assess whether the difference between the loads exerted by the fore and hind limbs differs in wild-type and HD^{+/-} mice the mean loads across the hind limbs were subtracted from that of the fore limbs and the resultant measure of weight distribution analysed by the Mann-Whitney U statistical test. The median difference between the fore and hind limb loads in wild-type mice was 4.9 \pm 1 % and in HD^{+/-} mice 6.3 \pm 1.4 %. There was no significant difference (p=0.2) between the median difference of the loads transmitted through the fore and hind limbs in wild-type mice and HD^{+/-} mice (Table 3.3).

Table 3.3 The median distribution of weight between the fore and hind limbs and the left and right limbs in all cohorts and the p values resulting from the Mann-Whitney U statistical test when comparing the median difference between loadings in wild-type and HD^{+/-} mice

Genotype /Sex	Number of mice	Weight Distribution			
		F-H (%BW \pm S.E.)	p value*	L-R (%BW \pm S.E.)	*p value
WT	10	4.9 \pm 1	0.2	0.93 \pm 0.8	0.1
HD ^{+/-}	10	6.3 \pm 1.4		-1.5 \pm 1.5	
Male WT	5	6.1 \pm 1.9	0.09	1.32 \pm 1.2	0.1
Male HD ^{+/-}	5	11.9 \pm 1.5		-1.4 \pm 2.1	
Female WT	5	4.8 \pm 0.85	0.7	0.54 \pm 0.95	0.3
Female HD ^{+/-}	5	3.9 \pm 1.33		-1.6 \pm 2.4	

F-H = the median of the values obtained for the difference between the mean loads of the fore and hind limbs. L-R = the median of the values obtained for the difference between the mean loads of the left and right limbs. * comparing F-H and L-R in wild-type and HD^{+/-} mice using the Mann-Whitney U test.

Previous investigations into normal mouse gait have illustrated that the loads transmitted through the left and right limbs are similar, resulting in a symmetrical gait (Clarke and Still, 1999). In agreement with these findings, the mean loads for left and right limbs in 4 month old wild-type mice were $70.03 \pm 1.82 \%$ and $69.4 \pm 1.43 \%$, respectively (Figure 3.1B and Table 3.2). The left and right limbs of HD^{+/-} mice were also very similar, $72.3 \pm 1.92 \%$ and $73.8 \pm 1.80 \%$, respectively (Figure 3.1B and Table 3.2). No significant difference ($p=0.1$) was found when the median difference between the left and right limb loads in wild-type mice ($0.93 \pm 0.8 \%$) and HD^{+/-} mice ($-1.5 \pm 1.5 \%$) were compared suggesting a symmetrical gait for mice with and without the HD mutation (Table 3.3).

The limb loadings of 4 month old wild-type and HD^{+/-} mice all showed the pattern of weight distribution expected of a normal mouse gait. When comparing the differences between the limb loadings across the fore/hind and left/right axis no significant differences were observed between wild-type and HD^{+/-} mice. These studies have illustrated that the gait of 4 month old HD^{+/-} mice does not differ from the wild-type controls.

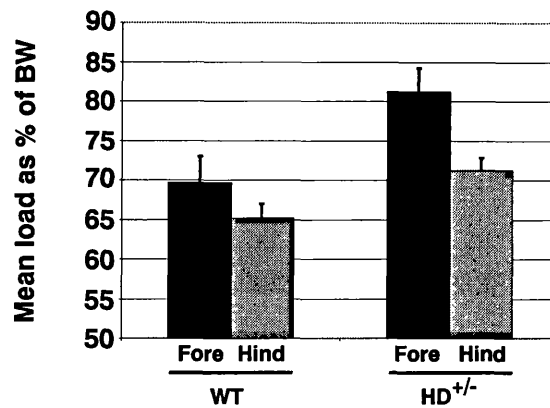
3.2.2.1 Investigating sex differences in gait of 4 month old mice

The cohorts of 4 month old mice used in section 3.2.2 consisted of equal numbers of male and female animals. In order to establish if mean loads transmitted, difference between limb loadings and body weight differ in male and female mice, the data were separated according to sex, and re-analysed.

3.2.2.1.1 Male mice

The mean load transmitted by the fore limbs of wild-type male mice was measured at $69.6 \pm 3.73 \%$ and the mean load transmitted through the hind limbs was $65.16 \pm 1.81 \%$ (Table 3.2). Again this corresponds to the typical mouse gait as the fore limbs exert more force than the hind limbs (Figure 3.2A). This pattern is also repeated in the male HD^{+/-} mice with the load from the fore limbs measured at $81.2 \pm 3.05 \%$ and the hind limbs at $71.2 \pm 1.61 \%$ (Table 3.2, Figure 3.2A). The maintenance of a typical asymmetrical gait in male mice carrying the HD mutation was confirmed when the median difference between the fore and hind limb loads was statistically compared to wild-type controls and no difference was found (Table 3.3, $p=0.09$).

A.



B.

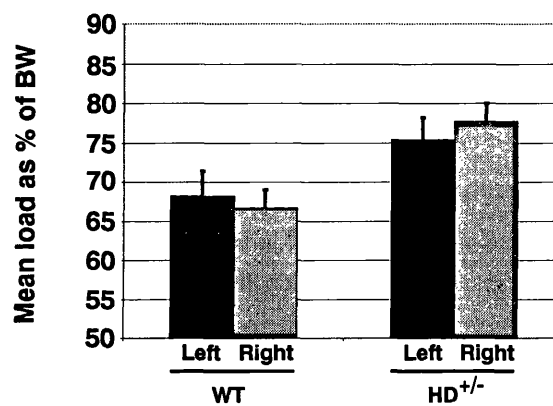


Figure 3.2 The mean load exerted through the limbs of male 4 month old wild-type and HD^{+/-} mice

The bar graphs show the mean load, expressed as a percentage of body weight (BW) \pm one standard error, transmitted through all four groups of limbs (fore, hind, left and right) in male 4 month old wild-type and HD^{+/-} mice. **A.** A normal mouse gait displays asymmetry across the fore/hind axis with the fore limb transmitting greater load than the hind limb. The median difference between the fore and hind limb loads in wild-type (n=5) and HD^{+/-} mice (n=5) were compared using the Mann-Whitney U statistical test and no significant difference in weight distribution was detected (p=0.09). **B.** A normal mouse gait displays symmetry across the left/right axis. The median difference between the left and right limb loads in wild-type (n=5) and HD^{+/-} mice (n=5) were compared using the Mann-Whitney U statistical test and no significant difference in weight distribution was detected (p=0.1). Male HD^{+/-} mice seemed to transmit greater loads through all limb groups compared to their wild-type controls. Statistical analysis of each limb group between wild-type and HD^{+/-} mice showed a significantly greater load transmitted through the hind (p=0.04) and right (p=0.04) limbs of HD^{+/-} mice compared to wild-type controls (Mann-Whitney, Fore, p=0.06, Left, p=0.3).

Male mice also demonstrate retention of the symmetrical gait when investigating left and right limb loadings. The wild-type mice showed a mean load of 68.1 ± 3.31 % for the left limbs and a mean load of 66.71 ± 2.26 % for the right limbs (Table 3.2, Figure 3.2B). In HD^{+/-} mice the left limbs transmitted a mean load of 75.4 ± 2.78 % and the right limbs a mean load of 77.6 ± 2.4 % (Table 3.2, Figure 3.2B). When the median differences between left and right limb loading in wild-type and HD^{+/-} mice were compared there was no significant difference between the cohorts (Table 3.3, $p=0.1$).

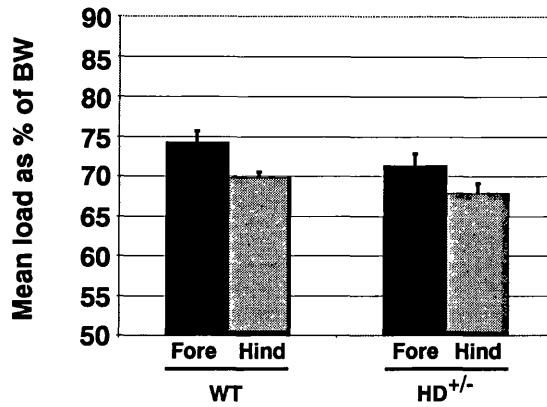
Male HD^{+/-} mice do, however, transmit greater peak loads from all limbs compared to their wild-type counterparts. When the mean loads for each limb were compared using the Mann-Whitney U statistical test, the hind ($p=0.04$) and right ($p=0.04$) limbs were found to exert significantly more force in HD^{+/-} mice compared to their wild-type littermates (Figure 3.2). As no significant difference between body weight in wild-type (28.1 ± 1.4 g) and HD^{+/-} (28.3 ± 1.5 g) male mice (Table 3.1) was detected and the velocity between wild-type and HD^{+/-} mice, at a later time point (section 3.2.5), showed no significant difference, the reason male mice exert greater peak loads through their hind and right limbs is unknown but suggests some variation in limb placement perhaps due to poorer co-ordination between limb placements or different posture during movement.

The limb loadings of male 4 month old mice all displayed the pattern of weight distribution expected of a normal mouse gait. When the median differences between the mean loads across the fore/hind and left/right axis were compared between wild-type and HD^{+/-} mice, no significant differences were detected. Male 4 month old HD^{+/-} mice displayed a gait that was not significantly different from their wild-type controls. This result was consistent with the results obtained from the cohorts containing both male and female mice in section 3.2.2.

3.2.2.1.2 Female mice

In female wild-type mice the fore and hind limb mean loads were 74.2 ± 1.42 % and 69.8 ± 0.78 %, respectively and HD^{+/-} mice exerted mean loads of 71.3 ± 1.46 % through the fore limbs and 67.9 ± 1.21 % through the hind limbs (Table 3.2, Figure 3.3A). The asymmetrical gait across the fore/hind axis previously observed in both male wild-type and HD^{+/-} mice is also apparent in their female counterparts. The weight distribution for the two cohorts was not significantly different when the median difference between the fore and hind limb loads in wild-type animals (4.8 %) and HD^{+/-} mice (3.9 %) were compared (Table 3.3, $p=0.7$).

A.



B.

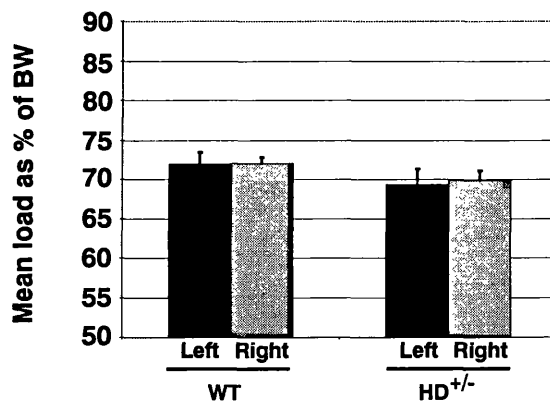


Figure 3.3 The mean load exerted through the limbs of female 4 month old wild-type and HD^{+/-} mice

The bar graphs show the mean load, expressed as a percentage of body weight (BW) \pm one standard error, transmitted through all four groups of limbs (fore, hind, left and right) in female 4 month old wild-type (n=5) and HD^{+/-} mice (n=5). **A.** A normal mouse gait displays asymmetry across the fore/hind axis with the fore limb transmitting greater load than the hind limb. The median difference between the fore and hind limb loads in wild-type (n=5) and HD^{+/-} mice (n=5) were compared using the Mann-Whitney U statistical test and no significant difference in weight distribution was detected (p=0.7). **B.** A normal mouse gait displays symmetry across the left/right axis. The median difference between the left and right limb loads in wild-type and HD^{+/-} mice were compared using the Mann-Whitney U statistical test and no significant difference in weight distribution was detected (p=0.3).

A symmetrical gait was observed in wild-type mice as the left limb mean load was 71.9 ± 1.48 % and the right limb mean load was 72.05 ± 0.75 (Table 3.2, Figure 3.3B). The HD^{+/-} mice followed this pattern and displayed mean loads for the left limbs of 69.3 ± 2.06 % and 69.92 ± 1.21 % for the right limbs (Table 3.2, Figure 3.3B). As previously shown for the combined wild-type and HD^{+/-} mice cohorts and male cohorts, the median difference between left and right limb loadings was not significantly different in the female HD^{+/-} mice compared to the wild-type controls (Table 3.3, $p=0.3$).

Unlike the male HD^{+/-} mice (section 3.2.2.1.1), female HD^{+/-} mice did not seem to exert significantly more load through their limbs when the same limb groups were compared in wild-type and HD^{+/-} mice (Figure 3.3).

In analysing the mean load data and assessing weight distributions in female 4 month old wild-type and HD^{+/-} mice a typical mouse gait was observed, consistent with the previous findings in male mice (section 3.2.2.1.1) and the combined cohort (section 3.2.2) of the same age.

The female HD^{+/-} mice displayed a mean body weight of 22.2 ± 0.9 g, a significant reduction in body weight compared to their wild-type controls (25.1 ± 0.86 g, $p=0.03$) (Table 3.1). This difference in body weight was not observed in male mice at this age. At this time point male wild-type mice do weigh significantly more than their female counterparts ($p=0.05$), however in HD^{+/-} mice the difference between male and female animals was greater ($p=0.004$). It may be that the HD mutation prevents normal weight gain at this age in female mice although previous publications have shown no difference in weight between wild-type and HD^{+/-} mice (Shelbourne *et al.*, 1999). This discrepancy may be due to the previous investigations analysing larger cohorts.

3.2.3 Gait analysis in 9 month old wild-type and HD^{+/-} mice

Gait analysis was again carried out on the wild-type and HD^{+/-} mice used in section 3.2.2 at 9 months of age to investigate any alterations in gait at a later time point.

Consistent with results from 4 month old female mice a significantly lower body weight ($p=0.03$) was observed when all HD^{+/-} (27.7 ± 0.83 g) mice were compared to wild-type mice (30.7 ± 1.27 g) at 9 months of age (Table 3.4).

Table 3.4 Summary of mean body weight for 9 month old mice assessed for gait parameters

Genotype /Sex	Number of mice	Mean body weight (grams ± S.E.)	*p value
WT	9	30.7 ± 1.27	0.03
HD ^{+/-}	10	27.7 ± 0.83	
Male WT	4	33.4 ± 1.67	0.03
Male HD ^{+/-}	5	29.36 ± 0.91	
Female WT	5	28.54 ± 1.23	0.08
Female HD ^{+/-}	5	26.12 ± 0.97	

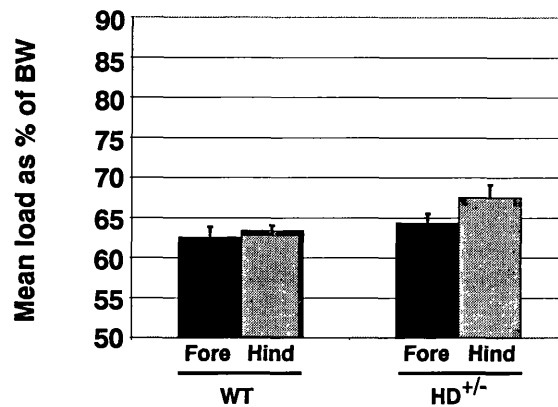
* comparing mean body weight between wild-type and HD^{+/-} mice using the unpaired, one-tailed, Student's *t*-test.

When investigating the fore and hind limb mean loads the wild-type mice displayed mean loads of 62.5 ± 1.39 % for the fore limbs and 63.3 ± 0.69 % for the hind limbs (Table 3.5). The difference in limb loadings between the fore and hind limbs was uncharacteristically symmetrical for wild-type animals (0.3 ± 1.76 %) (Table 3.6, Figure 3.4A). The mean loads in HD^{+/-} mice were observed as 64.4 ± 1.07 % for the fore limbs and 67.5 ± 1.57 % for the hind limbs (Table 3.5). This median difference between the limb loadings for the fore and hind limbs in HD^{+/-} mice (-4.8 ± 1.48 %) illustrated an even larger change from the previously normal gait observed in HD^{+/-} mice at 4 months of age. HD^{+/-} mice at 9 months of age exert greater force through their hind limbs than their fore limbs (Figure 3.4A). However, when the median difference between the fore and hind limb loadings were compared, weight distribution in the wild-type and HD^{+/-} mice was not significantly different (Table 3.6, p=0.4).

Table 3.5 Summary of the mean loads, as a percentage of body weight, exerted through all groups of limbs in 9 month old mice

Genotype/ Sex	Number of mice	Mean load (% BW ± S.E.)			
		Fore	Hind	Left	Right
WT	9	62.5 ± 1.39	63.3 ± 0.69	62.88 ± 0.78	62.93 ± 0.75
HD ^{+/-}	10	64.4 ± 1.07	67.5 ± 1.57	66.6 ± 1.66	65.29 ± 1.58
Male WT	4	63.6 ± 0.32	62.96 ± 0.43	63.3 ± 0.52	63.2 ± 0.08
Male HD ^{+/-}	5	64.7 ± 0.93	71.2 ± 0.51	67.2 ± 2.63	68.7 ± 1.91
Female WT	5	61.62 ± 2.55	63.6 ± 1.25	62.5 ± 1.40	62.74 ± 1.41
Female HD ^{+/-}	5	64 ± 2.06	63.9 ± 2.02	66 ± 2.32	61.9 ± 1.40

A.



B.

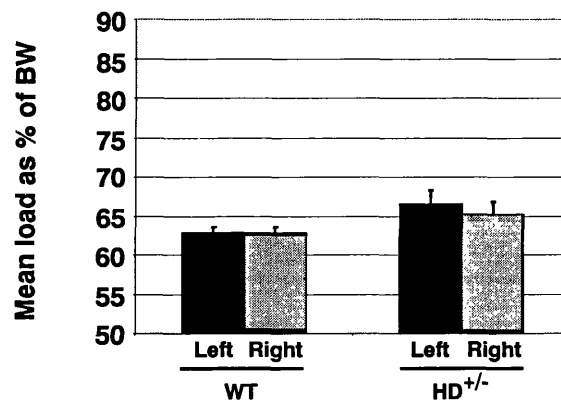


Figure 3.4 The mean load exerted through the limbs of 9 month old wild-type and HD^{+/-} mice

The bar graphs show the mean load, expressed as a percentage of body weight (BW) \pm one standard error, transmitted through all four groups of limbs (fore, hind, left and right) in 9 month old wild-type and HD^{+/-} mice. **A.** A normal mouse gait displays asymmetry across the fore/hind axis with the fore limb transmitting greater load than the hind limb. The median difference between the fore and hind limb loads in wild-type (n=9) and HD^{+/-} mice (n=10) were compared using the Mann-Whitney U statistical test and no significant difference in weight distribution was detected (p=0.4). **B.** A normal mouse gait displays symmetry across the left/right axis. The median difference between the left and right limb loads in wild-type (n=9) and HD^{+/-} mice (n=10) were compared using the Mann-Whitney U statistical test and no significant difference in weight distribution was detected (p=0.1).

Table 3.6 The median distribution of weight between the fore and hind limbs and the left and right limbs in all cohorts and the p values resulting from the Mann-Whitney U statistical test when comparing the median difference between loadings in wild-type and HD^{+/-} mice.

Genotype /Sex	Number of mice	Weight Distribution			
		F-H (%BW + S.E.)	*p value	L-R (%BW + S.E.)	*p value
WT	9	0.3 ± 1.76	0.4	0.3 ± 0.78	0.1
HD ^{+/-}	10	-4.8 ± 1.48		3.5 ± 2.35	
Male WT	4	0.65 ± 0.6	0.02	0.1 ± 0.54	0.9
Male HD ^{+/-}	5	-6.4 ± 0.9		0.9 ± 4.4	
Female WT	5	-2.8 ± 3.19	0.8	0.6 ± 1.86	0.1
Female HD ^{+/-}	5	0.6 ± 1.4		4.9 ± 1.2	

F-H = the median of the values obtained for the difference between the mean loads of the fore and hind limbs. L-R = the median of the values obtained for the difference between the mean loads of the left and right limbs. * comparing F-H and L-R in wild-type and HD^{+/-} mice using the Mann-Whitney U test.

When analysing the mean loads and weight distributions for the left and right limbs the normal symmetrical gait was observed (Figure 3.4B). Wild-type mice displayed mean loads of 62.88 ± 0.78 % for the left limbs and 62.93 ± 0.75 % for the right limbs (Table 3.5). The HD^{+/-} mice transmitted 66.6 ± 1.66 % mean load through their left limbs and 65.29 ± 1.58 % through their right limbs (Table 3.5). The median difference between left and right limb loads was not significantly different ($p=0.1$) in wild-type (0.3 ± 0.78 %) compared to HD^{+/-} mice (3.5 ± 2.35 %)(Table 3.6).

In summary, the left/right limb axis symmetry of a normal mouse gait was maintained in 9 month old wild-type and HD^{+/-} mice. Wild-type mice showed an uncharacteristic symmetrical gait when analysing the distribution of weight across the fore/hind axis. The abnormal gait was also demonstrated in HD^{+/-} mice, however, the distribution of weight was not significantly different when compared to wild-type mice.

3.2.3.1 Investigating sex differences in gait of 9 month old mice

The cohorts used in this study were the same animals investigated in section 3.2.2 and so the cohort was again separated according to sex and re-analysed.

3.2.3.1.1 Male mice

Male wild-type mice transmitted 63.6 ± 0.32 % mean load through their fore limbs and 62.96 ± 0.43 % through their hind limbs (Table 3.5). These loads illustrated an uncharacteristic symmetrical gait. The HD^{+/-} mice showed mean loads of 64.7 ± 0.93 % and 71.2 ± 0.51 % for their fore and hind limbs, respectively (Table 3.5). Taking into account the symmetry of the wild-type mouse gait

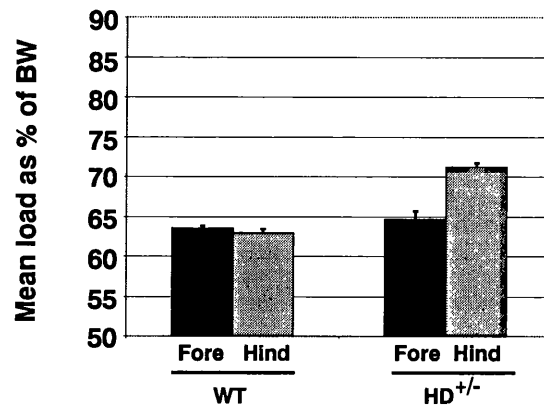
HD^{+/-} mice displayed an abnormal gait with the hind limbs transmitting a greater load than the fore limbs (Figure 3.5A). When the median difference between the fore and hind limb loadings were compared, weight distribution in the HD^{+/-} and wild-type mice was significantly different ($p=0.02$)(Table 3.6).

The alteration in gait of male HD^{+/-} mice appeared only for the distribution of weight through the fore and hind limbs as the left and right limbs continued to transmit symmetrical loads (Figure 3.5B). The wild-type mice transmitted 63.3 ± 0.52 % load through their left limbs and 63.2 ± 0.08 % through their right limbs (Table 3.5). HD^{+/-} mice exerted mean loads of 67.2 ± 2.63 % on their left limbs and 68.7 ± 1.91 % on their right limbs (Table 3.5). When the median differences between left and right limb loadings were compared between wild-type mice (0.1 ± 0.54 %), and HD^{+/-} mice (0.9 ± 4.4 %), a symmetrical gait was demonstrated with no significant difference ($p=0.9$) between the cohorts detected (Table 3.6).

When the mean body weight of male wild-type mice ($33.4 + 1.67$ g) was compared to that of male HD^{+/-} mice ($29.36 + 0.91$ g), the HD^{+/-} mice displayed a significantly lower mean body weight than the wild-type controls ($p=0.03$) (Table 3.4). This difference is consistent with female mice at 4 months of age and the combined cohort at 9 months of age.

As male mice at 4 months of age exerted significantly more load through their hind and right limbs compared to their wild-type controls the load exerted through all limbs were compared between HD^{+/-} and wild-type male mice at 9 months of age. Significantly greater load was transmitted through the hind ($p=0.02$) and right limbs ($p=0.02$) of HD^{+/-} mice compared to wild-type controls at this time point. This significant difference was not observed for the fore ($p=0.6$) and left limbs ($p=0.2$). These findings are consistent with those found at 4 months of age in these animals. It is unknown whether this difference in the amount of load transmitted through some limbs is connected to the abnormal weight distribution observed in male HD^{+/-} mice. If a significant increase in load transmitted through certain limbs plays a role in generating gait abnormality then an early subtle alteration in male gait may be detected at 4 months of age.

A.



B.

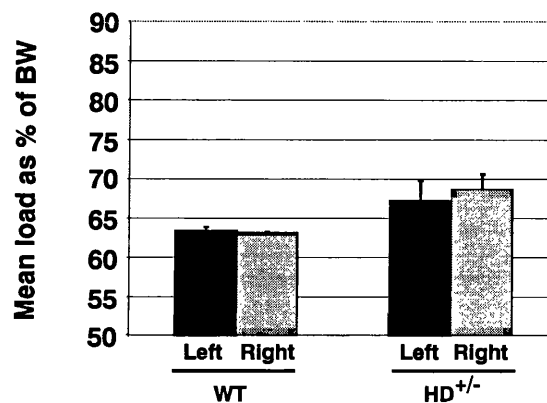


Figure 3.5 The mean load exerted through the limbs of male 9 month old wild-type and HD^{+/-} mice

The bar graphs show the mean load, expressed as a percentage of body weight (BW) \pm one standard error, transmitted through all four groups of limbs (fore, hind, left and right) in male 9 month old wild-type and HD^{+/-} mice. **A.** A normal mouse gait displays asymmetry across the fore/hind axis with the fore limb transmitting greater load than the hind limb. The median difference between the fore and hind limb loads in wild-type (n=4) and HD^{+/-} mice (n=5) were compared using the Mann-Whitney U statistical test and a significant difference in weight distribution was detected (p=0.02). **B.** A normal mouse gait displays symmetry across the left/right axis. The median difference between the left and right limb loads in wild-type (n=4) and HD^{+/-} mice (n=5) were compared using the Mann-Whitney U statistical test and no significant difference in weight distribution was detected (p=0.9). Male HD^{+/-} mice seemed to transmit greater loads through all limb groups compared to their wild-type controls. Statistical analysis of each limb group between wild-type and HD^{+/-} mice showed a significantly greater load transmitted through the hind (p=0.02) and right (p=0.02) limbs of HD^{+/-} mice compared to wild-type controls (Mann-Whitney, Fore, p=0.6, Left, p=0.2).

The male wild-type mice at 9 months of age display a symmetrical gait across the fore/hind axis. This differs from the normal gait observed in all animals at 4 months of age. The HD^{+/-} mice display an abnormal gait when investigating the fore/hind axis as a greater load is transmitted through the hind limbs. The difference between the fore and hind limb loads is significantly different in HD^{+/-} mice compared to wild-type controls. No alteration from the typical mouse gait is observed in wild-type and HD^{+/-} mice when investigating the loads transmitted across the left/right axis. Consistent with male HD^{+/-} mice at 4 months of age, male HD^{+/-} mice transmit significantly more load through their hind and right limbs compared to the wild-type controls.

In summary, these data suggest that male HD^{+/-} mice at 9 months of age display a gait that is significantly different when compared to their wild-type controls.

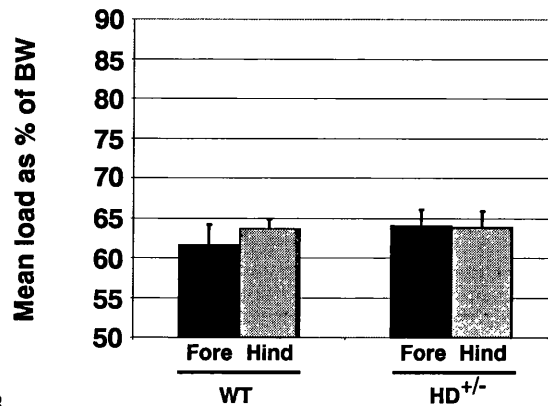
3.2.3.1.2 Female mice

The 9 month old female wild-type mice transmitted 61.62 ± 2.55 % load through their fore limbs and 63.6 ± 1.25 % through their hind limbs (Table 3.5). The female wild-type mice showed an uncharacteristic distribution of weight across the fore and hind limbs with the fore limb failing to transmit a greater load than the hind limb, also seen in the male wild-type 9 month old mice. The HD^{+/-} mice exerted mean loads of 64 ± 2.06 % through their fore limbs and 63.9 ± 2.02 % through their hind limbs (Table 3.5). Female HD^{+/-} mice also displayed a relatively symmetrical gait across the fore/hind axis (Figure 3.6A). The median differences in loads for the fore and hind limbs in the wild-type and HD^{+/-} female mice were not significantly different (Table 3.6, $p=0.8$).

The left to right symmetry normally observed was apparent in wild-type female mice at 9 months (Figure 3.6B). Wild-type mice transmitted 62.5 ± 1.40 % load through their left limbs and 62.74 ± 1.41 % through their right limbs (Table 3.5). The HD^{+/-} mice displayed mean loads of 66 ± 2.32 % and 61.9 ± 1.40 % for their left and right limbs, respectively (Table 3.5). This HD^{+/-} mouse gait shows slight asymmetry, however, the median differences between the left and right limbs for wild-type and HD^{+/-} mice are not significantly different (Table 3.6, $p=0.1$).

Female HD^{+/-} mice do have a lower mean body weight when compared to their wild-type controls however, this difference does not reach significance ($p=0.08$)(Table 3.4). This finding is not consistent with the significant reduction in weight of HD^{+/-} male mice when compared to their wild-type controls at 9 months of age.

A.



B.

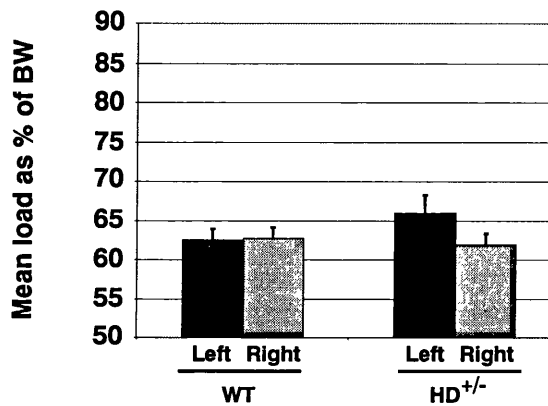


Figure 3.6 The mean load exerted through the limbs of female 9 month old wild-type and HD^{+/-} mice

The bar graphs show the mean load, expressed as a percentage of body weight (BW) \pm one standard error, transmitted through all four groups of limbs (fore, hind, left and right) in female 9 month old wild-type and HD^{+/-} mice. **A.** A normal mouse gait displays asymmetry across the fore/hind axis with the fore limb transmitting greater load than the hind limb. The median difference between the fore and hind limb loads in wild-type (n=5) and HD^{+/-} mice (n=5) were compared using the Mann-Whitney U statistical test and no significant difference in weight distribution was detected (p=0.8). **B.** A normal mouse gait displays symmetry across the left/right axis. The median difference between the left and right limb loads in wild-type (n=5) and HD^{+/-} mice (n=5) were compared using the Mann-Whitney U statistical test and no significant difference in weight distribution was detected (p=0.1).

Female HD^{+/-} mice at 9 months of age do not display any alteration in gait when compared to their wild-type controls. Male HD^{+/-} mice did display a significant difference in gait compared to wild-type controls at this age suggesting that there may be sex-specific factors influencing the phenotypic consequences of the HD mutation. Studies at later time points would be needed to assess whether this change in gait of male HD^{+/-} mice does eventually occur in female HD^{+/-} mice.

3.2.4 Gait analysis in 12 month old wild-type and HD^{+/-} mice

Investigations of gait in wild-type and HD^{+/-} mice at 12 months of age were carried out. Each cohort contained 3 male and 3 female mice.

At 12 months of age there was no significant difference in mean body weight detected between wild-type (34.98 ± 1.85 g) and HD^{+/-} (37.3 ± 3.32 g) mice (Table 3.7, $p=0.3$).

Table 3.7 Summary of mean body weight for 12 month old mice assessed for gait parameters

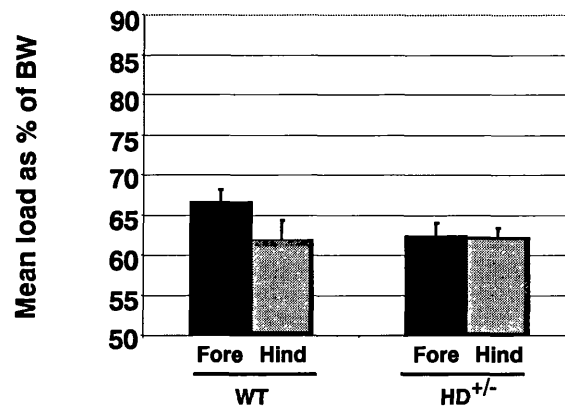
Genotype	Number	Mean body weight of mice (grams \pm S.E.)	*p value
WT	6	34.98 ± 1.85	0.3
HD ^{+/-}	6	37.3 ± 3.32	

* comparing mean body weight between wild-type and HD^{+/-} mice using the unpaired, one-tailed, Student's *t*-test.

The mean load for the fore limbs in wild-type mice was 66.7 ± 1.52 % and for the hind limbs was 61.96 ± 2.37 % (Table 3.8). The weight distribution illustrated that the fore limbs transmitted a greater load than the hind limbs, as expected in a normal mouse gait. HD^{+/-} mice showed a mean load of 62.5 ± 1.62 % for the fore limbs and 62.2 ± 1.26 % for the hind limbs (Table 3.8). This symmetrical gait differs from the normal gait across the fore/hind limb axis. The median differences between the loads for the fore and hind limbs in wild-type and HD^{+/-} mice were nearly significantly different (Table 3.9, $p=0.065$).

The left and right limb mean loads were 64.5 ± 1.27 % for the left limb and 64.2 ± 2.52 % for the right, showing a symmetrical and normal gait in wild-type mice at 12 months of age (Table 3.8, Figure 3.7B). The mean loads in HD^{+/-} mice were 61.7 ± 1.64 % for the left limbs and 63 ± 0.63 % for the right limbs (Table 3.8). The median difference between the left and right limb loads in wild-type and HD^{+/-} mice were not significantly different (Table 3.9, $p=0.6$).

A.



B.

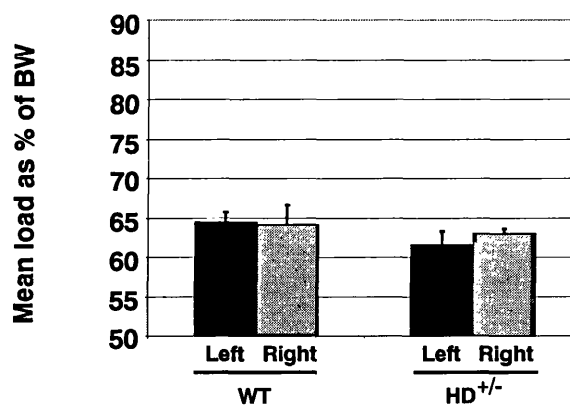


Figure 3.7 The mean load exerted through the limbs of 12 month old wild-type and HD^{+/-} mice

The bar graphs show the mean load, expressed as a percentage of body weight (BW) \pm one standard error, transmitted through all four groups of limbs (fore, hind, left and right) in 12 month old wild-type and HD^{+/-} mice. **A.** A normal mouse gait displays asymmetry across the fore/hind axis with the fore limb transmitting greater load than the hind limb. The median difference between the fore and hind limb loads in wild-type ($n=6$) and HD^{+/-} mice ($n=6$) were compared using the Mann-Whitney U statistical test and a nearly significant difference in weight distribution was detected ($p=0.065$). **B.** A normal mouse gait displays symmetry across the left/right axis. The median difference between the left and right limb loads in wild-type ($n=6$) and HD^{+/-} mice ($n=6$) were compared using the Mann-Whitney U statistical test and no significant difference in weight distribution was detected ($p=0.6$).

Table 3.8 Summary of the mean loads, as a percentage of body weight, exerted through all groups of limbs in 12 month old mice

Genotype/ Sex	Number of mice	Mean load (% BW \pm S.E.)			
		Fore	Hind	Left	Right
WT	6	66.7 \pm 1.52	61.96 \pm 2.37	64.5 \pm 1.27	64.2 \pm 2.52
HD ^{+/-}	6	62.5 \pm 1.62	62.2 \pm 1.26	61.7 \pm 1.64	63 \pm 0.63

Table 3.9 The median distribution of weight between the fore and hind limbs and the left and right limbs in all cohorts and the p values resulting from the Mann-Whitney U statistical test when comparing the median difference between the loadings in wild-type and HD^{+/-} mice

Genotype	Weight Distribution			
	F-H (%BW)	*p value	L-R (%BW)	*p value
WT	5.3 \pm 1.4	0.065	0.9 \pm 1.96	0.6
HD ^{+/-}	0.9 \pm 1.4		-1.8 \pm 1.24	

F-H = the median of the values obtained for the difference between the mean loads of the fore and hind limbs. L-R = the median of the values obtained for the difference between the mean loads of the left and right limbs. * comparing F-H and L-R in wild-type and HD^{+/-} mice using the Mann-Whitney U test.

At 12 months of age HD^{+/-} mice displayed gait that was not significantly different from wild-type controls. However, a trend towards an abnormality in the fore/hind axis load distributions within the HD^{+/-} mice was observed. The HD^{+/-} mice fail to exert a greater load through their fore limbs than their hind limbs, as expected for normal mouse gait. This trend towards an abnormal gait in HD^{+/-} mice may represent the alteration in gait of male mice observed at 9 months worsening and affecting the results in the combined cohort or an alteration in female gait that may now be contributing. It is not possible to determine if gait varies between sexes at this time point as data separation is not recommended with so few animals in each test cohort.

3.2.5 Velocity of 9 and 12 month old wild-type and HD^{+/-} mice

As the velocity of each animal was calculated for each run used in the analysis of limb loadings, a mean velocity for each mouse was obtained. As the runs were captured on video, velocity was measured by the number of video frames, taken at known time intervals that were required for the animal to cross the load cell of known length. The mean velocity of wild-type and HD^{+/-} mice was therefore assessed during spontaneous locomotion.

The mean velocity of wild-type mice at 9 months of age was calculated as described in section 2.6.1.2 and found to be 23.01 cms⁻¹. The velocity of HD^{+/-} mice at the same age was established as 24.78 cms⁻¹. These velocities were not significantly different when compared using the unpaired,

one-tailed, Student's *t*-test ($p=0.2$) (Table 3.10). At 12 months of age wild-type mice displayed a mean velocity of 23.38 cms^{-1} . 12 month old HD^{+/-} mice showed a reduction in mean velocity (19.6 cms^{-1}) when compared to their wild-type littermates, however, this reduction just failed to reach statistical significance ($p=0.06$) (Table 3.10).

When investigating the progressive nature of velocity in animals of the same genotype, wild-type mice showed no sign of change in velocity from 9 to 12 months of age (Table 3.11, $p=0.4$). The trend towards a reduction in velocity of HD^{+/-} mice compared to wild-type mice at 12 months of age is supported by a significant progressive change in velocity of HD^{+/-} mice from 9 months to 12 months of age (Table 3.11, $p=0.007$).

Velocity data were not available for 4 months old animals, however, the lack of any significant difference between HD^{+/-} and wild-type mice at 9 months of age suggests no long term alteration in velocity occurred prior to this age.

Table 3.10 Summary of cohorts used and the mean velocities during locomotion in 9 and 12 month old wild-type and HD^{+/-} mice

Age (months)	Genotype	Number of mice	Mean velocity (cms ⁻¹ ± S.E.)	*p value
9	WT	9	23.01 ± 1.17	0.2
	HD ^{+/-}	10	24.78 ± 1.14	
12	WT	6	23.38 ± 1.73	0.06
	HD ^{+/-}	6	19.6 ± 1.46	

* comparing mean body velocity between wild-type and HD^{+/-} mice using the unpaired, one-tailed, Student's *t*-test.

Table 3.11 Summary of cohorts used and the mean velocities during locomotion in mice of the same genotype at different ages

Genotype	Age (months)	Number of mice	Mean velocity (cms ⁻¹ ± S.E.)	*p value
WT	9	9	23.01 ± 1.17	0.4
	12	6	23.38 ± 1.73	
HD ^{+/-}	9	10	24.78 ± 1.14	0.007
	12	6	19.6 ± 1.46	

* comparing mean velocity between 9 month and 12 month old mice of the same genotype using the unpaired, one-tailed, Student's *t*-test.

3.2.6 Summary of Results

Both wild-type and HD^{+/-} mice displayed a typical mouse gait during spontaneous locomotion at 4 months of age. When the cohorts were separated into males and females both sexes of each genotype showed a typical mouse gait. The retention of the normal left/right axis symmetry in limb loadings was observed throughout life for both wild-type and HD^{+/-} mice. The distribution of weight across the fore/hind axis, typically asymmetrical with greater load transmitted through the fore limb, was observed in wild-type mice at 4 months and 12 months, however, became more symmetrical in 9 month old mice. This change in wild-type mouse gait may reflect the smaller number of measurements taken at the intermediate time point (see section 2.6.1.2) or a natural variation in gait within this cohort.

At 9 and 12 months of age alterations of gait were detected in HD^{+/-} mice compared to their wild-type littermates. The male HD^{+/-} mice at 9 months of age did not exhibit the normal mouse gait or the more symmetrical gait observed in 9 month old wild-type mice, they displayed an asymmetrical gait across the fore/hind axis with the hind limb exerting the greatest load. At 9 months the slight alteration in gait of the combined HD^{+/-} mice cohort was apparently the result of a significant alteration in the gait of male HD^{+/-} mice and no change in the gait of the female HD^{+/-} mice. Results from the 12 month old cohort nearly reached significance and again illustrated a change across the fore/hind axis suggesting that the alteration in gait within HD^{+/-} mice may be progressive. It is not possible to establish from this study if this alteration is due to a further change in male HD^{+/-} mouse gait or the initiation of an abnormality in female HD^{+/-} mouse gait. Further evidence supporting a change in gait in HD^{+/-} mice at 12 months of age was obtained with a trend towards a reduction in velocity of HD^{+/-} mice compared to wild-type mice ($p=0.06$). This difference between HD^{+/-} and wild-type mice was not observed at 9 months of age. Further analysis did demonstrate that HD^{+/-} mice at 12 months of age did display a significant reduction in velocity compared to their 9 month old HD^{+/-} counterparts ($p=0.007$).

In summary, these studies have provided evidence to support a late onset alteration in gait and velocity within HD^{+/-} mice compared to their wild-type littermates.

3.3 Investigating spatial learning and memory in wild-type and HD^{+/-} mice

3.3.1 Aims of the study

The aim of this study was to investigate spatial learning and memory in wild-type and HD^{+/-} mice. Cognitive deficits, in the form of memory dysfunction, are one of the principal symptoms associated with human HD. Other prominent features of the human HD phenotype such as movement disorder and behavioural abnormalities have previously been observed in this HD mouse model (Shelbourne *et al.*, 1999) and section 3.2). In order to determine if this HD mouse model exhibits other behavioural aspects of the HD phenotype, cognitive functioning was investigated. Spatial learning and memory was investigated using the behavioural paradigm called the rotating holeboard (Brosnan-Watters and Wozniak, 1997) described in section 2.6.2. Mice were first assessed at 6 months of age, allowing time for repeated testing throughout life to establish the onset and progression of possible deficits.

3.3.2 Results

Practice experiments were carried out in the rotating holeboard apparatus to assess the effectiveness of the apparatus design and protocol. Three mice, of unknown genotype, were chosen to run through the full protocol. Previous reports of investigations using the rotating holeboard to assess cognitive functioning in mice had suggested that learning would be achieved in approximately 25 trials (Brosnan-Watters and Wozniak, 1997). As each trial was estimated to take up to 4 minutes (3 minutes per trial plus apparatus cleaning and rotation) the expected duration of the experiment was approximately 1 h 40 min. As responses to behavioural paradigms can fluctuate depending on sex and mouse strain slight variation was expected. The results from the practice experiments using the rotating holeboard are presented in Table 3.12.

Table 3.12 Summary of the animals used and the results and conclusions from the practice sessions in the rotating holeboard paradigm

Sex/ Genotype	Acquisition	Retention	Problems	Modifications
F HD ^{+/-}	Yes 34 trials	No 42 trials	Scraping and moving punctuated hole screens	Redesign hole screens
M WT	No 64 trials			Redesign start box
M WT	Yes 46 trials	No 54 trials	Removal of the start box disruptive	

F = Female, M = Male, WT = Wild-type, HD^{+/-} = Heterozygote HD mice

During the first attempt using the rotating holeboard the mouse showed acquisition of the task after 34 trials. This was in spite of the mouse regularly attempting to remove the punctuated screens covering the inaccessible bait and taking a prolonged time to emerge from the start box. However, the following day retention of learning in this animal failed to occur after 42 trials. The second mouse experienced the same disruption due to the apparatus and became so preoccupied with removing the punctuated screens to access the large bait that acquisition was not achieved after 64 trials. Acquisition of learning with the third mouse was again successful after 46 trials however, the punctuated screens and start box caused disruption and retention of the task failed after 54 trials.

It has previously been observed that mice are easily distracted and sensitive to environmental stress during behavioural assessment. However, the failure of these animals to complete the task was primarily attributed to apparatus design problems.

The initial experiments suggested that placing mice in a darkened start box and allowing voluntary emergence was unfavourable as the mice, preferring the dark, failed to explore the apparatus. The start box also had to be removed from the apparatus after emergence, which again disrupted the animals. The start box was redesigned to contain a sliding trap door. After placement of the box into the apparatus the floor was removed and the box lifted leaving the mouse in the centre of the apparatus with no cover and no further need for contact with the experimenter.

An important feature of the rotating holeboard design was the punctuated hole screens. These grids prevented access to the large bait in the holes but allowed a food odour around the apparatus, eliminating any olfactory cues. It was established in the initial trials that mouse claws could grip the screens and remove them, so tempting the mice to retrieve the large bait and ignore the small accessible bait. The grids were therefore redesigned and attached to the holes, eliminating the possibility of movement or removal.

Once the appropriate design modifications were carried out all remaining animals were fully re-habituated to the new apparatus. This habituation consisted of thrice weekly handling and exposure to the new apparatus for 2 weeks. Animals were handled for 1 minute and then transferred into the apparatus by placement into the new start box and removing the sliding floor. This procedure was carried out approximately 5 times per habituation session.

Four fully habituated male mice were assessed in the new rotating holeboard apparatus and the results are presented in Table 3.13.

Table 3.13 Summary of rotating holeboard experiments using the modified apparatus

Sex/ Genotype	Acquisition	Retention	Problems	Modifications
M WT	No 14 trials		Ignoring bait	Retry acquisition after second nights starvation
M WT	No 4 trials			
	No 10 trials			
M HD ^{+/-}	No 10 trials			Retry acquisition after second nights starvation
	Yes 40 trials	Yes 26 trials		Correct trial criteria changed
M WT	No 50 trials			Varying bait size

F = Female, M = Male, WT = Wild-type, HD^{+/-} = Heterozygote HD mice

The first two attempts of the rotating holeboard paradigm were terminated following a small number of trials as the animals were ignoring the accessible bait. Animals would carry out a nose poke on the hole containing the accessible bait but fail to present the correct response and eat the bait. These incorrect nose pokes into the correct hole continued throughout the trial and no bait was eaten. Food deprivation overnight prior to testing was carried out to induce an incentive to learn through hunger. Ignoring the accessible bait was suggestive of insufficient hunger induced by overnight food deprivation.

To test this the second animal was deprived of food over a second night and acquisition re-tested. The animal continued to ignore the bait from the first trial of the second acquisition experiment.

The third animal was also subjected to two nights food deprivation as it ignored the bait on the first attempt at acquisition. As the animals were failing to eat the bait but frequently picked it up the criteria for a correct response was changed. The bait no longer needed to be eaten but only removed from the correct hole. These criteria resulted in the successful acquisition and retention of the task. However, as the animal would either ignore the bait or pick it up, the response was not fuelled by hunger and appeared to occur randomly. The new criterion was used on a second mouse, which, failed to demonstrate acquisition after 50 trials, suggesting that without the hunger incentive, learning was not induced.

To assess the animals response to food under normal conditions crude testing of olfactory functioning was carried out by placing each animal in a fresh home cage with a hidden piece of bait. The behaviour of the animals was assessed for 5 minutes and all subjects spent a high proportion of time (~3 min) investigating around the hidden bait. Three male and three female mice were tested and all females and two males mice found the bait within 1.5 minutes illustrating a positive response to the hidden food. The animals would either pick up the bait or walk away, behaviour reminiscent of that observed in the rotating holeboard paradigm. The bait could elicit a response but there was not enough incentive to consistently do so. Three animals tested for responsiveness to food were subjected to the rotating holeboard and none successfully achieved acquisition of the task (Table 3.14).

The size of both the inaccessible and accessible bait was varied to ensure that the small pieces of bait when eaten were not too large to dampen hunger within the first few trials. Varying the type of bait used to establish if the mice responded in the same way failed to elicit an alteration in behaviour.

Table 3.14 Summary of the rotating holeboard carried out with animals known to respond to food

Sex/ Genotype	Acquisition	Retention	Problems	Modifications
F WT	No 38 trials		Ignoring bait	New kind of bait
F WT	No 43 trials			Retry acquisition after second nights starvation
	No 45 trials			
F WT	No 32 trials			

F = Female, M = Male, WT = Wild-type, HD^{+/-} = Heterozygote HD mice

3.3.3 Summary of findings

The rotating holeboard experiments were discontinued after testing 10 mice and achieving successful acquisition and retention for the task in 1 animal. This success rate was deemed too low to acquire the animal numbers required for statistical analysis. Following initial design modifications the incentive to find and eat the bait seemed to be absent. Bait type and size was varied and mice elicited a positive response to hidden bait. Many mice still showed no sign of learning after more than 4 hours of testing despite previous reports suggesting that approximately

1 h 40 min should be sufficient for learning under these conditions (Brosnan-Watters and Wozniak, 1997). In reports of successful rotating holeboard studies, mice were systematically deprived of food until they achieved 80 % of their original body weight and were held at this weight throughout testing. According to Home Office advice, food was only withheld overnight prior to testing, and as a result no animal used in this study lost any weight. Under these circumstances it may be that mice will not learn as the hunger incentive to find the bait is missing. Due to these problems the aim of demonstrating cognitive deficits in the HD^{+/-} mice was not achieved and the onset and progressive nature of any spatial learning and memory could not be established.

3.3.4 Future studies on HD knock-in mouse cognition

Although this cognitive paradigm did not work well under the above conditions other paradigms may be suitable for this task. There are many other possible paradigms designed to assess learning and memory in rodents. Basic T or radial mazes could be utilised, however, these paradigms also rely on hunger-induced incentive. The most common alternative is adverse conditioning designed to force animals into learning an escape or prevention strategy. The Morris water maze is frequently used to assess spatial learning and memory by mice utilising spatial cues to find a hidden platform under the surface of a water tank (Morris, 1984). This test however, due to the involvement of water, can elicit a large stress response (Francis *et al.*, 1995). An alternative paradigm may be the Barnes circular maze utilising the more subtle adverse stimuli of light and noise (Barnes, 1979) to encourage the mouse to learn which hole around the outside of a domed circle leads to a darkened escape tunnel. This paradigm or ones like it may overcome the problem of incentive and minimise the stress response and therefore, may be suitable for the assessment of cognitive ability in HD^{+/-} mice and their wild-type littermates in the future.

4 Neurotransmitter receptor profiles in a knock-in mouse model of Huntington's disease

4.1 Aims of the study

To further elucidate the underlying mechanisms of neuronal dysfunction observed in the early stages of human HD (Andrews *et al.*, 1999; Antonini *et al.*, 1996; Lawrence *et al.*, 1998b) an investigation into the integrity of the neuronal circuitry of mice modelling early HD pathology was carried out. Any alterations in the density or distribution of neurotransmitter receptors could affect neuronal functioning. Changes in opioid, benzodiazepine, dopamine D₁ and dopamine D₂ receptors have all previously been associated with early HD pathogenesis (Ginovart *et al.*, 1997; Holthoff *et al.*, 1993; Weeks *et al.*, 1997). The density of these neurotransmitter receptors within the striatum and cortex of HD mice was investigated by quantitative ligand binding autoradiography (section 2.5).

The study was designed to address the following questions:

- Are neurotransmitter receptor densities altered in the striatum of HD^{+/-} mice compared to wild-type controls? The striatum was selected for investigation as this brain region shows the earliest pathological changes in HD. The question was investigated by determining the density of opioid, benzodiazepine, dopamine D₁ and dopamine D₂ neurotransmitter receptors in the striatum of 18 month old HD^{+/-} and wild-type mice. HD^{+/-} mice of this age have previously demonstrated late onset and progressive consequences of the HD mutation (Shelbourne *et al.*, 1999; Usdin *et al.*, 1999), L.K., unpublished data, chapter 3).
- Are neurotransmitter receptor densities altered in the cortex of HD^{+/-} mice compared to wild-type controls, and if so, do the changes parallel with changes in the striatum? Neurotransmitter receptor densities were investigated in the cortex because the neurodegenerative process associated with HD spreads to this brain region in the later stages of the disease. This suggests that the disease process, although less severe than in the striatum, does influence cortical cells. Cortical projection neurons innervate the striatum and any disruption of neurotransmission in cortical neurons may contribute to dysfunction within the striatum. In order to make comparisons with neurotransmitter receptor densities in the striatum, the receptor binding assays mentioned in the previous paragraph were performed on brain sections encompassing the striatum and the cerebral cortex.

- Is there any evidence that genetic background influences the effect of the HD mutation on neurotransmitter receptor densities? The cohorts used to investigate neurotransmitter receptor densities in the striatum and cortex contained animals with different genetic backgrounds. This question will be investigated by subdividing the data obtained for striatal and cortical receptor densities according to genetic background and carrying out re-analysis. If a genetic background influence is detected one possible interpretation is that genetic modifiers of the disease process are present. Subsequent identification of the molecular basis of any genetic modifiers may provide potential targets for future therapeutic interventions.
- Do changes in neurotransmitter receptor densities in HD^{+/-} mice occur as a result of a progressive process? This question will be addressed by investigating neurotransmitter receptor densities within the striatum and cortex of HD^{+/-} mice at different ages. HD is a progressive disorder, characterised by a prolonged symptom-free period during early life. Therefore, it is predicted that changes in neurotransmitter receptor densities would have a late onset and progress with age. Determining the time point at which neurotransmitter receptor density alterations occur would allow a comparison with the phenotypic alterations observed in the HD^{+/-} mice. This may uncover a potential involvement of these molecular changes in the symptomatology of HD.

Insights into other questions may also be provided by these studies. These include; Is the molecular basis of pathology the same in different regions of the brain? Is there a temporal gradient of brain region involvement?

In addition to investigating the possible molecular basis of neuronal dysfunction in HD, studies into neurotransmitter receptor densities may provide useful biochemical markers of the disease process in HD^{+/-} mice that may be utilised when assessing future HD therapies.

4.2 Optimisation of binding protocols

The concentration of the ligands used and the length of exposure time to autoradiographic film were optimised to ensure clear images of the appropriate intensity were produced for all brain regions examined.

4.2.1 Ligand concentration

The effect of ligand concentration on the results obtained from the receptor binding assays was investigated. For each ligand a series of 5-6 different concentrations was selected. For each ligand concentration, the total binding solution was added to 3 alternate brain sections from one wild-type

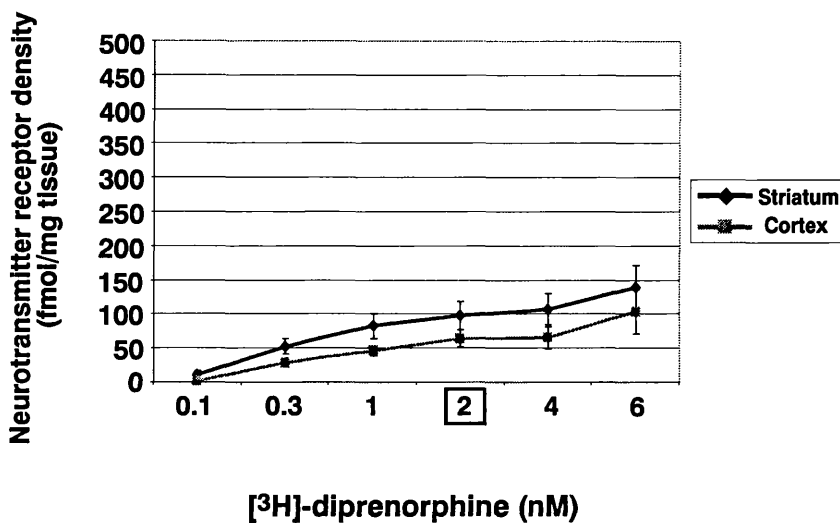
animal, and the same animal was used to assess all concentrations of a particular ligand. As described in section 2.5.3, non-specific binding associated with each ligand concentration was then assessed using the 2 intervening brain sections. Binding assays were performed as described in section 2.5.

The effect of increasing ligand concentrations on the resultant neurotransmitter receptor densities within the striatum and cortex can be seen in Figures 4.1 and 4.2. The ligand concentration chosen for the main study was one where binding saturation had not yet been reached and a clear autoradiographic image was produced.

4.2.2 Time of exposure

Tritium standards are composed of polymer representing eight different values of the tissue equivalent (TE) tritium concentration as calibrated for the auto-absorptive features of intact brain grey matter. Image analysis readings (section 2.5.5) must be taken when the relationship between the standard's tritium concentration and the corresponding optical density is linear. Densitometry errors may occur below or above this range as small optical density increments may represent large increments of tissue radioactivity. In order to produce autoradiographic images of an optical density within the linear range of the radioactive standards, brain sections bound with the chosen ligand concentration used in the assays described in section 4.2.1 were exposed to autoradiographic film for varying periods of time.

A. Opioid receptors



B. Benzodiazepine receptors

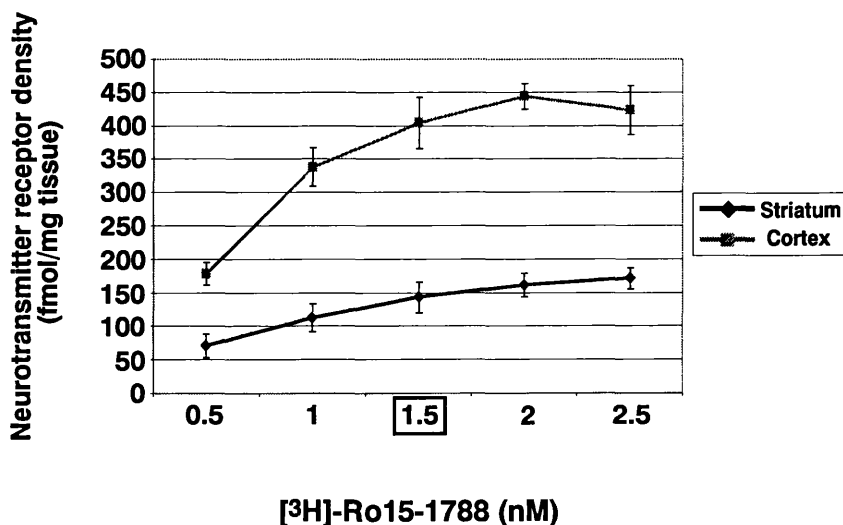


Figure 4.1 The effect of radiolabelled ligand concentration on striatal and cortical receptor binding

A. Neurotransmitter receptor density in the striatum and cortex of a wild-type mouse after receptor binding with increasing concentrations of [³H]-diprenorphine. The boxed value indicates the ligand concentration used in subsequent studies. **B.** Neurotransmitter receptor density in the striatum and cortex of a wild-type mouse after receptor binding with increasing concentrations of [³H]-Ro15-1788. The boxed value indicates the ligand concentration used in subsequent studies. Values representing neurotransmitter receptor density are expressed as a mean ± S.D. (fmol/mg tissue).

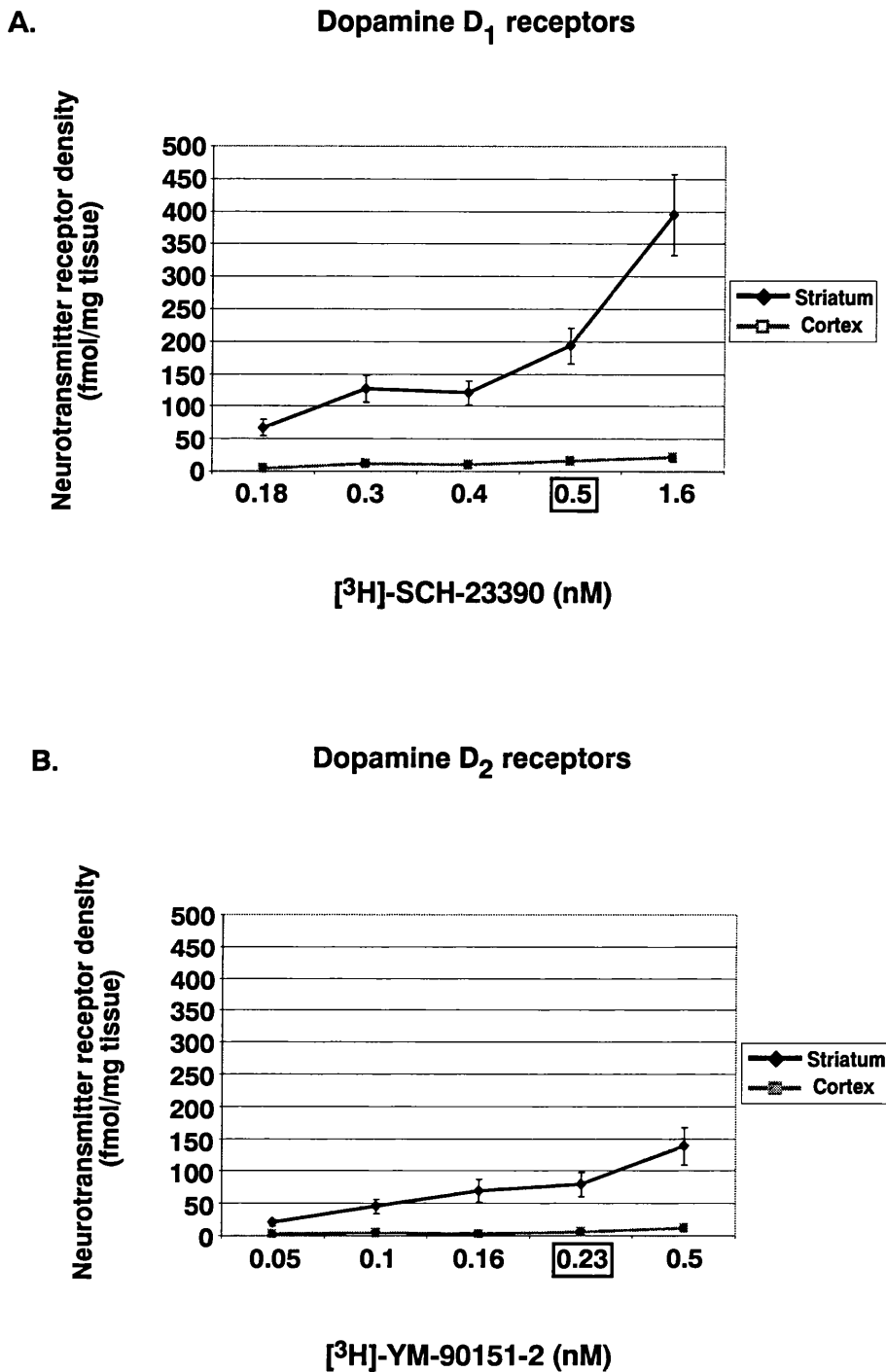


Figure 4.2 The effect of radiolabelled ligand concentration on striatal and cortical receptor binding

A. Neurotransmitter receptor density in the striatum and cortex of a wild-type mouse after receptor binding with increasing concentrations of [³H]-SCH-23390. The boxed value indicates the ligand concentration used in subsequent studies.

B. Neurotransmitter receptor density in the striatum and cortex of a wild-type mouse after receptor binding with increasing concentrations of [³H]-YM-90151-2. The boxed value indicates the ligand concentration used in subsequent studies. Values representing neurotransmitter receptor density expressed as a mean ± S.D. (fmol/mg tissue).

The ligand concentrations and exposure times that resulted in the neurotransmitter receptor densities shown in Table 4.1 were chosen for the main study.

Table 4.1 The mean specific binding obtained from the brain sections bound with the optimised ligand concentration after the chosen exposure times. Values are calculated from comparison with the [³H]-micro-scales

[³H]-Micro-scales (nCi/mg estimated Tissue Equivalent)	Receptor type and brain region (Mean specific binding (nCi/mg))	Exposure Time (Hyperfilm)
33.3	Benzodiazepine cortical binding (28.5)	3 wks
21.8		
13.9	Dopamine D ₁ striatal binding (14.6)	2 wks
	Benzodiazepine striatal binding (10)	3 wks
8.4	Dopamine D ₂ striatal binding (7)	2 wks
5.6	Opioid striatal binding (5)	3 wks
3.4	Opioid cortical binding (3.2)	3 wks
2.2		
1.4	Dopamine D ₁ cortical binding (1)	2 wks
	Dopamine D ₂ cortical binding (0)	2 wks

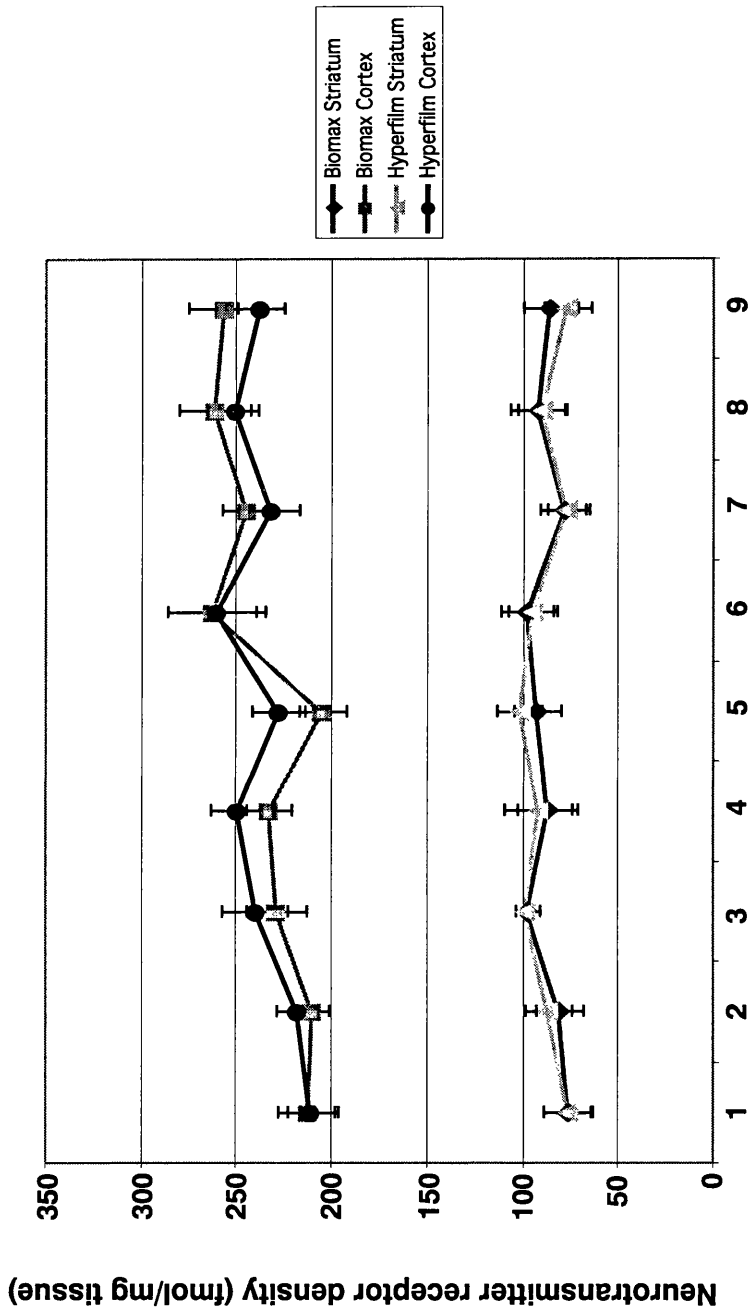
- - - values between the dashed lines represent the linear range of the [³H]-Micro-scales

The resultant neurotransmitter receptor density for the striatum and cortex under these conditions for opioid receptors were within the linear range of the radioactive standards. The striatal binding for both dopamine receptor types was within the linear range, however, cortical binding was extremely low. Although dopamine receptor cortical binding could have been established with longer exposure times, the length of exposure time needed to produce values within the linear range was deemed too long to enable completion of the study within the designated time. Studies examining the densities of both dopamine receptors in other HD mouse models have also obtained insufficient binding within the cortex to include these data within their analyses (Cha *et al.*, 1998). As dopamine D₁ neurotransmitter receptor densities could be detected for cortical regions, binding was analysed and the results included in the discussion. Benzodiazepine striatal binding was within the linear range of the radioactive standards, but benzodiazepine cortical binding produced high optical density readings out with the linear range. To obtain data for cortical benzodiazepine

receptors, shorter exposure times were planned. However, when analysing the initial exposures in the subsequent studies for striatal binding the values for the cortical region of all animals fell within the linear range and a second exposure was not necessary (Table 4.3). Therefore the excessively high optical density within the cortex, produced by benzodiazepine receptor binding, appeared to be restricted to the one animal used in the optimisation study.

4.2.3 Autoradiographic Film

An investigation into possible differences in the values of neurotransmitter receptor densities acquired from the same brain sections on different types of autoradiographic films was carried out. This was necessary as the Hyperfilm initially used in these studies was discontinued before the experiments were completed. The autoradiographic film, Biomax MR-1 (Kodak Scientific Imaging) and Hyperfilm™-³H (Amersham) were both used to produce autoradiographic images in the main studies. To assess any disparity that may have arisen in the results by using different films, brain sections processed to examine benzodiazepine binding were used to produce images on both films. Biomax MR-1 film, found to be less susceptible to physical damage, resulted in a duller image and required longer exposure times. When the striata and cortices from nine different mice were analysed on both kinds of film no significant differences in neurotransmitter receptor density were obtained (Figure 4.3).



Individual mice represented by numbers 1 - 9

Figure 4.3 Benzodiazepine receptor density in the striatum and cortex using Biomax-MR1 film and Hyperfilm

The same brain sections were used to produce images on both Biomax-MR1 and Hyperfilm. Neurotransmitter receptor density in each brain region was analysed independently from 3 total binding sections and 2 non-specific binding sections from 9 mice. Values for neurotransmitter receptor density are shown for each animal and expressed as a mean \pm S.D. (fmol/mg tissue). Neurotransmitter receptor density showed no significant differences in any animal on Biomax-MR1 film or Hyperfilm when analysed with the unpaired, two-tailed, Student's t-test.

4.2.4 Summary of optimised binding conditions

Table 4.2 The chosen ligand concentrations and exposure times used to detect neurotransmitter receptor densities of all four receptor types. The percentage of the data obtained for each receptor type on Hyperfilm and Biomax film is indicated.

Conditions for both the striatum and cortex*				
	Opioid	Benzodiazepine	D₁	D₂
Ligand concentration				
	2 nM	1.5 nM	0.5 nM	0.23 nM
Film exposure				
Hyperfilm	3 wks	3 wks	2 wks	2 wks
Biomax	4 wks	4 wks	3 wks	3 wks
Film used (% of sections exposed in main study)				
Hyperfilm	100%	87.5%	62.5 %	87.5%
Biomax	0%	12.5%	37.5%	12.5%

*values of neurotransmitter receptor density for both cortex and striatum were obtained from the same film. D₁ = dopamine D₁ and D₂ = dopamine D₂ receptors.

4.2.5 Evaluation of optimised binding protocols

Table 4.3 shows mean specific binding in nCi/mg for the conditions chosen from the optimisation experiment and used in the subsequent main study.

Table 4.3 Average specific binding in nCi/mg for all ligands within the striatum and cortex and a comparison with the radioactive standard range

[³H]-Micro-scales (nCi/mg estimated Tissue Equivalent)	Mean specific binding (nCi/mg) Optimisation	Mean specific binding (nCi/mg) Main study
33.3	Benzodiazepine cortical binding (28.5)	
21.8		Benzodiazepine cortical binding and Dopamine D ₁ striatal binding (16)
13.9	Benzodiazepine striatal binding (10)	Dopamine D ₂ striatal binding (10)
8.4	Dopamine D ₂ striatal binding (7)	Opioid and benzodiazepine striatal binding (6)
5.6	Opioid striatal binding (5)	Opioid cortical binding (4)
3.4	Opioid cortical binding (3.2)	
2.2		
1.4	Dopamine D ₁ cortical binding (1)	Dopamine D ₁ cortical binding (1)
	Dopamine D ₂ cortical binding (0)	Dopamine D ₂ cortical binding (0)

--- values between the dashed lines represent the linear range of the [³H]-Micro-scales

The results obtained from the chosen ligand concentrations and exposure times in the optimisation experiment and the main study suggest that repetition of the chosen protocols produced consistent levels of binding in the striatum and cortex when examining dopamine D₁, dopamine D₂ and opioid receptors. This was also the case when investigating striatal benzodiazepine receptor binding. However, cortical benzodiazepine showed significant alteration in values obtained in the optimisation and main study. A significantly higher value of neurotransmitter receptor densities in the cortex for benzodiazepine receptors was observed in the optimisation experiment. This variation may be accounted for by the fact that the optimisation study consisted of one experiment

using one control brain and the data from the main study represents the neurotransmitter receptor density results from a large cohort of wild-type mice. However, no individual animal in the main study demonstrated a cortical binding as high as that found in the optimisation study.

In other rodent studies investigating the chosen receptor types receptor binding levels are consistent with those found in this investigation (Cha *et al.*, 1999; McCabe *et al.*, 1988; Savasta *et al.*, 1986; Sur *et al.*, 1999).

4.2.6 Non-specific binding

Varying levels of non-specific binding were achieved with each optimised binding protocol (Table 4.4). Non-specific binding was consistent within all brain sections processed through each binding protocol. Non-specific binding, expressed as a percentage of total binding, was detected at low levels (<20 %) in the striatum and cortex for opioid and benzodiazepine receptor binding (Figure 4.4A and B). Binding conditions also achieved low non-specific binding within the striatum for dopamine D₁ receptors. The non-specific binding detected in the cortex for dopamine D₁ binding was relatively high, but may reflect the low levels of total binding achieved (Figure 4.4C). The highest non-specific binding was detected for dopamine D₂ receptor binding (Figure 4.4D). The level within the striatum was considered acceptable (<40 %) and data analysis carried out. Non-specific binding within the cortex for dopamine D₂ receptor binding was too high (90 %) to allow interpretation of the specific binding obtained, however, as dopamine D₂ receptor binding within the cortex was negligible this analysis was not required.

Table 4.4 Non-specific binding levels in the striatum and cortex for all binding protocols as a percentage of the total binding obtained

	Opioid	Benzodiazepine	D ₁	D ₂
Striatum	11 %	2.5 %	5 %	25 %
Cortex	17 %	1 %	35 %	90 %

D₁ = dopamine D₁ and D₂ = dopamine D₂ receptors.

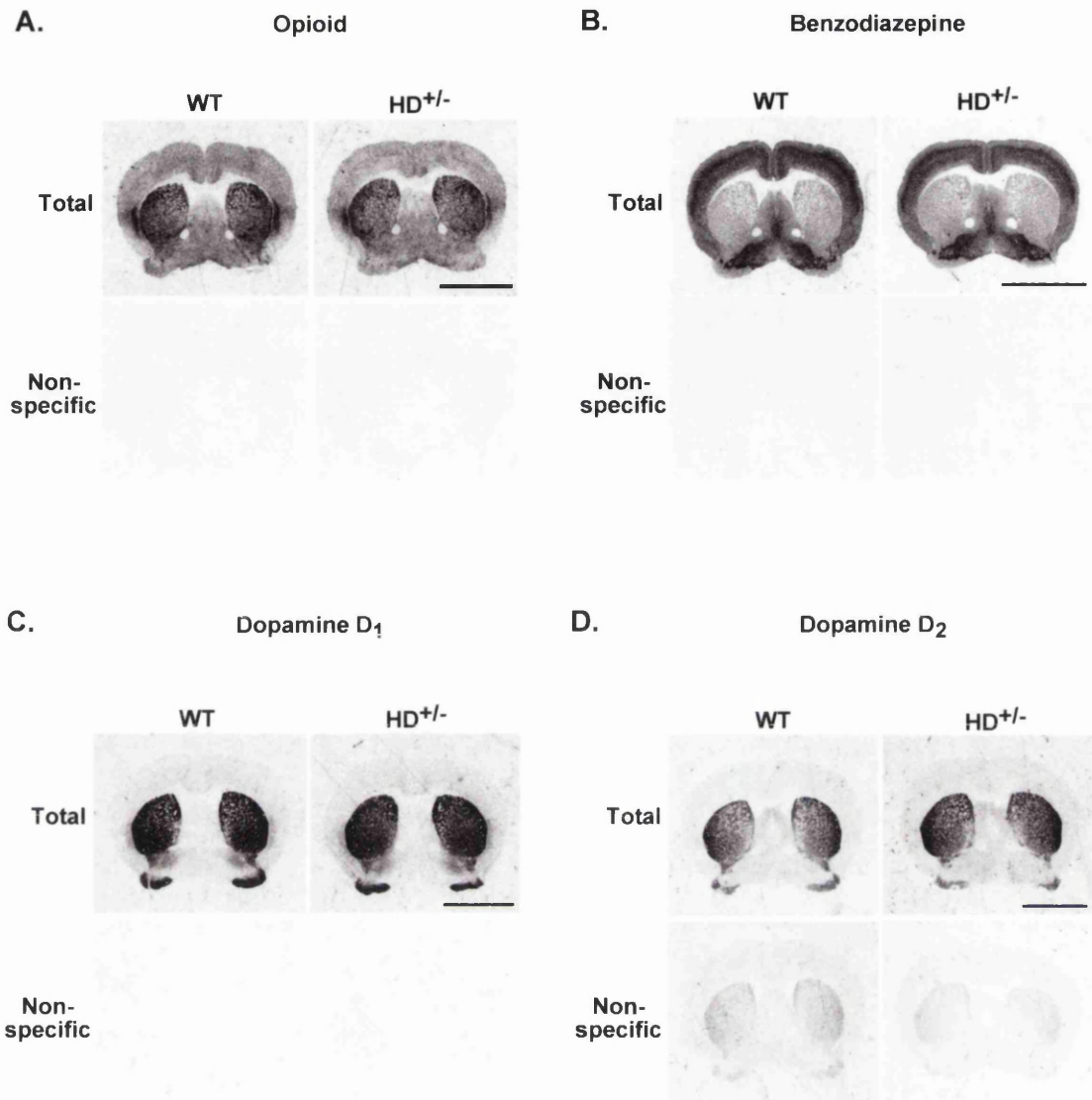


Figure 4.4 Specific and non-specific binding for all ligand binding protocols

A. Coronal brain sections incubated with [³H]-diprenorphine to assess opioid neurotransmitter receptor binding. **B.** Coronal brain sections incubated with [³H]-Ro15-1788 to assess benzodiazepine neurotransmitter receptor binding. **C.** Coronal brain sections incubated with [³H]-SCH23390 to assess dopamine D₁ neurotransmitter receptor binding. **D.** Coronal brain sections incubated with [³H]-YM-09151-2 to assess dopamine D₂ neurotransmitter receptor binding. An example of a total binding section and the corresponding non-specific binding section for one wild-type and one HD^{+/-} mouse. Scale bar = 5 mm.

4.3 Neurotransmitter receptor profiles in the striatum of 18 month old wild-type and HD^{+/-} mice

Investigations into neurotransmitter receptor densities first concentrated on the striatum, the brain region predominantly associated with HD pathology. The initial study compared results from 18 month old female wild-type and HD^{+/-} mice. This time point was selected because phenotypic and cellular consequences of the HD mutation have been observed at this age (Shelbourne *et al.*, 1999; Usdin *et al.*, 1999) and L.K., unpublished data, chapter 3). Initial analyses were carried out on pooled data from animals on three different genetic backgrounds. All wild-type and HD^{+/-} mice used were matched for age and genetic background. This was frequently achieved by using HD^{+/-} and wild-type littermates. The exact numbers of mice on each genetic background in each pooled cohort are indicated in Table 4.5.

Table 4.5 The number of mice on three different genetic backgrounds used for striatal analysis of each receptor type

Genetic background	Genotype	Striatum			
		Op	Ben	D ₁	D ₂
FVB/N	WT	6	6	6	5
	HD ^{+/-}	5	5	5	4
C57BL/6	WT	9	9	7	9
	HD ^{+/-}	9	10	6	6
DBA/2	WT	3	2	4	3
	HD ^{+/-}	6	2	5	5
Total	WT	18	17	17	17
	HD ^{+/-}	20	17	16	15

Op = Opioid, Ben = Benzodiazepine, D₁ = Dopamine D₁, D₂ = Dopamine D₂ neurotransmitter receptors.

The striatum of each mouse in the cohort was assessed for opioid, benzodiazepine, dopamine D₁ and dopamine D₂ neurotransmitter receptor densities. The number included in the final analysis (Table 4.5) varies between receptor assay due to the number of brain sections successfully processed to produce images of suitable quality. The neurotransmitter receptor densities for each pooled cohort are summarised in Table 4.6.

Table 4.6 The number of animals utilised and the neurotransmitter receptor density for each study investigating the receptor profiles within the striatum of 18 month old HD^{+/-} and wild-type mice

Receptor type	Genotype	Number of mice	Mean neurotransmitter receptor density \pm S.D. (fmol/mg tissue)	*p value
Opioid	WT	18	124 \pm 24	0.07
	HD ^{+/-}	20	141 \pm 33	
Benzodiazepine	WT	17	87 \pm 12	0.005
	HD ^{+/-}	17	99 \pm 10	
Dopamine D ₁	WT	17	191 \pm 23	0.9
	HD ^{+/-}	16	190 \pm 26	
Dopamine D ₂	WT	17	127 \pm 18	0.006
	HD ^{+/-}	15	109 \pm 14	

*Values in bold represent statistical significance ($p < 0.05$) obtained using two tailed, Student's *t*-test.

Opioid receptor binding sites were found at moderate levels within the striatum (Figure 4.4A). The neurotransmitter receptor density revealed by this ligand (³H]-diprenorphine) in wild-type mice was 124 \pm 24 fmol/mg tissue. No significant difference was detected between this value and that of the 141 \pm 33 fmol/mg tissue detected in HD^{+/-} mice using the two tailed, Student's *t*-test ($p = 0.07$) (Figure 4.5A).

Benzodiazepine receptors displayed the lowest binding in the striatum within this study with a neurotransmitter receptor density in wild-type mice of 87 \pm 12 fmol/mg tissue (Figure 4.4B). In comparison, the neurotransmitter receptor density in HD^{+/-} mice was 99 \pm 10 fmol/mg tissue. Statistical analysis of the results revealed a significant increase in benzodiazepine binding in the striatum of HD^{+/-} mice (two tailed, Student's *t*-test, $p = 0.005$) when compared to wild-type mice (Figure 4.5B).

Dopamine D₁ receptors were expressed at high levels in the striatum and the neurotransmitter receptor density in wild-type mice was 191 \pm 23 fmol/mg tissue, (Figure 4.4C) and in HD^{+/-} mice was 190 \pm 26 fmol/mg tissue. Statistical analysis of these results illustrated no significant difference in dopamine D₁ receptor density in mice with or without the HD mutation (two-tailed, Student's *t*-test, $p = 0.9$) (Figure 4.5C).

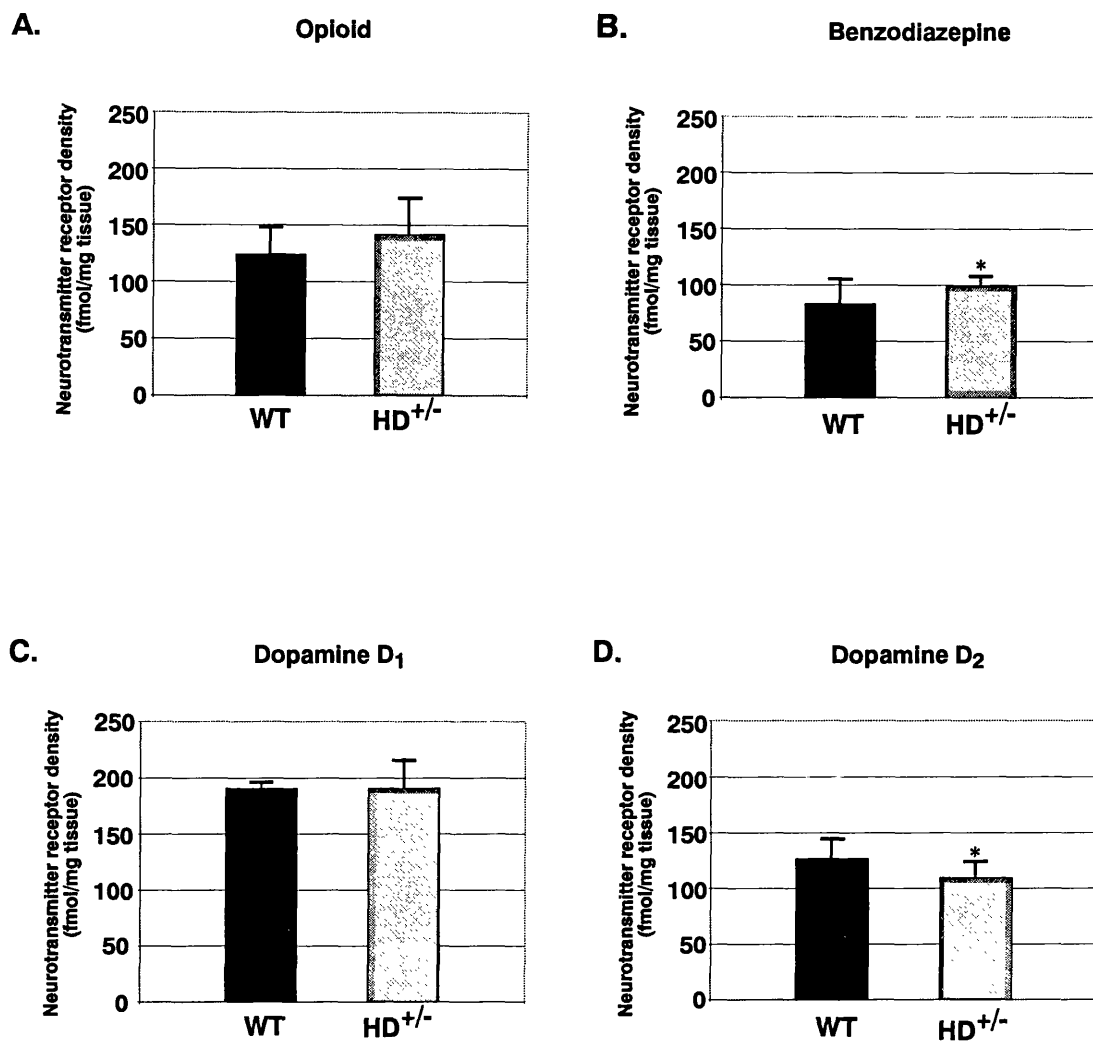


Figure 4.5 Striatal neurotransmitter receptor density

A. A bar graph illustrating the neurotransmitter receptor density in wild-type ($n=18$) and HD^{+/-} ($n=20$) mice. No significant difference was detected when opioid receptor density in the striatum of HD^{+/-} and wild-type mice were compared using the unpaired, two-tailed, Student's t -test ($p=0.07$).

B. A bar graph illustrating the neurotransmitter receptor density in wild-type ($n=17$) and HD^{+/-} ($n=17$) mice. A significant increase in benzodiazepine receptor density in HD^{+/-} mice was detected when compared to wild-type mice using the unpaired, two-tailed, Student's t -test ($*p=0.005$).

C. A bar graph illustrating the neurotransmitter receptor density in wild-type ($n=17$) and HD^{+/-} ($n=16$) mice. No significant difference in dopamine D₁ receptor density was detected in HD^{+/-} mice compared to wild-type when compared using the unpaired, two-tailed, Student's t -test ($p=0.9$).

D. A bar graph illustrating the neurotransmitter receptor density in wild-type ($n=17$) and HD^{+/-} mice ($n=15$). HD^{+/-} mice demonstrated a significant reduction in dopamine D₂ receptors when compared to wild-type mice using the unpaired, two-tailed, Student's t -test ($*p=0.006$).

Values of neurotransmitter receptor density expressed as a mean \pm S.D. (fmol/mg tissue).

Wild-type mice displayed a moderate dopamine D₂ binding within the striatum with a neurotransmitter receptor density of 127 ± 18 fmol/mg tissue (Figure 4.4D). In comparison HD^{+/-} mice displayed a neurotransmitter receptor density of 109 ± 14 fmol/mg tissue. Statistical analysis of the data revealed that HD^{+/-} mice exhibit a significantly lower striatal dopamine D₂ receptor density than their wild-type controls (two-tailed, Student's *t*-test, $p = 0.006$) (Figure 4.5D).

In summary, these studies revealed alterations in the neurotransmitter receptor profile within the striatum of mice carrying the HD mutation compared to wild-type controls. These changes are restricted to specific receptor types with no alterations observed in the opioid and dopamine D₁ receptor binding densities. In contrast, a significant reduction in the density of dopamine D₂ receptors and a significant increase of benzodiazepine receptor number within the striatum were observed in HD^{+/-} mice, compared to wild-type controls (Table 4.6).

4.4 Neurotransmitter receptor profiles in the cortex of 18 month old wild-type and HD^{+/-} mice

As in the striatal study (section 4.3), all values for neurotransmitter receptor density in the cortex were obtained from image analysis carried out as described in section 2.5.5. All measurements were taken from the same brain sections used for the striatal binding studies, since they included motor and somatosensory cortical regions (section 2.5.3). The numbers of animals included in the final analysis are indicated in Table 4.7.

Table 4.7 The number of mice on three different genetic backgrounds used for cortical analysis of each receptor type

Genetic background	Genotype	Cortex			
		Op	Ben	D ₁	D ₂
FVB/N	WT	6	6	6	N/A
	HD ^{+/-}	5	5	5	N/A
C57BL/6	WT	9	9	7	N/A
	HD ^{+/-}	10	10	6	N/A
DBA/2	WT	3	2	4	N/A
	HD ^{+/-}	6	2	5	N/A
Total	WT	18	17	17	N/A
	HD ^{+/-}	21	17	16	N/A

Op = Opioid, Ben = Benzodiazepine, D₁ = Dopamine D₁, D₂ = Dopamine D₂ neurotransmitter receptors. N/A= not analysed

The results indicated that opioid receptor binding was lower in the cortex than the striatum (Figure 4.4A). Cortical opioid receptor density in wild-type mice was 78 ± 16 fmol/mg tissue and in HD^{+/-} mice was 86 ± 17 fmol/mg tissue. No significant difference in opioid receptor density was detected between wild-type and HD^{+/-} mice, consistent with the findings in the striatum (two-tailed, Student's *t*-test, $p = 0.1$, Table 4.8) (Figure 4.6A).

Benzodiazepine binding sites were observed at high levels within the cortex (Figure 4.4B) and a mean neurotransmitter receptor density value of 225 ± 44 fmol/mg tissue was found in wild-type mice. HD^{+/-} mice displayed even higher neurotransmitter receptor density of 266 ± 30 fmol/mg tissue. Statistical analysis of the data revealed significantly more benzodiazepine binding sites within the cortex of HD^{+/-} mice, compared to wild-type controls (two-tailed, Student's *t*-test, $p = 0.003$) (Figure 4.6B). These results are consistent with the increased levels of benzodiazepine binding within the striatum of HD^{+/-} mice, when compared to wild-type controls.

Dopamine D₁ receptor density was detected at low levels within the cortex (Figure 4.4C). The neurotransmitter receptor density in wild-type mice was 12.4 ± 3.5 fmol/mg tissue and in HD^{+/-} mice was 14 ± 4 fmol/mg tissue. No statistically significant difference in dopamine D₁ receptor density in the cortex of wild type and HD^{+/-} mice was detected, consistent with the observations in the striatum (two-tailed, Student's *t*-test, $p=0.2$) (Figure 4.6C).

Receptor binding demonstrated very low levels of dopamine D₂ binding sites within the cortex (Figure 4.4D). In addition, the level of non-specific binding obtained with [³H]-YM09151-2 was 90 %, the highest non-specific binding obtained in this study. These factors contributed to a negligible detection of cortical dopamine D₂ receptor binding and therefore no data analysis was carried out. Although both dopamine D₁ and D₂ receptors are expressed on cortical neurons, the low levels of binding were not unexpected as previous reports have suggested that dopamine receptors have a lower expression in the cortex, especially in the motor and parietal cortex (Gaspar *et al.*, 1995), which represent the regions examined in this study. The slightly higher level of dopamine D₁ receptor density compared to dopamine D₂ receptors obtained in this study is also consistent with previously published data (Camps *et al.*, 1990).

These studies have demonstrated alterations in the neurotransmitter receptor profiles within the cortex of HD^{+/-} mice compared to their wild-type controls. Whilst dopamine D₁ and opioid receptor binding were unaffected, benzodiazepine receptor binding within the cortex of HD^{+/-} mice was significantly increased, when compared to wild-type controls (Table 4.8).

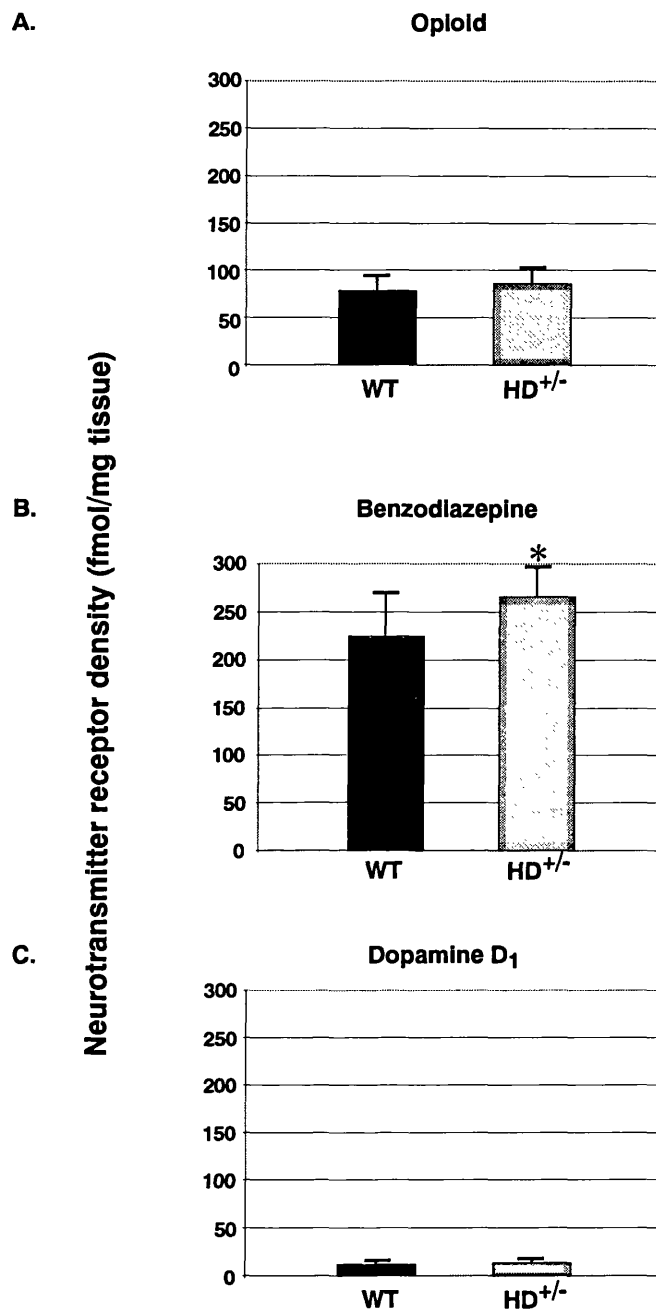


Figure 4.6 Cortical neurotransmitter receptor densities

Bar graphs comparing cortical neurotransmitter receptor densities in wild-type and HD^{+/-} mice. **A.** Opioid neurotransmitter receptor densities expressed as a mean \pm S.D. (fmol/mg tissue). No significant difference between cortical opioid receptor densities were detected when comparing wild-type and HD^{+/-} mice using the unpaired, two-tailed, Student's *t*-test, ($p=0.1$).

B. Benzodiazepine neurotransmitter receptor densities expressed as a mean \pm S.D. (fmol/mg tissue). A significant increase in cortical benzodiazepine receptor density in HD^{+/-} mice was detected when compared to wild-type mice using the unpaired, two-tailed, Student's *t*-test, ($*p=0.003$).

C. Dopamine D₁ neurotransmitter receptor densities expressed as a mean \pm S.D. (fmol/mg tissue). No significant difference between cortical dopamine D₁ receptor densities were detected when comparing wild-type and HD^{+/-} mice using the unpaired, two-tailed, Student's *t*-test, ($p=0.2$).

Table 4.8 The number of animals utilised and the neurotransmitter receptor density for each study investigating the receptor profiles within the cortex of 18 month old HD^{+/-} and wild-type mice

Receptor type	Genotype	Number of mice	Mean neurotransmitter receptor density \pm S.D. (fmol/mg tissue)	*p value
Opioid	WT	18	78 \pm 16	0.1
	HD ^{+/-}	21	86 \pm 17	
Benzodiazepine	WT	17	225 \pm 44	0.003
	HD ^{+/-}	17	266 \pm 30	
Dopamine D ₁	WT	17	12.4 \pm 3.5	0.2
	HD ^{+/-}	16	14 \pm 4	

* Values in bold represent statistical significance ($p < 0.05$) obtained using the two tailed, Student's *t*-test.

4.5 Investigating the influence of genetic background on neurotransmitter receptor profiles in mouse striatum and cortex

To explore the possible presence of genetic modifiers of the HD disease process the effect of three different genetic backgrounds on neurotransmitter receptor profiles was investigated. The previous experiments investigating neurotransmitter receptor density (sections 4.3 and 4.4) were carried out using cohorts of wild-type and HD^{+/-} mice containing animals on the FVB/N, C57BL/6 and DBA/2 inbred genetic backgrounds (Table 4.5 and 4.7). To determine whether genetic background has any influence on the neurotransmitter receptor densities obtained, the striatal and cortical neurotransmitter receptor densities were re-analysed following the subdivision of cohorts according to genetic background. As fewer animals were present in these cohorts statistical analysis using Student's *t*-test was not possible. A two-way ANOVA was subsequently carried out to detect possible trends in the data suggesting an influence of genetic background or the HD mutation on neurotransmitter receptor densities in these cohorts. The mean neurotransmitter receptor densities detected in HD^{+/-} and wild-type animals on the three different genetic backgrounds are presented in Tables 4.9- 4.12.

Table 4.9 Opioid neurotransmitter receptor densities in 18 month old wild-type and HD^{+/-} mice on different genetic backgrounds

Genetic Background	Genotype	Number of mice	Striatum Mean receptor density \pm S.D. (fmol/mg tissue)	Cortex Mean receptor density \pm S.D. (fmol/mg tissue)
FVB/N	WT	6	140 \pm 16	87 \pm 11
	HD ^{+/-}	5	167 \pm 34	95 \pm 8
C57BL/6	WT	9	113 \pm 25	70 \pm 15
	HD ^{+/-}	9	124 \pm 29	80 \pm 21
DBA/2	WT	3	125 \pm 18	85 \pm 19
	HD ^{+/-}	6	149 \pm 22	88 \pm 8

Table 4.10 Benzodiazepine neurotransmitter receptor densities in 18 month old wild-type and HD^{+/-} mice on different genetic backgrounds

Genetic Background	Genotype	Number of mice	Striatum Mean receptor density \pm S.D. (fmol/mg tissue)	Cortex Mean receptor density \pm S.D. (fmol/mg tissue)
FVB/N	WT	6	85 \pm 15	225 \pm 26
	HD ^{+/-}	5	98 \pm 9	258 \pm 31
C57BL/6	WT	9	88 \pm 11	218 \pm 54
	HD ^{+/-}	10	98 \pm 11	262 \pm 18
DBA/2	WT	2	89 \pm 13	258 \pm 37
	HD ^{+/-}	2	107 \pm 12	254 \pm 29

Table 4.11 Dopamine D₁ neurotransmitter receptor densities in 18 month old wild-type and HD^{+/-} mice on different genetic backgrounds

Genetic Background	Genotype	Number of mice	Striatum Mean receptor density \pm S.D. (fmol/mg tissue)	Cortex Mean receptor density \pm S.D. (fmol/mg tissue)
FVB/N	WT	6	196 \pm 24	12 \pm 3
	HD ^{+/-}	5	171 \pm 22	11 \pm 5
C57BL/6	WT	7	181 \pm 25	11 \pm 3
	HD ^{+/-}	6	212 \pm 7	17 \pm 3
DBA/2	WT	4	200 \pm 14	16 \pm 1
	HD ^{+/-}	5	184 \pm 27	14 \pm 2

Table 4.12 Dopamine D₂ neurotransmitter receptor densities in 18 month old wild-type and HD^{+/-} mice on different genetic backgrounds

Genetic Background	Genotype	Number of mice	Striatum Mean receptor density \pm S.D. (fmol/mg tissue)	Cortex Mean receptor density \pm S.D. (fmol/mg tissue)
FVB/N	WT	5	139 \pm 16	N/A
	HD ^{+/-}	4	117 \pm 15	N/A
C57BL/6	WT	9	125 \pm 16	N/A
	HD ^{+/-}	6	113 \pm 15	N/A
DBA/2	WT	3	112 \pm 18	N/A
	HD ^{+/-}	5	100 \pm 9	N/A

This study was designed to ask three important questions:

1. In a cohort of HD^{+/-} and WT mice on the same genetic background, does the presence of the HD mutation influence neurotransmitter receptor densities?
2. Does genetic background influence the neurotransmitter receptor densities of cohorts containing either HD^{+/-} or WT mice?
3. Does genetic background influence the effect that the HD mutation has on neurotransmitter receptor densities, i.e. is there an interaction between genetic background and the consequences of the mutation?

4.5.1 Investigating the influence of the HD mutation on neurotransmitter receptor densities in animals with the same genetic background

To investigate whether the influence of the HD mutation on neurotransmitter receptor densities can still be detected following subdivision of the previously used cohorts (sections 4.3 and 4.4) according to genetic background, a comparison of neurotransmitter receptor densities in WT and HD^{+/-} mice on the same genetic background was carried out (Table 4.13).

Table 4.13 Comparing neurotransmitter receptor densities in wild-type and HD^{+/-} mice divided into cohorts of the same genetic background. Values represent the p values obtained after the two-way ANOVA was used to compare the wild-type and HD^{+/-} neurotransmitter receptor density data

	Striatum				Cortex			
	Op	Ben	D ₁	D ₂	Op	Ben	D ₁	D ₂
Two-way ANOVA (effect of mutation)	0.03	0.01	0.7	0.01	0.2	0.02	0.4	N/A

Values in bold represent statistical significance (p<0.05) obtained using the two-way ANOVA. Op = Opioid, Ben = Benzodiazepine, D₁ = Dopamine D₁, D₂ = Dopamine D₂ neurotransmitter receptors.

When opioid neurotransmitter receptor density in HD^{+/-} and wild-type mice were analysed previously (section 4.3 and 4.4), pooling data from animals on different genetic backgrounds, no significant differences in opioid receptor densities between HD^{+/-} and wild-type mice were detected (Tables 4.6 and 4.8). This was mirrored by the two-way ANOVA suggesting no significant influence of the HD mutation on cortical opioid receptor density. The previous comparison did, however, produce a near significant result (p = 0.07) supporting a trend towards an increase in striatal opioid receptor density in HD^{+/-} mice compared to wild-type. The two-way ANOVA analysis supported this by suggesting an effect of the HD mutation on opioid receptor densities within the striatum (Table 4.13).

In previous studies (sections 4.3 and 4.4), a significant increase in benzodiazepine receptor densities was detected in the striatum and cortex of HD^{+/-} mice compared to wild-type (Tables 4.6 and 4.8). The two-way ANOVA, analysing the effect of the HD mutation when the cohort is divided according to genetic background, suggested that the HD mutation does have an influence on benzodiazepine neurotransmitter receptor densities in the striatum and cortex (Table 4.13).

The two-way ANOVA suggests that the HD mutation does not significantly influence the densities of dopamine D₁ neurotransmitter receptors in the striatum or cortex. In agreement, dopamine D₁ neurotransmitter receptors displayed no significant differences when analysed previously (sections 4.3 and 4.4) where data from mice with different genetic backgrounds was pooled (Tables 4.6 and 4.8).

Previous studies (section 4.3 and 4.4) had detected a significant reduction of dopamine D₂ receptors in the striatum of HD^{+/-} mice compare to wild-type (Table 4.6). The two-way ANOVA analysis suggested a significant influence of the HD mutation on the densities of striatal dopamine D₂ neurotransmitter receptors (Table 4.13).

Dividing the cohorts according to genetic background and statistical analysis by the two-way ANOVA determined whether the influence of the HD mutation on neurotransmitter receptor

densities, shown in previous experiments, could still be illustrated when comparing cohorts of wild-type and HD^{+/-} mice when distinguishing between different genetic backgrounds.

4.5.2 Investigating the influence of genetic background on neurotransmitter receptor densities in 18 month old HD^{+/-} or wild-type mice

To investigate whether genetic background influences neurotransmitter receptor densities in animals of the same genotype comparisons of neurotransmitter receptor densities in wild-type or HD^{+/-} mice on different genetic backgrounds were carried out by the two-way ANOVA (Table 4.14).

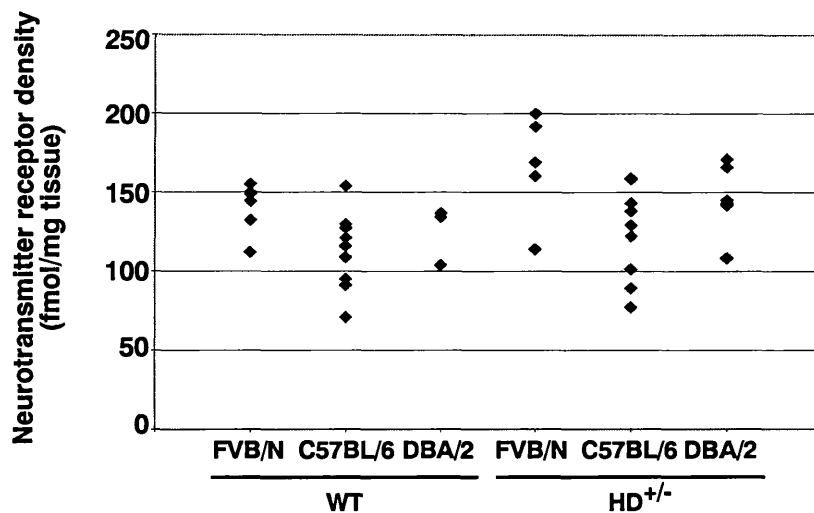
Table 4.14 The results of the two-way ANOVA comparing wild-type or HD^{+/-} mice on different genetic backgrounds

	Striatum				Cortex			
	Op	Ben	D ₁	D ₂	Op	Ben	D ₁	D ₂
Two-way ANOVA (effect of genetic background)	0.004	0.7	0.3	0.02	0.2	0.2	0.04	N/A

Values in bold represent statistical significance ($p < 0.05$) obtained using the two-way ANOVA. Op = Opioid, Ben = Benzodiazepine, D₁ = Dopamine D₁, D₂ = Dopamine D₂ neurotransmitter receptors.

Data for all mice included in the study of opioid neurotransmitter receptor density is shown in Figure 4.7. This illustration of the data, as well as supporting the suggestion that there is a subtle increase in opioid receptors in HD^{+/-} mice compared to wild-type (section 4.5.1), demonstrates that this subtle increase may not occur to the same extent in animals on all genetic backgrounds. HD^{+/-} mice on the FVB/N genetic background appear to exhibit a marked increase in striatal receptor density compared to all other cohorts (Figure 4.7A). The two-way ANOVA also suggests that genetic background does significantly influence opioid receptor density in the striatum. This suggestion is not repeated for the opioid receptor densities in the cortex and is supported by the raw data presented in Figure 4.7B.

A. Striatal opioid receptors



B. Cortical opioid receptors

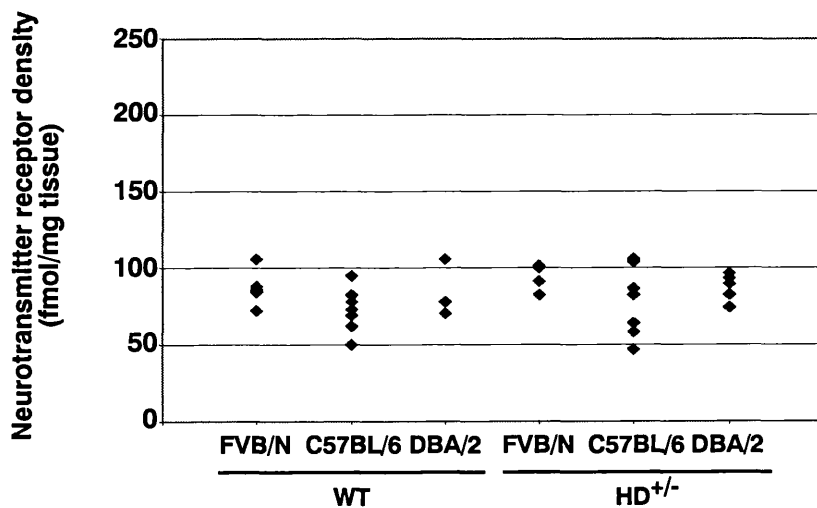


Figure 4.7 Opioid receptor density in the striatum and cortex

Scattergraphs illustrating the neurotransmitter receptor densities in individual mice grouped according to genotype and genetic background.

A. A scattergraph where each point represents the mean opioid receptor density in the striatum of an individual mouse.

B. A scattergraph where each point represents the mean opioid receptor density in the cortex of an individual mouse.

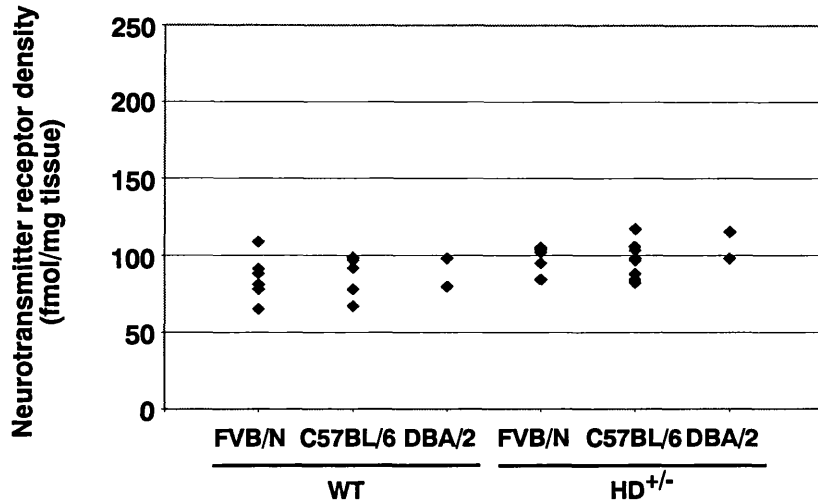
The two-way ANOVA suggests that genetic background did not influence the striatal or cortical density of benzodiazepine receptors (Table 4.14). These findings are supported as no obvious variation between mice of the same genotype on different genetic backgrounds can be seen when the data are presented in scattergraphs (Figure 4.8A and B). As the HD mutation has been previously shown to significantly effect benzodiazepine receptor binding in the striatum and cortex (sections 4.3, 4.4 and 4.5.1), the data are consistent with the notion that it is the HD mutation, not genetic background, that is responsible for the increase in benzodiazepine neurotransmitter receptor densities in HD^{+/-} mice compared to wild-type controls.

The two-way ANOVA suggested that genetic background was influencing dopamine D₁ receptor densities within the cortex but not in the striatum. The scattergraph does show fluctuations between animals of different genetic backgrounds in the striatum, however, this may be due to variance within the cohorts (Figure 4.9A). In addition, as the receptor densities observed for dopamine D₁ receptors within the cortex were extremely low and below the linear range of the radioactive standards, the significance of the results must be interpreted with caution. These findings suggest some influence of genetic background on the consequences of the HD mutation, however, this influence would need further investigation to establish its exact nature.

The two-way ANOVA suggested an influence of genetic background on dopamine D₂ receptor densities and Figure 4.9B illustrates variations between animals of the same genotype on different genetic backgrounds. However, the same general variations are seen between wild-type and HD^{+/-} mice on each genetic background. The previous studies (sections 4.3, 4.4 and 4.5.1) detected a significant decrease in dopamine D₂ receptors in HD^{+/-} mice compared to wild-type controls. However, the data discussed in this paragraph could mean that the extent of this HD mutation influence may be modified by genetic background.

In summary, these analyses have illustrated that genetic background alone can influence neurotransmitter receptor densities in wild-type and HD^{+/-} mice. It was also demonstrated that the effect of genetic background could vary depending on the particular combination of genetic background and receptor type under investigation.

A. Striatal benzodiazepine receptors



B. Cortical benzodiazepine receptors

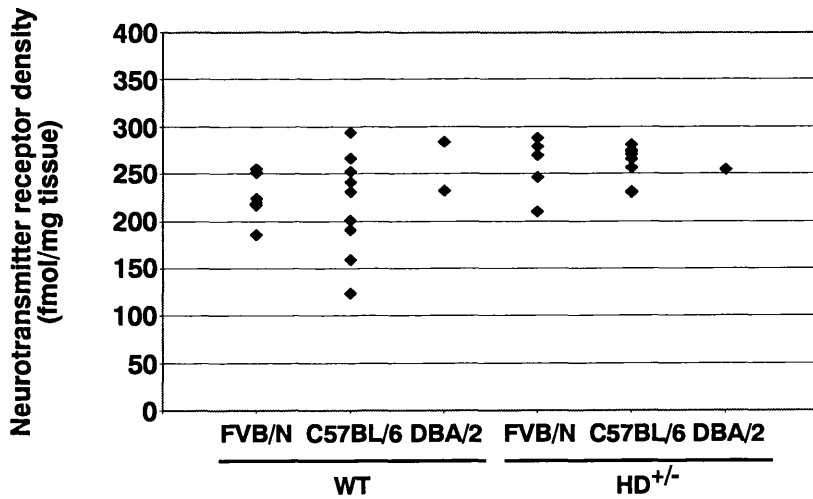


Figure 4.8 Benzodiazepine receptor density in the striatum and cortex

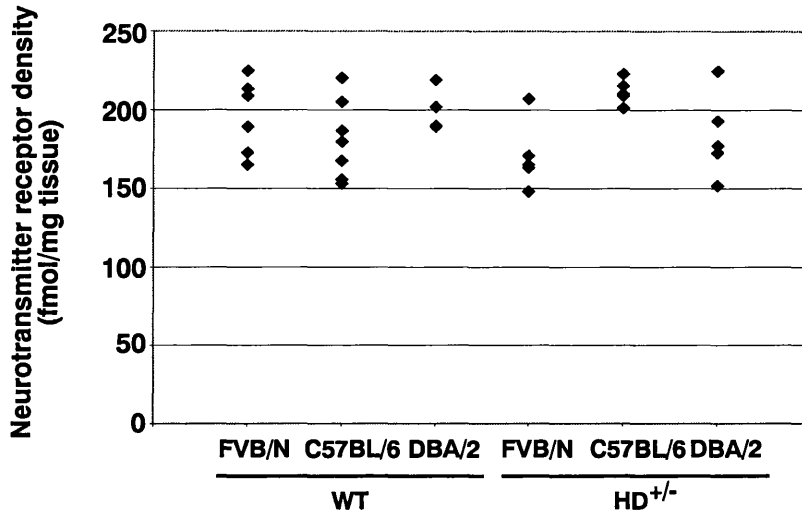
Scattergraphs illustrating the neurotransmitter receptor densities in individual mice grouped according to genotype and genetic background.

A. A scattergraph where each point represents the mean benzodiazepine receptor density in the striatum of an individual mouse.

B. A scattergraph where each point represents the mean benzodiazepine receptor density in the cortex of an individual mouse.

A.

Striatal Dopamine D₁ receptors



B.

Striatal Dopamine D₂ receptors

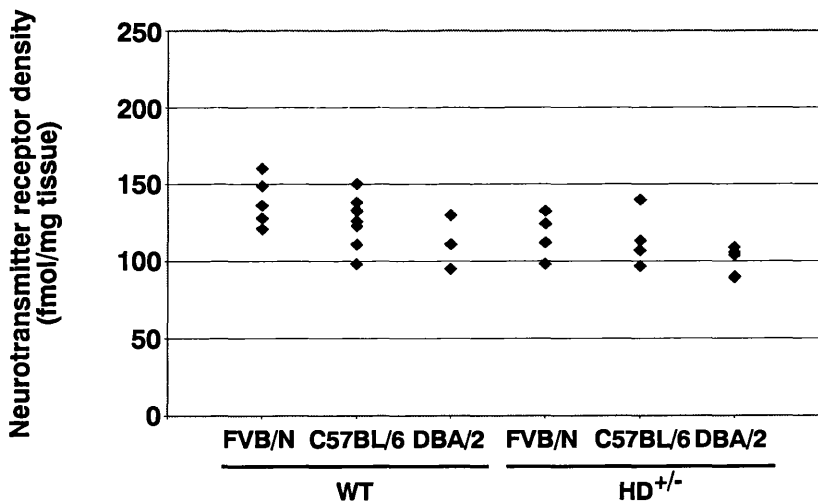


Figure 4.9 Dopamine D₁ and D₂ receptor densities in the striatum

Scattergraphs illustrating the neurotransmitter receptor densities in individual mice grouped according to genotype and genetic background.

A. A scattergraph where each point represents the mean dopamine D₁ receptor density in the striatum of an individual mouse.

B. A scattergraph where each point represents the mean dopamine D₂ receptor density in the striatum of an individual mouse.

4.5.3 Investigating whether genetic background influences the consequences of the HD mutation

To investigate whether genetic background influences the effect that the HD mutation has on neurotransmitter receptor densities, two-way ANOVA was carried out (Table 4.15). This analysis determines whether there is any interaction between the genetic background of the animal and the consequences of the HD mutation.

Table 4.15 The presence of any interaction between genetic background and the consequences of the HD mutation for the previously investigated neurotransmitter receptors

	Striatum				Cortex			
	Op	Ben	D ₁	D ₂	Op	Ben	D ₁	D ₂
Two-way ANOVA (interaction?)	No	No	Yes	No	No	No	Yes	N/A

Op = Opioid, Ben = Benzodiazepine, D₁ = Dopamine D₁, D₂ = Dopamine D₂ neurotransmitter receptors.

The analysis suggests there is no interaction between genetic background and the consequences of the HD mutation when considering opioid, benzodiazepine and dopamine D₂ neurotransmitter receptor densities in cortex and striatum. This enables the two influencing factors on neurotransmitter receptor densities, genetic background and HD mutation, to be analysed separately. However, an interaction was suggested when investigating the influence of genetic background and the HD mutation on the neurotransmitter receptor densities of dopamine D₁ receptors. This means that analysing these factors individually may lead to misleading conclusions about the influence of each factor on receptor densities.

In summary, it has been demonstrated that genetic background can influence neurotransmitter receptor profiles in wild-type and HD^{+/-} mice. This effect varies depending on the receptor type analysed. For example, it appears that benzodiazepine receptor binding is not affected by the genetic backgrounds included in this study and the alterations between wild-type and HD^{+/-} mice are due to the HD mutation. However, it has also been established that mice bred onto different genetic backgrounds can exhibit differences in receptor densities between mice of the same genotype (e.g. opioid receptors).

These findings have implications when interpreting data obtained from mice on mixed genetic backgrounds and comparing mice on different genetic backgrounds. Future experimental design should incorporate these findings by utilising cohorts of animals with the same genetic backgrounds. These studies also demonstrate the possible presence of genetic modifiers of the HD

disease process. Identification of the molecular nature of these modifiers may provide potential candidates for new targets in therapeutic intervention.

4.6 Investigating the influence of mouse age on neurotransmitter receptor profiles

As alterations in neurotransmitter receptor densities were demonstrated in old (18 month) HD^{+/-} mice, when compared to wild-type a pilot study was instigated to investigate the progressive nature and onset of the receptor changes. In order to determine the effect of age on neurotransmitter receptor density, cohorts of wild-type and HD^{+/-} mice of three different ages were examined. The time points investigated were 4 months, 10 months and 18 months of age. All cohorts were made up of male mice on the C57BL/6 genetic background. Neurotransmitter receptor density was obtained by measurements collected as previously described in section 2.5.3 and the results analysed by the two-way ANOVA. The mean receptor densities detected for each neurotransmitter receptor in animals of three different ages are presented in Tables 4.16 - 4.19.

Table 4.16 Opioid neurotransmitter receptor densities in wild-type and HD^{+/-} mice of different ages

Age	Genotype	Number of mice	Striatum Mean receptor density ± S.D. (fmol/mg tissue)	Cortex (months) Mean receptor density ± S.D. (fmol/mg tissue)
4	WT	5	131 ± 26	87 ± 17
	HD ^{+/-}	5	143 ± 10	91 ± 10
10	WT	5	142 ± 16	89 ± 8
	HD ^{+/-}	5	150 ± 30	96 ± 14
18	WT	4	117 ± 8	74 ± 3
	HD ^{+/-}	4	138 ± 36	84 ± 17

Table 4.17 Benzodiazepine neurotransmitter receptor densities in wild-type and HD^{+/-} mice of different ages

Age (months)	Genotype	Number of mice	Striatum Mean receptor density ± S.D. (fmol/mg tissue)	Cortex Mean receptor density ± S.D. (fmol/mg tissue)
4	WT	5	90 ± 19	251 ± 52
	HD ^{+/-}	5	90 ± 9	244 ± 16
10	WT	5	93 ± 13	253 ± 28
	HD ^{+/-}	4	95 ± 9	232 ± 20
18	WT	4	98 ± 5	249 ± 15
	HD ^{+/-}	4	95 ± 6	222 ± 35

Table 4.18 Dopamine D₁ neurotransmitter receptor densities in wild-type and HD^{+/-} mice of different ages

Age (months)	Genotype	Number of mice	Striatum Mean receptor density \pm S.D. (fmol/mg tissue)	Cortex Mean receptor density \pm S.D. (fmol/mg tissue)
4	WT	5	203 \pm 22	9 \pm 4
	HD ^{+/-}	4	240 \pm 16	17 \pm 1
10	WT	5	224 \pm 21	18 \pm 3
	HD ^{+/-}	5	222 \pm 17	15 \pm 2
18	WT	4	222 \pm 6	16 \pm 2
	HD ^{+/-}	4	231 \pm 11	17 \pm 3

Table 4.19 Dopamine D₂ neurotransmitter receptor densities in wild-type and HD^{+/-} mice of different ages

Age (months)	Genotype	Number of mice	Striatum Mean receptor density \pm S.D. (fmol/mg tissue)	Cortex Mean receptor density \pm S.D. (fmol/mg tissue)
4	WT	5	129 \pm 11	N/A
	HD ^{+/-}	3	128 \pm 20	N/A
10	WT	4	117 \pm 5	N/A
	HD ^{+/-}	5	136 \pm 21	N/A
18	WT	4	107 \pm 18	N/A
	HD ^{+/-}	4	113 \pm 11	N/A

The initial comparisons in this pilot study of neurotransmitter receptor densities in the striatum and cortex of animals at different ages were carried out by Student's *t*-tests comparing HD^{+/-} and wild-type animals in the same age groups (Table 4.20). The absence of any receptor alterations at 18 months of age disagreed with the previously reported receptor changes (sections 4.3, 4.4 and 4.5) and illustrated that smaller cohorts fail to demonstrate the subtle receptor density alterations previously detected in these HD mice.

Table 4.20 The results of the Student’s *t*-tests comparing wild-type or HD^{+/-} mice of the same age

	Striatum				Cortex			
	Op	Ben	D ₁	D ₂	Op	Ben	D ₁	D ₂
WT₄ vs HD^{+/-}₄	0.30	0.85	0.03	0.69	0.65	0.81	0.02	N/A
WT₁₀ vs HD^{+/-}₁₀	0.61	0.70	0.92	0.12	0.69	0.31	0.6	N/A
WT₁₈ vs HD^{+/-}₁₈	0.66	0.66	0.20	0.52	0.28	0.20	0.49	N/A

Values in bold represent statistical significance ($p < 0.05$) obtained using the two tailed, Student’s *t*-test. Op = Opioid, Ben = Benzodiazepine, D₁ = Dopamine D₁, D₂ = Dopamine D₂ neurotransmitter receptors. 4, 10, 18 = age in months.

The only significant differences detected were increases in dopamine D₁ receptor density in the striatum ($p = 0.03$) and cortex ($p = 0.02$) of HD^{+/-} mice compared to their wild-type controls at 4 months of age. These were the only significant differences observed at any of the time points examined (Table 4.20).

In an attempt to investigate any trends in this data a two-way ANOVA was carried out (Table 4.21). The results of the two-way ANOVA tests are consistent with those in Table 4.20, in as much as the striatal dopamine D₁ neurotransmitter receptor density is the only effect of the HD mutation. An effect of age was suggested to produce the significant changes in dopamine D₁ receptors within the cortex. The interpretation of this data is complicated by the previously detected interaction between the consequences of the HD mutation and genetic background when analysing dopamine D₁ receptor density.

Table 4.21 The significance of the effect of the HD mutation and age on neurotransmitter receptor densities. Whether there is an interaction between the two factors influencing neurotransmitter receptor densities.

	Striatum				Cortex			
	Op	Ben	D ₁	D ₂	Op	Ben	D ₁	D ₂
Two-way ANOVA (effect of mutation)	0.15	0.97	0.04	0.3	0.15	0.15	0.09	N/A
Two-way ANOVA (effect of age)	0.29	0.58	0.84	0.08	0.08	0.72	0.02	N/A
Two-way ANOVA (interaction?)	No	No	No	No	No	No	Yes	N/A

Values in bold represent statistical significance ($p < 0.05$) obtained using the two-way ANOVA. Op = Opioid, Ben = Benzodiazepine, D₁ = Dopamine D₁, D₂ = Dopamine D₂ neurotransmitter receptors.

These results suggest no alterations in neurotransmitter receptor densities in 18 month old HD^{+/-} mice compared to wild-type controls. This does not support the findings in sections 4.3, 4.4 and 4.5, using larger cohorts of animals. This pilot study suggests that the changes in neurotransmitter receptor densities in these HD^{+/-} mice at 18 months of age are subtle and larger cohorts are needed to detect significant changes. The findings also suggest that any progressive changes in HD^{+/-} or wild-type mice may be masked or confounded by small numbers of animals in each cohort. The subtlety of changes observed in this study are emphasised by reports that similar sized cohorts (n=6-12) of other HD mouse models provided highly significant results when used in autoradiographic binding studies (Cha *et al.*, 1998).

4.7 Summary of Results

This study has demonstrated that there are alterations in the neurotransmitter receptor profiles within the brains of 18 month old mice carrying the HD mutation. Within the striatum a significant increase in the density of benzodiazepine neurotransmitter receptors has been shown in HD^{+/-} mice. This alteration was also observed in the cerebral cortex demonstrating that the effects of the HD mutation are not restricted to the striatum. Further investigation would be required to determine if these alterations occur at the same time point in the animals life and occur in the same progressive manner. In keeping with previous studies in human HD subjects and HD mice (Andrews *et al.*, 1999; Cha *et al.*, 1998; Kunig *et al.*, 2000; Lawrence *et al.*, 1998b; Turjanski *et al.*, 1995; Weeks *et al.*, 1996) a significant reduction in dopamine D₂ receptor density within the striatum was also detected in the mutant mice. The lack of neurodegeneration observed within the brains of the HD^{+/-} mice (section 1.5.3.2) suggests that the neurotransmitter receptor changes may not be the result of depleted neuronal populations but may represent cellular alterations involved in early HD pathogenesis. By investigating the effect of mutation and genetic background on these results it was demonstrated that genetic background could, to varying extents, influence the receptor densities reported. This effect was most obvious when investigating opioid and dopamine D₁ receptor types. In contrast genetic background was found to have no effect on the result when examining benzodiazepine receptor binding and the alterations observed were due to the HD mutation. These findings illustrate the care needed when designing experiments and interpreting data obtained from mice on mixed or different genetic backgrounds. An attempt was also made to establish the temporal nature of receptor density alterations. By examining mice of different ages it was anticipated that the onset and association with phenotypic changes could be assessed. However, the pilot study demonstrated that the subtle changes in receptor densities occurring in this HD mouse model cannot be assessed using cohorts that contain a small number of animals. Therefore, in order to further explore the temporal nature of any receptor density alterations, it is likely that cohorts consisting of > 15 mice on the same genetic background would probably be required.

5 Characterisation of somatic repeat instability in a knock-in mouse model of Huntington's disease

5.1 Aims of the study

The mutation responsible for Huntington's disease is the expansion of the trinucleotide (CAG) repeat within exon 1 of the *HD* gene ((HDCRG), 1993). The number of repeats present is inversely correlated to age at onset and the degree of neuropathology at death (Andrew *et al.*, 1993; Duyao *et al.*, 1993; Ranen *et al.*, 1995; Telenius *et al.*, 1993; Trottier *et al.*, 1994). Cell-selective vulnerability has been observed in HD with the medium spiny neurons within the striatum initially affected by the disease process (Vonsattel *et al.*, 1985). The ubiquitous expression pattern of the *HD* gene does not correlate with the tissue-selective pattern of HD neuropathology. We hypothesise that somatic repeat instability could play a role in the selective vulnerability observed in HD. Specific cell-types may be more prone to changes in repeat length producing a population of cells, expressing longer CAG repeats, that would be more vulnerable to the disease process. The aim of this study was to explore the existence of somatic repeat instability in the HD mouse model and, if found, to characterise the pattern and extent of repeat instability present. This study utilised the sensitive technique of small pool PCR, which allows the determination of the CAG repeat copy number on individual mutant alleles and therefore reveals the distribution of repeat sizes within a tissue.

The study was designed to address the following questions:

- Is somatic repeat instability present in HD^{+/-} mice? This question was investigated by small pool PCR analysis to determine the length of the CAG repeat present in the mouse *Hdh* gene in DNA obtained from 16 different tissues. 24 month old HD^{+/-} mice were used as previous investigations have indicated late-onset and progressive consequences of the HD mutation in these animals (Shelbourne *et al.*, 1999; Usdin *et al.*, 1999), L.K., unpublished data, chapters 3 and 4).
- Does the striatum display significantly greater repeat instability compared to other tissues and brain regions? Quantification of repeat size distributions within selected tissues by single molecule small pool PCR analysis was used to determine if the striatum, the brain region predominantly affected by HD pathology, exhibits the greatest repeat instability. This investigation was carried out on several 24 month old animals to determine the reproducibility of the results.

- Is somatic repeat instability apparent from birth or does it display a late onset? Does somatic repeat instability occur in a progressive manner and what is the nature of the progression? Does somatic repeat instability maintain the same pattern of tissue-specificity at all ages where repeat instability is observed? HD is a late onset and progressive disorder, and molecular events such as repeat instability, if involved in or acting as a surrogate marker of the disease process, would be expected to occur in a similar manner. Investigating the nature and timing of the molecular consequences of the HD mutation and its association with phenotypic alterations in HD^{+/-} mice will provide insights into the possible molecular mechanisms underlying these phenotypic changes. If repeat instability is a molecular marker of the disease process, the knowledge of its onset and progression may have implications for the timing and duration of any HD treatment strategies. These questions were addressed by investigating repeat instability within several brain regions of HD^{+/-} mice at 5 different time points throughout life.
- Does somatic repeat instability occur in human HD patients? It is essential to establish if molecular changes observed in HD^{+/-} mice are present in human HD patients to assess the relevance of the findings. Investigating somatic repeat instability in human tissue may uncover an early molecular mechanism underlying pathogenesis in human HD. To answer this question small pool PCR analysis was carried out on several brain regions from a human juvenile HD patient.
- Does experimental technique influence the extent of somatic repeat instability detected? This study aims to evaluate the relative sensitivity of techniques used to detect somatic repeat instability. To address this issue, identical samples were analysed using both small pool PCR and Genescan technology.

By investigating somatic repeat instability, early molecular events contributing to HD pathogenesis may be uncovered and present possible targets for future therapeutic intervention. Somatic repeat instability may also be a molecular marker of the disease process and, as such, may provide one approach to assess the efficacy of future therapies.

5.2 Investigating somatic repeat instability in 24 month old HD^{+/-} mice

Small pool PCR (section 2.4) was utilised to investigate the presence of somatic repeat instability in HD^{+/-} mice. This technique amplifies relatively small amounts of template DNA (1.2 ng - 3 pg) and visualises the PCR products by Southern blotting. Reduced competition during amplification and the sensitive visualisation technique enables PCR products from individual alleles to be

detected. Small pool PCR can therefore establish if alleles within the same tissue carry different sized repeats.

Initially, multiple (5-6) PCR amplifications with serial dilutions (1.2 ng - 3 pg of template DNA per reaction) of template DNA were carried out (Figure 5.1). The PCR products obtained from amplifications using the highest DNA concentrations (e.g. >300 pg) allowed the general spectrum of repeat sizes within a tissue to be demonstrated. Lower DNA concentrations (e.g. <12 pg) revealed PCR products representing the CAG repeat lengths within the *Hdh* gene from individual cells. Several different dilutions of template DNA were used as analysis of small numbers of genomes alone can produce misleading patterns of repeat instability due to random sampling variation.

Small pool PCR amplifications using 5 different dilutions (1.2 ng - 12 pg) of template DNA allowed semi-quantitative analysis to be carried out on between 1000-3000 mutant alleles from 16 different tissues (Table 5.1) obtained from 24 month old HD^{+/-} mice (Table 2.1). The HD^{+/-} mice originated from a line carrying a mutant *Hdh* allele with 72 CAG repeats (Shelbourne *et al.*, 1999). The 16 tissues analysed included major somatic organs, sperm and several regions of the central nervous system, as HD is a neurological disorder. Analysis was carried out for all 16 tissues in two 24 month old HD^{+/-} mice and selected tissues from a further four 24 month old HD^{+/-} mice.

It was apparent from the small pool PCR autoradiograms that somatic repeat instability occurred in the tissues of old HD^{+/-} mice (Figure 5.2).

The maximum repeat length observed for each tissue and the percentage of alleles that appeared to exhibit a repeat size change distinguishable from the prominent band representing the mutant progenitor allele repeat length were determined. The maximum repeat length observed, although dependent on the number of mutant alleles examined, does give a general indication of the potential for repeat length changes in each tissue.

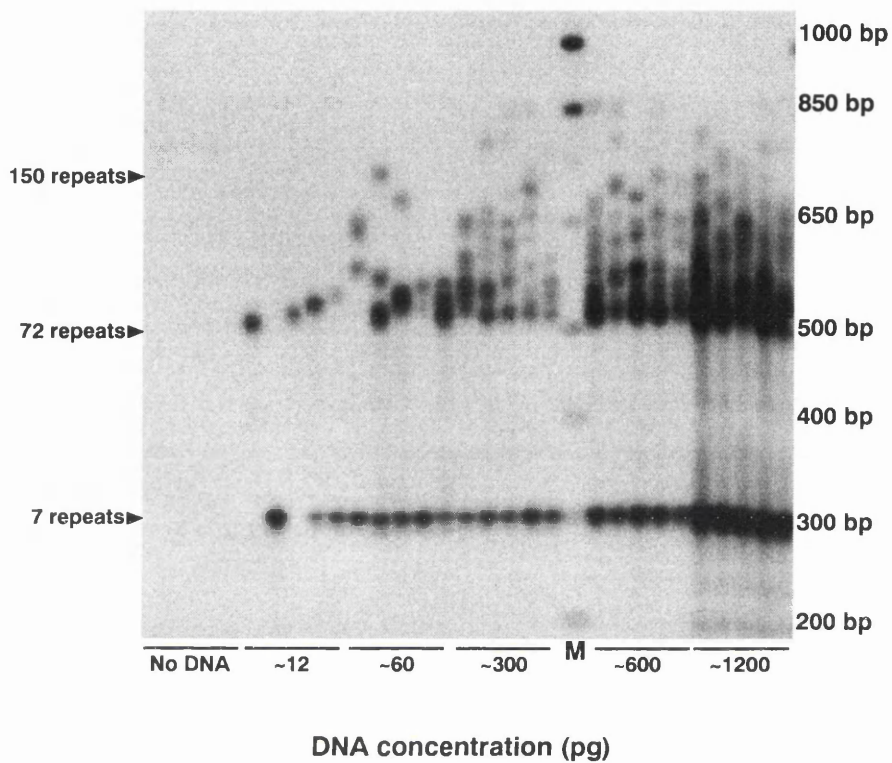


Figure 5.1 Serial dilutions of striatal DNA from a 24 month old HD^{+/-} mouse analysed by small pool PCR (SP-PCR)

A representative autoradiogram of five SP-PCR amplification replicates for each DNA concentration plus five lanes representing the negative control reactions containing no DNA template. M denotes the lane containing the 1 kb plus size marker used to establish the size of the PCR products. The numbers listed on the right of the panel correspond to the values present in the 1 kb plus size marker and the numbers on the left indicate the estimated number of CAG repeats. The DNA concentration indicated under the panel represents the amount added as template to each PCR amplification. The band in each lane found at ~300 bp represents the wild-type allele carrying 7 CAG repeats. The PCR products found at ~500 bp and above represent the *Hdh* mutant allele. The varying sized PCR products represent individual mutant alleles demonstrating somatic repeat instability.

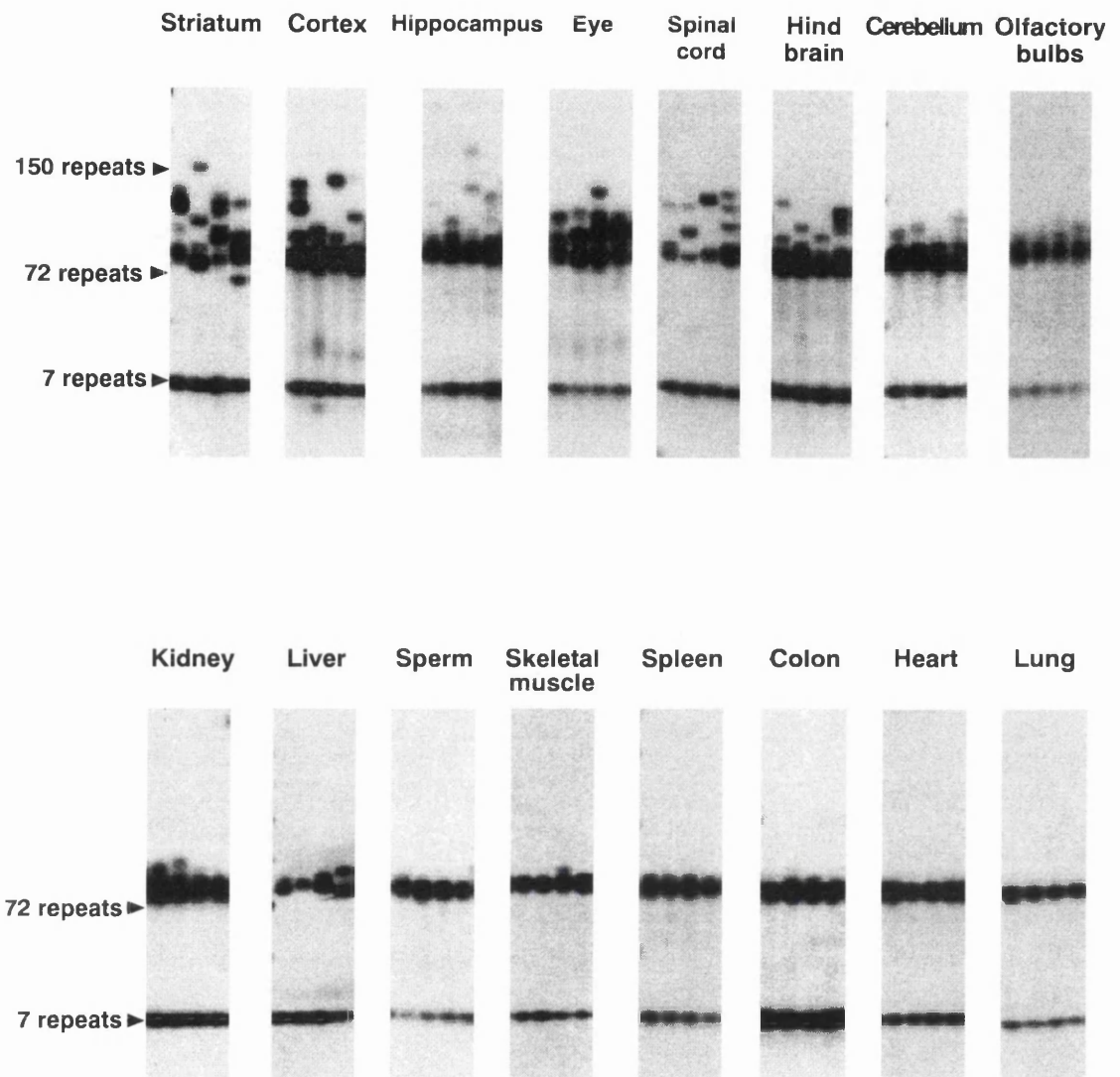


Figure 5.2 Somatic repeat instability of the CAG repeat mutation in 24 month old HD^{+/-} mice

A comparison of the CAG repeat mutation instability in 16 different tissues from 24 month old HD^{+/-} mice. Each panel shows 4 lanes of SP-PCR products derived from approximately 10 cells worth (~60 pg) of DNA obtained from the tissues specified above each panel. The tissues are ordered across the page from the top left to the bottom right to represent the order of variability and magnitude of repeat instability observed in these reactions and confirmed in others (data not shown). The numbers on the far left of the panels indicate the estimated number of CAG repeats carried by the PCR products.

Table 5.1 Semi-quantitative analysis of 1000-3000 mutant alleles for 16 different tissues in 24 month old HD^{+/-} mice

	% of alleles unstable	largest alleles detected
Striatum	>80%	398
Cortex, Hippocampus, Cerebellum, Hindbrain Spinal cord, Eye, Olfactory bulbs, Kidney	30-80%	124-192
Liver, Colon, Spleen, Heart, Skeletal muscle Sperm, Lung	2-30%	85-112

'% of alleles unstable' is the percentage of total alleles analysed, which produced bands, not contained within the prominent mutant allele band. In semi-quantitative analysis, to discriminate unstable alleles from the progenitor allele band, it is estimated that the repeat size change must be $> \pm 2$ repeats from the progenitor allele repeat length.

'Largest alleles detected' is the range of alleles that encompasses the individual maximum repeat lengths for every tissue within the category.

When ordered with respect to the variability and magnitude of repeat instability, the highest ranked tissues were predominantly regions of the central nervous system. The region that consistently displayed the highest repeat instability was the striatum, the region selectively involved in HD pathology (Figure 5.2). The striatum contained a high percentage (>80 %) of cells that no longer contained the progenitor allele repeat size (Table 5.1). This brain region also displayed cells containing the longest repeat lengths when compared to other tissues. It was estimated that ~5 % of striatal cells in 24 month old HD^{+/-} mice contained a repeat length double that of the progenitor allele length and ~0.5 % of cells contained a repeat of >250 CAG repeats.

Two male and four female mice were included in these investigations and no significant difference in the pattern and extent of somatic repeat instability was observed between the sexes.

Repeat instability of the mutant allele appeared to occur in an expansion-biased manner. Bands in a size range between the wild-type allele (7 CAG) and the prominent mutant band (~72 CAG) were rarely observed (Figure 5.1 and 5.2) suggesting that although contractions of the mutant CAG repeat may occur, they do not occur as frequently as expansions.

An investigation into the stability of the repeat on the wild-type allele was necessary to allow full evaluation of the mutation repeat instability. The wild-type allele in heterozygous HD^{+/-} mice consistently produced a discrete band and failed to display any obvious fluctuation in repeat size. The absence of bands representing intermediate allele sizes between the wild-type and mutant

allele suggested that if significant repeat instability of the wild-type allele were occurring, the resulting PCR products would fall within the mutant allele repeat range (i.e. >500 bp). To investigate whether the wild-type allele was contributing to the mutation repeat instability profile, the occurrence of bands within the mutant range in DNA from wild-type animals was investigated. Striatal DNA from two wild-type animals, matched for age and genetic background to the HD^{+/-} mice investigated, was analysed and ~1000 wild-type alleles amplified in serial dilutions. No bands other than those representing the wild-type (7 CAG) allele were detected, suggesting that no significant repeat instability occurs on the *Hdh* allele within wild-type mice (Figure 5.3). However, this investigation does not account for the possibility that the wild-type allele may display greater repeat instability in the presence of an HD mutant allele. However, it seems unlikely that repeat length changes, of the magnitude required for the wild-type allele to contribute to the mutation profile, are generated from the short, interrupted repeat sequence found on the wild-type allele within these HD^{+/-} mice.

In summary, repeat length variability of the mutant allele was observed in HD^{+/-} mice and occurred in a tissue-specific, expansion-biased manner. The striatum, the brain region selectively vulnerable in early HD pathology, was the brain region in all HD^{+/-} mice examined that displayed the greatest repeat instability.

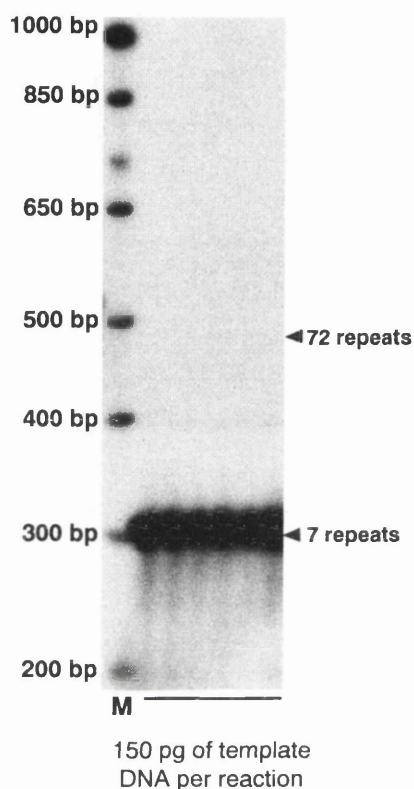


Figure 5.3 The CAG repeat length variability in 24 month old wild-type mice

A representative autoradiogram of 6 lanes of PCR products obtained from approximately 150 pg of template DNA derived from the striatum of a wild-type mouse. M denotes the lane containing the 1 kb plus size marker used to establish the number of CAG repeats carried by the PCR products. SP-PCR analysis of striatal DNA for two 24 month old wild-type mice demonstrated the absence of any significant repeat size variation when ~1000 wild-type alleles were examined.

5.3 Quantification of somatic repeat instability in 24 month old HD^{+/-} mice

5.3.1 Quantitative small pool PCR

Analysis of single genomes by small pool PCR allows the quantification of the mutation spectrum present within different tissues (Jeffreys *et al.*, 1994; Monckton *et al.*, 1995). Obtaining the mutation spectrum for different tissues permits more detailed characterisation of repeat instability and allows statistical comparison in order to further investigate tissue-specificity and inter-animal differences.

To quantify repeat instability the number of amplifiable molecules present within a sample must be accurately determined. This calculation must be carried out empirically for each DNA sample investigated. Calculating the dilution needed to obtain one amplifiable molecule in each PCR allows the CAG repeat length within the mutant *Hdh* gene in individual cells to be determined.

To determine the concentration of amplifiable molecules within a sample, 8-10 small pool PCR amplifications of several low (estimated at <12 pg of template DNA per reaction) dilutions were carried out to obtain a dilution that provided several lanes that displayed a radioactive signal (positive lanes), and in addition, several which failed to produce a signal (blank lanes). The resultant autoradiograms were then used to accurately determine the exact number of amplifiable templates in the known DNA dilution.

As the concentration of DNA template for each PCR amplification was obtained by dilution it is possible that amplifications producing one band could contain more than one template DNA molecule, as both may have the same repeat length giving rise to bands of equal size. Thus using lanes that display a radioactive signal (positive lanes) to calculate the number of template molecules in each PCR may under-estimate the DNA concentration of the dilution. However, there is no ambiguity concerning the concentration of amplifiable DNA molecules within reactions that produce blank lanes (lanes with no radioactive signal) as no products are observed.

$p(0)$, the proportion of blank lanes was calculated for a known dilution,

$$p(0) = (\text{total number of lanes} - \text{number of positive lanes}) / \text{total number of lanes}$$

The Poisson distribution is then exploited to calculate the exact number of DNA templates in that dilution,

$$\text{Number of amplifiable molecules per reaction} = -\ln p(0)$$

5.3.2 Quantification of selected tissues from a 24 month old HD^{+/-} mouse

Small pool PCR analysis was carried out to determine the repeat copy number carried by individual mutant *Hdh* alleles in striatal and cortical brain regions, as these regions are implicated in HD neuropathology. In addition, hippocampal and cerebellar brain regions, thought to be less involved in HD pathology, were investigated for comparison. The kidney, the non-CNS somatic tissue displaying the highest variability of repeat lengths, was also investigated for comparison with the brain regions.

Multiple amplifications were carried out using single molecule dilutions (section 5.3.1) and each resultant PCR product sized as described in section 2.4.6.5. To illustrate the distribution of CAG repeat lengths on the mutant *Hdh* allele in individual tissues, histograms were produced showing the percentage of alleles investigated containing a specific repeat length. The mutant allele repeat size distributions for these selected tissues from a HD^{+/-} mouse (animal 1) are shown in Figure 5.4.

Small pool PCR analysis utilising DNA derived from a tail-tip sample obtained at weaning established this animal's progenitor mutant allele repeat size as 77 CAG repeats. To investigate the mutation spectra observed in different tissues, several characteristics of the repeat size distributions were examined and are presented in Tables 5.2 and 5.3.

Table 5.2 presents the 'median repeat length' to assess whether an overall change in repeat size within a tissue has occurred and the 'median repeat change' to establish the magnitude of the repeat changes, which typically occur. The range of repeat lengths present within each tissue were determined by the maximum and minimum repeat lengths (Table 5.2, Max and Min repeat length).

To further assess the mutation spectra, Table 5.3 presents the 'percentage of total alleles undergone repeat size change' illustrating the number of mutant alleles that have undergone a change in mutation load. The 'percentage of total alleles double the progenitor repeat' was calculated to assess the occurrence of large repeat lengths within a tissue. To assess the direction and magnitude of the repeat length changes that have occurred, the relationship between expansions and contractions was investigated by examining the 'percentage of altered alleles that have expanded'. To assess the typical magnitude of changes the proportion of alleles that have undergone expansion or contraction, which remained within 3 repeats of the progenitor allele '% of expansions < 3 repeats' and '% of contractions < 3 repeats' were calculated.

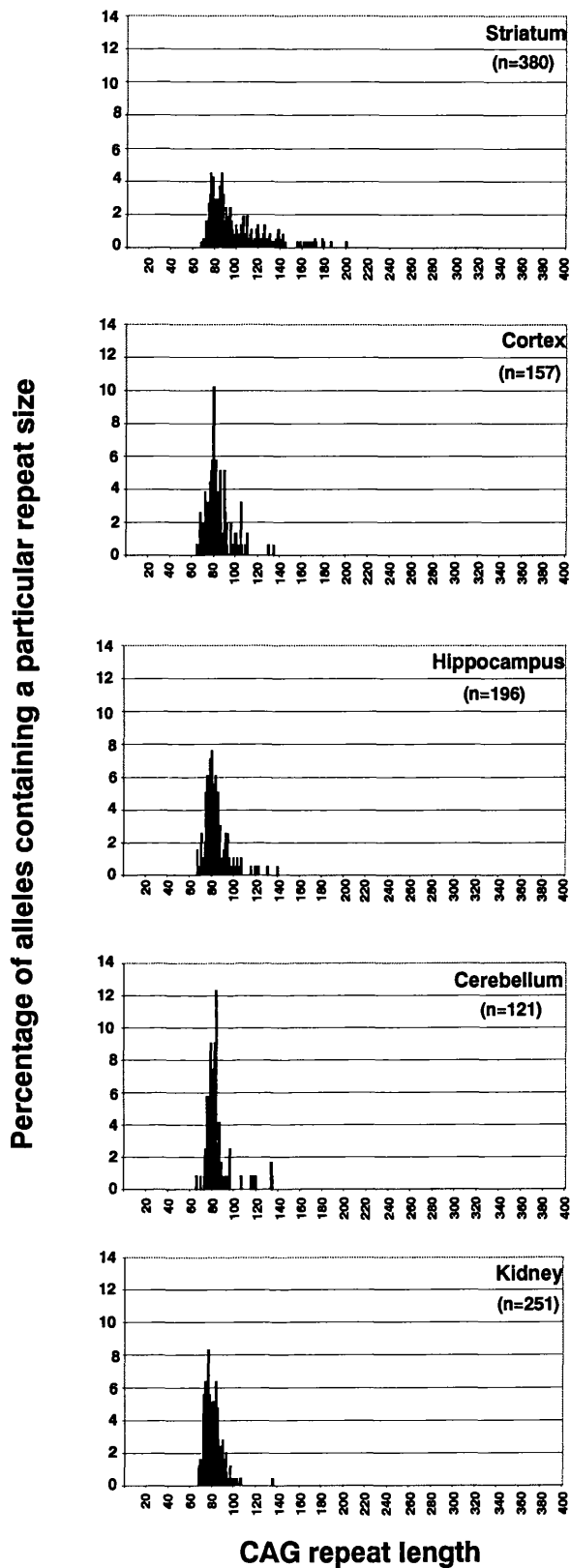


Figure 5.4 The distribution of CAG repeat lengths carried by individual alleles within tissues of a 24 month old HD^{+/-} mouse

Histograms illustrating the distribution of repeat sizes within each tissue by demonstrating the proportion of alleles analysed containing the designated repeat length. The tissue type is denoted in the top right of each panel. n = the number of mutant alleles analysed for each tissue. The median repeat length and statistical comparisons of these distributions are shown in Tables 5.2, 5.3. and 5.4.

Table 5.2 Mutation length profiles of 5 different tissues from a 24 month old HD^{+/-} mouse with a progenitor allele of 77 CAG repeats (animal 1)

Tissue	Number of alleles examined	Median repeat length	Median repeat change	Max repeat length	Min repeat length
Striatum (St)	380	89	+ 12	201	68
Cortex (Ctx)	157	82	+ 5	135	65
Cerebellum (Cb)	121	82	+ 5	135	66
Hippocampus (Hip)	196	81	+ 4	140	67
Kidney (K)	251	79	+ 2	136	68

max = maximum, min = minimum.

Table 5.3 Mutation length profiles of 5 different tissues from a 24 month old HD^{+/-} mouse with a progenitor allele of 77 CAG repeats (animal 1)

Tissue	% of total alleles undergone repeat size change	% of total alleles double progenitor repeat	% of altered alleles that have expanded	% of expansions < 3 repeats	% of contractions < 3 repeats
Striatum (St)	95 %	4.5 %	89 %	11 %	68 %
Cortex (Ctx)	95 %	0 %	96 %	28 %	33 %
Cerebellum (Cb)	94 %	0 %	88 %	24 %	79 %
Hippocampus (Hip)	95 %	0 %	79 %	27 %	67 %
Kidney (K)	92 %	0 %	63 %	24 %	52 %

‘% of total alleles undergone repeat size change’ is the percentage of mutant alleles investigated that no longer carried 77 CAG repeats.

‘% of total alleles double progenitor repeat’ is the percentage of mutant alleles investigated that carried > 154 CAG repeats.

‘% of altered alleles that have expanded’ is the percentage of all the mutant alleles which no longer carried 77 CAG repeats which carried > 77 CAG repeats.

‘% of expansions < 3 repeats’ is the percentage of alleles with > 77 CAG repeats which carried 78 - 80 CAG repeats.

‘% of contractions < 3 repeats’ is the percentage of alleles displaying < 77 CAG repeats which carried 74 -76 CAG repeats.

As expected from previous small pool PCR experiments investigating serial dilutions of DNA samples (section 5.2), the distribution of mutant allele repeat lengths in the kidney was relatively limited (Figure 5.4). The kidney had a median repeat length of 79 CAG repeats and displayed a small median repeat length change of + 2 repeats (Table 5.2). The maximum and minimum repeat lengths observed from 251 mutant alleles were 136 repeats and 68 repeats, respectively (Table 5.2). Very large changes in repeat length within kidney cells appeared to be relatively rare as no alleles carrying a repeat size that had doubled in length, compared to the mutant progenitor allele, were obtained (Table 5.3). Repeat instability occurred in an expansion-biased manner, accounting for 63 % of all changes in repeat length (Table 5.3). The magnitude of expansions was commonly greater than 3 repeats as only 24 % of expansions remained within 3 repeats of the progenitor allele. Contractions displayed a reduced propensity to produce alleles with large repeat length changes, as 52 % of all contractions remained within 3 repeats of the progenitor allele (Table 5.3).

A high percentage (95 %) of hippocampal cells displayed a change in repeat length and 79 % of these changes were expansions (Table 5.3). A preponderance of large expansions and small contractions (as seen in the kidney) was also observed (Table 5.3). The median repeat length was 81 repeats and the median repeat length change + 4 repeats (Table 5.2). The maximum repeat length detected from 196 mutant alleles was 140 repeats and the minimum was 67 repeats (Table 5.2). No alleles with a repeat size that was over double the mutant progenitor allele size were detected (Table 5.3).

The patterns of repeat instability in the cerebellum and hippocampus were similar. Within the cerebellum approximately 88 % of all changes in repeat length on the mutant allele were expansions and only 24 % of these remained within 3 repeats of the progenitor mutation size (Table 5.3). Of the few contractions observed, 79 % remained within 3 repeats of the progenitor mutation repeat length (Table 5.3). The cerebellum displayed a median repeat length of 82 repeats with a median repeat length change of + 5 repeats (Table 5.2). A maximum of 135 repeats and a minimum of 66 repeats were detected in the 121 mutant alleles sampled (Table 5.2). No alleles were detected carrying a repeat size that had doubled in length compared to the mutant progenitor allele size (Table 5.3).

The cortex displayed a median repeat length of 82 repeats and a median repeat change of + 5 repeats (Table 5.2). Amongst the 157 mutant alleles sampled, the maximum repeat size detected was 135 repeats and the minimum was 65 repeats (Table 5.2). No cortical cells carrying a repeat size that had doubled in length, compared to the mutant progenitor allele size, were detected (Table 5.3). The same expansion-biased pattern of repeat instability was observed and the propensity for large expansions but small contractions was seen (Table 5.3).

In contrast, the profile of repeat sizes in the striatum encompassed a significantly wider range of repeat lengths, compared to other tissues (Figure 5.4). The maximum repeat length detected from 380 mutant alleles sampled was 201 repeats and the minimum was 68 repeats (Table 5.2). A higher median repeat length (89 repeats) was observed and the median repeat change was + 12 repeats (Table 5.2). To illustrate the magnitude of repeat size changes, approximately 4.5 % of all striatal cells analysed contained a repeat size over double the mutant progenitor length (Table 5.3). Expansion-biased repeat instability was observed in the striatum with 89 % of altered alleles displaying an expansion and 89 % of the expansions over three repeats longer than the progenitor allele repeat length (Table 5.3). The mutation profiles observed within the striatum of this HD^{+/-} mouse were consistent with the semi-quantitative analysis in section 5.3.

In summary, the mutation profile data showed that the kidney displayed the narrowest range of repeat sizes and the highest number of mutant alleles that retained the progenitor allele repeat length. The cortex, cerebellum and hippocampus all showed similar patterns of repeat instability. However, the striatum displayed a significantly wider repeat length distribution than the other tissues, with the highest values for median repeat length and median repeat length change. The results suggest that the cells within the striatum contain the largest mutation sizes and greatest variability.

Statistical comparison of the mutation profiles obtained for each tissue was carried out to further examine the tissue-specific pattern of repeat instability. Statistical comparisons of the repeat length distributions from different tissues were made using the Mann-Whitney U statistical test (Table 5.4). The Mann-Whitney U test is used to compare the elements of two populations to assess whether the bulk of elements in one population are larger than those in the other, by asking whether the median repeat length of one population is significantly different from the other.

Statistical comparison of the repeat length distributions revealed that the median repeat length in the kidney was significantly smaller than that in all other tissues examined (Table 5.4). The repeat size distributions of the cortex, hippocampus and cerebellum were not significantly different (Table 5.4) suggesting several regions of the brain display similar patterns of repeat instability. The median repeat length of the striatum was significantly higher than the median repeat lengths observed in all other tissues examined. This suggests that the striatum displays significantly greater somatic repeat instability than all other tissues examined in old HD^{+/-} mice (Table 5.4).

Table 5.4 Statistical comparison of the mutation length distributions of five different tissues from one 24 month old HD^{+/-} mouse (animal 1)

Tissue	Comparison	*p value
Striatum (St)	St vs Ctx	<0.0001
	St vs Hip	<0.0001
	St vs Cb	<0.0001
	St vs K	<0.0001
Cortex (Ctx)	Ctx vs Hip	0.9
	Ctx vs Cb	0.6
	Ctx vs K	0.004
Hippocampus (Hip)	Hip vs Cb	0.6
	Hip vs K	0.0004
Cerebellum (Cb)	Cb vs K	0.0002

K = Kidney , * Values in bold represent statistical significance ($p < 0.05$) of data analysed using the Mann-Whitney U statistical test. All comparisons are based on the median repeat lengths found in Table 5.2. obtained from the size distributions shown in Figure 5.4.

5.3.3 Reproducibility of repeat instability profiles in 24 month old HD^{+/-} mice

The studies carried out in section 5.3.2 were replicated to establish the reproducibility of the pattern and distribution of repeat instability observed in a single 24 month old HD^{+/-} mouse (animal 1). The variability and magnitude of somatic repeat instability was investigated in a second HD^{+/-} mouse (animal 2) matched for genetic background and age to animal 1. The progenitor allele repeat length for animal 2 was established at 79 CAG repeats by small pool PCR analysis of DNA obtained from a tail-tip sample taken at weaning. The characteristics of the mutation profiles obtained from animal 2 are presented in Tables 5.5 and 5.6. The repeat distributions for the 5 selected tissues are shown in Figure 5.5.

Statistical analysis was carried out to assess the relationship between the mutation profiles of different tissues within animal 2 (Table 5.7) followed by statistical comparison of the mutation profiles obtained from animals 1 and 2 (Table 5.8 and 5.9).

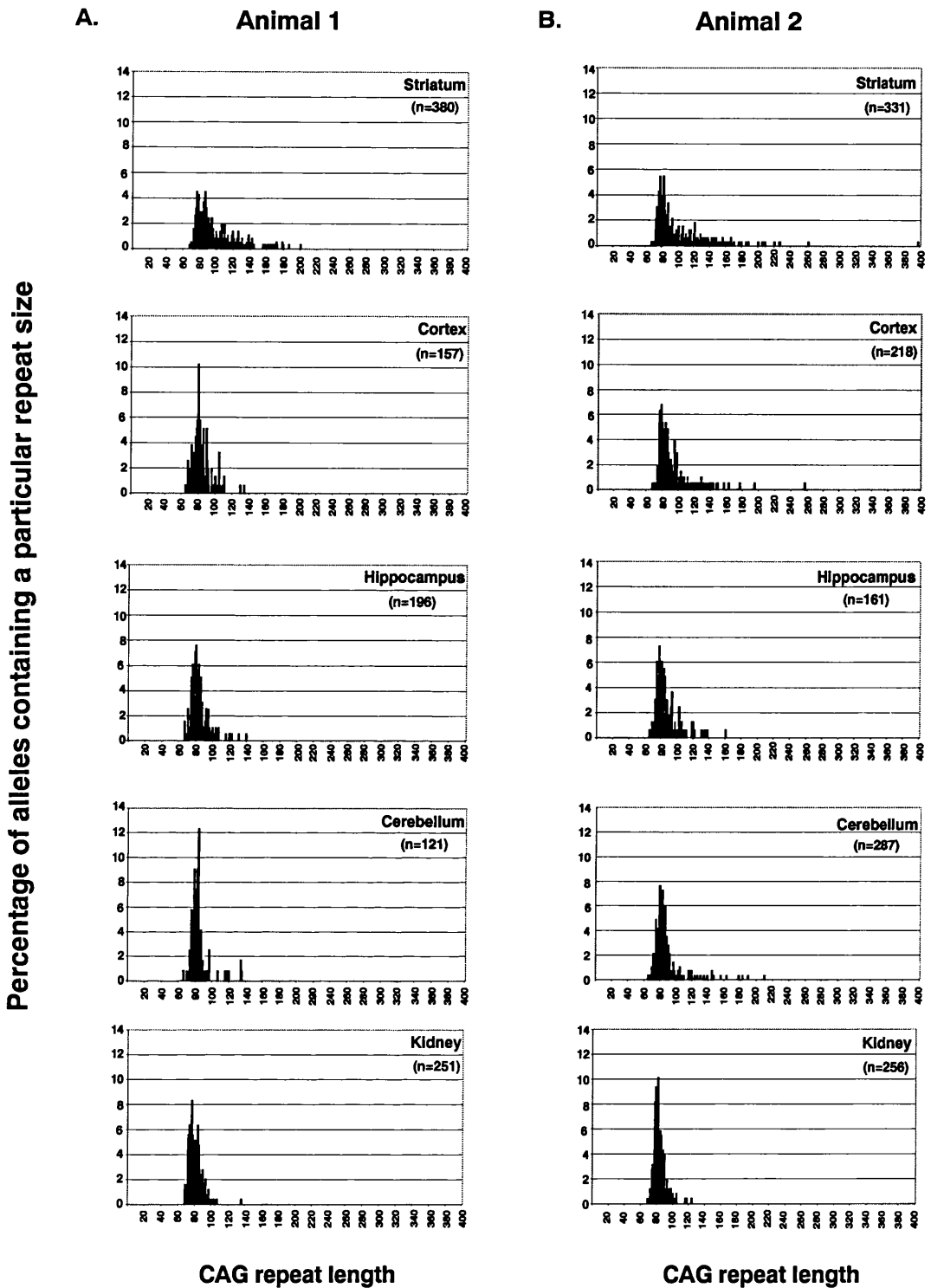


Figure 5.5 Comparison of the mutation profiles in old HD^{+/-} mice

Histograms illustrating the distribution of repeat sizes within each tissue by demonstrating the proportion of cells analysed containing a particular repeat length. The tissue type is denoted in the top right of each panel. **A.** Repeat size distributions for the HD^{+/-} mouse previously shown in Figure 5.4. **B.** Repeat size distributions for a second HD^{+/-} mouse. n = the number of mutant *Hdh* alleles analysed for each tissue. The median repeat lengths and statistical comparisons between the tissues of animal 2 can be seen in Table 5.5, 5.6 and 5.7 and for the same tissues between the two HD^{+/-} mice in Table 5.8 and 5.9.

Table 5.5 Mutation length profiles of 5 different tissues from a 24 month old HD^{+/-} mouse with a progenitor allele of 79 repeats (animal 2)

Tissue	Number of alleles examined	Median repeat length	Median repeat change	Max repeat	Min repeat
Striatum (St)	331	87	+ 8	398	68
Cortex (Ctx)	218	84.5	+ 5.5	258	68
Cerebellum (Cb)	287	83	+ 4	210	66
Hippocampus (Hip)	161	82	+ 3	161	66
Kidney (K)	256	82	+ 3	124	69

max = maximum, min = minimum

Table 5.6 Mutation length profiles of 5 different tissues from a 24 month old HD^{+/-} mouse with a progenitor allele of 79 repeats (animal 2)

Tissue	% of total alleles undergone repeat size change	% of total alleles double progenitor repeat	% of altered alleles that have expanded	% of expansions < 3 repeats	% of contractions < 3 repeats
Striatum (St)	95 %	6 %	80 %	13 %	61 %
Cortex (Ctx)	94 %	1.4 %	77 %	19 %	74 %
Cerebellum (Cb)	94 %	1.4 %	75 %	25 %	47 %
Hippocampus (Hip)	94 %	1 %	65 %	25 %	51 %
Kidney (K)	91 %	0 %	76 %	37 %	64 %

'% of total alleles undergone repeat size change' is the percentage of mutant alleles investigated that no longer carried 79 CAG repeats.

'% of total alleles double progenitor repeat' is the percentage of mutant alleles investigated that carried > 158 CAG repeats.

'% of altered alleles that have expanded' is the percentage of all the alleles which no longer carried 79 CAG repeats which carried > 79 CAG repeats.

'% of expansions < 3 repeats' is the percentage of alleles displaying > 79 CAG repeats which carried 80 - 82 CAG repeats.

'% of contractions < 3 repeats' is the percentage of alleles displaying < 79 CAG repeats which carried 76 - 78 CAG repeats.

The data obtained from animal 2 illustrates that the repeat instability in this HD^{+/-} mouse appears similar to that found in animal 1. The somatic repeat instability in animal 2 also occurred in an expansion-biased manner with a small percentage of cells retaining the progenitor allele repeat length. Variation in the magnitude of expansions and contractions was again observed, with contractions tending to be small (1-3 repeats) and expansions tending to be > 3 repeats greater than the progenitor allele. However, the magnitude of mutation size appeared to be greater in animal 2 (when compared to animal 1) as all brain regions contained repeats twice the size of the progenitor allele.

Despite this difference, features of the overall pattern of tissue-specificity were maintained, as the striatum still displayed a significantly higher median repeat length compared to all other tissues examined (Table 5.7) and the kidney still displayed the most limited variation in repeat size (Figure 5.5). The cortex displayed a significantly higher median repeat length than all other tissues except the striatum (Table 5.7) and the hippocampus, cerebellum and kidney did not differ statistically from each other but all showed significantly smaller median repeat lengths than the cortex and striatum (Table 5.7).

Table 5.7 Statistical comparison of the repeat size distributions of five different tissues from one 24 month old HD^{+/-} mouse (animal 2)

Tissue	Comparison	*p value
Striatum (St)	St vs Ctx	0.02
	St vs Hip	<0.0001
	St vs Cb	<0.0001
	St vs K	<0.0001
Cortex (Ctx)	Ctx vs Hip	0.003
	Ctx vs Cb	0.005
	Ctx vs K	<0.0001
Hippocampus (Hip)	Hip vs Cb	0.5
	Hip vs K	0.8
Cerebellum (Cb)	Cb vs K	0.1

K = Kidney, * Values in bold represent statistical significance ($p < 0.05$) of data analysed using the Mann-Whitney U statistical test. All comparisons are based on the median repeat lengths found in Table 5.5, obtained from the repeat distributions shown in Figure 5.5.

Statistical comparison of the repeat size distributions from the same tissues in animal 1 and 2 revealed similar repeat size distributions in both animals (Table 5.8). However, there were significant differences in the mutation profiles displayed by the cortex and kidney (Table 5.8). These differences may be a consequence of random sampling variation or inter-animal variation.

Table 5.8 Statistical comparison of the repeat size distributions of the same tissues in different 24 month old HD^{+/-} mice

Tissue	Median repeat lengths		Comparison	p value* repeat length
	Animal 1 (# alleles)	Animal 2 (# alleles)		
Striatum (St)	89 (380)	87 (331)	St vs St	0.4
Cortex (Ctx)	82 (157)	84.5 (218)	Ctx vs Ctx	0.0002
Cerebellum (Cb)	82 (121)	83 (287)	Cb vs Cb	0.2
Hippocampus (Hip)	81 (196)	82 (161)	Hip vs Hip	0.4
Kidney (K)	79 (251)	82 (256)	K vs K	<0.0001

* Values in bold represent statistical significance ($p < 0.05$) of data analysed using the Mann-Whitney U statistical test. All comparisons are based on the median repeat lengths found in Tables 5.2 and 5.5.

As longer repeats display a greater tendency to expand, it is possible that the slight variation in the mutation profiles of the two HD^{+/-} mice is due to the two repeats difference in the progenitor allele repeat length. To take the progenitor allele repeat length into account, re-analysis of the distributions was carried out using the change in repeat length (median repeat length change) rather than the absolute repeat length for each comparison (Table 5.9). When comparing the median repeat length change in the striatum of animal 1 and 2, a significant difference was obtained. The median repeat length change distributions for all other tissues did not display statistically significant variation between animals. It is still unknown whether the comparisons between the animals yielded significant differences due to sampling variation or natural variation between individual mice.

Table 5.9 Statistical comparison of the repeat change distributions of the same tissues in different 24 month old HD^{+/-} mice

Tissue	Median repeat change		Comparison	p value* repeat change
	Animal 1 (# alleles)	Animal 2 (# alleles)		
Striatum (St)	+ 12 (380)	+ 8 (331)	St vs St	0.007
Cortex (Ctx)	+ 5 (157)	+ 5.5 (218)	Ctx vs Ctx	0.06
Cerebellum (Cb)	+ 5 (121)	+ 4 (287)	Cb vs Cb	0.1
Hippocampus (Hip)	+ 4 (196)	+ 3 (161)	Hip vs Hip	0.1
Kidney (K)	+ 2 (251)	+ 3 (256)	K vs K	0.1

* Values in bold represent statistical significance ($p < 0.05$) of data analysed using the Mann-Whitney U statistical test. All comparisons are based on the median repeat changes found in Table 5.2. and 5.5.

In summary, although some differences in the extent of repeat instability were detected when absolute repeat length or repeat length change distributions were compared, the general pattern of tissue-specificity in both HD^{+/-} mice analysed, in terms of the variability and magnitude of repeat instability, was maintained. The striatum consistently displayed a significantly greater variability and magnitude of repeat instability compared to all other tissues examined in both animals.

5.4 Investigating the progressive nature of somatic repeat instability within HD^{+/-} mice

In order to ascertain the time course of mutation instability in HD^{+/-} mice, DNA samples from the striatum, cortex, hippocampus and cerebellum were analysed from animals of 3, 9, 15, 19 and 24 months of age (Figure 5.6). Approximately 1000 mutant alleles were examined from the chosen brain regions of several HD^{+/-} mice (2-6 animals) of each time point, matched for genetic background and mutation line (Table 2.1).

Negligible repeat instability was observed at 3 months of age in all brain regions (Figure 5.6) suggesting somatic repeat instability has an onset in adult life.

Consistent with this speculation, small changes of 3-5 repeats were seen infrequently but to a similar extent in all brain regions of 9 month old mice (Figure 5.6). This suggests that the mechanism responsible for repeat size change may initiate at the same time and have a similar effect in all brain regions sampled.

At 15 months of age larger changes in repeat length were observed and these seemed to occur in a tissue-specific manner. The repeat instability had increased in all brain regions compared to that observed at 9 months. However, analysis of ~ 1000 mutant alleles from each brain region showed that the striatum displayed the greatest variability and magnitude of repeat size changes, when compared to the other brain regions examined (Figure 5.6).

The progressive increase in repeat instability in all brain regions continued at 19 and 24 months of age (Figure 5.6). At all time points after the initial appearance of repeat instability, the striatum demonstrated the greatest variability and magnitude of repeat instability. These observations suggest that the underlying mechanism responsible for repeat instability occurs in all brain regions and initiates at a similar time point during adult life. However, the tissue-specific mutation profiles within older mice suggest that a brain region-specific factor may be responsible for the greater repeat length variability and mutation size observed in the striatum.

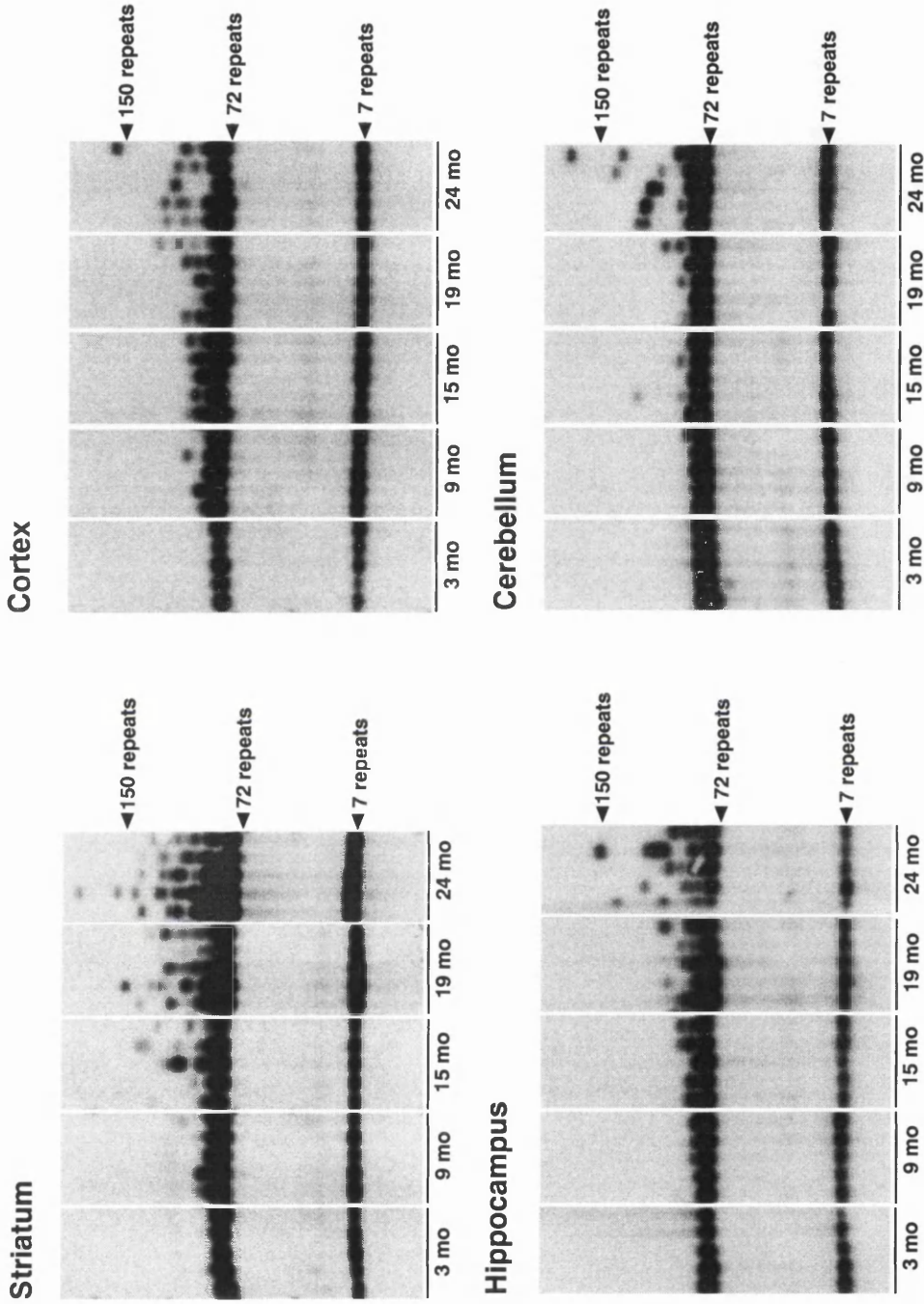


Figure 5.6 The progressive nature of CAG repeat instability in the brain of HD^{+/-} mice. Each panel shows 5 lanes of SP-PCR analysis of 10-20 cells worth of template DNA. All tissues originate from HD^{+/-} mice of the age indicated below the panel. mo = months. The numbers on the right side of the panels represent the number of CAG repeats for the corresponding PCR products.

5.5 Investigating somatic repeat instability in human HD

To investigate the occurrence of somatic repeat instability in human HD patients, small pool PCR was carried out on human HD tissue obtained from a juvenile HD patient. Post-mortem examination of the brain established extensive neurodegeneration within the caudate nucleus and confirmed the diagnosis of HD.

The predominant mutant allele repeat size obtained from the post-mortem tissue was estimated at 87 CAG repeats. As earlier DNA samples were not available for this individual, it is unknown if this repeat length was carried on the mutant *HD* allele at birth.

Tissue samples from the cortex, hippocampus, substantia nigra and caudate nucleus brain regions were obtained. Two different regions of the cortex, the temporal lobe and the parietal lobe were available for comparison. The small sample denoted the caudate nucleus was collected from a region that had suffered extensive degenerative changes, as noted in the post-mortem report. The results obtained from this sample must therefore be interpreted with caution, as the cell populations retained will not necessarily reflect that of an intact caudate nucleus.

Small pool PCR analysis was carried out on DNA from all available brain regions by multiple amplifications of serial DNA concentrations as described in sections 5.3 and 2.4.

Based on data obtained from wild-type mouse tissue (section 5.3), it is assumed that wild-type alleles within human tissue would not exhibit a significant degree of repeat instability. The human wild-type allele in this patient contained approximately 24 CAG repeats (Figure 5.7) and demonstrated no obvious fluctuations in repeat length in all brain regions. As in mouse tissue, no intermediate bands between the products from the wild-type and prominent mutant allele were observed. This suggests that repeat instability on the wild-type allele would have to produce PCR products within the mutant allele range. It is deemed unlikely that the wild-type allele is capable of expanding to an extent in which it contributes to the mutant allele mutation spectrum.

Expansion-biased somatic repeat instability of the mutant allele repeat was detected in brain regions from this human HD patient (Figure 5.7). Extensive repeat instability was observed in both cortical regions analysed (Figure 5.7). High variability and magnitude of repeat size changes were observed and a maximum repeat length of >700 repeats from ~500 mutant alleles was detected. No expanded CAG repeat of this length, associated with HD, has previously been reported in the literature.

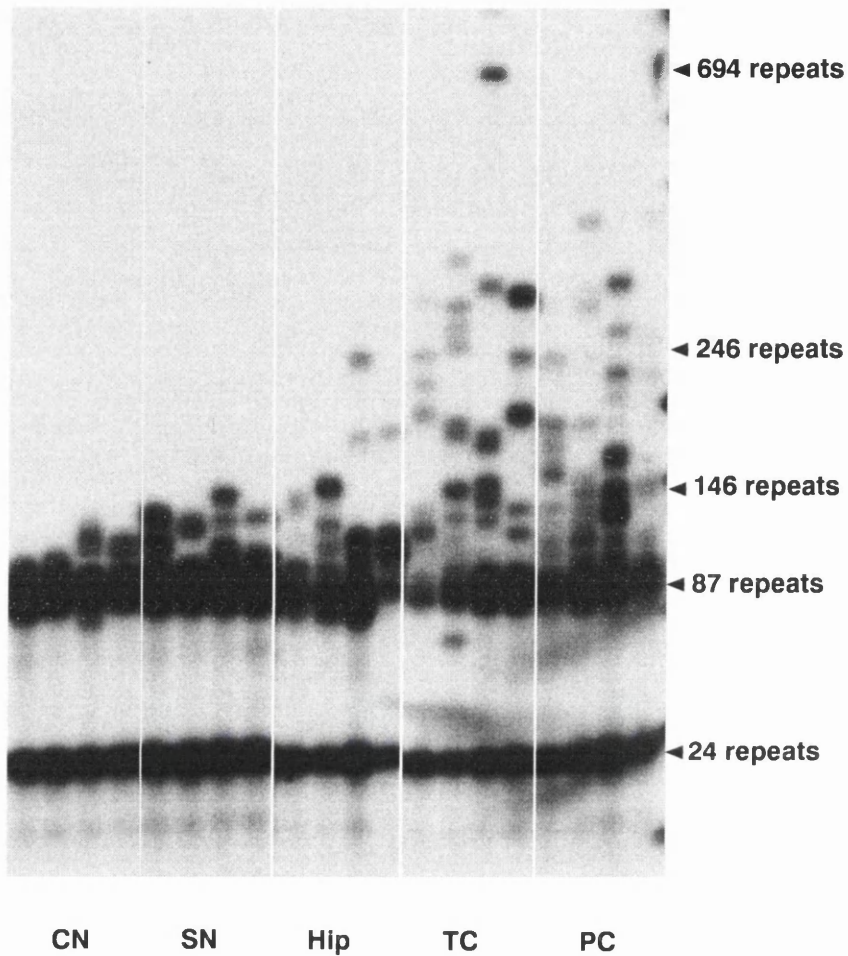


Figure 5.7 Somatic repeat instability of the CAG repeat mutation in human juvenile HD brain tissue

Each panel illustrates 4 lanes of SP-PCR products from 10-30 cells worth of template DNA. The numbers on the right side of the panels represent the estimated CAG repeat number carried by the PCR products of the wild-type, progenitor mutant allele and the further expanded alleles. The brain regions examined are denoted as CN = caudate nucleus, SN = substantia nigra, Hip = hippocampus, TC = temporal cortex and PC = parietal cortex.

The hippocampus also displayed repeat length variation and a maximum repeat length of 246 repeats was detected from ~500 mutant alleles (Figure 5.7). The variability and magnitude however, appeared substantially lower than that observed in the cortex.

The substantia nigra displayed repeat instability and a maximum repeat size of 146 repeats was detected from ~500 mutant alleles (Figure 5.7). The variability and magnitude of repeat instability appeared lower than that observed in the hippocampus and considerably lower than that in the cortex.

The caudate nucleus, the brain region most affected by the HD disease process showed the lowest level of repeat instability (Figure 5.7). As this region had undergone extensive neurodegeneration it is possible that the surviving cell populations were the least affected by the disease process. Our hypothesis predicts that cells containing the largest repeats will be more vulnerable to the disease process and will therefore be absent from the post-mortem sample. The lack of mutation length variability is consistent with the cells containing the largest repeats having succumbed to the disease process first.

In summary, this study has illustrated that extensive somatic repeat instability does occur in human HD tissue. Whilst this somatic repeat instability occurs in a tissue-specific manner, the significance of this variability must be investigated in tissue that has not undergone neurodegeneration.

The dramatic tissue-specific pattern of repeat instability in human tissue is similar to that observed in HD^{+/+} mice and suggests that the findings in this mouse model may be relevant to human HD. As subtle phenotypic changes and no neurodegeneration are observed in the HD mouse model, variations in repeat length may be an early molecular change in the HD disease process. Further studies are needed to assess the occurrence of repeat instability in human tissue obtained from earlier time points in the disease process. More in-depth characterisation of the somatic repeat instability in the HD mouse model will present an opportunity to further investigate the molecular mechanisms underlying repeat instability and the resulting phenotypic consequences. Deciphering these mechanisms may therefore, present possible targets for therapeutic intervention that would be relevant to human HD.

5.6 Investigating experimental techniques utilised to detect somatic repeat instability

5.6.1 Methods used to investigate somatic repeat instability

5.6.1.1 Radioactive PCR

Investigations into CAG repeat length variation in somatic tissues have previously been carried out by radioactive PCR amplification, typically using 100 ng of template DNA (De Rooij *et al.*, 1995; MacDonald *et al.*, 1993; Telenius *et al.*, 1994; Zuhlke *et al.*, 1993). The PCR products were separated through polyacrylamide gels, visualised by autoradiography and the image densitometrically analysed. PCR amplification of this number of DNA templates (~33000 genomes) usually generates a smear of fragments on an autoradiogram. There have been several suggested origins of the various sizes of PCR products responsible for the smear, including slippage of the *Taq* polymerase through the repeat sequence during the amplification process and/or CAG repeat length variation in the template DNA. These varying interpretations of the results have led to confusion regarding the presence of somatic CAG repeat length variation (De Rooij *et al.*, 1995; MacDonald *et al.*, 1993; Telenius *et al.*, 1994; Zuhlke *et al.*, 1993) in HD tissues.

5.6.1.2 Genescan Analysis

Analysis of PCR products from 100 ng of template DNA electrophoresed through polyacrylamide gels is commonly carried out by Genescan technology. PCR amplification is carried out using a fluorescently tagged primer and the subsequent fluorescent signal from the PCR products is visualised by a laser. Highly accurate sizing of the PCR products is carried out by comparison to internal standards within every lane by the Genescan software. As the PCR amplification is carried out using ~100 ng of template DNA, the resultant smear does prevent the detection of individual alleles. However, the technique has been successfully used in assessing the occurrence of somatic repeat instability in a number of HD mouse models (Ishiguro *et al.*, 2001; Mangiarini *et al.*, 1996; Manley *et al.*, 1999).

5.6.1.3 Small pool PCR

Small pool PCR (section 2.4) investigates the presence of somatic repeat instability by quantifying the CAG repeat length on individual alleles within a tissue. Techniques described in sections 5.6.1.1 and 5.6.1.2 use relatively large amounts of template DNA so that the repeat length of thousands of alleles is analysed simultaneously. The expanded alleles are therefore observed as a smear made up of multiple unresolved bands. The technique of small pool PCR allows the

resolution of this smear into discrete bands by analysing small amounts of template DNA (1.2 ng - 3 pg) and visualising the products by Southern blotting.

5.6.2 Comparison of somatic repeat instability analysed by SP-PCR and Genescan technology

Previous investigations into somatic repeat instability in other HD mouse models (Ishiguro *et al.*, 2001; Mangiarini *et al.*, 1997; Manley *et al.*, 1999) have failed to detect the levels of somatic repeat instability observed in this model. One possible reason for this disparity is the difference in experimental techniques utilised. To determine if Genescan technology and small pool PCR differ in their representation of mutation length within the same sample of DNA, half of a PCR amplification was investigated with Genescan technology (section 2.3.6) and the other half was subjected to the small pool PCR visualisation and image analysis protocol (sections 2.4.5 and 2.4.6). Three different concentrations of striatal DNA from a 24 month old HD^{+/-} mouse were used as PCR template.

When small pool PCR was carried out using 100 ng (~33000 genomes) of striatal template DNA, the vast number of PCR products resulted in a large smear on the autoradiogram (Figure 5.8A). The smear prevented the different sized products from individual cells, seen previously (Figure 5.1), being elucidated. This large amount of template DNA, commonly used for Genescan technology, reduces the chance of observing rarer large changes in repeat size as they may not be amplified due to preferential amplification of smaller DNA fragments and increased competition for reaction components. When 100 ng of DNA was used as PCR template and Genescan technology used to detect the products, a obvious range of repeat sizes representing 70 to 80 repeats on the mutant allele was apparent. The resolution of this technique allowed the possible detection of a maximum repeat size of approximately 86 repeats.

300 pg (~100 genomes) of striatal template DNA is a common concentration used to assess the overall pattern of repeat instability within a tissue during small pool PCR analysis. The products from this number of individual alleles can be distinguished on a small pool PCR autoradiogram if repeat length variability is significantly high (Figure 5.8A). A range of 77 to >150 CAG repeats was observed in this sample. This repeat size range is greater than the range previously observed using Genescan technology with 100 ng of DNA template from the same tissue. Genescan technology using 300 pg of striatal template DNA detects less repeat instability than at the higher dilution and is again unsuccessful in detecting the range of repeat lengths observed in the small pool PCR analysis. The result suggests that Genescan technology, at this DNA concentration, fails to detect the entire spectrum of repeat sizes, as the smaller amount of PCR product does not produce an adequate fluorescent signal.

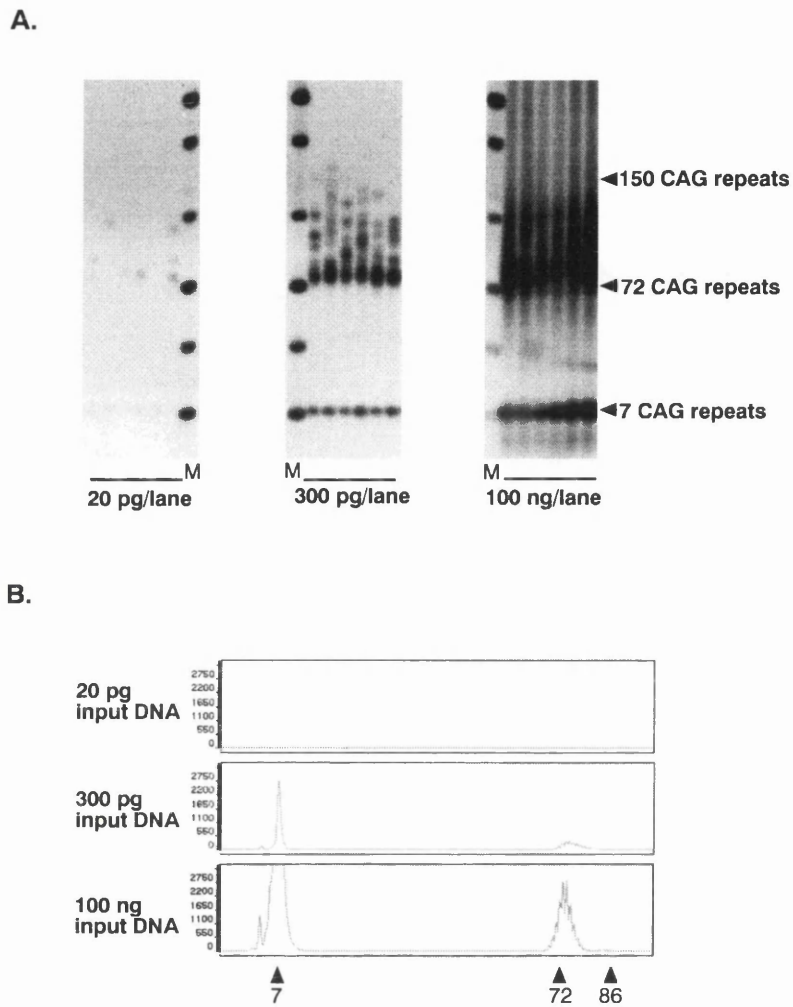


Figure 5.8 Comparison of CAG repeat length variation detected in striatal tissue from a 24 month old HD^{+/-} mouse using SP-PCR analyses and Genescan-based technology

A. SP-PCR analyses demonstrating the level of CAG repeat length variation detectable in PCR amplifications generated from differing amounts of input genomic DNA. The amount of template DNA can be seen under each panel. M indicates the 1 kb plus size marker. The numbers on the far right side of the panels indicate the estimated number of CAG repeats carried by the PCR products. **B.** Representative Genescan traces generated by the same PCR products in the SP-PCR autoradiograms. The vertical scale on the traces is arbitrary units of fluorescence intensity.

Genescan technology failed to detect a fluorescent signal from the products generated by PCR amplification of 20 pg (~7 genomes) of striatal template DNA. In small pool PCR analyses, the sensitivity of the Southern blotting visualisation technique allowed the amplified products from individual molecules to be detected, thus more fully revealing the extent of the somatic repeat instability within the tissue.

Comparisons of repeat size distributions obtained by SP-PCR and Genescan technologies must take into account the use of denaturing polyacrylamide gels in association with Genescan in contrast to the non-denaturing agarose gels used in SP-PCR. As both techniques separate DNA fragments according to size, it is proposed that this technical difference will not account for the significant differences in repeat size distributions observed. The range of repeat sizes detected using autoradiography of radioactive PCR separated on polyacrylamide gels, has also failed to demonstrate significant repeat instability in human HD tissue (De Rooij *et al.*, 1995; Telenius *et al.*, 1994; Zuhlke *et al.*, 1993). These studies, like those using Genescan technology, presumably suffer from the use of bulk quantities of DNA template (~100 ng) impeding the resolution and visualisation of products from individual mutant alleles.

In summary, this study has illustrated one reason why significant levels of somatic repeat instability in HD has not been detected previously. The sensitivity offered by small pool PCR permits the detection and quantification of the full range of repeat sizes. Other techniques including Genescan technology have been shown to lack the sensitivity capable of detecting all PCR products and therefore, the true spectrum of repeat sizes present.

5.7 Summary of results

In summary, these studies have uncovered extensive somatic repeat instability in HD^{+/-} mice. In 24 month old HD^{+/-} mice the 16 different tissues investigated presented mutation profiles that vary in a tissue-specific manner. The brain regions examined displayed higher variability and magnitude of repeat instability than non-CNS somatic tissues and sperm. The striatum, the region of the brain selectively involved in HD neuropathology, was found to display the greatest degree of repeat instability. It was observed that repeat instability on the mutant allele occurred in an expansion-biased manner. The mutation lengths carried by individual alleles in selected tissues were compiled and distributions of the mutant allele repeat sizes were produced. It was shown independently in two animals that the striatum has a distribution of repeat sizes that differs significantly from all other tissues examined. In general, the rank order of repeat instability in other tissues was also consistent.

After identifying somatic repeat instability in the HD mouse model and discovering the dramatic and significant difference in repeat instability of the striatum, further studies were carried out to assess the temporal nature of this somatic repeat instability. Small pool PCR analysis of brain regions at different ages, demonstrated that this tissue-specific somatic repeat instability is not present in early life and occurs in a progressive manner. The repeat instability becomes obvious at 15 months of age and occurs in a tissue-specific manner. The striatum, at all time points when significant repeat instability was detected, displayed the greatest variability and magnitude of repeat lengths.

A dramatic pattern of somatic repeat instability was also detected in human HD tissue. Brain regions from a juvenile HD patient were analysed by small pool PCR and extensive somatic repeat instability was observed. Within the cortical regions mutations over 700 CAG repeats were detected, over 8 times longer than the original expansion mutation. However, it was not possible to determine if the striatum displayed significantly higher levels of repeat instability in human HD as profound neurodegenerative changes in this region were reported.

The fact that previous studies had failed to report significant levels of somatic HD mutation instability, led to an examination of HD^{+/-} mouse striatal samples using the commonly utilised Genescan technology. It was demonstrated that rare large expansions in repeat length were not detected using this approach and a highly truncated distribution of the more common allele sizes was obtained. These findings suggest that the variability and magnitude of repeat instability in HD human and mouse tissue may have been under-estimated in previous studies. The increased sensitivity offered by reduced competition during amplification and the visualisation technique utilised in small pool PCR technology provides a more detailed mutation profile of a tissue.

6 Investigating the underlying mechanisms of somatic repeat instability in HD mouse models

6.1 Aims of the study

The aim of this study was to investigate the possible underlying mechanisms of somatic repeat instability observed in human and mouse HD tissues. The studies were designed to address the following questions:

- Is the underlying mechanism of brain repeat instability in HD^{+/-} mice replication based? A number of mechanisms proposed to explain repeat size changes are based on DNA strand slippage during replication (section 1.6.2). As the most striking somatic repeat instability observed in this HD mouse model was detected in the brain, a predominantly post-mitotic tissue, further investigations were carried out to determine if cell division may play a role in brain repeat instability.

In order to ascertain whether replication is involved in mutation length variability in the brains of HD mice, the following issues were addressed.

- Is the dramatic pattern of striatal repeat instability produced by replication-competent cells within this brain region? The striatal samples used in previous studies (Chapter 5) may have contained the brain region called the subventricular zone (SVZ). The SVZ is known to include replication-competent progenitor cells and to generate neurons destined for the olfactory bulbs (Barres, 1999; Doetsch *et al.*, 1999). Small pool PCR analysis of striatal samples from a 24 month old HD^{+/-} mouse that either contained or omitted the SVZ, was performed to determine whether the extensive pattern of repeat instability observed in the striatum was altered due to the inclusion of these replication-competent cells.
- Does repeat instability occur in the brain during periods of significant cell proliferation? During neurogenesis neural stem cells go through extensive proliferation to provide adequate numbers of cells to ensure the correct connections are made in the developing brain. Once the appropriate connections are made the surplus cells are culled by apoptosis (Gordon, 1995). If the replication process is the underlying mechanism responsible for repeat instability it is postulated that mutation length variability would be observed during this period of increased cell division. Negligible levels of repeat instability within the brain were previously demonstrated at 3 months of age in HD^{+/-} mice (section 5.4). If repeat instability does occur during neurogenesis,

the absence of repeat instability in the early post-natal period may be due to the selective advantage of cells with smaller mutations. This selection may occur because the detrimental effects of large repeats may prevent the cells from making the appropriate connections and therefore promote their elimination by apoptosis. To investigate whether there is repeat instability during neurogenesis, brain samples from different embryonic time points were analysed by small pool PCR.

- Is the pattern of somatic repeat instability reflected in the germline? By comparing the pattern of repeat instability in sperm and striatal samples the repeat size changes produced in a post-mitotic environment can be compared to that in mature sperm, cells that are the products of many cell divisions (Drost and Lee, 1995).
- Does carrying two copies of the HD mutation affect the pattern and extent of somatic repeat instability? One possible mechanism involved in producing repeat instability is DNA repair. The repair process may utilise the wild-type *Hdh* allele through recombinational mechanisms such as homologous recombination/unequal crossing over or gene conversion/break repair (section 1.6.5). Greater scope for large repeat size changes would be provided during recombinational DNA repair if both *Hdh* alleles carried an expanded CAG repeat. Therefore, the mutation profiles of several different tissues were determined to establish if the pattern and extent of somatic repeat instability differed in homozygous ($HD^{-/-}$) and heterozygous ($HD^{+/-}$) mice.
- Is the pattern and extent of somatic repeat instability previously observed in $HD^{+/-}$ mice maintained in mice expressing a truncated form of the mutant huntingtin protein? By comparing the somatic repeat instability in heterozygous mice expressing full-length mutant huntingtin ($HD^{+/-}$) and mice expressing a mutant N-terminal region of the protein (HD^{trunc}), the involvement of the sequence downstream of the expanded CAG repeat in repeat instability can be investigated. Small pool PCR analysis was carried out on selected tissues from 24 month old $HD^{+/-}$ and HD^{trunc} mice.

6.2 Investigating the possible involvement of replication in brain repeat instability in $HD^{+/-}$ mice

Replication has been suggested as one possible underlying mechanism responsible for generating repeat instability. The detection of extensive repeat instability in the brain, a predominantly post-mitotic tissue merits further investigation to determine any possible connection between replication and brain repeat instability in the $HD^{+/-}$ mice.

Replication-competent progenitor cells have been found within the adult brain. A known population of these stem cells, which give rise to olfactory bulb neurons, are found within the subventricular zone (SVZ) (Barres, 1999; Doetsch *et al.*, 1999). This brain region is located between the striatum and the lateral ventricle and was probably included in the striatal samples previously analysed (Chapter 5). To establish whether the inclusion of a small population of these replication-competent cells is responsible for the extensive repeat instability observed in the striatum compared to other brain regions, striatal samples containing or omitting the SVZ were analysed by small pool PCR. To obtain striatal samples without the SVZ, 1 mm thick coronal brain sections, at the level of the head of the caudate putamen (striatum), were visualised under a dissection microscope (Nikon SMZ-U). Hole punches of several regions of the striatum distant from the lateral ventricle were obtained.

Small pool PCR using several dilutions of template DNA (1.2 ng - 60 pg) allowed the analysis of ~1000 mutant alleles from each striatal sample and demonstrated no significant difference, in terms of variability and magnitude of repeat instability, between striatal samples with or without the SVZ (Figure 6.1A).

During neurogenesis, embryonic stem cells participate in a period of vast cell division. If the process of DNA replication contributes to somatic repeat instability, it is postulated that the resultant neuronal population would display mutant repeat length variation.

Small pool PCR analysis was carried out on whole brain samples collected from HD^{+/-} embryos at embryonic day 14 and 18. Investigations were restricted to whole brain samples as distinguishing and dissecting the defined brain regions analysed previously (Chapter 5) was difficult due to the early developmental stage and technical restraints.

Small pool PCR of ~2000 mutant alleles by amplifying 1.2 pg - 60 ng of template DNA per reaction failed to detect repeat instability at either embryonic time point (Figure 6.1B).

Comparison of the repeat instability within striatal and sperm cells from the same HD^{+/-} mice was carried out. The extensive repeat instability seen in the striatum contrasted to the low-level repeat instability seen in sperm (Figure 6.1C). The extent of repeat instability in sperm is supported by the modest amount of intergenerational changes in repeat length observed in this HD mouse model (see section 1.5.3.6). The results suggest that the extent of repeat instability detected does not correlate with increased cell division, as adult brain is a predominantly post-mitotic tissue and mouse mature sperm cells are the products of ~165 cell divisions (24 month old mouse) (Drost and Lee, 1995).

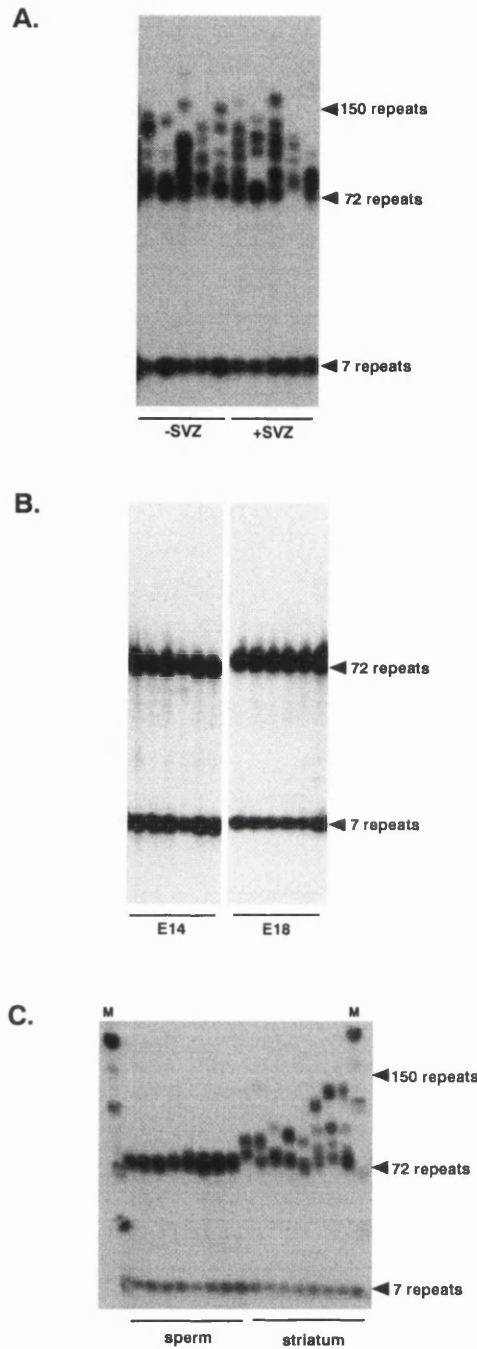


Figure 6.1 Investigating the possible role of replication in somatic repeat instability

A. Repeat instability in striatal samples with or without the subventricular zone (SVZ). A representative SP-PCR autoradiogram in which each lane contains the products of ~20 cells worth of template DNA. Both samples, obtained from the same 24 month old HD^{+/-} mouse, either contained or omitted the replication competent cells derived from the SVZ. The SP-PCR data obtained from several concentrations of template DNA (12 pg - 60 pg) demonstrated no apparent difference between the striatal samples. **B.** Repeat instability in embryonic brain from HD^{+/-} mice. Representative SP-PCR autoradiogram showing multiple reactions using ~20 cells worth of DNA from brain sample collected from HD^{+/-} embryos at day 14 (E14) and 18 (E18) of gestation, the period of maximal neuronal precursor cell division. Negligible repeat instability was observed in embryonic brain at both time points examined. **C.** Somatic and germline repeat instability in 24 month old HD^{+/-} mice. A comparison of somatic (striatum) and germline (sperm) repeat instability of the mutation in a 24 month old HD^{+/-} mouse. Each lane of SP-PCR analysis contains the products of ~10 cells worth of template DNA. M indicates the 1 kb plus DNA marker. The numbers on the right side of each panel indicate the estimated number of triplet repeats carried by the amplified alleles.

Microglia are present within the normal adult brain in a resting state (Barron 1995). However, they are capable of vast cell division in response to neuronal injury or toxicity, such as that associated with neurodegenerative disorders (Meda et al 2000, Brown 2001, Rozemuller and Muiswinkel 2000). Increased gliosis has been reported in post-mortem human HD tissue (Sapp *et al.*, 2001) and several HD mouse models (Lin *et al.*, 2001; Reddy *et al.*, 1998; Yamamoto *et al.*, 2000). If this gliotic reaction occurs within the brain of the HD mouse model, the increased rate of cell proliferation may account for the increased occurrence of repeat instability. However, no neurodegeneration or gliosis have been observed in this HD mouse model (Shelbourne *et al.*, 1999) and although microglia are capable of proliferating in normal brain, the rate is thought to be extremely low. It is therefore postulated that the extensive brain repeat instability detected in this HD mouse model is not the consequence of a gliotic reaction.

In addition, microglia are unlikely to be entirely responsible for the extensive repeat instability previously observed within the striatum of HD^{+/-} mice (section 5.2) as a high percentage (90 %) of the neuronal population within the striatum is made up of medium spiny neurons (Gerfen, 1988), the cell-type selectively affected in early HD. The extent of repeat instability observed and the cell proportions within the striatum suggest that repeat size changes are unlikely to be solely restricted to the glial cell-type.

In summary, these studies illustrate that repeat instability in brain is not directly correlated to the levels of cell division. The contrast in repeat instability in germline and somatic tissues suggests that different underlying mechanisms may be responsible for the respective repeat size changes. The observation of extensive repeat instability in post-mitotic cells and negligible repeat instability in highly replicating neuronal progenitor cells suggests that the underlying mechanism of brain repeat instability may not be replication based.

6.3 Investigating somatic repeat instability in 24 month old homozygous HD mice

Repeat instability was quantified using small pool PCR by determining the mutation length on individual alleles (section 5.3.1) in tissues from two 24 month old homozygous HD ($HD^{-/-}$) mice. The repeat size distributions of striatal, cortical and kidney DNA samples were obtained and compared within each animal to determine the tissue specificity of somatic repeat instability. The consistency of the variability and magnitude of the repeat size changes detected in $HD^{-/-}$ mice were investigated by comparing the distributions obtained for the same tissues in different mice. To establish if somatic repeat instability differs in animals carrying two copies of the HD mutation from those with one, the repeat size distributions from $HD^{-/-}$ mice were compared to those previously obtained from $HD^{+/-}$ mice (section 5.3.2 and 5.3.3). The $HD^{-/-}$ mice used in this study were matched with respect to age, mutation and genetic background to each other and the previously studied $HD^{+/-}$ animals (Table 2.1). It was determined (section 5.3.2) that the mutant progenitor allele lengths were similar in both $HD^{-/-}$ mice investigated, 78 repeats for animal 3 and 76 repeats for animal 4.

6.3.1 Quantification of somatic repeat instability in a 24 month old $HD^{-/-}$ mouse

The characteristics of the somatic repeat instability pattern within the striatum, cortex and kidney of a $HD^{-/-}$ mouse (animal 3) were examined in the same manner as the $HD^{+/-}$ mice (animal 1 and 2, see section 5.3.2 and 5.3.3) and the data presented in Tables 6.1 and 6.2.

Table 6.1 Mutation length profiles of 3 different tissues from a 24 month old $HD^{-/-}$ mouse with a progenitor allele size of 78 repeats (animal 3)

Tissue	Number of alleles examined	Median repeat length	Median repeat change	Max repeat length	Min repeat length
Striatum (St)	499	90	+ 12	252	63
Cortex (Ctx)	332	84	+ 6	172	61
Kidney (K)	218	80	+ 2	104	63

max = maximum, min = minimum.

Table 6.2 Mutation length profiles of 3 different tissues from a 24 month old HD^{-/-} mouse with a progenitor allele of 78 CAG repeats (animal 3)

Tissue	% of total alleles undergone repeat size change	% of total alleles double progenitor repeat	% of altered alleles that have expanded	% of expansions < 3 repeats	% of contractions < 3 repeats
Striatum (St)	95 %	6 %	85 %	11 %	47 %
Cortex (Ctx)	95 %	1 %	80 %	20 %	94 %
Kidney (K)	95 %	0 %	61 %	37 %	52 %

‘% of total alleles undergone repeat size change’ is the percentage of mutant alleles investigated that no longer carried 78 CAG repeats.

‘% of total alleles double progenitor repeat’ is the percentage of mutant alleles investigated that carried > 156 CAG repeats.

‘% of altered alleles that have expanded’ is the percentage of all the alleles which no longer carried 78 CAG repeats which carried > 78 CAG repeats.

‘% of expansions < 3 repeats’ is the percentage of alleles displaying > 78 CAG repeats which carried 79 - 81 CAG repeats.

‘% of contractions < 3 repeats’ is the percentage of alleles displaying < 78 CAG repeats which carried 75 - 77 CAG repeats.

The repeat size distribution within the kidney spanned a narrow range of repeat lengths (Figure 6.2). The median repeat size detected was 80 CAG repeats and the median repeat length change was + 2 repeats (Table 6.1). The maximum repeat length observed when 218 individual alleles were investigated was 104 repeats and the minimum 63 repeats (Table 6.1). The low level of large repeat size changes within kidney cells was illustrated by the absence of kidney cells containing a repeat size double the mutant progenitor allele repeat length (Table 6.3). Somatic repeat instability occurred in an expansion-biased manner as 61 % of all alleles, which displayed an altered, repeat length exhibited an expansion (Table 6.3).

The cortex displayed a wider range of repeat sizes than the kidney (Figure 6.2) with a minimum repeat size of 61 and a maximum of 172 repeats from 332 mutant alleles investigated (Table 6.1). The cortex displayed a median repeat length of 84 repeats and a median repeat length change of + 6 repeats (Table 6.1). The cortical repeat size distribution showed that 1 % of cortical cells contained a repeat that had doubled in length compared to the mutant progenitor allele (Table 6.2). The expansion-biased nature of the somatic repeat instability was illustrated by 80 % of all alleles having undergone a change in repeat size resulting in an expansion (Table 6.2). Approximately 20 % of the expansions remained within 3 repeats of the progenitor allele repeat size, in contrast to the 94 % of all contractions that remained within 3 repeats of the progenitor allele (Table 6.2).

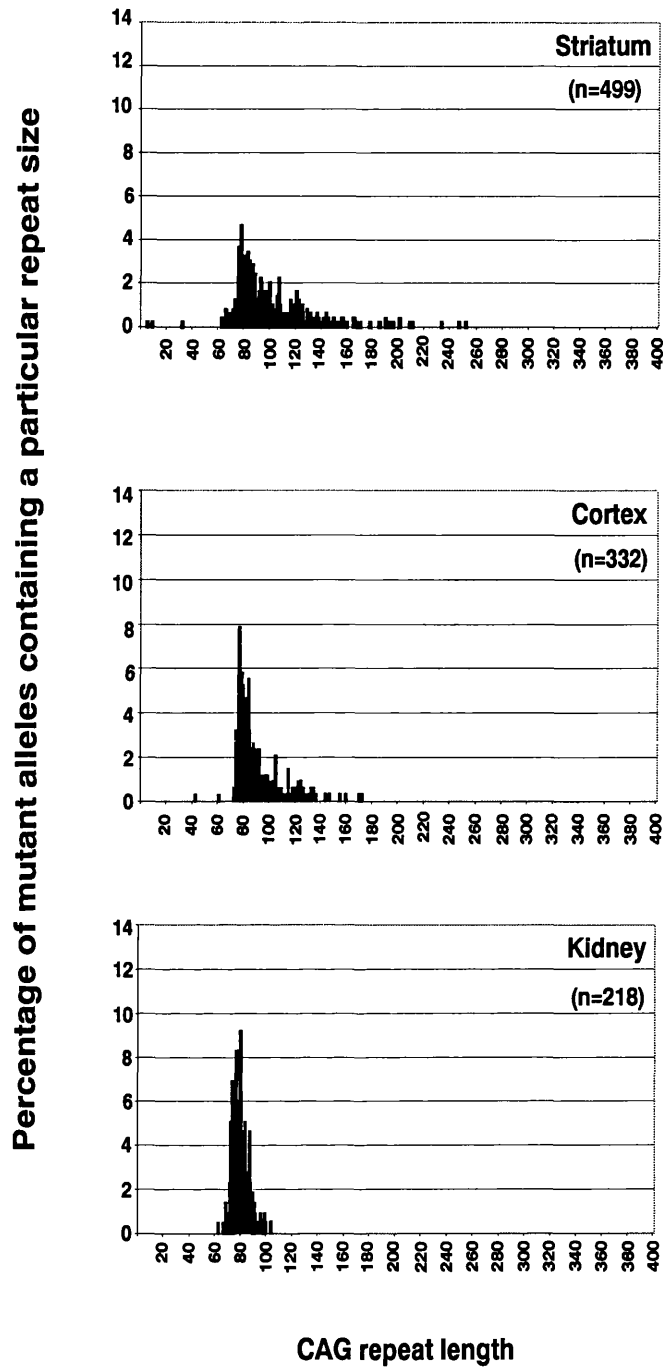


Figure 6.2 Mutation profiles in tissues from a 24 month old HD^{-/-} mouse

Histograms illustrating the distribution of repeat sizes within each tissue by demonstrating the percentage of alleles analysed containing the appropriate repeat length. The tissue type is denoted in the top right of each panel. n = the number of mutant alleles analysed for each tissue. The median repeat length and statistical comparisons of these distributions are shown in Tables 6.1, 6.2, 6.3, 6.7 and 6.8.

The striatal repeat size distribution comprised of a wider range of repeat lengths than the cortex or kidney (Figure 6.2). A median repeat length of 90 repeats was observed and the median repeat length change was + 12 repeats (Table 6.1). The largest allele detected from 499 mutant alleles investigated carried 252 repeats and the minimum 63 repeats. In this brain region, 6 % of cells contained a repeat that had doubled in length compared to the mutant progenitor allele size (Table 6.2). The expansion-biased pattern of repeat instability was once again observed with only 11 % of the high number of expansions (85 %) remaining within 3 repeats of the mutant progenitor allele repeat length (Table 6.2).

When the repeat size distributions for all three tissues were compared using the Mann-Whitney U statistical test, the results suggested that the kidney displayed a significantly smaller median repeat length than the cortex and striatum (Table 6.3). The mutation distribution in the cortex and striatum were also significantly different, with the striatal cells carrying the largest median repeat length (Table 6.3).

Table 6.3 Statistical comparison of the repeat size distributions of three different tissues from one 24 month old HD^{+/-} mouse (animal 3)

Tissue	Comparison	*p value
Striatum (St)	St vs Ctx	<0.0001
	St vs K	<0.0001
Cortex (Ctx)	Ctx vs K	<0.0001

K=Kidney, * Values in bold represent statistical significance ($p < 0.05$) when comparing the median repeat lengths quoted in Table 6.1 using the Mann-Whitney U statistical test.

In summary, the results suggest that mutation profiles in HD^{+/-} mice are similar to those previously detected in HD^{+/-} mice (section 5.3.2 and 5.3.3). Both the median repeat lengths and the median repeat length changes within the tissues are comparable and the expansion-biased repeat instability apparent. The percentage of cells containing repeat sizes double the mutant progenitor allele is also consistent with the findings in HD^{+/-} mice (Table 5.2 and 5.4). The pattern of tissue-specificity was maintained for the tissues examined, and in all mice investigated the striatum shows the greatest variability and magnitude of repeat instability.

6.3.2 Reproducibility of somatic repeat instability in 24 month old HD^{+/-} mice

The studies carried out in section 6.3.1 were replicated to establish the reproducibility of the pattern of repeat instability observed in a single 24 month old HD^{+/-} mouse (animal 3, Figure 6.2). A second HD^{+/-} mouse (animal 4), matched for genetic background and age to animals 1, 2 and 3 was

investigated by small pool PCR to determine the variability and magnitude of the somatic repeat instability in selected tissues. Statistical analysis of the repeat size distributions obtained for the striatum, cortex and kidney of animal 4 were compared to determine the tissue-specificity of somatic repeat instability present (Table 6.6). The mutation profiles for these tissues were also compared to those obtained from animal 3 in order to assess the consistency of somatic repeat instability between HD^{-/-} mice (Table 6.7 and 6.8). The general characteristics of the somatic repeat instability observed in animal 4 is shown in Tables 6.4 and 6.5.

Table 6.4 Mutation length profiles of 3 different tissues from a 24 month old HD^{-/-} mouse with a progenitor allele size of 76 repeats (animal 4)

Tissue	Number of alleles examined	Median repeat length	Median repeat change	Max repeat length	Min repeat length
Striatum (St)	92	93	+ 17	252	72
Cortex (Ctx)	196	87.5	+ 11.5	172	72
Kidney (K)	274	82	+ 6	104	72

max = maximum, min = minimum.

Table 6.5 Mutation length profiles of 3 different tissues from a 24 month old HD^{-/-} mouse with a progenitor allele of 76 CAG repeats (animal 4)

Tissue	% of total alleles undergone repeat size change	% of total alleles double progenitor repeat	% of altered alleles that have expanded	% of expansions < 3 repeats	% of contractions < 3 repeats
Striatum (St)	92 %	7 %	97 %	7 %	67 %
Cortex (Ctx)	94 %	2 %	96 %	8 %	57 %
Kidney (K)	93 %	0 %	97 %	19 %	86 %

'% of total alleles undergone repeat size change' is the percentage of mutant alleles investigated that no longer carried 76 CAG repeats.

'% of total alleles double progenitor repeat' is the percentage of mutant alleles investigated that carried > 152 CAG repeats.

'% of altered alleles that have expanded' is the percentage of all the alleles which no longer carried 76 CAG repeats which carried > 76 CAG repeats.

'% of expansions < 3 repeats' is the percentage of alleles displaying > 76 CAG repeats which carried 77 - 79 CAG repeats.

'% of contractions < 3 repeats' is the percentage of alleles displaying < 76 CAG repeats which carried 73 - 75 CAG repeats.

Somatic repeat instability was observed in the second HD^{-/-} mouse in an expansion-biased manner, with similar numbers of large changes in repeat sizes demonstrated (% of alleles double the progenitor) compared to the previously investigated HD^{-/-} mouse (animal 3). The percentage of repeat changes which resulted in expansions was high in all tissues (>95%) and the median repeat length changes were larger than previously detected. These factors resulted in a slight increase in the median repeat lengths in the tissues of animal 4 compared to those in animal 3 (Figure 6.3 and Table 6.7).

Despite these variations in repeat instability, features of the overall pattern of tissue-specificity were maintained (Table 6.6). The kidney displayed a significantly smaller median repeat length compared to the cortex and striatum. The striatum displayed a significantly larger median repeat length compared to all other tissues. The striatum demonstrated the greatest variability and magnitude of repeat size changes (Figure 6.3).

Table 6.6 Statistical comparison of the repeat size distributions of three different tissues from a second 24 month old HD^{-/-} mouse (animal 4)

Tissue	Comparison	*p value
Striatum (St)	St vs Ctx	0.0342
	St vs K	<0.0001
Cortex (Ctx)	Ctx vs K	<0.0001

K=Kidney, * Values in bold represent statistical significance ($p < 0.05$) when comparing the median repeat lengths quoted in Table 6.4 using the Mann-Whitney U statistical test.

The repeat size distributions from the same tissue from animals 3 and 4 were compared to assess if mutation profiles were reproducible in HD^{-/-} mice (Table 6.7). The overall variability and magnitude of repeat instability in both HD^{-/-} mice appeared to be similar (Figure 6.3). The mutation profiles obtained from the striatum of both HD^{-/-} mice were not significantly different (Table 6.7). However, there were significant differences in the mutation profiles displayed by the cortex and kidney. Variations in repeat size distributions were previously detected in the tissues with lower levels of repeat instability relative to the striatum (section 5.3.3). Sampling error introduced to these mutation profiles by the number of mutant alleles investigated may be responsible for these small statistical variations in repeat length distributions.

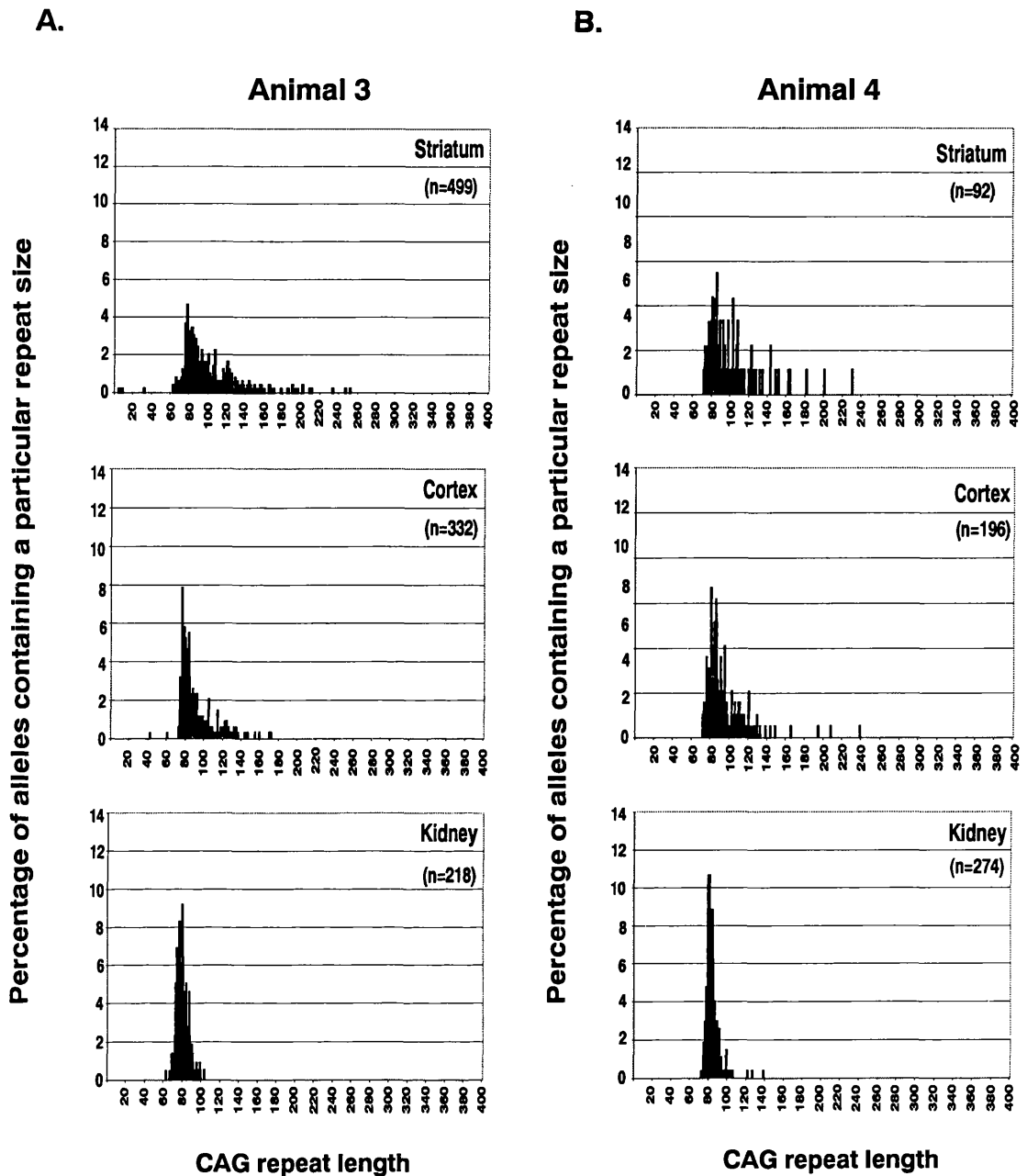


Figure 6.3 Mutation profiles in 24 month old HD^{-/-} mice

Histograms illustrating the distribution of repeat sizes within each tissue. The proportion of alleles carrying a particular mutation length are indicated. The tissue type is denoted in the top right of each panel. n = the number of mutant alleles analysed for each tissue.

A. The repeat size distributions of a HD^{-/-} mouse previously shown in Figure 6.2 (animal 3). **B.** Repeat size distributions for a second HD^{-/-} mouse (animal 4). Statistical comparison between the striatum, cortex and kidney animal 4 displayed a tissue-specific pattern in repeat instability consistent with the first HD^{-/-} mouse analysed (animal 3). The median repeat length and statistical comparisons of the distributions in the second animal are shown in Tables 6.4, 6.5 and 6.6. Statistical comparison between the animals can be seen in Tables 6.7 and 6.8.

Table 6.7 Statistical comparison of the repeat size distributions from the same tissues in different 24 month old HD^{-/-} mice

Tissue	Median repeat lengths		Comparison	*p value repeat length
	Animal 3 (# alleles)	Animal 4 (# alleles)		
Striatum (St)	90 (499)	93 (92)	St vs St	0.2
Cortex (Ctx)	84 (332)	87.5 (196)	Ctx vs Ctx	0.0001
Kidney (K)	80 (218)	82 (274)	K vs K	<0.0001

* Values in bold represent statistical significance at p<0.05 using the Mann-Whitney U statistical test. All comparisons are based on the median repeat lengths found in Tables 6.1 and 6.3.

The slight variations in the mutation profiles of the two HD^{-/-} mice may be due to the two repeats difference in the progenitor allele repeat length. To take the progenitor allele repeat length into account, re-analysis of the distributions was carried out using the change in repeat length (median repeat length change) rather than the absolute repeat length for each comparison (Table 6.8). As animal 4 had displayed a relative propensity for expansions in repeat size the repeat length change distributions proved to be statistically different for each tissue when comparing animals 3 and 4 (Table 6.8). It is still unknown whether the comparisons between the animals yielded statistical differences due to random sampling variation or natural variation between individual mice.

Table 6.8 Statistical comparison of the repeat change distributions of the same tissues in different 24 month old HD^{+/-} mice

Tissue	Median repeat change		Comparison	p value* repeat change
	Animal 3 (# alleles)	Animal 4 (# alleles)		
Striatum (St)	+ 12 (499)	+ 17 (92)	St vs St	0.03
Cortex (Ctx)	+ 6 (332)	+ 11.5 (196)	Ctx vs Ctx	<0.0001
Kidney (K)	+ 2 (218)	+ 6 (274)	K vs K	<0.0001

* Values in bold represent statistical significance (p<0.05) of data analysed by using the Mann-Whitney U statistical test. All comparisons are based on the median repeat changes found in Table 6.1 and 6.4.

In both HD^{-/-} mice (animals 3 and 4), a consistent pattern of somatic repeat instability was observed. In general, the variability and magnitude of repeat instability was preserved with the kidney demonstrating the least amount of repeat instability and the striatum displaying the greatest

magnitude and variability of repeat length changes. The mutation profiles within the striatum, when statistically compared between animals, were not significantly different. Some variation was detected when comparing the mutation profiles of other tissues.

In summary, repeat instability has been detected in mice that are homozygous for the HD mutation. The repeat instability occurs in a tissue-specific and expansion-biased manner and quantitative analysis has revealed repeat size distributions indicating that the striatum displays the greatest variability and magnitude of somatic repeat instability.

6.3.3 Comparing mutation profiles in HD^{-/-} and HD^{+/-} mice

Qualitative analysis suggested that there was little difference between the somatic repeat instability observed in the three tissues investigated in homozygous and heterozygous HD mice (Figure 6.4). A consistent pattern of extensive repeat instability was observed in the striatum of HD^{-/-} and HD^{+/-} animals. When the striatal repeat size distributions for each HD^{-/-} and HD^{+/-} mouse were compared there were no significant differences (Table 6.9) and only one significant result when using the median repeat length change distributions (Table 6.10). Previous comparisons had demonstrated that all striatal repeat size distributions were significantly different, carrying a larger median repeat length, compared to all other tissues examined (Figure 6.5 and Tables 5.4, 5.7, 6.3 and 6.6). The kidney was the tissue examined, in animals of both genotypes, which consistently displayed the least amount of repeat instability (Figure 6.5). The repeat size distributions for the kidney and cortex did yield some statistical differences between HD^{-/-} and HD^{+/-} mice (Tables 6.9 and 6.10). As repeat size distributions derived from these tissues in different HD^{+/-} animals had previously displayed statistical variation (Tables 5.8, 6.7 and 6.8), this is unsurprising and unlikely to signify any overall difference between HD^{+/-} and HD^{-/-} mice.

In summary, when comparing the repeat instability in HD^{+/-} and HD^{-/-} mice qualitative analysis suggested no obvious difference in the pattern of repeat instability. Statistical analysis of the repeat size distributions obtained revealed only minor variations between the striatal repeat instability but slightly greater differences in the tissues that displayed less extensive repeat instability in HD^{-/-} and HD^{+/-} mice.

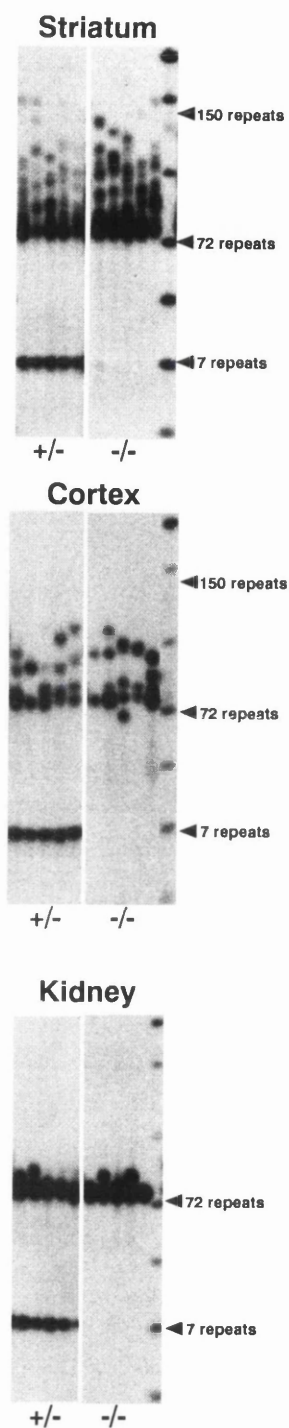
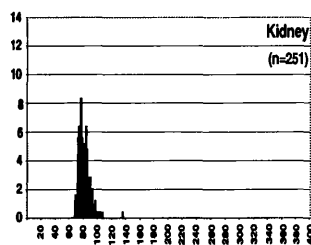
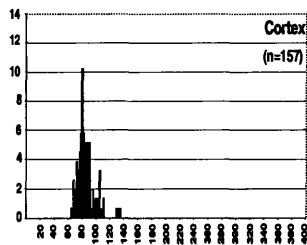
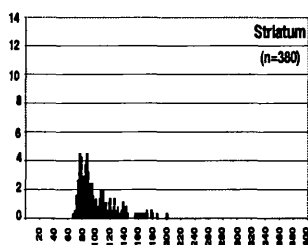


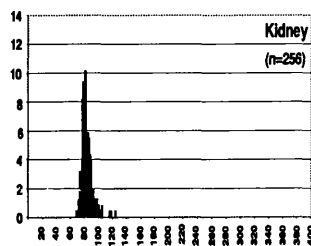
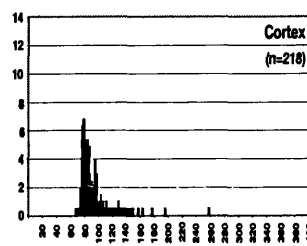
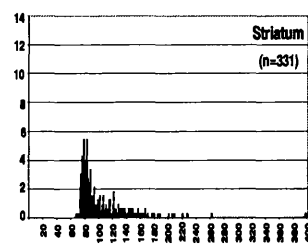
Figure 6.4 Comparison of repeat instability in selected tissues from HD^{-/-} and HD^{+/-} mice

Representative data from SP-PCR analyses demonstrating repeat instability in the striatum, cortex and kidney of 24 month old HD^{-/-} and HD^{+/-} mice. 5 reactions containing ~ 10-20 cells worth of DNA are shown for the striatum and ~ 5-10 cells worth for the cortex and kidney. No apparent differences in the variability and magnitude or tissue-specific pattern of repeat instability was observed when comparing HD^{-/-} and HD^{+/-} mice.

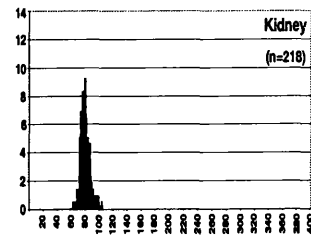
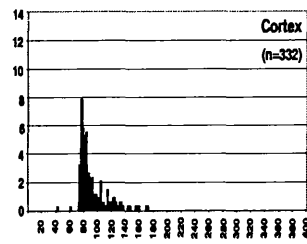
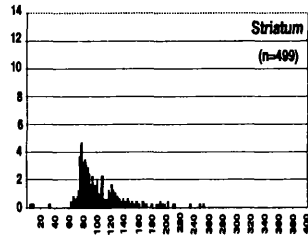
**Heterozygote
Animal 1**



**Heterozygote
Animal 2**



**Homozygote
Animal 3**



**Homozygote
Animal 4**

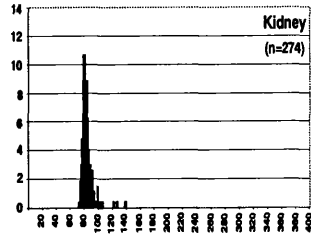
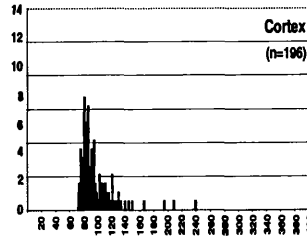
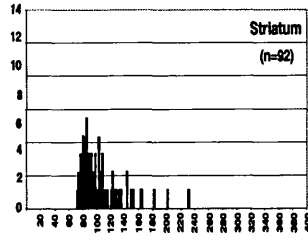


Figure 6.5 Mutation profiles in tissues from 24 month old HD^{-/-} and HD^{+/-} mice

Histograms illustrating the distribution of repeat sizes within each tissue examined from HD^{+/-} and HD^{-/-} mice. The proportion of alleles carrying a particular mutation length are indicated. The tissue type is denoted in the top right of each panel. n = the number of mutant alleles analysed for each tissue. Statistical comparisons of the distributions between all animals are shown in Tables 6.9 and 6.10.

Table 6.9 Statistical comparison of the repeat size distributions of the same tissues in 24 month old mice of different genotypes

Tissue	Animal	Median repeat lengths	Comparison	*p value repeat length
Striatum (St)	Animal 1	89	1 vs 3	0.9
	Animal 2	87	1 vs 4	0.2
	Animal 3	90	2 vs 3	0.4
	Animal 4	93	2 vs 4	0.06
Cortex (Ctx)	Animal 1	82	1 vs 3	0.001
	Animal 2	84.5	1 vs 4	<0.0001
	Animal 3	84	2 vs 3	0.3
	Animal 4	87.5	2 vs 4	0.01
Kidney (K)	Animal 1	79	1 vs 3	0.7
	Animal 2	82	1 vs 4	<0.0001
	Animal 3	80	2 vs 3	<0.0001
	Animal 4	82	2 vs 4	0.3

* Values in bold represent statistical significance ($p < 0.05$) when using the Mann-Whitney U statistical test. All comparisons are based on the median repeat lengths found in Tables 6.1 and 6.4.

Table 6.10 Statistical comparison of the repeat change distributions of the same tissues in 24 month old mice of different genotypes

Tissue	Animal	Median repeat change	Comparison	*p value repeat change
Striatum (St)	Animal 1	+ 12	1 vs 3	0.4
	Animal 2	+ 8	1 vs 4	0.07
	Animal 3	+ 12	2 vs 3	0.07
	Animal 4	+ 17	2 vs 4	0.0005
Cortex (Ctx)	Animal 1	+ 5	1 vs 3	0.03
	Animal 2	+ 8	1 vs 4	<0.0001
	Animal 3	+ 6	2 vs 3	0.9
	Animal 4	+ 11.5	2 vs 4	<0.0001
Kidney (K)	Animal 1	+ 2	1 vs 3	0.2
	Animal 2	+ 3	1 vs 4	<0.0001
	Animal 3	+ 2	2 vs 3	0.004
	Animal 4	+ 6	2 vs 4	<0.0001

* Values in bold represent statistical significance ($p < 0.05$) when using the Mann-Whitney U statistical test. All comparisons are based on the median repeat changes found in Tables 6.2 and 6.5.

6.4 Investigating somatic repeat instability in 24 month old HD^{trunc} mice

During the production of the HD mouse model discussed in this thesis (HD^{+/-} and HD^{-/-} mice), mice were generated carrying a mutant copy of the *Hdh* gene interrupted, in intron 1, by the neomycin resistant (neo) marker gene. This mutant *Hdh* allele expresses a truncated form of the mutant huntingtin protein (HD^{trunc} mice). As HD^{+/-} mice express the full-length mutant huntingtin protein, comparison of these mice with HD^{trunc} mice presents the opportunity to investigate the consequences of expressing a truncated mutant huntingtin peptide. Any alterations in the mechanism of HD pathogenesis caused by the failure to express the *Hdh* DNA sequence downstream of the expanded CAG repeat can be determined in mice matched for age, genetic background and mutation length. By comparing the pattern of repeat instability in HD^{+/-} and HD^{trunc} mice it may be examined whether the expression of the full-length *Hdh* gene sequence influences the variability and magnitude of the molecular changes found in HD mice.

Investigations into somatic repeat instability in mice heterozygous for the allele that produces the truncated form of mutant huntingtin protein (HD^{trunc}) were carried out by small pool PCR analysis. Multiple PCR amplifications of serial dilutions of DNA template (1.2 ng - 12 pg template DNA per reaction)(section 5.2) were performed allowing examination of between 1000-2000 mutant alleles for each tissue. Somatic repeat instability in the striatum, cortex, hippocampus, cerebellum and kidney was investigated in three HD^{trunc} littermates matched for age and genetic background to the HD^{+/-} mice previously studied (Table 2.1). Small pool PCR analysis of DNA from tail-tip samples obtained at weaning indicated that these HD^{trunc} littermates all possessed a progenitor allele repeat length of 69 CAG repeats, 8-10 repeats smaller than the HD^{+/-} mice used for comparison (section 5.3.2 and 5.3.3). As longer repeats are more prone to repeat size changes, this difference in mutant progenitor allele length should be taken into account when interpreting the data.

The kidney from HD^{+/-} mice exhibited minimal variability of repeat sizes on the mutant allele (section 5.3). Small pool PCR analysis of the kidney in HD^{trunc} mice illustrated a similar low level of repeat size changes (Figure 6.6). The maximum repeat sizes observed in the kidney from HD^{trunc} and HD^{+/-} mice were 134 and 136 repeats, respectively. The kidney in HD^{trunc} mice (as previously detected in HD^{+/-} mice) displayed the least repeat instability compared to the other tissues examined.

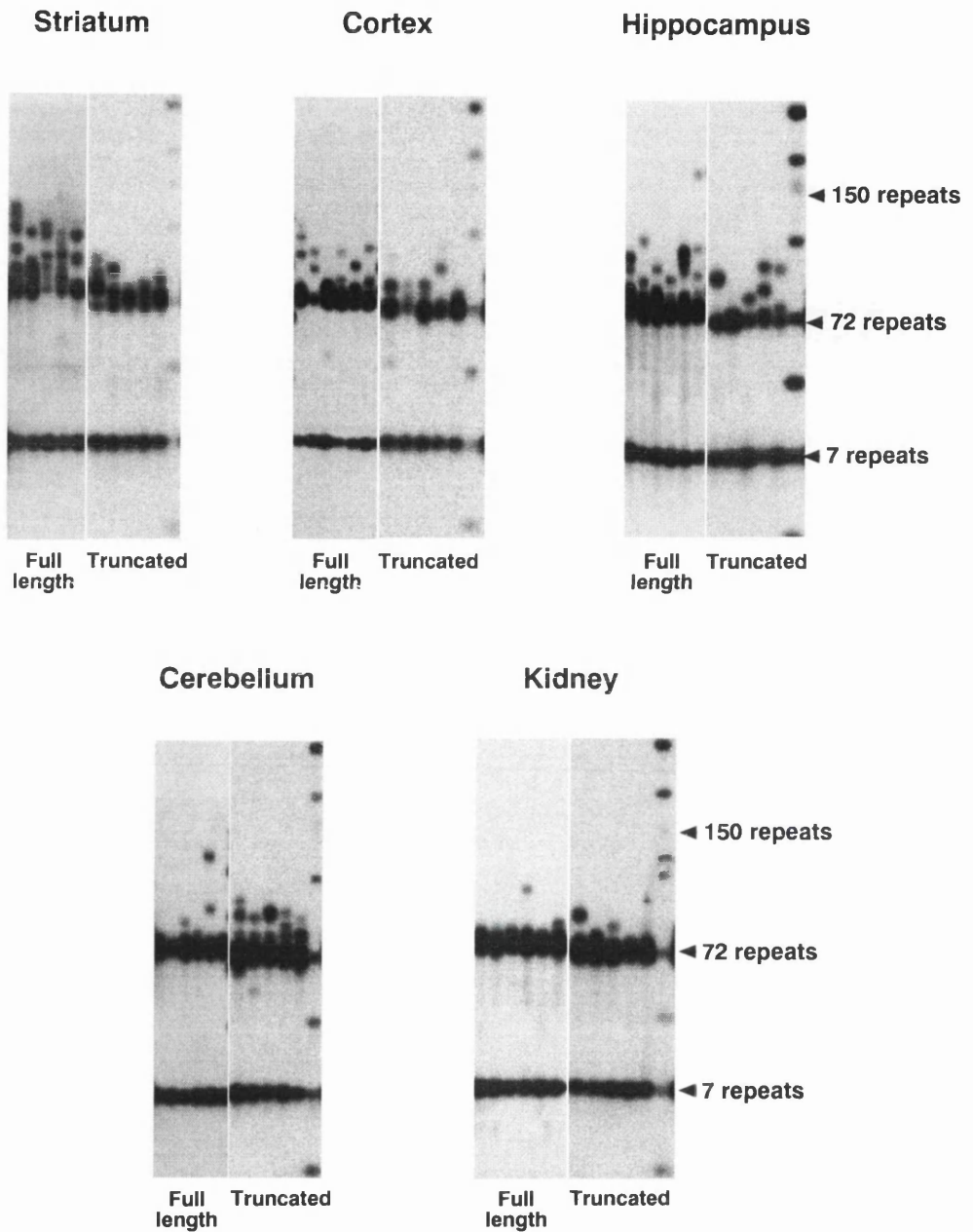


Figure 6.6 Comparison of somatic repeat instability in HD^{+/-} mice and HD^{trunc} mice

Representative data from SP-PCR analyses of the striatum, cortex, hippocampus, cerebellum and kidney from 24 month old HD^{+/-} and HD^{trunc} mice. Each lane represents the PCR products of ~ 10-20 cells worth of DNA. HD^{+/-} mice express a full-length mutant copy of the *Hdh* gene and HD^{trunc} mice express an interrupted form of the mutant *Hdh* gene generating a truncated mutant huntingtin peptide.

In HD^{+/-} mice the pattern of repeat instability observed within the brain regions demonstrated that the striatum displayed a significantly greater variability and magnitude of repeat instability compared to all other brain regions examined (section 5.2 and 5.3). The cortex was shown to be the brain region that generally displayed a repeat instability profile that was second only to the striatum. The hippocampus and the cerebellum displayed repeat instability at a higher variability and magnitude compared to the non-CNS tissues but significantly lower repeat instability than the striatum.

When the four brain regions were investigated in HD^{trunc} mice, analysis revealed an altered brain region specific pattern of repeat instability, compared to HD^{+/-} mice.

In general, no significant differences between the HD^{trunc} and HD^{+/-} mice were suggested by the analysis of cortical and hippocampal samples (Figure 6.6). The cortex within HD^{trunc} mice displayed a maximum repeat of 126 repeats and the hippocampus was similar with a maximum of 121 repeats. In comparison the cortex from HD^{+/-} mice displayed a maximum repeat length of 258 and 161 repeats in the hippocampus. However, the general profile of repeat sizes appeared similar between these brain regions in HD^{trunc} and HD^{+/-} mice, and the larger maximum repeat lengths in the HD^{+/-} mice may be due to the smaller number (~60 %) of alleles sampled in the HD^{trunc} mice.

In contrast, variation between HD^{trunc} and HD^{+/-} mice in the pattern of brain repeat instability was detected when analysis of the striatum and cerebellum was carried out. HD^{trunc} mice displayed reduced variability and magnitude of repeat size changes in the striatum compared to HD^{+/-} mice (Figure 6.6). Since the HD^{trunc} mice in this study carried progenitor alleles containing shorter repeat stretches than those carried by the HD^{+/-} mice used for comparison, a slight reduction in repeat instability might be expected. However, HD^{+/-} mice display significantly greater levels of repeat instability within the striatum compared to the cortex and hippocampus and in HD^{trunc} mice this pattern of tissue-specificity was not as apparent. The maximum repeat length detected in HD^{trunc} striatal samples was 131 repeats compared to the maximum of 398 observed from HD^{+/-} mice. Again a smaller number of alleles (~60 %) have been sampled for HD^{trunc} mice, however, the reduced variability of repeat sizes (Figure 6.6) and the absence of any alleles containing a repeat length double the progenitor allele in HD^{trunc} mice (something commonly observed within the striatum of HD^{+/-} mice), suggested an overall reduction in striatal repeat instability compared to HD^{+/-} mice.

The cerebellum in HD^{trunc} mice demonstrated a repeat instability profile that differed from that observed in HD^{+/-} mice (Table 6.11). The mutation lengths in some cerebellar cells within HD^{+/-} mice are much greater than those in the HD^{trunc} mice. However, larger numbers of cells in the HD^{trunc} cerebellum appeared to contain smaller repeat length changes (20-30 repeat expansions).

The maximum repeat size observed in HD^{trunc} mice was 174 repeats and the maximum repeat size observed in HD^{+/-} mice was 210 repeats. HD^{trunc} mice carrying shorter progenitor allele repeats would perhaps be expected to display a reduction in repeat instability compared to the HD^{+/-} mice. Therefore, it is possible that these alterations in repeat variability may be even more prominent if comparisons were made between HD^{trunc} and HD^{+/-} mice with the same mutation size.

Table 6.11 Semi-quantitative analysis of 1000-2000 mutant alleles for 5 different tissues in 24 month old HD^{+/-} and HD^{trunc} mice. HD^{+/-} data reproduced from Table 5.1.

	% of alleles unstable		largest allele detected	
	HD ^{+/-}	HD ^{trunc}	HD ^{+/-}	HD ^{trunc}
Cerebellum	30-80 %	>60%	210	174
Striatum	>80 %	30-80 %	398	131
Cortex	30-80 %	30-80 %	258	126
Hippocampus	30-80 %	30-80 %	161	121
Kidney	30-80 %	20-50 %	136	134

'% of alleles unstable' is the percentage of total alleles analysed which produced bands which were not contained within the prominent mutant allele band. In semi-quantitative analysis, to discriminate unstable alleles from the progenitor allele band, it is estimated that the repeat size change must be $> \pm 2$ repeats from the progenitor allele repeat length.

In summary, the tissue-specific pattern of repeat instability within HD^{trunc} mice was altered in comparison to HD^{+/-} mice. In HD^{trunc} mice it appeared that the cerebellum was the brain region, which displayed the greatest variability and magnitude of repeat size changes. Although this brain region is not generally thought to be involved in HD pathology HD^{trunc} mice do display a higher level of cerebellar huntingtin aggregates, a cellular hallmark of the HD disease process, providing supportive evidence that the cerebellar cells do express longer repeats. If longer repeats are more toxic to cells this would suggest that cells within the cerebellum maybe more vulnerable to HD pathogenesis in HD^{trunc} mice. The pattern of repeat instability in the brains of HD^{trunc} mice suggested a loss of the region specific repeat instability previously observed in the striatum of HD^{+/-} mice which reflects the selective pattern of HD pathology.

It is important to determine if the full-length and truncated forms of mutant huntingtin vary in their downstream cellular effects, as this may provide insights into the molecular events influencing early HD pathogenesis. If repeat instability is involved in HD pathogenesis, variations in the extent

or pattern of repeat size changes in HD^{+/-} and HD^{trunc} mice suggest that the expression of the entire sequence downstream of the expanded CAG repeat maybe required to produce the specific mechanism of toxicity responsible for HD pathogenesis. A number of HD mouse models have been generated by integration of truncated forms of the mutant *HD* gene into the mouse genome (Mangiarini *et al.*, 1996; Schilling *et al.*, 1999; Yamamoto *et al.*, 2000). If expression of a truncated form of the mutant *HD* gene or peptide initiates an altered time course or nature of pathogenesis this should be taken into account when interpreting findings from these models.

6.5 Summary of results

In summary, investigations into repeat instability within different tissues demonstrate that repeat size changes did not correlate with the rate of cell division. These findings are not consistent with the suggested mechanism underlying repeat instability based on strand slippage during replication. Contrasting repeat instability profiles observed in the brain and sperm cells also suggested that different mechanisms maybe responsible for somatic and germline repeat instability. The extensive repeat instability observed in the brain, a predominantly post-mitotic tissue, suggested that the underlying mechanism of this repeat instability might not be replication-based.

Quantitative small pool PCR analysis demonstrated similar tissue-specific patterns of repeat instability in mice homozygous for the HD mutation. These findings confirmed a similar magnitude and pattern of somatic repeat instability in HD^{-/-} mice and HD^{+/-} animals. The striatum in all mice analysed consistently displayed the greatest repeat instability compared to other tissues examined. The tissues that showed repeat instability below that observed in the striatum did demonstrate variation between animals. It is not clear whether this is due to the random sampling variation or inter-animal variation.

The absence of a significant difference in repeat instability between HD^{+/-} and HD^{-/-} mice suggested, if repeat instability is a molecular marker of the HD disease process, that the severity of this process is not significantly higher in animals carrying two copies of the HD mutation. This hypothesis is supported by the observation that human HD patients carrying two expanded HD alleles appear clinically similar to their heterozygous siblings (Wexler *et al.*, 1987).

It is hypothesised that if recombinational forms of DNA repair are involved in the process of repeat size change, animals with two expanded repeats possess greater scope for larger changes in repeat length. The observation that the variability and magnitude of repeat instability in HD^{-/-} mice is similar in HD^{+/-} mice suggests that the underlying mechanism responsible for repeat size changes occurs independently on both mutant alleles.

Somatic repeat instability was detected in mice heterozygous for a mutant *Hdh* allele that produced a truncated form of the mutant huntingtin protein (HD^{trunc}). Repeat instability appeared to occur in a similar pattern in the cortex, hippocampus and kidney of HD^{trunc} mice when compared to HD^{+/-} mice. In all HD mice expressing the full-length mutant huntingtin protein the striatum, the brain region selectively involved in HD pathology, displayed the greatest repeat instability. However, the striatum of HD^{trunc} mice exhibited repeat instability that appeared nearer the variability and magnitude of mutations in the cortex and hippocampus. These findings suggest a loss of the tissue-specific pattern of repeat instability in the brain that reflects tissue-specific HD pathology.

However, a brain-region specific pattern of repeat instability was observed in HD^{trunc} mice. The cerebellum in HD^{trunc} mice displayed a greater variability in repeat sizes than previously observed in HD^{+/-} mice. The cerebellum within HD^{trunc} mice appeared to exhibit greater repeat instability compared to the striatum. The tissue-specific pattern of repeat instability in HD^{trunc} mice therefore, does not reflect the tissue-specific pathology in HD.

This alteration in the pattern of repeat instability in HD^{trunc} mice compared to HD^{+/-} mice suggests that the expression of the sequence downstream of the expanded CAG repeat within the mutant *Hdh* gene might influence the mechanism involved in producing repeat instability.

7 Discussion

The aim of the work presented within this thesis is to contribute to the understanding of the cellular and molecular mechanisms underlying HD pathogenesis. In order to achieve this aim a knock-in HD mouse model expressing the HD mutation within the appropriate genomic and protein context was utilised to study HD pathogenesis. Previous studies have demonstrated cellular dysfunction and subtle phenotypic alterations reminiscent of HD, in the absence of obvious neurodegeneration (Shelbourne *et al.*, 1999; Usdin *et al.*, 1999). These studies have suggested that the HD knock-in mice model early stages of the disease process and provide the opportunity to investigate the initial cellular and molecular events involved in HD pathogenesis and perhaps elucidate targets for early therapeutic intervention.

7.1 Investigating phenotypic alterations in a knock-in mouse model of Huntington's disease

Further characterisation of the phenotypic changes within HD^{+/-} knock-in mice was carried out to assess aspects of their phenotype and to relate the changes detected to the symptom profile of human HD patients. These studies may also provide clues to the mechanisms of neuronal dysfunction responsible for the phenotypic alterations observed. Gathering detailed knowledge of the phenotypic changes that occur in the HD^{+/-} mice will also aid in assessing the efficiency of future HD therapies.

7.1.1 Investigating gait abnormalities in HD knock-in mice

Movement disorder is one of the most prominent symptoms associated with human HD (section 1.1.1.1). Among the earliest signs of motor disturbance in HD patients is an awkward gait due to abnormalities in voluntary movement (Kirkwood *et al.*, 2001). However, general observations of the HD^{+/-} knock-in mice had previously failed to reveal any obvious motor disturbances. As reaction force analyses have been used to reveal consistent and quantifiable features of mouse gait (Clarke and Still, 1999), this sensitive technique was used to examine the gait of HD^{+/-} and wild-type mice.

In the present study wild-type mice displayed a typical mouse gait, consistent with published data (Clarke and Still, 1999) at 4 and 12 months of age. However, wild-type mice analysed at 9 months of age displayed an abnormal gait, with respect to weight distribution, across the fore/hind axis. Although these data could reflect a natural alteration in gait with age, this seems unlikely as published reports depicting a typical mouse gait are based on mice of ~8 months of age (Clarke and Still, 1999). In addition, the typical fore/hind weight distribution resumed in HD mice at 12 months

of age. It therefore seems more likely that the slight deviation from the typical weight distribution during locomotion in wild-type mice at 9 months of age is due to the smaller number of observations (section 2.6.1.2) in this dataset, dictated by time constraints during experimentation.

HD^{+/-} mice also displayed a typical mouse gait during spontaneous locomotion at 4 months of age. The male HD^{+/-} mice at 9 months of age did not exhibit the normal mouse gait or the slightly altered gait observed in 9 month old wild-type mice. They displayed an abnormal gait across the fore/hind axis. In contrast, there was no difference in gait between female HD^{+/-} and wild-type mice at this age. It was not possible to establish from this study if the slight alteration observed in the mixed-sex cohort at 12 months of age was due to a further change in male HD^{+/-} mouse gait or the initiation of an abnormality in female HD^{+/-} mouse gait, because the numbers of animals in each cohort were so small. These studies suggest that further gait analyses are warranted to determine if and when motor abnormalities can be observed in female HD^{+/-} mice.

Studies of wild-type mouse gait have previously indicated that there are no differences between males and females (Clarke and Still, 1999). However, the sex-bias in the HD^{+/-} mouse gait abnormalities is supported by data generated using the rotarod apparatus that investigates coordination and balance. Rotarod deficits in both male and female HD^{+/-} mice have been detected as early as 4 months of age but they appear to be more prominent in males (C-M Chen, unpublished data). Behavioural changes in the form of hyperaggression have been reported in the HD^{+/-} mice (Shelbourne *et al.*, 1999). These were also expressed to a greater extent in male mice. Although aggression is a typical male trait and this may be sufficient to explain these findings, the difference may be due to possible underlying sex-specific influences within these animals. The reason why the HD mutation would manifest greater phenotypic alterations in male HD^{+/-} mice compared to their female counterparts is unknown but may suggest some sex-specific genetic modifiers of the HD disease process. It is also possible that different phenotypic alterations interact with each other. For example, the hyperaggression and hyperactivity displayed by male mice may make motor alterations more noticeable. To date, no sex-specific differences in the clinical manifestation of HD have been reported in human HD patients. However, gait analysis of this sensitivity has not been carried out on humans and the subtlety of these differential deficits could go undetected. In addition, human HD symptoms can be highly variable between individuals and this issue is further complicated by the fact that differing repeat sizes cause varying onset ages and disease severity. Given these confounding effects, small differences between the sexes in human HD may be overlooked.

Previous studies in other HD mouse models have reported motor disturbances. The demonstration of limb claspings on suspension by the tail has been used to indicate motor dysfunction. Progressive claspings has been observed in all transgenic HD mice expressing a mutant huntingtin fragment

(Mangiarini *et al.*, 1996; Schilling *et al.*, 1999; Yamamoto *et al.*, 2000). However, this observation does not necessarily indicate a striatal-specific abnormality but may represent a cerebellar deficit, as in the case of the *weaver* and *staggerer* mouse mutants that display loss of cerebellar neurons (Lalonde, 1987a; Lalonde, 1987b). Additional reports of resting tremor and involuntary movements (Mangiarini *et al.*, 1996; Schilling *et al.*, 1999; Yamamoto *et al.*, 2000) have suggested motor abnormalities that are probably more relevant to HD. Obvious lack of coordination and abnormal gait have also been observed in end-stage N171-Q82 HD mice (5-6 months old) with progressive rotarod deficits presenting from 3 months of age (Schilling *et al.*, 1999).

Transgenic HD mice expressing full-length mutant human huntingtin also display motor abnormalities in the form of late onset involuntary movements (~9 months) (Hodgson *et al.*, 1999), followed by gait ataxia (Hodgson *et al.*, 1999; Reddy *et al.*, 1998). No obvious movement disorder has been reported in any of the knock-in HD mouse models (Ishiguro *et al.*, 2001; Lin *et al.*, 2001; Shelbourne *et al.*, 1999; Wheeler *et al.*, 1999). However, in agreement with the findings of the present study, a late-onset, subtle variability in gait has been observed at ~10 months of age (Lin *et al.*, 2001) in *Hdh*¹⁵⁰ knock-in mice, although no comment about sex-specific differences were made. Motor deficits on the rotarod apparatus were also observed in a cohort of *Hdh*¹⁵⁰ mice aged between 4-10 months (Lin *et al.*, 2001). At 24 months the *Hdh*^{Q111} knock-in mice display gait abnormalities with imprecise hind/fore paw placement (Wheeler *et al.*, 2002) supporting the observed alteration in fore/hind weight distribution of HD^{+/-} mice in the present study.

From published reports of motor abnormalities in HD patients and mouse models it appears that movement disorders occur early in the HD disease process (Carter *et al.*, 1999; Kirkwood *et al.*, 1999) and begin with involuntary movement deficits generating abnormalities in gait. The data presented in this thesis has also demonstrated a subtle gait abnormality, supporting the notion that the HD^{+/-} knock-in mice are modelling early stages of the HD disease process. The broad similarities in movement disorder between mouse models and humans raise the possibility that similar underlying cellular dysfunction may be involved.

7.1.2 Investigating spatial learning and memory in HD knock-in mice

Reports that detectible cognitive deficits are present in presymptomatic HD gene carriers (Foroud *et al.*, 1995; Jason *et al.*, 1997; Kirkwood *et al.*, 1999; Lawrence *et al.*, 1998a) have supported the suggestion that cognitive deficits occur early in the HD process (section 1.1.1.2) and indicate that cognitive impairment may be caused by neuronal dysfunction rather than cell death. Previous studies in the HD^{+/-} mice have demonstrated hippocampal synaptic deficits affecting long-term potentiation, implicated in forms of hippocampal-dependent learning and memory (Usdin *et al.*, 1999). Does this cellular dysfunction manifest as phenotypic changes in HD^{+/-} mice? Although behavioural changes and motor disturbances have been detected in the HD knock-in mice,

cognitive function had not been studied previously. Therefore an investigation of possible cognitive deficits was attempted in the present study.

Common cognitive deficits observed in HD that can be studied in mice, are those involving memory and visuospatial functioning. The paradigm chosen to assess spatial learning and memory in HD^{+/-} and wild-type mice was the rotating holeboard (sections 2.6.2 and 3.3). The rotating holeboard determines spatial learning and memory by assessing the ability to learn the position of a hidden food bait using constant spatial clues. The learning process is encouraged by food deprivation and the ability to remember the constant location of the food bait in the test area is assessed the following day. Despite, a number of experimental design modifications, the success rate of task completion was still very low. Further changes such as varying bait type and size and verifying a positive response to hidden food did not improve the situation as many mice still showed no signs of learning after more than 4 hours of testing. Previous reports of rotating holeboard experiments have suggested that approximately 1 h 40 min should be sufficient for learning under these conditions (Brosnan-Watters and Wozniak, 1997). The experiments were discontinued after testing 10 mice and achieving successful acquisition and retention of the task in 1 animal. Due to these problems the aim of investigating cognitive deficits in the HD^{+/-} mice was not achieved.

Successful studies of spatial learning and memory utilising the rotating holeboard paradigm have previously been reported (Brosnan-Watters *et al.*, 1996; Brosnan-Watters *et al.*, 1999; Hartman *et al.*, 2001; Wozniak *et al.*, 1996) suggesting that, under the right conditions, this paradigm can be used to obtain robust data. Although the mice in this study were fully habituated to the apparatus and the experimental conditions kept constant, there was one known deviation from the published protocol. In previous studies the mice had been systematically deprived of food until they achieved 80 % of their original body weight, after which time this weight was maintained throughout testing. According to Home Office advice, food was only withheld for the night prior to testing in this study and as a result no animal lost weight. Under these circumstances it is possible that mice would not learn the task as the hunger incentive to find the bait was missing. This restriction also modified the habituation process. In published work, the animals undergo food deprivation during this time, encouraging them to retrieve hidden food from the apparatus. Although bait was present within the apparatus during habituation of HD^{+/-} mice, the incentive to eat was missing as food deprivation had not occurred. Therefore, it is possible that whilst habituation with respect to the apparatus was successful, this did not extend to the task of retrieving the bait. In support of this suggestion, a recent successful rotating holeboard experiment describes a habituation process that trained food-deprived animals to carry out the task until 8 out of 9 trials were correct and then proceeded with the learning session by simply changing the position of the bait (Hartman *et al.*,

2001). This form of task habituation was only possible because the animals possessed the hunger incentive during the habituation period.

Although it is not known whether the HD^{+/-} knock-in mice display cognitive deficits previous studies in other HD mouse models have successfully reported cognitive deficits. Lione *et al.* (1999) presented a series of cognitive tasks carried out on the R6/2 mice that demonstrated a differential pattern of deficits depending on the paradigm used. No obvious deficits were detected in the two-choice swim tank or the Morris water maze. However, the application of more stringent criteria to the Morris water maze data revealed progressive deficits between 3.5-5.5 weeks of age (Lione *et al.*, 1999). A candidate for the underlying cellular mechanism of these cognitive deficits has been suggested by the study that demonstrated impaired synaptic plasticity in the R6/2 mice at a time prior to overt phenotypic abnormalities (Murphy *et al.*, 2000). Impairment of LTP in the CA1 synapses has also been observed in other HD mice, including the YAC72 knock-in mice (Hodgson *et al.*, 1999) and those used in this study (Usdin *et al.*, 1999). These findings suggest that synaptic alterations may occur early in HD animals, and may be responsible for the presentation of cognitive deficits. They also suggest that both cellular dysfunction and cognitive impairment occur early in HD pathogenesis. It is possible that the HD^{+/-} mice express cellular dysfunction but possess a functional reserve, which will prevent detectable cognitive deficits. However, as other behavioural changes have been observed and other HD mice with similar cellular dysfunction do express cognitive deficits, further studies into the possible cognitive impairment in HD^{+/-} mice are warranted.

7.2 Investigating the cellular mechanisms underlying pathogenesis in HD knock-in mice by examining neurotransmitter receptor density

The integrity of the neuronal circuitry in HD knock-in mice was examined in order to establish possible cellular mechanisms underlying the neuronal dysfunction and phenotypic changes observed in HD. Changes in the neuronal circuitry could contribute to the clinical features of HD by altering normal neurotransmission and/or contribute to HD pathogenesis by producing an environment that, over time, could contribute to neuronal degeneration e.g. by promoting glutamate or dopamine toxicity. Alterations in synaptic activity have previously been implicated in HD pathogenesis as a result of studies that demonstrate progressive reductions in cerebral blood flow and glucose metabolism, processes intimately coupled to synaptic activity (Hasselbalch *et al.*, 1992; Hayden *et al.*, 1986; Holthoff *et al.*, 1993; Kuwert *et al.*, 1990; Sax *et al.*, 1996; Young *et al.*, 1986). Further studies have shown that a proportion of relatives at risk of HD already display a significant reduction in striatal glucose metabolism (Grafton *et al.*, 1992; Hayden *et al.*, 1986; Kuwert *et al.*, 1993), suggesting that altered synaptic activity could contribute to early HD

pathogenesis. Neurotransmitter receptors are vital for normal neurotransmission and alterations in their distribution and/or expression levels could disrupt synaptic functioning. Many studies have previously demonstrated alterations in several neurotransmitter receptor types throughout the disease process in human HD brains (section 1.2.8). These HD-associated changes in synaptic activity and receptor levels have been observed prior to obvious cell loss, suggesting that synaptic dysfunction and alterations in receptor density may contribute to neuronal dysfunction early in the disease process. To explore the integrity of the neuronal circuitry in the HD^{+/-} knock-in mice the density of specific neurotransmitter receptors was investigated.

7.2.1 GABA_A/Benzodiazepine receptor density

In this study a significant increase in the density of BNZ neurotransmitter receptor binding sites was shown within the striatum and cortex of 18 month old HD^{+/-} mice compared to wild-type littermates. As detectable phenotypic changes and neuronal dysfunction have been observed in HD^{+/-} mice without obvious cell loss, neuronal dysfunction may be inducing compensatory up-regulation of receptor expression.

Previous studies in human HD post-mortem tissue have revealed reductions in GABA_A/BNZ binding within the striatum of HD patients (Faull *et al.*, 1993; Penney and Young, 1982; Reisine *et al.*, 1979; Walker *et al.*, 1984). Several brain imaging studies in early HD patients have also found reduced BNZ binding within the caudate nucleus (Holthoff *et al.*, 1993; Kunig *et al.*, 2000; Pinborg *et al.*, 2001). However, as significant neurodegenerative changes were observed within these subjects, the reductions in receptor density may simply reflect cell loss. Conversely, post-mortem studies have also demonstrated a ~30-40 % increase in BNZ binding, despite brain atrophy in the mid-frontal cortex, globus pallidus and the substantia nigra pars reticulata (Glass *et al.*, 2000; Penney and Young, 1982; Reisine *et al.*, 1979; Trifiletti *et al.*, 1987). Brain imaging studies have also shown substantial increases in GABA_A/BNZ receptor density within the putamen despite concomitant reductions in glucose metabolism and dopamine D₂ receptor density in early HD patients (Kunig *et al.*, 2000; Pinborg *et al.*, 2001). These findings have shown that increased BNZ receptor density can occur within the striatum, cortex and pallidum despite cell loss, suggesting compensatory receptor up-regulation in the remaining cells. Human studies have also shown increases in BNZ receptor binding in other basal ganglia regions (e.g. globus pallidus) early in the disease process suggesting that cellular dysfunction alone may initiate receptor expression changes (Walker *et al.*, 1984).

In human HD the reduction in receptor density within the caudate nucleus probably reflects 1. cell loss and 2. a disease stage that follows the phase of receptor up-regulation. The increases within the putamen and cortex may reflect brain regions that lag behind the caudate nucleus with respect to neuropathological changes and are still able to elicit a compensatory up-regulation response. As the

caudate nucleus and putamen are an integrated structure in mouse brain, it is difficult to make structural distinctions. However, the up-regulation observed in the striatum of the HD^{+/-} mice may be due to the fact that the HD mice are modelling an earlier time point in HD pathogenesis than that represented by many of the human HD subjects.

7.2.2 Dopamine receptor density

In this study a significant reduction in dopamine D₂ receptor density within the striatum was detected in the HD^{+/-} mice. However, no alteration in dopamine D₁ receptor density was observed between HD^{+/-} and wild-type mice. Significant reductions in striatal, dopamine D₂ receptor density in asymptomatic and early HD patients has been observed suggesting a role contributing to neuronal dysfunction early in HD pathogenesis (Antonini *et al.*, 1996; Lawrence *et al.*, 1998b). An absence of dopamine D₁ receptor reduction suggests that the mice are modelling a time point in HD pathogenesis where no cell loss has occurred, but where D₂ expression is declining. However, this time point precedes the onset of dopamine D₁ receptor reduction, previously observed in clinical HD (Ginovart *et al.*, 1997; Lawrence *et al.*, 1998b; Turjanski *et al.*, 1995).

Based on the observation that the indirect pathway MSN are selectively vulnerable to early HD neuropathology (Albin, 1995) and that these MSN preferentially express dopamine D₂ receptors (Gerfen *et al.*, 1990), a preferential decline in dopamine D₂ receptors may be expected. However, this may not be the case as studies have reported that the indirect pathway is not preferentially targeted in HD (Storey and Beal, 1993) and have questioned the selective expression of dopamine receptors on MSN (Surmeier *et al.*, 1996).

Initial post-mortem studies of early human HD tissue reported a greater reduction of striatal dopamine D₁ receptors than dopamine D₂ receptors (Joyce *et al.*, 1988; Richfield *et al.*, 1991). However, brain-imaging studies have gone on to illustrate a parallel reduction in both dopamine receptors in early clinical HD (Ginovart *et al.*, 1997; Lawrence *et al.*, 1998b; Turjanski *et al.*, 1995) and asymptomatic HD gene carriers (Weeks *et al.*, 1996). Conversely autoradiographic studies in grade 0 HD brains have reported a significant reduction in dopamine D₂ receptors and no decline of dopamine D₁ receptors (Glass *et al.*, 2000). Brain-imaging studies, which have shown decline of both dopamine D₁ and D₂ receptor density in early HD have noted an earlier and greater annual loss of dopamine D₂ receptors compared to that of dopamine D₁ receptors in presymptomatic HD gene carriers (Andrews *et al.*, 1999). The discrepancies between these studies may be due to differences in the stage of HD pathogenesis at which the receptor levels were assessed and warrant further studies to clarify the temporal relationship between dopamine receptors and their involvement in HD.

7.2.3 Opioid receptor density

No significant difference in opioid receptor density was observed in the striatum and cortex of HD^{+/-} mice when compared to wild-type, although there was a strong trend towards increased opioid receptor density in the striatum (section 4.3). The findings presented here may indicate that the absence of opioid receptor reductions reflects the lack of cell loss in the HD^{+/-} mice. The trend towards an increase of opioid receptor density within the striatum may be another example of receptor up-regulation, occurring in response to cellular dysfunction in the brains of HD^{+/-} mice.

Brain imaging studies of early HD patients have demonstrated significantly reduced opioid receptor binding in the striatum, globus pallidus, midbrain and cortex, and increased binding in the thalamus and prefrontal areas (Weeks *et al.*, 1997). The reductions in some brain regions could be due to cell loss whereas the increases in other brain regions suggest the capacity for compensatory up-regulation. Up-regulation may not have been observed in the striatum of clinically affected HD patients as the extent of cell loss and/or cellular dysfunction may be too great or too advanced to elicit a change in receptor expression.

7.2.4 Receptor alterations and the effect on brain function

Consideration of the localisation and function of the neurotransmitter receptors that are altered within HD^{+/-} mouse brain tissue may provide information concerning the possible cellular mechanisms underlying HD pathogenesis.

Approximately 50 % of all cells within the rat striatum are positive for dopamine D₁ receptor mRNA and ~75 % of all cells contain dopamine D₂ receptor mRNA, with co-localisation of both D₁ and D₂ receptors ~ 30 % of all cells in the striatum (Meador-Woodruff *et al.*, 1991). Dopamine D₁ and/or D₂ receptor mRNA is found in all MSN within the striatum (Meador-Woodruff *et al.*, 1991). Dopamine D₁ and D₂ receptors are also thought to be present on large cholinergic interneurons and dopamine D₂ receptors on NAPDH-diaphorase interneurons (Dawson *et al.*, 1990; Joyce and Marshall, 1987).

Stimulation of dopamine D₂ receptors leads to inhibition of adenylylcyclase (Stoof and Keibadian, 1981), which attenuates neurotransmitter actions (Cepeda *et al.*, 1993; Flores-Hernandez *et al.*, 1997; Levine *et al.*, 1996). The postsynaptic (Joyce and Marshall, 1987) and presynaptic (Filloux *et al.*, 1988; Garau *et al.*, 1978; Schwarcz *et al.*, 1978) distribution of dopamine D₂ receptors on neurons means that this inhibitory function could either attenuate the excitability of postsynaptic neurons or prevent the release of neurotransmitters from presynaptic neurons. The loss of a mechanism mediating these processes could contribute to neuronal toxicity since the excessive stimulation of neurotransmitter receptors (e.g. through glutamate excitotoxicity) or excessive

concentrations of neurotransmitters (e.g. dopamine toxicity) have both been implicated as mechanisms of HD pathogenesis (section 1.3). Loss of attenuating postsynaptic dopamine D₂ receptors would bring the membrane potential of striatal neurons closer to activation thereby enhancing the responsiveness of striatal neurons to physiological concentrations of excitatory neurotransmitters. Several studies have already shown that excessive concentrations of or an increased sensitivity to glutamate can cause neurodegeneration (section 1.3.1.1). Loss of presynaptic dopamine D₂ receptors would attenuate the control of glutamate and dopamine release onto the MSN, causing excess neurotransmitter release and opposing the negative feedback control mechanism. In addition, the highest expression levels of dopamine D₂ receptors can be found in the ventral lateral striatum with decreasing levels along the medial and dorsal axes. This gradient correlates with neuropathological profiles in HD (section 1.1.2.3), with lower levels of dopamine D₂ receptors associated with areas that are most vulnerable to HD pathology (Dubois and Scatton, 1985).

In support of this proposed mechanism, increased release of glutamate occurs in dopamine D₂ receptor-deficient mice (Cepeda *et al.*, 2001b). The resulting structural dendritic alterations in striatal neurons, consistent with neurodegeneration, are thought to be caused by long term exposure to increased levels of glutamate. The early reduction in presynaptic dopamine D₂ receptors in HD may initiate a chronic exposure to excessive concentrations of glutamate that would result in dendritic alterations in the MSN, which have been previously reported in HD^{+/-} mice (Li *et al.*, 2001) and other HD mouse models (Petersen *et al.*, 2001). In addition, mild movement impairments (Kelly *et al.*, 1998) and alterations in synaptic plasticity (Calabresi *et al.*, 1997b) have also been observed in dopamine D₂-deficient mice, changes that have been previously observed in HD^{+/-} mice (Usdin *et al.*, 1999), section 3.2).

Conversely, stimulation of dopamine D₂ receptors expressed on NADPH-diaphorase and cholinergic interneurons appear to activate production of toxic NO (Xia *et al.*, 2001). The loss of dopamine D₂ receptors could therefore reduce the production of NO, resulting in a neuroprotective effect. This neuroprotection may provide a mechanism to slow down the cellular toxicity and dysfunction generated by the loss of dopamine D₂ receptors on the MSN. In addition, if the dopamine D₂ receptor reduction extends to the interneurons, it provides a possible mechanism that explains the selective resistance of interneurons to HD pathogenesis.

In general, stimulation of dopamine D₁ receptors results in the activation of adenylylcyclase (Stoof and Kebabian, 1981), resulting in postsynaptic (Joyce *et al.*, 1988) signal enhancement (Cepeda *et al.*, 1998; Flores-Hernandez *et al.*, 1997). A decline in dopamine D₁ receptors could reflect cell loss or an active neuroprotective mechanism that reduces the excitatory capabilities of neurons. In the present study no reduction was observed in dopamine D₁ receptor density was observed in HD^{+/-}

mice compared to wild-type. These findings suggest that HD^{+/-} mice may be modelling a time point of HD pathogenesis before dopamine D₁ receptor reduction occurs as a result of cell loss or as a compensatory response.

Three different subtypes (μ , δ , κ) of opioid receptors are expressed in brain (Mansour *et al.*, 1993; Nishi *et al.*, 1993; Wang *et al.*, 1993). Evidence that opioid receptors are expressed presynaptically and postsynaptically in the striatum has been presented (Rawls *et al.*, 1999; Svingos *et al.*, 1998). The opiates are predominantly inhibitory in their actions and the endogenous opioid receptor ligands include ENK and DN (Pleuvry, 1991), both of which are expressed in the striatum.

The suggested up-regulation of opioid receptors in HD^{+/-} mice may be an attempt to dampen the excessive excitation caused by a loss of dopamine D₂ receptors. An overlap of function may occur between opioid and dopamine D₂ receptors, as they are both found presynaptically on the same projection neurons and both mediate the release of glutamate. An increase in opioid receptors may be a direct substitution mechanism for the loss of dopamine D₂ receptors. Postsynaptic opioid receptors could exert an inhibitory effect on the cells that are being bombarded with increased levels of glutamate and dopamine.

Benzodiazepines (BNZ) bind to a modulatory site on the GABA_A receptor complex mediating GABA-induced chloride flux (Mehta and Ticku, 1999). The GABA_A/BNZ receptor complex is highly expressed on virtually all cortical and striatal neurons and axon terminals (Olsen, 1981; Olsen and Tobin, 1990). The up-regulation of BNZ receptors would have a non-specific inhibitory influence within the brain region. This may occur in an attempt to reduce the excess stimulation of the MSN and their firing, which may be responsible for the HD symptoms such as involuntary movements.

7.2.5 Future studies into neurotransmitter receptor densities in HD

Further studies should be carried out to determine the progression of receptor changes observed in the HD^{+/-} mice. Human studies suggest that receptor levels in HD brains are eventually reduced, probably because the disease process renders it impossible for the cells to exert an up-regulation in expression. Do BNZ, opioid and dopamine D₁ receptors show reductions at any time point in the lifespan of the HD^{+/-} mice? It is most probable that the entire HD disease process cannot be modelled in the two-year life span of a mouse and that the HD^{+/-} mice, if modelling an early stage in HD pathogenesis, will never display the general receptor reductions associated with late stage human HD. Despite this limitation, the temporal nature of receptor changes in HD^{+/-} mice might provide answers to questions such as: When do the receptor changes begin? And what is the relationship to the onset of phenotypic changes? Do dopamine D₂ receptors decline prior to the compensatory increases in BNZ receptors?

Deciphering the relationship between the onset and progression of receptor changes and the phenotypic alterations in HD would help to determine if alterations in different receptor types are responsible for different HD-associated symptoms. If aspects of clinical HD have different aetiologies, this would have implications for treatment strategies. If future studies demonstrate that receptor changes occur prior to phenotypic alterations, one interpretation would be that HD pathogenesis has a preclinical period. This would have implications for the timing of any potential treatment regimes in order to maximise efficacy. If a significant preclinical period does exist and the HD^{+/-} mice are used to assess the efficacy of potential treatments in the future, it will be important to have sensitive biological markers of disease progression. In addition, by defining the nature of the early neuronal dysfunction in HD, potential targets for the new therapies may be revealed.

Changes in receptor levels within other regions of the basal ganglia in HD have been demonstrated (Enna *et al.*, 1976; Kunig *et al.*, 2000; Penney and Young, 1982; Richfield *et al.*, 1995). The temporal nature of these extra-striatal changes would help determine if all changes initiate in the striatum or whether specific receptor changes occur in different brain regions. The studies may also indicate whether other brain regions are responsible for the phenotypic alterations observed in HD.

Whilst this study has demonstrated alterations in the density of neurotransmitter receptors, it has not determined whether the changes are due to alterations in gene transcription or protein processing, trafficking or folding. Changes in receptor expression levels in HD could be due to transcriptional dysregulation (section 1.2.7.2), abnormal protein trafficking to the synapse (section 1.2.4), or sequestering of the receptor protein into aggregates (section 1.2.6). Further studies that explore the relationship between the onset of receptor density changes and aggregate formation might provide clues to which mechanism is responsible. As demonstrated in other human and HD mouse model studies (Augood *et al.*, 1997; Cha *et al.*, 1998), *in situ* hybridisation techniques could be used to determine whether the receptor changes observed are a consequence of reduced mRNA levels.

Human HD studies have demonstrated early loss of adenosine A_{2A} receptors within the striatum (Glass *et al.*, 2000; Varani *et al.*, 2001). Adenosine A_{2A} receptors are exclusively expressed alongside dopamine D₂ receptors on ENK/GABA MSN (Ferre *et al.*, 1993) and a concurrent reduction in adenosine A_{2A} receptors might establish whether the consequences of the HD mutation produce general neuronal dysfunction or alterations in specific neurotransmission pathways. Interestingly, adenosine A_{2A} receptor knock-out mice display a phenotype that consists of hyper-aggression (Ledent *et al.*, 1997). This similarity with the first phenotypic alterations observed in HD^{+/-} mice, raise the possibility that adenosine A_{2A} receptor loss may play a role in early HD pathogenesis.

7.2.6 Additional issues raised by the receptor density studies

By examining the receptor densities in HD^{+/-} mice of different ages it was anticipated that the onset and association with phenotypic alterations could be assessed. However, a pilot study (section 4.6) demonstrated that the subtlety of changes observed in HD^{+/-} knock-in mice requires large cohorts in order to obtain statistically valid data. From previous experiments it is estimated that in order to further explore the temporal nature of any receptor density alterations, it is likely that cohorts of > 15 mice would probably be required. As these numbers are high it may be prudent to find more sensitive techniques to assess receptor expression (e.g. *in situ* hybridisation) or explore other cellular mechanisms that may be responsible for early neuronal dysfunction in HD.

The congenic HD^{+/-} mice in the present study have been backcrossed onto 3 different genetic backgrounds, providing an opportunity to address the influence of genetic background on receptor densities within the striatum and cortex of HD^{+/-} and wild-type mice. By investigating the effect of mutation and genetic background on these results it was demonstrated that genetic background could, to varying extents, influence the receptor densities reported (section 4.5). This effect was most obvious when investigating opioid and dopamine D₁ receptor types. In contrast genetic background was found to have no effect on the result when examining benzodiazepine receptor binding and in this case it was concluded that the alterations observed were due to the HD mutation.

The process of generating gene targeted mouse models generally utilises embryonic stem cells obtained from the 129 inbred mouse strain and other mouse strains (e.g. C57BL/6) for subsequent breeding. The mice generated often have a mixed genetic background and therefore the behaviour and cellular phenotypes of the resulting mouse may not only reflect the functional consequences of the targeted gene but also the interactions between different background genes and other unknown mutations carried by the parental strains. In addition to these problems, even when progeny mice are backcrossed for several generations to a stated inbred strain, a small section of the 129 genome will continue to flank the targeted gene. Genes or cis-acting factors within this flanking region may have phenotypic or molecular consequences for the mutant mice.

Maintaining mutant mice on hybrid genetic backgrounds has implications for experimental design. The variability in the genetic background of the experimental mice has the potential of generating variability in the resulting data set. This increased variability may require larger cohorts in order to observe significant differences between wild-type and mutant mice. The variable background of each hybrid animal also has implications when choosing experimental control animals. Parental strains may differ in the trait under investigation and so the particular trait should be assessed in both parental strains as well as hybrid controls to determine if detected alterations are caused solely by the mutation.

Backcrossing progeny mice onto one background strain to produce congenic animals, should reduce intra-cohort variability and allow the use of smaller cohorts to obtain significant results. When investigating congenic animals, wild-type littermates can be used as controls since the influence of different background strains should be minimised. In addition, comparisons of mutant mice on different congenic background may result in the detection of genetic modifiers of the disease process. This may provide clues to cellular processes involved in pathogenesis and offer novel ways to manipulate the disease process.

Interesting indications that genetic modifiers influence the extent of cell death following systemic injections of kainic acid (Schauwecker and Steward, 1997) have been presented in recent studies. For example, strains such as FVB/N and DBA/2J appear to be relatively vulnerable to kainic acid administration whereas 129SvJ and C57BL/6 relatively invulnerable. As excitotoxicity has been implicated in HD pathogenesis these findings demonstrate the importance of genetic background when interpreting results obtained from different HD mouse models. Further studies have also shown that the C57BL/6 strain is more susceptible to the neurotoxic effects of 1-methyl-4-phenyl-1,2,3,6-tetrahydropyridine (MPTP), which causes nigrostriatal dopaminergic damage, another pathway implicated in HD pathogenesis (Muthane *et al.*, 1994; Zimmer and Geneser, 1987).

7.3 Investigating molecular mechanisms underlying HD pathogenesis by characterising somatic repeat instability

It has previously been suggested that instability of the mutation in somatic tissues may contribute to HD pathogenesis (De Rooij *et al.*, 1995; Telenius *et al.*, 1994). Investigations in HD^{+/-} mice have demonstrated somatic repeat instability. Repeat size changes occur in a tissue-specific and expansion-biased manner, with the greatest variability and magnitude of somatic repeat size changes within the brain. In particular, the striatum displays the most dramatic pattern of repeat instability (section 5.2). Conversely, the cerebellum has a relatively low level of repeat instability compared to other brain regions. In the periphery it is predominantly the kidney and liver cells that display low levels of repeat instability in HD^{+/-} mice. Tissue-specific somatic repeat instability was also detected within human juvenile HD brain tissue (section 5.5). Extensive repeat size changes (>600 repeats) were observed within the human HD cortex compared to other brain regions. Due to the extensive neurodegeneration within the caudate nucleus it was not possible to determine the extent of somatic repeat instability in this brain region. In order to resolve this issue, investigations on early human HD brain tissue that has not undergone any neuropathological cell loss would be needed.

Prominent expansion-biased somatic repeat instability in the brain, with the largest repeat length changes in the striatum and lower levels of repeat instability in the cerebellum, has been

demonstrated in other mouse models of HD (Ishiguro *et al.*, 2001; Mangiarini *et al.*, 1997; Wheeler *et al.*, 1999). The reduced extent of repeat instability within the cerebellum compared to other brain regions observed in HD mouse models may mask cell-type specific repeat instability. For example, the Purkinje neurons are the least numerous cell-type in the cerebellum (Nairn *et al.*, 1989) and significantly increased levels of repeat size changes within these cells might be concealed by the inclusion of many other cell-types within the tissue samples used for analysis. In peripheral tissues repeat instability is also consistently demonstrated in the kidney and liver (Ishiguro *et al.*, 2001; Mangiarini *et al.*, 1997; Wheeler *et al.*, 1999). Previously published data on human somatic repeat instability initially reported no heterogeneity of repeat size within different HD tissues (MacDonald *et al.*, 1993; Zuhlke *et al.*, 1993). However, subsequent studies of juvenile HD patients demonstrated minor, but consistent levels of increased repeat instability associated with the striatum compared to other brain regions (De Rooij *et al.*, 1995; Telenius *et al.*, 1995).

Whilst the patterns of somatic repeat instability are broadly similar between the previously published data and the present study significant differences are apparent when comparing the magnitude of the repeat size changes observed. The largest expansions detected within the striatum of HD mice expressing significantly longer progenitor repeat tracts (111-145 repeats) than the HD^{+/-} mice in this study, were only ~3 repeats in the knock-in mouse (Wheeler *et al.*, 1999) and ~25 repeats in the R6/2 mice (Mangiarini *et al.*, 1997). A knock-in HD mouse model carrying a progenitor repeat size of 77 repeats, similar to the progenitor allele size of HD^{+/-} mice, demonstrated expansions of ~20 repeats within the striatum (Ishiguro *et al.*, 2001) compared to regular increases of over 80 repeats observed in HD^{+/-} mice in this study. Expansion-biased (<15 repeats) changes in repeat length within the striatum and cortex of juvenile HD patients have been reported (Ishiguro *et al.*, 2001) compared to the repeat size changes of >600 repeats observed in juvenile HD tissue in this study.

To determine whether different experimental techniques could contribute to the discrepancies in mutation profiles observed, the PCR products from the same PCR amplification were analysed by both small pool PCR and Genescan imaging techniques (section 5.6). The increased sensitivity of the visualisation technique and the lower numbers of DNA templates amplified in small pool PCR permits the detection of a significantly wider spectrum of repeat lengths (section 5.6). Therefore, the use of a small pool PCR approach may be responsible for the more dramatic mutation profiles observed in this study compared to others.

7.3.1 Small pool PCR

Small pool PCR was used to detect the extensive somatic repeat instability in brain regions of HD^{+/-} mice and human HD patients. However, it is well established that the amplification of DNA templates by PCR is associated with the production of PCR artefacts due to slippage of *Taq*

polymerase or preferential amplification of smaller molecules. Several observations suggest that the spectrum of PCR products obtained from the small pool PCR analyses in this study are not PCR artefacts and do represent the products from individual templates.

- The PCR products observed are not merely a reflection of the progenitor allele repeat length as a tissue-specific pattern of repeat instability is observed in individual animals and a consistent pattern of somatic repeat instability is generated for animals of a particular age. Previous studies have also illustrated that the variability of repeat lengths observed in different samples reflects the variation observed on Southern blot analysis of genomic DNA (Monckton *et al.*, 1995).
- In sperm analyses the frequency of individual mutant PCR products is proportional to the amount of input template DNA (over the range of 60-960 pg of sperm DNA per reaction) (Jeffreys *et al.*, 1994). This suggests that heteroduplex formation, which would produce additional bands leading to a disproportionate increase in PCR products with increasing concentrations of template DNA, does not occur.
- The PCR signal from a mutant allele is similar to that seen for progenitor alleles in single molecule dilutions of sperm DNA. This observation is consistent with the signal being derived from a single input molecule (Jeffreys *et al.*, 1994).
- Although PCR artefacts could arise at any stage of the PCR amplification process and produce bands of different intensities longer autoradiography exposures do not pick up any additional faint bands compared to the strong signal from the original PCR products.

7.3.2 Polyglutamine load and HD pathogenesis

In an attempt to further elucidate the possible role of somatic repeat instability in HD pathogenesis, the pattern and extent of somatic repeat instability was investigated in homozygous HD^{-/-} mice (section 6.3). The tissue-specific pattern of somatic repeat instability was similar in homozygous and heterozygous HD mice, with comparable size changes observed.

The overall similarities between homozygous and heterozygous HD patients and HD^{+/-} mice support the idea that the HD mutation is dominant and therefore 50 % of total huntingtin protein carrying an extended polyglutamine stretch is sufficient to initiate the disease process. However, it has been shown that the disease process can be influenced by increasing the toxicity of mutant huntingtin protein (Andrew *et al.*, 1993; Duyao *et al.*, 1995; (HDCRG), 1993; Penney *et al.*, 1997; Snell *et al.*, 1993). Therefore, the length of the polyglutamine tract rather than the overall polyglutamine concentration appears to influence the degree of cellular dysfunction. As there are

no significant differences in the extent and magnitude of repeat instability in homozygous and heterozygous HD mice, the likelihood that an individual cell within the striatum contains a repeat length above the threshold number required to precipitate neuronal dysfunction, would be the same in both genotypes. This hypothesis may explain the absence of a earlier disease onset in homozygous compared to heterozygous HD mice.

Homozygous HD^{-/-} mice are phenotypically similar to heterozygous HD^{+/-} mice and this is consistent with previous reports that homozygous human HD patients appear to be phenotypically indistinguishable from their heterozygous counterparts (Wexler *et al.*, 1987). However, some studies of HD knock-in mice have reported that disease progression is faster in homozygous animals (Lin *et al.*, 2001; Wheeler *et al.*, 2000). These findings suggest that a higher cellular polyglutamine load may expedite disease progression, perhaps at a later stage in the disease process when both mutations have crossed the threshold length.

7.3.3 Expression of full-length mutant huntingtin and HD pathogenesis

The present study demonstrates that the pattern of tissue-specific repeat instability is altered in mice expressing a truncated form of mutant huntingtin protein when compared to mice expressing full-length mutant huntingtin protein (section 6.4). Although there were tissue-specific differences in somatic repeat instability, the striatum of HD^{trunc} mice no longer showed significantly greater repeat instability than other brain regions. In addition, the cerebellum displayed the greatest extent and magnitude of repeat length variation. It is interesting to note that a higher incidence of protein aggregates have been reported within the cerebellum of mice expressing truncated mutant huntingtin, suggesting that these cells may have an increased polyglutamine load (Xiao-Jiang Li, unpublished data). This study raises the possibility that the expression of a mutant huntingtin protein lacking the protein sequence downstream of the elongated polyglutamine stretch influences patterns of tissue-specific repeat instability.

These findings may have implications for HD transgenic mouse models that have been generated using transgenes expressing a truncated form of the human mutant huntingtin protein (Mangiarini *et al.*, 1996; Schilling *et al.*, 1999; Yamamoto *et al.*, 2000). The expression of a truncated mutant huntingtin protein is associated with a more progressive phenotype and widespread distribution of protein aggregates (Davies *et al.*, 1997; Schilling *et al.*, 1999). Aggregates, a cellular hallmark of HD pathology, are restricted to brain cells vulnerable to HD pathogenesis in humans (Becher *et al.*, 1998; DiFiglia *et al.*, 1997), suggesting that the expression of truncated mutant huntingtin could alter the selective pattern of cellular changes in HD. Full-length mutant huntingtin may influence cell-selective vulnerability by cell-specific protein-protein interactions (section 1.2.7) and/or tissue-specific protein processing prior to nuclear translocation (section 1.2.6.1). The absence of the full-length protein could disrupt or bypass these tissue-specific steps in HD pathogenesis and allow

other cellular factors to determine the specificity of pathology. However, the pattern of somatic repeat instability in HD^{trunc} mice and other HD mouse models expressing truncated huntingtin cannot be accurately compared as the different experimental techniques used in these investigations have previously shown significantly different detection sensitivities (section 5.6).

7.3.4 Somatic repeat instability and mechanisms of HD pathogenesis

The progressive somatic repeat instability in the HD^{+/-} mice (section 5.4) suggests a role for repeat length expansions in the initiation and/or progression of HD pathogenesis. Behavioural alterations in the HD^{+/-} mice are present from 3 months of age (Shelbourne *et al.*, 1999). However, clear tissue-specific repeat instability does not occur until ~ 9 months of age. These findings suggest that somatic repeat instability does not contribute to the initiation of HD pathogenesis in the HD^{+/-} mice. However, huntingtin-mediated pathogenesis and repeat instability could interact and initiate a vicious cycle, as longer repeats are more toxic to cells but are also more prone to expansion. Tissue-specific differences in the extent and magnitude of repeat instability might result in more rapid progression of the disease process in specific regions with the temporal gradient of neuropathology matching the pattern of somatic repeat instability.

It is postulated that somatic repeat instability might play a role in the initiation of HD pathogenesis. As all mouse models have been generated using repeat lengths significantly larger than those generally seen in human HD, it is possible that subtle forms of neuronal dysfunction are already apparent at birth since the repeat threshold required to initiate HD pathogenesis has already been exceeded. Initial HD pathogenesis observed in HD mice would therefore be independent of repeat instability. Conversely, the mutation length that most human patients inherit may be below the threshold required to initiate neuronal dysfunction. The late onset of clinical HD symptoms may reflect the time taken to generate a significant proportion of neurons with repeat lengths above this threshold and cause observable dysfunction. The selective vulnerability of the striatum may occur as a greater proportion of striatal cells reach the threshold repeat length earlier than other regions of the brain. This hypothesis would suggest that the 36 CAG repeat threshold, distinguishing non-pathogenic and pathogenic HD mutations in humans, may not encode the polyglutamine length required to initiate pathogenesis but the size at which repeat instability becomes more likely.

7.3.5 Future studies into somatic repeat instability in HD

In order for somatic repeat instability to contribute to HD pathogenesis in the manner indicated in previous sections, repeat length must be correlated with the degree of cellular dysfunction. To directly relate cellular function and repeat length an examination of the electrophysiological properties of visualised MSN followed by collection of the nucleus and mutation length

determination could be carried out. It is postulated that the cells with larger repeats would display greater cellular dysfunction.

Based on this assumption it would be expected that the MSN, the cell-type most vulnerable to the HD disease process, would carry the longest repeats. As a high (~95 %) percentage of the neurons within the striatum are MSN and a high percentage of cells (~95 %) investigated exhibit repeat length changes, it is almost certain that the MSN will exhibit some level of somatic repeat instability. However, it is possible that other cell-types within the striatum also display repeat instability. An investigation to harvest single cells from striatal tissue using laser capture microdissection followed by PCR amplification of the mutation would allow the assessment of the range of repeat lengths within specific cell-types.

An alternative approach of assessing the contribution of somatic repeat instability to HD pathogenesis would be to generate a mouse model that expresses a long polyglutamine stretch within the mutant huntingtin molecule encoded by an extended but stable repeat stretch. This could be achieved by generating a HD mouse in which the extended CAG repeat within the *Hdh* gene is frequently interrupted by CAA codons. This would still encode a pure glutamine stretch but should display reduced instability as studies have demonstrated that interruptions to CAG repeat tracts can dramatically reduce levels of repeat instability (Goldberg *et al.*, 1995; McNeil *et al.*, 1997).

7.3.6 Underlying mechanisms of somatic repeat instability

As mutation length variability in somatic tissue may play a crucial role in the initiation and progression of HD pathogenesis, elucidation of the mechanisms underlying the CAG repeat instability may provide targets for future therapeutic intervention strategies. Studies of the somatic repeat instability in HD^{+/-} mice have provided clues to the mechanisms that might be responsible for repeat size changes.

Although many of the previously reported mechanisms for repeat instability are replication-based (section 1.6.2) the progressive somatic repeat instability observed in HD^{+/-} mice is predominantly observed in brain regions, tissues that are largely comprised of post-mitotic cells. These findings suggest that brain repeat instability within HD^{+/-} mice may not be caused by a replication-based process. Further studies of repeat instability in cells with differing proliferation capacities also demonstrated a lack of correlation between cell division rate and repeat instability (section 6.2). This observation is also supported by studies of triplet repeat instability in other mouse models (Fortune *et al.*, 2000) and cell culture systems (Gomes-Pereira *et al.*, 2001).

It has been suggested that recombination-based mechanisms of DNA repair can generate repeat instability (section 1.6.5.1). If recombinational repair is responsible for repeat instability then it

might be postulated that homozygous HD^{-/-} mice, carrying two elongated CAG repeats, would have a greater propensity for expansion because longer repair templates are present. The observation that there is no significant difference in the somatic repeat instability profiles of homozygous and heterozygous HD mice suggests that repeat instability is generated by a mechanism working independently on each chromosome. This suggestion has also been supported by the observations that repeat instability occurs in post-mitotic haploid sperm cells (Kovtun and McMurray, 2001).

Studies have shown that a functional mismatch repair (MMR) system is required to generate somatic repeat instability within R6/2 HD mouse tissues (Manley *et al.*, 1999) (section 1.6.3.2) and mouse models of other triplet repeat diseases (van den Broek *et al.*, 2002). The ability of the MMR protein MSH2 to bind looped DNA structures (Pearson *et al.*, 1997) that can form in repetitive sequences (Sinden and Wells, 1992), has been postulated to stabilise these structures and aid with their incorporation into the genome (section 1.6.3.2).

In cycling *E.coli* cells, loop formation during replication would activate MMR methylation-directed strand-specific repair to excise the looped structure and preventing repeat instability. As brain cells are predominantly post-mitotic this loop formation and repair cannot occur. However, single-stranded DNA is still generated during processes such as transcription and/or during DNA repair. Formation of secondary structures during DNA repair could be exacerbated in non-replicating cells by increased levels of DNA damage associated with enhanced oxidative stress. It is predicted that there will be no methylation-based recognition of the loops formed during repair and therefore either DNA strand may be processed. When presented with the choice of either deleting DNA and perhaps potentially important sequence or adding new repeat units to incorporate the loop, incorporation might be favoured, generating an expansion-biased pattern of repeat instability (M. Gomes-Pereira and D. Monckton, personal communication).

If mutation length variability plays a role in the initiation and progression of HD pathogenesis further investigation of the mechanisms responsible for repeat instability, particularly in non-replicating cells, are needed to identify *cis*- and *trans*-acting factors that could be manipulated to prevent repeat instability. If increased oxidative stress associated with HD pathogenesis exacerbates the process of repeat instability, then early administration of antioxidants may be a straightforward and effective treatment for HD.

References

- Acharya, S., Wilson, T., Gradia, S., Kane, M. F., Guerrette, S., Marsischky, G. T., Kolodner, R., and Fishel, R. (1996). hMSH2 forms specific mismatch-binding complexes with hMSH3 and hMSH6. *Proc Natl Acad Sci U S A* 93, 13629-13634.
- Albin, R. L. (1995). Selective Neurodegeneration In Huntingtons Disease. *Ann Neurol* 38, 835-836.
- Albin, R. L., and Greenamyre, J. T. (1992). Alternative excitotoxic hypotheses. *Neurology* 42, 733-738.
- Albin, R. L., Young, A. B., Penney, J. B., Handelin, B., Balfour, R., Anderson, K. D., Markel, D. S., Tourtellotte, W. W., and Reiner, A. (1990). Abnormalities of striatal projection neurons and N-methyl-D-aspartate receptors in presymptomatic Huntington's disease. *N Engl J Med* 322, 1293-1298.
- Albright, S. R., and Tjian, R. (2000). TAFs revisited: more data reveal new twists and confirm old ideas. *Gene* 242, 1-13.
- Altar, C. A., Cai, N., Bliven, T., Juhasz, M., Conner, J. M., Acheson, A. L., Lindsay, R. M., and Wiegand, S. J. (1997). Anterograde transport of brain-derived neurotrophic factor and its role in the brain. *Nature* 389, 856-860.
- Anderson, K. E., and Marder, K. S. (2001). An overview of psychiatric symptoms in huntington's disease. *Curr Psychiatry Rep* 3, 379-388.
- Andreassen, O. A., Dedeoglu, A., Ferrante, R. J., Jenkins, B. G., Ferrante, K. L., Thomas, M., Friedlich, A., Browne, S. E., Schilling, G., Borchelt, D. R., *et al.* (2001). Creatine increase survival and delays motor symptoms in a transgenic animal model of Huntington's disease. *Neurobiol Dis* 8, 479-491.
- Andrew, S. E., Goldberg, Y. P., Kremer, B., Telenius, H., Theilmann, J., Adam, S., Starr, E., Squitieri, F., Lin, B., Kalchman, M. A., and *et al.* (1993). The relationship between trinucleotide (CAG) repeat length and clinical features of Huntington's disease. *Nat Genet* 4, 398-403.
- Andrews, T. C., Weeks, R. A., Turjanski, N., Gunn, R. N., Watkins, L. H., Sahakian, B., Hodges, J. R., Rosser, A. E., Wood, N. W., and Brooks, D. J. (1999). Huntington's disease progression. PET and clinical observations. *Brain* 122, 2353-2363.
- Antonini, A., Leenders, K. L., Spiegel, R., Meier, D., Vontobel, P., WeigellWeber, M., SanchezPernaute, R., De Yebenez, J. G., Boesiger, P., Weindl, A., and Maguire, R. P. (1996). Striatal glucose metabolism and dopamine D₂ receptor binding in asymptomatic gene carriers and patients with Huntington's disease. *Brain* 119, 2085-2095.
- Aronin, N., Chase, K., Young, C., Sapp, E., Schwarz, C., Matta, N., Kornreich, R., Landwehrmeyer, B., Bird, E., Beal, M. F., *et al.* (1995). CAG Expansion Affects the Expression Of Mutant Huntingtin In the Huntingtons Disease Brain. *Neuron* 15, 1193-1201.
- Arzberger, T., Krampfl, K., Leimgruber, S., and Weindl, A. (1997). Changes of NMDA receptor subunit (NR1, NR2B) and glutamate transporter (GLT1) mRNA expression in Huntington's disease An *in situ* hybridization study. *J Neuropath Exp Neurol* 56, 440-454.
- Augood, S. J., Faull, R. L., and Emson, P. C. (1997). Dopamine D₁ and D₂ receptor gene expression in the striatum in Huntington's disease. *Ann Neurol* 42, 215-221.
- Augood, S. J., Faull, R. L., Love, D. R., and Emson, P. C. (1996). Reduction in enkephalin and substance P messenger RNA in the striatum of early grade Huntington's disease: a detailed cellular *in situ* hybridization study. *Neuroscience* 72, 1023-1036.
- Aylward, E. H., Codori, A. M., Barta, P. E., Pearlson, G. D., Harris, G. J., and Brandt, J. (1996). Basal ganglia volume and proximity to onset in presymptomatic Huntington disease. *Arch Neurol* 53, 1293-1296.
- Bacolla, A., Gellibolian, R., Shimizu, M., Amirhaeri, S., Kang, S., Ohshima, K., Larson, J. E., Harvey, S. C., Stollar, B. D., and Wells, R. D. (1997). Flexible DNA: Genetically unstable CTGCAG and CGGCCG from human hereditary neuromuscular disease genes. *J Bio Chem* 272, 16783-16792.
- Bal-Price, A., and Brown, G. C. (2001). Inflammatory neurodegeneration mediated by nitric oxide from activated glia-inhibiting neuronal respiration, causing glutamate release and excitotoxicity. *J Neurosci* 21, 6480-6491.
- Balakumaran, B. S., Freudenreich, C. H., and Zakian, V. A. (2000). CGG/CCG repeats exhibit orientation-dependent instability and orientation-independent fragility in *Saccharomyces cerevisiae*. *Hum Mol Genet* 9, 93-100.
- Banfi, S., Servadio, A., Chung, M. Y., Capozzoli, F., Duvick, L. A., Elde, R., Zoghbi, H. Y., and Orr, H. T. (1996). Cloning and Developmental Expression Analysis Of the Murine Homolog Of the Spinocerebellar Ataxia Type 1 Gene (SCA1). *Hum Mol Genet* 5, 33-40.
- Barnes, C. A. (1979). Memory deficits associated with senescence: a neurophysiological and behavioral study in the rat. *J Comp Physiol Psychol* 93, 74-104.

- Barnes, G. T., Duyao, M. P., Ambrose, C. M., McNeil, S., Persichetti, F., Srinidhi, J., Gusella, J. F., and MacDonald, M. E. (1994). Mouse Huntington's disease gene homolog (*Hdh*). *Somat Cell Mol Genet* 20, 87-97.
- Barr, A. N., Heinze, W. J., Dobben, G. D., Valvassori, G. E., and Sugar, O. (1978). Bicaudate index in computerized tomography of Huntington disease and cerebral atrophy. *Neurology* 28, 1196-1200.
- Barres, B. A. (1999). A new role for glia: generation of neurons! *Cell* 97, 667-670.
- Barron, L. H., Warner, J. P., Porteous, M., Holloway, S., Simpson, S., Davidson, R., and Brock, D. J. (1993). A study of the Huntington's disease associated trinucleotide repeat in the Scottish population. *J Med Genet* 30, 1003-1007.
- Baxendale, S., Abdulla, S., Elgar, G., Buck, D., Berks, M., Micklem, G., Durbin, R., Bates, G., Brenner, S., and Beck, S. (1995). Comparative sequence analysis of the human and pufferfish Huntington's disease genes. *Nat Genet* 10, 67-76.
- Beal, M. F. (1992a). Does impairment of energy metabolism result in excitotoxic neuronal death in neurodegenerative illnesses? *Ann Neurol* 31, 119-130.
- Beal, M. F. (1992b). Role of excitotoxicity in human neurological disease. *Curr Opin Neurobiol* 2, 657-662.
- Beal, M. F. (1994). Neurochemistry and toxin models in Huntington's disease. *Curr Opin Neurol* 7, 542-547.
- Beal, M. F. (1995). Aging, energy, and oxidative stress in neurodegenerative diseases. *Ann Neurol* 38, 357-366.
- Beal, M. F., Brouillet, E., Jenkins, B. G., Ferrante, R. J., Kowall, N. W., Miller, J. M., Storey, E., Srivastava, R., Rosen, B. R., and Hyman, B. T. (1993). Neurochemical and histologic characterization of striatal excitotoxic lesions produced by the mitochondrial toxin 3-nitropropionic acid. *J Neurosci* 13, 4181-4192.
- Beal, M. F., Ferrante, R. J., Swartz, K. J., and Kowall, N. W. (1991). Chronic quinolinic acid lesions in rats closely resemble Huntington's disease. *J Neurosci* 11, 1649-1659.
- Beal, M. F., Kowall, N. W., Ellison, D. W., Mazurek, M. F., Swartz, K. J., and Martin, J. B. (1986). Replication of the neurochemical characteristics of Huntington's disease by quinolinic acid. *Nature* 321, 168-171.
- Becher, M. W., Kotzruk, J. A., Sharp, A. H., Davies, S. W., Bates, G. P., Price, D. L., and Ross, C. A. (1998). Intranuclear neuronal inclusions in Huntington's disease and dentatorubral and pallidolusian atrophy: Correlation between the density of inclusions and IT15 CAG triplet repeat length. *Neurobio Dis* 4, 387-397.
- Bernard, V., Somogyi, P., and Bolam, J. P. (1997). Cellular, subcellular, and subsynaptic distribution of AMPA type glutamate receptor subunits in the neostriatum of the rat. *J Neurosci* 17, 819-833.
- Berrios, G. E., Wagle, A. C., Markova, I. S., Wagle, S. A., Ho, L. W., Rubinsztein, D. C., Whittaker, J., Ffrench-Constant, C., Kershaw, A., Rosser, A., *et al.* (2001). Psychiatric symptoms and CAG repeats in neurologically asymptomatic Huntington's disease gene carriers. *Psychiatry Res* 102, 217-225.
- Bertaux, F., Sharp, A. H., Ross, C. A., Lehrach, H., Bates, G. P., and Wanker, E. (1998). HAP1 huntingtin interactions do not contribute to the molecular pathology in Huntington's disease transgenic mice. *Febs Letters* 426, 229-232.
- Bhide, P. G., Day, M., Sapp, E., Schwarz, C., Sheth, A., Kim, J., Young, A. B., Penney, J., Golden, J., Aronin, N., and Difiglia, M. (1996). Expression Of Normal and Mutant Huntingtin In the Developing Brain. *J Neurosci* 16, 5523-5535.
- Bi, X., and Liu, L. F. (1994). *recA*-independent and *recA*-dependent intramolecular plasmid recombination. Differential homology requirement and distance effect. *J Mol Biol* 235, 414-423.
- Bi, X., and Liu, L. F. (1996). A replicational model for DNA recombination between direct repeats. *J Mol Biol* 256, 849-858.
- Biscoe, T. J., Duggan, A. W., and Lodge, D. (1972). Effect of etorphine, morphine and diprenorphine on neurones of the cerebral cortex and spinal cord of the rat. *Br J Pharmacol* 46, 201-212.
- Bolanos, J. P., Almeida, A., Fernandez, E., Medina, J. M., Land, J. M., Clark, J. B., and Heales, S. J. (1997). Potential mechanisms for nitric oxide-mediated impairment of brain mitochondrial energy metabolism. *Biochem Soc Trans* 25, 944-949.
- Bolt, J. M. (1970). Huntington's chorea in the West of Scotland. *Br J Psychiatry* 116, 259-270.
- Borlongan, C. V., Cahill, D. W., and Sanberg, P. R. (1995a). Asymmetrical behavior in rats following striatal lesions and fetal transplants: The elevated body swing test. *Res Neurol and Neurosci* 9, 15-19.
- Borlongan, C. V., Koutouzis, T. K., Freeman, T. B., Cahill, D. W., and Sanberg, P. R. (1995b). Behavioral pathology induced by repeated systemic injections of 3 nitropropionic acid mimics the motoric symptoms of Huntington's disease. *Brain Res* 697, 254-257.
- Bossi, S. R., Simpson, J. R., and Isacson, O. (1993). Age dependence of striatal neuronal death caused by mitochondrial dysfunction. *Neuroreport* 4, 73-76.

- Boutell, J. M., Thomas, P., Neal, J. W., Weston, V. J., Duce, J., Harper, P. S., and Jones, A. L. (1999). Aberrant interactions of transcriptional repressor proteins with the Huntington's disease gene product, huntingtin. *Hum Mol Genet* 8, 1647-1655.
- Boutell, J. M., Wood, J. D., Harper, P. S., and Jones, A. L. (1998). Huntingtin interacts with cystathionine beta synthase. *Hum Mol Genet* 7, 371-378.
- Bouyer, J. J., Miller, R. J., and Pickel, V. M. (1984). Ultrastructural relation between cortical efferents and terminals containing enkephalin-like immunoreactivity in rat neostriatum. *Regul Pept* 8, 105-115.
- Bowater, R. P., Jaworski, A., Larson, J. E., Parniewski, P., and Wells, R. D. (1997). Transcription increases the deletion frequency of long CTG.CAG triplet repeats from plasmids in *Escherichia coli*. *Nucleic Acids Res* 25, 2861-2868.
- Bowater, R. P., Rosche, W. A., Jaworski, A., Sinden, R. R., and Wells, R. D. (1996). Relationship between *Escherichia coli* growth and deletions of CTG.CAG triplet repeats in plasmids. *J Mol Biol* 264, 82-96.
- Bowater, R. P., and Wells, R. D. (2001). The intrinsically unstable life of DNA triplet repeats associated with human hereditary disorders. *Prog Nucleic Acid Res Mol Biol* 66, 159-202.
- Brandt, J., Bylsma, F. W., Gross, R., Stine, O. C., Ranen, N., and Ross, C. A. (1996). Trinucleotide Repeat Length and Clinical Progression In Huntingtons Disease. *Neurology* 46, 527-531.
- Braun, A., and Grossman, L. (1974). An endonuclease from *Escherichia coli* that acts preferentially on UV-irradiated DNA and is absent from the *uvrA* and *uvrB* mutants. *Proc Natl Acad Sci U S A* 71, 1838-1842.
- Brennan, W. A., Jr., Bird, E. D., and Aprille, J. R. (1985). Regional mitochondrial respiratory activity in Huntington's disease brain. *J Neurochem* 44, 1948-1950.
- Brinkman, R. R., Mezei, M. M., Theilmann, J., Almqvist, E., and Hayden, M. R. (1997). The likelihood of being affected with huntington disease by a particular age, for a specific CAG size. *Am J Hum Genet* 60, 1202-1210.
- Brock, G. J., Anderson, N. H., and Monckton, D. G. (1999). Cis-acting modifiers of expanded CAG/CTG triplet repeat expandability: associations with flanking GC content and proximity to CpG islands. *Hum Mol Genet* 8, 1061-1067.
- Brook, J. D., McCurrach, M. E., Harley, H. G., Buckler, A. J., Church, D., Aburatani, H., Hunter, K., Stanton, V. P., Thirion, J. P., Hudson, T., and et, a. I. (1992). Molecular basis of myotonic dystrophy: expansion of a trinucleotide (CTG) repeat at the 3' end of a transcript encoding a protein kinase family member. *Cell* 69.
- Brosnan-Watters, G., and Wozniak, D. F. (1997). A rotating holeboard procedure for testing drug effects on spatial learning and memory in mice. *Brain Res Brain Res Protoc* 1, 331-338.
- Brosnan-Watters, G., Wozniak, D. F., Nardi, A., and Olney, J. W. (1996). Acute behavioral effects of MK-801 in the mouse. *Pharmacol Biochem Behav* 53, 701-711.
- Brosnan-Watters, G., Wozniak, D. F., Nardi, A., and Olney, J. W. (1999). Parallel recovery of MK-801-induced spatial learning impairment and neuronal injury in male mice. *Pharmacol Biochem Behav* 62, 111-122.
- Brouillet, E., Conde, F., Beal, M. F., and Hantraye, P. (1999). Replicating Huntington's disease phenotype in experimental animals. *Prog Neurobiol* 59, 427-468.
- Brouillet, E., Jenkins, B. G., Hyman, B. T., Ferrante, R. J., Kowall, N. W., Srivastava, R., Roy, D. S., Rosen, B. R., and Beal, M. F. (1993). Age-dependent vulnerability of the striatum to the mitochondrial toxin 3-nitropropionic acid. *J Neurochem* 60, 356-359.
- Brown, L. L., Schneider, J. S., and Lidsky, T. I. (1997). Sensory and cognitive functions of the basal ganglia. *Curr Opin Neurobiol* 7, 157-163.
- Brown, R. G., and Marsden, C. D. (1988). 'Subcortical dementia': the neuropsychological evidence. *Neuroscience* 25, 363-387.
- Brown, W. T., Houck, G. E., Jr., Ding, X., Zhong, N., Nolin, S., Glicksman, A., Dobkin, C., and Jenkins, E. C. (1996). Reverse mutations in the fragile X syndrome. *Am J Med Genet* 64, 287-292.
- Browne, S. E., Bowling, A. C., MacGarvey, U., Baik, M. J., Berger, S. C., Muqit, M. M., Bird, E. D., and Beal, M. F. (1997). Oxidative damage and metabolic dysfunction in Huntington's disease: selective vulnerability of the basal ganglia. *Ann Neurol* 41, 646-653.
- Budd, S. L., and Nicholls, D. G. (1996). Mitochondria, calcium regulation, and acute glutamate excitotoxicity in cultured cerebellar granule cells. *J Neurochem* 67, 2282-2291.
- Buisson, A., Pateau, V., Plotkine, M., and Boulu, R. G. (1991). Nigrostriatal pathway modulates striatum vulnerability to quinolinic acid. *Neurosci Lett* 131, 257-259.
- Burke, J. R., Enghild, J. J., Martin, M. E., Jou, Y. S., Myers, R. M., Roses, A. D., Vance, J. M., and Strittmatter, W. J. (1996). Huntington and DRPLA Proteins Selectively Interact With the Enzyme GAPDH. *Nat Med* 2, 347-350.
- Butters, N., Sax, D., Montgomery, K., and Tarlow, S. (1978). Comparison of the neuropsychological deficits associated with early and advanced Huntington's disease. *Arch Neurol* 35, 585-589.

- Caine, E. D., Hunt, R. D., Weingartner, H., and Ebert, M. H. (1978). Huntington's dementia. Clinical and neuropsychological features. *Arch Gen Psychiatry* *35*, 377-384.
- Calabresi, P., Ascone, C. M., Centonze, D., Pisani, A., Sancesario, G., D'Angelo, V., and Bernardi, G. (1997a). Opposite membrane potential changes induced by glucose deprivation in striatal spiny neurons and in large aspiny interneurons. *J Neurosci* *17*, 1940-1949.
- Calabresi, P., Centonze, D., Pisani, A., and Bernardi, G. (1999). Metabotropic glutamate receptors and cell-type-specific vulnerability in the striatum: Implication for ischemia and Huntington's disease. *Exp Neurol* *158*, 97-108.
- Calabresi, P., Centonze, D., Pisani, A., Sancesario, G., Gubellini, P., Marfia, G. A., and Bernardi, G. (1998). Striatal spiny neurons and cholinergic interneurons express differential ionotropic glutamatergic responses and vulnerability: Implications for ischemia and Huntington's disease. *Ann Neurol* *43*, 586-597.
- Calabresi, P., De Murtas, M., Pisani, A., Stefani, A., Sancesario, G., Mercuri, N. B., and Bernardi, G. (1995). Vulnerability of medium spiny striatal neurons to glutamate: role of Na⁺/K⁺ ATPase. *Eur J Neurosci* *7*, 1674-1683.
- Calabresi, P., Pisani, A., Mercuri, N. B., and Bernardi, G. (1996). The Corticostriatal Projection From Synaptic Plasticity to Dysfunctions Of the Basal Ganglia. *Trends Neurosci* *19*, 19-24.
- Calabresi, P., Saiardi, A., Pisani, A., Baik, J. H., Centonze, D., Mercuri, N. B., Bernardi, G., and Borrelli, E. (1997b). Abnormal synaptic plasticity in the striatum of mice lacking dopamine D₂ receptors. *J Neurosci* *17*, 4536-4544.
- Campodónico, J. R., Codori, A. M., and Brandt, J. (1996). Neuropsychological stability over two years in asymptomatic carriers of the Huntington's disease mutation. *J Neurol Neurosurg Psychiatry* *61*, 621-624.
- Camps, M., Kelly, P. H., and Palacios, J. M. (1990). Autoradiographic localization of dopamine D₁ and D₂ receptors in the brain of several mammalian species. *J Neural Transm Gen Sect* *80*, 105-127.
- Campuzano, V., Montermini, L., Molto, M. D., Pianese, L., Cossee, M., Cavalcanti, F., Monros, E., Rodius, F., Duclos, F., Monticelli, A., *et al.* (1996). Friedreichs Ataxia Autosomal Recessive Disease Caused By an Intronic GAA Triplet Repeat Expansion. *Science* *271*, 1423-1427.
- Cancel, G., Gourfinkel-An, I., Stevanin, G., Didierjean, O., Abbas, N., Hirsch, E., Agid, Y., and Brice, A. (1998). Somatic mosaicism of the CAG repeat expansion in spinocerebellar ataxia type 3/Machado-Joseph disease. *Hum Mutat* *11*, 23-27.
- Carmichael, J., Chatellier, J., Woolfson, A., Milstein, C., Fersht, A. R., and Rubinsztein, D. C. (2000). Bacterial and yeast chaperones reduce both aggregate formation and cell death in mammalian cell models of Huntington's disease. *Proc Natl Acad Sci U S A* *97*, 9701-9705.
- Carter, R. J., Lione, L. A., Humby, T., Mangiarini, L., Mahal, A., Bates, G. P., Dunnett, S. B., and Morton, A. J. (1999). Characterization of progressive motor deficits in mice transgenic for the human Huntington's disease mutation. *J Neurosci* *19*, 3248-3257.
- Cass, W. A. (1997). Decreases in evoked overflow of dopamine in rat striatum after neurotoxic doses of methamphetamine. *J Pharmacol Exp Ther* *280*, 105-113.
- Cattaneo, E., Rigamonti, D., Goffredo, D., Zuccato, C., Squitieri, F., and Sipione, S. (2001). Loss of normal huntingtin function: new developments in Huntington's disease research. *Trends Neurosci* *24*, 182-188.
- Cepeda, C., Ariano, M. A., Calvert, C. R., Flores-Hernandez, J., Chandler, S. H., Leavitt, B. R., Hayden, M. R., and Levine, M. S. (2001a). NMDA receptor function in mouse models of Huntington disease. *J Neurosci Res* *66*, 525-539.
- Cepeda, C., Buchwald, N. A., and Levine, M. S. (1993). Neuromodulatory actions of dopamine in the neostriatum are dependent upon the excitatory amino acid receptor subtypes activated. *Proc Natl Acad Sci U S A* *90*, 9576-9580.
- Cepeda, C., Colwell, C. S., Itri, J. N., Gruen, E., and Levine, M. S. (1998). Dopaminergic modulation of early signs of excitotoxicity in visualized rat neostriatal neurons. *Eur J Neurosci* *10*, 3491-3497.
- Cepeda, C., Hurst, R. S., Altemus, K. L., Flores-Hernandez, J., Calvert, C. R., Jokel, E. S., Grandy, D. K., Low, M. J., Rubinstein, M., Ariano, M. A., and Levine, M. S. (2001b). Facilitated glutamatergic transmission in the striatum of D₂ dopamine receptor-deficient mice. *J Neurophysiol* *85*, 659-670.
- Cha, J. H., Kosinski, C. M., Kerner, J. A., Alsdorf, S. A., Mangiarini, L., Davies, S. W., Penney, J. B., Bates, G. P., and Young, A. B. (1998). Altered brain neurotransmitter receptors in transgenic mice expressing a portion of an abnormal human huntington disease gene. *Proc Natl Acad Sci U S A* *95*, 6480-6485.
- Cha, J. H. J., Frey, A. S., Alsdorf, S. A., Kerner, J. A., Kosinski, C. M., Mangiarini, L., Penney, J. B., Davies, S. W., Bates, G. P., and Young, A. B. (1999). Altered neurotransmitter receptor expression in transgenic mouse models of Huntington's disease. *Phil Trans R Soc Lond B* *354*, 981-989.
- Chan, E. Y., Nasir, J., Gutekunst, C. A., Coleman, S., Maclean, A., Maas, A., Metzler, M., Gertsenstein, M., Ross, C. A., Nagy, A., and Hayden, M. R. (2002). Targeted disruption of Huntingtin-associated

- protein-1 (Hap1) results in postnatal death due to depressed feeding behavior. *Hum Mol Genet* 11, 945-959.
- Chang, C., and Jang, T. (1995). Age-dependent neurotoxicity of striatal lesions produced by aminoxyacetic acid: quantitative *in vitro* ¹H NMR spectroscopic studies. *J Neurochem* 65, 1192-1198.
- Chapman, A. G., Durmuller, N., Lees, G. J., and Meldrum, B. S. (1989). Excitotoxicity of NMDA and kainic acid is modulated by nigrostriatal dopaminergic fibres. *Neurosci Lett* 107, 256-260.
- Chen, N., Luo, T., Wellington, C., Metzler, M., McCutcheon, K., Hayden, M. R., and Raymond, L. A. (1999). Subtype-specific enhancement of NMDA receptor currents by mutant huntingtin. *J Neurochem* 72, 1890-1898.
- Cheng, N., Maeda, T., Kume, T., Kaneko, S., Kochiyama, H., Akaike, A., Goshima, Y., and Misu, Y. (1996). Differential neurotoxicity induced by L-DOPA and dopamine in cultured striatal neurons. *Brain Res* 743, 278-283.
- Chong, S. S., Almqvist, E., Telenius, H., LaTray, L., Nichol, K., BourdelatParks, B., Goldberg, Y. P., Haddad, B. R., Richards, F., Sillence, D., *et al.* (1997). Contribution of DNA sequence and CAG size to mutation frequencies of intermediate alleles for Huntington disease: Evidence from single sperm analyses. *Hum Mol Genet* 6, 301-309.
- Chong, S. S., McCall, A. E., Cota, J., Subramony, S. H., Orr, H. T., Hughes, M. R., and Zoghbi, H. Y. (1995). Gametic and somatic tissue-specific heterogeneity of the expanded SCA1 CAG repeat in spinocerebellar ataxia type 1. *Nat Genet* 10, 344-350.
- Chun, W., Lesort, M., Lee, M., and Johnson, G. V. (2002). Mutant huntingtin aggregates do not sensitize cells to apoptotic stressors. *FEBS Lett* 515, 61-65.
- Cicchetti, F., and Parent, A. (1996). Striatal interneurons in Huntington's disease: Selective increase in the density of calretinin immunoreactive medium sized neurons. *Mov Dis* 11, 619-626.
- Ciechanover, A. (1994). The ubiquitin-proteasome proteolytic pathway. *Cell* 79, 13-21.
- Clarke, K. A., and Still, J. (1999). Gait analysis in the mouse. *Physiol Behav* 66, 723-729.
- Cleary, J. D., Nichol, K., Wang, Y. H., and Pearson, C. E. (2002). Evidence of cis-acting factors in replication-mediated trinucleotide repeat instability in primate cells. *Nat Genet* 31, 37-46.
- Connop, B. P., Boegman, R. J., Beninger, R. J., and Jhamandas, K. (1996). Attenuation of malonate-induced degeneration of the nigrostriatal pathway by inhibitors of nitric oxide synthase. *Neuropharm* 35, 459-465.
- Cooper, J. K., Schilling, G., Peters, M. F., Herring, W. J., Sharp, A. H., Kaminsky, Z., Masone, J., Khan, F. A., Delanoy, M., Borchelt, D. R., *et al.* (1998). Truncated N-terminal fragments of huntingtin with expanded glutamine repeats form nuclear and cytoplasmic aggregates in cell culture. *Hum Mol Genet* 7, 783-790.
- Coyle, J. T., and Puttfarcken, P. (1993). Oxidative stress, glutamate, and neurodegenerative disorders. *Science* 262, 689-695.
- Coyle, J. T., and Schwarcz, R. (1976). Lesion of striatal neurones with kainic acid provides a model for Huntington's chorea. *Nature* 263, 244-246.
- Crossman, A. R., Clarke, C. E., Boyce, S., Robertson, R. G., and Sambrook, M. A. (1987). MPTP-induced parkinsonism in the monkey: neurochemical pathology, complications of treatment and pathophysiological mechanisms. *Can J Neurol Sci* 14, 428-435.
- David, G., Abbas, N., Stevanin, G., Durr, A., Yvert, G., Cancel, G., Weber, C., Imbert, G., Saudou, F., Antoniou, E., *et al.* (1997). Cloning of the SCA7 gene reveals a highly unstable CAG repeat expansion. *Nat Genet* 17, 65-70.
- David, G., Giunti, P., Abbas, N., Coullin, P., Stevanin, G., Horta, W., Gemmill, R., Weissenbach, J., Wood, N., Cunha, S., *et al.* (1996). The gene for autosomal dominant cerebellar ataxia type II is located in a 5 cM region in 3p12 p13: Genetic and physical mapping of the SCA7 locus. *Am J Hum Genet* 59, 1328-1336.
- Davies, S. W., and Roberts, P. J. (1987). No evidence for preservation of somatostatin-containing neurons after intra-striatal injections of quinolinic acid. *Nature* 327, 326-329.
- Davies, S. W., Turmaine, M., Cozens, B. A., DiFiglia, M., Sharp, A. H., Ross, C. A., Scherzinger, E., Wanker, E. E., Mangiarini, L., and Bates, G. P. (1997). Formation of neuronal intranuclear inclusions underlies the neurological dysfunction in mice transgenic for the HD mutation. *Cell* 90, 537-548.
- Davies, S. W., Turmaine, M., Cozens, B. A., Raza, A. S., Mahal, A., Mangiarini, J. B., and Bates, G. P. (1999). From neuronal inclusions to neurodegeneration; neuropathological investigation of a transgenic mouse model of Huntington's disease. *Phil Trans R Soc Lond B* 354, 971-980.
- Dawson, T. M., Dawson, V. L., and Snyder, S. H. (1993). Nitric oxide as a mediator of neurotoxicity. *NIDA Res Monogr* 136, 258-271.
- Dawson, V. L. (1995). Nitric oxide: role in neurotoxicity. *Clin Exp Pharmacol Physiol* 22, 305-308.
- Dawson, V. L., Dawson, T. M., and Wamsley, J. K. (1990). Muscarinic and dopaminergic receptor subtypes on striatal cholinergic interneurons. *Brain Res Bull* 25, 903-912.

- de Almeida, L. P., Ross, C. A., Zala, D., Aebischer, P., and Deglon, N. (2002). Lentiviral-mediated delivery of mutant huntingtin in the striatum of rats induces a selective neuropathology modulated by polyglutamine repeat size, huntingtin expression levels, and protein length. *J Neurosci* 22, 3473-3483.
- de Boo, G. M., Tibben, A., Lanser, J. B., Jennekens-Schinkel, A., Hermans, J., Maat-Kievit, A., and Roos, R. A. (1997). Early cognitive and motor symptoms in identified carriers of the gene for Huntington disease. *Arch Neurol* 54, 1353-1357.
- De Rooij, K. E., De Koning Gans, P. A., Roos, R. A., Van Ommen, G. J., and Den Dunnen, J. T. (1995). Somatic expansion of the (CAG)_n repeat in Huntington disease brains. *Hum Genet* 95, 270-274.
- DiFiglia, M., Sapp, E., Chase, K., Schwarz, C., Meloni, A., Young, C., Martin, E., Vonsattel, J. P., Carraway, R., Reeves, S. A., and et al. (1995). Huntingtin is a cytoplasmic protein associated with vesicles in human and rat brain neurons. *Neuron* 14, 1075-1081.
- DiFiglia, M., Sapp, E., Chase, K. O., Davies, S. W., Bates, G. P., Vonsattel, J. P., and Aronin, N. (1997). Aggregation of huntingtin in neuronal intranuclear inclusions and dystrophic neurites in brain. *Science* 277, 1990-1993.
- Doetsch, F., Caille, I., Lim, D. A., Garcia-Verdugo, J. M., and Alvarez-Buylla, A. (1999). Subventricular zone astrocytes are neural stem cells in the adult mammalian brain. *Cell* 97, 703-716.
- Doyu, M., Sobue, G., Kimata, K., Yamamoto, K., and Mitsuma, T. (1994). Androgen receptor mRNA with increased size of tandem CAG repeat is widely expressed in the neural and nonneural tissues of X-linked recessive bulbospinal neuronopathy. *J Neurol Sci* 127, 43-47.
- Dragatsis, I., Levine, M. S., and Zeitlin, S. (2000). Inactivation of *Hdh* in the brain and testis results in progressive neurodegeneration and sterility in mice. *Nat Genet* 26, 300-306.
- Drost, J. B., and Lee, W. R. (1995). Biological basis of germline mutation: comparisons of spontaneous germline mutation rates among drosophila, mouse, and human. *Environ Mol Mutagen* 25, 48-64.
- Dubois, A., and Scatton, B. (1985). Heterogeneous distribution of dopamine D₂ receptors within the rat striatum as revealed by autoradiography of [3H]N-n-propylnorapomorphine binding sites. *Neurosci Lett* 57, 7-12.
- Dunah, A. W., Jeong, H., Griffin, A., Kim, Y. M., Standaert, D. G., Hersch, S. M., Mouradian, M. M., Young, A. B., Tanese, N., and Krainc, D. (2002). Sp1 and TAFIII130 Transcriptional Activity Disrupted in Early Huntington's Disease. *Science* 2, 2.
- Dunnett, S. B., Carter, R. J., Watts, C., Torres, E. M., Mahal, A., Mangiarini, L., Bates, G., and Morton, A. J. (1998). Striatal transplantation in a transgenic mouse model of Huntington's disease. *Exp Neurol* 154, 31-40.
- Dure, L. S. t., Young, A. B., and Penney, J. B. (1991). Excitatory amino acid binding sites in the caudate nucleus and frontal cortex of Huntington's disease. *Ann Neurol* 30, 785-793.
- Dure, L. S. t., Young, A. B., and Penney, J. B., Jr. (1992). Compartmentalization of excitatory amino acid receptors in human striatum. *Proc Natl Acad Sci U S A* 89, 7688-7692.
- Duyao, M., Ambrose, C., Myers, R., Novelletto, A., Persichetti, F., Frontali, M., Folstein, S., Ross, C., Franz, M., Abbott, M., and et, a. l. (1993). Trinucleotide repeat length instability and age of onset in Huntington's disease. *Nat Genet* 4, 387-392.
- Duyao, M. P., Auerbach, A. B., Ryan, A., Persichetti, F., Barnes, G. T., McNeil, S. M., Ge, P., Vonsattel, J. P., Gusella, J. F., Joyner, A. L., and MacDonald, M. E. (1995). Inactivation of the mouse Huntington's disease gene homolog *Hdh*. *Science* 269, 407-410.
- Ellison, D. W., Beal, M. F., Mazurek, M. F., Malloy, J. R., Bird, E. D., and Martin, J. B. (1987). Amino acid neurotransmitter abnormalities in Huntington's disease and the quinolinic acid animal model of Huntington's disease. *Brain* 110, 1657-1673.
- Enna, S. J., Bennett, J. P., Jr., Bylund, D. B., Snyder, S. H., Bird, E. D., and Iversen, L. L. (1976). Alterations of brain neurotransmitter receptor binding in Huntington's chorea. *Brain Res* 116, 531-537.
- Faber, P. W., Alter, J. R., MacDonald, M. E., and Hart, A. C. (1999). Polyglutamine mediated dysfunction and apoptotic death of a *Caenorhabditis elegans* sensory neuron. *Proc Natl Acad Sci U S A* 96, 179-184.
- Faull, R. L., Waldvogel, H. J., Nicholson, L. F., and Synek, B. J. (1993). The distribution of GABAA-benzodiazepine receptors in the basal ganglia in Huntington's disease and in the quinolinic acid-lesioned rat. *Prog Brain Res* 99, 105-123.
- Ferrante, R. J., Gutekunst, C. A., Persichetti, F., McNeil, S. M., Kowall, N. W., Gusella, J. F., MacDonald, M. E., Beal, M. F., and Hersch, S. M. (1997). Heterogeneous topographic and cellular distribution of Huntington expression in the normal human neostriatum. *J Neurosci* 17, 3052-3063.
- Ferrante, R. J., Kowall, N. W., Cipolloni, P. B., Storey, E., and Beal, M. F. (1993). Excitotoxin lesions in primates as a model for Huntington's disease: histopathologic and neurochemical characterization. *Exp Neurol* 119, 46-71.
- Ferre, S., O'Connor, W. T., Fuxe, K., and Ungerstedt, U. (1993). The striopallidal neuron: a main locus for adenosine-dopamine interactions in the brain. *J Neurosci* 13, 5402-5406.

- Ferrer, I., Oliver, B., Russi, A., Casas, R., and Rivera, R. (1994). Parvalbumin and calbindin-D28k immunocytochemistry in human neocortical epileptic foci. *J Neurol Sci* 123, 18-25.
- Figueredo-Cardenas, G., Chen, Q., and Reiner, A. (1997). Age-dependent differences in survival of striatal somatostatin-NPY- NADPH-diaphorase-containing interneurons versus striatal projection neurons after intrastriatal injection of quinolinic acid in rats. *Exp Neurol* 146, 444-457.
- Filloux, F., Dawson, T. M., and Wamsley, J. K. (1988). Localization of nigrostriatal dopamine receptor subtypes and adenylate cyclase. *Brain Res Bull* 20, 447-459.
- Flores-Hernandez, J., Galarraga, E., and Bargas, J. (1997). Dopamine selects glutamatergic inputs to neostriatal neurons. *Synapse* 25, 185-195.
- Flynn, G. A., Hirst, M. C., Knight, S. J., Macpherson, J. N., Barber, J. C., Flannery, A. V., Davies, K. E., and Buckle, V. J. (1993). Identification of the FRAXE fragile site in two families ascertained for X linked mental retardation. *J Med Genet* 30, 97-100.
- Folstein, S., Abbott, M. H., Chase, G. A., Jensen, B. A., and Folstein, M. F. (1983). The association of affective disorder with Huntington's disease in a case series and in families. *Psychol Med* 13, 537-542.
- Foroud, T., Gray, J., Ivashina, J., and Conneally, P. M. (1999). Differences in duration of Huntington's disease based on age at onset. *J Neurol Neurosurg Psychiatry* 66, 52-56.
- Foroud, T., Siemers, E., Kleindorfer, D., Bill, D. J., Hodes, M. E., Norton, J. A., Conneally, P. M., and Christian, J. C. (1995). Cognitive scores in carriers of Huntington's disease gene compared to noncarriers. *Ann Neurol* 37, 657-664.
- Fortune, M. T., Vassilopoulos, C., Coolbaugh, M. I., Siciliano, M. J., and Monckton, D. G. (2000). Dramatic, expansion-biased, age-dependent, tissue-specific somatic mosaicism in a transgenic mouse model of triplet repeat instability. *Hum Mol Genet* 9, 439-445.
- Francis, D. D., Zaharia, M. D., Shanks, N., and Anisman, H. (1995). Stress-induced disturbances in Morris water-maze performance: interstrain variability. *Physiol Behav* 58, 57-65.
- Franklin, K. B. J., and Paxinos, G. (1997). *The Mouse Brain in Stereotaxic Coordinates*, (San Diego, Academic Press).
- Freudenreich, C. H., Kantrow, S. M., and Zakian, V. A. (1998). Expansion and length-dependent fragility of CTG repeats in yeast. *Science* 279, 853-856.
- Freudenreich, C. H., Stavenhagen, J. B., and Zakian, V. A. (1997). Stability of a CTG/CAG trinucleotide repeat in yeast is dependent on its orientation in the genome. *Mol Cell Biol* 17, 2090-2098.
- Fu, Y. H., Kuhl, D. P., Pizzuti, A., Pieretti, M., Sutcliffe, J. S., Richards, S., Verkerk, A. J., Holden, J. J., Fenwick, R. G., Jr., Warren, S. T., and et al. (1991). Variation of the CGG repeat at the fragile X site results in genetic instability: resolution of the Sherman paradox. *Cell* 67, 1047-1058.
- Fujigasaki, H., Martin, J. J., De Deyn, P. P., Camuzat, A., Deffond, D., Stevanin, G., Dermaut, B., Van Broeckhoven, C., Durr, A., and Brice, A. (2001). CAG repeat expansion in the TATA box-binding protein gene causes autosomal dominant cerebellar ataxia. *Brain* 124, 1939-1947.
- Fusco, F. R., Chen, Q., Lamoreaux, W. J., Figueredo-Cardenas, G., Jiao, Y., Coffman, J. A., Surmeier, D. J., Honig, M. G., Carlock, L. R., and Reiner, A. (1999). Cellular localization of huntingtin in striatal and cortical neurons in rats: lack of correlation with neuronal vulnerability in Huntington's disease. *J Neurosci* 19, 1189-1202.
- Gacy, A. M., Goellner, G., Juranic, N., Macura, S., and McMurray, C. T. (1995). Trinucleotide repeats that expand in human disease form hairpin structures in vitro. *Cell* 81, 533-540.
- Garau, L., Govoni, S., Stefanini, E., Trabucchi, M., and Spano, P. F. (1978). Dopamine receptors: pharmacological and anatomical evidences indicate that two distinct dopamine receptor populations are present in rat striatum. *Life Sci* 23, 1745-1750.
- Garcia, E. P., Mehta, S., Blair, L. A., Wells, D. G., Shang, J., Fukushima, T., Fallon, J. R., Garner, C. C., and Marshall, J. (1998). SAP90 binds and clusters kainate receptors causing incomplete desensitization. *Neuron* 21, 727-739.
- Gaspar, P., Bloch, B., and Le Moine, C. (1995). D₁ and D₂ receptor gene expression in the rat frontal cortex: cellular localization in different classes of efferent neurons. *Eur J Neurosci* 7, 1050-1063.
- Gerfen, C. R. (1985). The neostriatal mosaic. I. Compartmental organization of projections from the striatum to the substantia nigra in the rat. *J Comp Neurol* 236, 454-476.
- Gerfen, C. R. (1988). Synaptic organization of the striatum. *J Electron Microscop Tech* 10, 265-281.
- Gerfen, C. R. (1992). The neostriatal mosaic: multiple levels of compartmental organization. *Trends Neurosci* 15, 133-139.
- Gerfen, C. R., Engber, T. M., Mahan, L. C., Susel, Z., Chase, T. N., Monsma, F. J., Jr., and Sibley, D. R. (1990). D₁ and D₂ dopamine receptor-regulated gene expression of striatonigral and striatopallidal neurons. *Science* 250, 1429-1432.
- Gerfen, C. R., and Young, W. S. (1988). Distribution of striatonigral and striatopallidal peptidergic neurons in both patch and matrix compartments: an in situ hybridization histochemistry and fluorescent retrograde tracing study. *Brain Res* 460, 161-167.

- Gerlach, M., Kuhn, W., Muller, T., Winkel, R., Lange, H., and Przuntek, H. (1996). Increased GABA synthesis in skin fibroblasts of patients with Huntington's disease: A possible role of glutamic acid decarboxylase? *Euro J Neurol* 3, 467-470.
- Ghasemzadeh, M. B., Sharma, S., Surmeier, D. J., Eberwine, J. H., and Chesselet, M. F. (1996). Multiplicity of glutamate receptor subunits in single striatal neurons: an RNA amplification study. *Mol Pharmacol* 49, 852-859.
- Ginovart, N., Lundin, A., Farde, L., Halldin, C., Backman, L., Swahn, C. G., Pauli, S., and Sedvall, G. (1997). PET study of the pre- and post-synaptic dopaminergic markers for the neurodegenerative process in Huntington's disease. *Brain* 120, 503-514.
- Giordani, B., Berent, S., Boivin, M. J., Penney, J. B., Lehtinen, S., Markel, D. S., Hollingsworth, Z., Butterbaugh, G., Hichwa, R. D., Gusella, J. F., and et al. (1995). Longitudinal neuropsychological and genetic linkage analysis of persons at risk for Huntington's disease. *Arch Neurol* 52, 59-64.
- Glass, M., Dragunow, M., and Faull, R. L. (2000). The pattern of neurodegeneration in Huntington's disease: a comparative study of cannabinoid, dopamine, adenosine and GABA(A) receptor alterations in the human basal ganglia in Huntington's disease. *Neuroscience* 97, 505-519.
- Goldberg, Y. P., Kremer, B., Andrew, S. E., Theilmann, J., Graham, R. K., Squitieri, F., Telenius, H., Adam, S., Sajoo, A., Starr, E., and et al. (1993). Molecular analysis of new mutations for Huntington's disease: intermediate alleles and sex of origin effects. *Nat Genet* 5, 174-179.
- Goldberg, Y. P., McMurray, C. T., Zeisler, J., Almqvist, E., Sillence, D., Richards, F., Gacy, A. M., Buchanan, J., Telenius, H., and Hayden, M. R. (1995). Increased instability of intermediate alleles in families with sporadic Huntington disease compared to similar sized intermediate alleles in the general population. *Hum Mol Genet* 4, 1911-1918.
- Goldberg, Y. P., Nicholson, D. W., Rasper, D. M., Kalchman, M. A., Koide, H. B., Graham, R. K., Bromm, M., Kazemi-Esfarjani, P., Thornberry, N. A., Vaillancourt, J. P., and Hayden, M. R. (1996). Cleavage of huntingtin by apopain, a proapoptotic cysteine protease, is modulated by the polyglutamine tract. *Nat Genet* 13, 442-449.
- Goldman-Rakic, P. S., and Selemon, L. D. (1990). New frontiers in basal ganglia research. Introduction. *Trends Neurosci* 13, 241-244.
- Gomes-Pereira, M., Fortune, M. T., and Monckton, D. G. (2001). Mouse tissue culture models of unstable triplet repeats: in vitro selection for larger alleles, mutational expansion bias and tissue specificity, but no association with cell division rates. *Hum Mol Genet* 10, 845-854.
- Gomez-Tortosa, E., del Barrio, A., Barroso, T., and Garcia Ruiz, P. J. (1996). Visual processing disorders in patients with Huntington's disease and asymptomatic carriers. *J Neurol* 243, 286-292.
- Gomez-Tortosa, E., del Barrio, A., Garcia Ruiz, P. J., Pernaute, R. S., Benitez, J., Barroso, A., Jimenez, F. J., and Garcia Yebenes, J. (1998). Severity of cognitive impairment in juvenile and late-onset Huntington disease. *Arch Neurol* 55, 835-843.
- Goodchild, R. E., Court, J. A., Hobson, I., Piggott, M. A., Perry, R. H., Ince, P., Jaros, E., and Perry, E. K. (1999). Distribution of histamine H3-receptor binding in the normal human basal ganglia: comparison with Huntington's and Parkinson's disease cases. *Eur J Neurosci* 11, 449-456.
- Gordenin, D. A., Kunkel, T. A., and Resnick, M. A. (1997). Repeat expansion--all in a flap? *Nat Genet* 16, 116-118.
- Gordon, N. (1995). Apoptosis (programmed cell death) and other reasons for elimination of neurons and axons. *Brain Dev* 17, 73-77.
- Goto, S., Hirano, A., and Rojas-Corona, R. R. (1989). An immunohistochemical investigation of the human neostriatum in Huntington's disease. *Ann Neurol* 25, 298-304.
- Gourfinkel-An, I., Cancel, G., Trottier, Y., Devys, D., Tora, L., Lutz, Y., Imbert, G., Saudou, F., Stevanin, G., Agid, Y., et al. (1997). Differential distribution of the normal and mutated forms of huntingtin in the human brain. *Ann Neurol* 42, 712-719.
- Grafton, S. T., Mazziotta, J. C., Pahl, J. J., St George-Hyslop, P., Haines, J. L., Gusella, J., Hoffman, J. M., Baxter, L. R., and Phelps, M. E. (1992). Serial changes of cerebral glucose metabolism and caudate size in persons at risk for Huntington's disease. *Arch Neurol* 49, 1161-1167.
- Graham, D. G., Tiffany, S. M., Bell, W. R., Jr., and Gutknecht, W. F. (1978). Autoxidation versus covalent binding of quinones as the mechanism of toxicity of dopamine, 6-hydroxydopamine, and related compounds toward C1300 neuroblastoma cells in vitro. *Mol Pharmacol* 14, 644-653.
- Grandy, D. K., and Civelli, O. (1992). G-protein-coupled receptors: the new dopamine receptor subtypes. *Curr Opin Neurobiol* 2, 275-281.
- Graveland, G. A., Williams, R. S., and DiFiglia, M. (1985). Evidence for degenerative and regenerative changes in neostriatal spiny neurons in Huntington's disease. *Science* 227, 770-773.
- Graybiel, A. M. (1990). Neurotransmitters and neuromodulators in the basal ganglia. *Trends Neurosci* 13, 244-254.
- Green, H. (1993). Human genetic diseases due to codon reiteration: relationship to an evolutionary mechanism. *Cell* 74, 955-956.

- Greene, E. L., and Paller, M. S. (1992). Xanthine oxidase produces O₂⁻ in posthypoxic injury of renal epithelial cells. *Am J Physiol* 263, F251-255.
- Grewe, C. W., Frey, E. A., Cote, T. E., and Keibabian, J. W. (1982). YM-09151-2: a potent antagonist for a peripheral D₂-dopamine receptor. *Eur J Pharmacol* 81, 149-152.
- Gu, M., Gash, M. T., Mann, V. M., Javoyagid, F., Cooper, J. M., and Schapira, A. H. V. (1996). Mitochondrial Defect In Huntingtons Disease On Caudate Nucleus. *Ann Neurol* 39, 385-389.
- Gutkunst, C. A., Levey, A. I., Heilman, C. J., Whaley, W. L., Yi, H., Nash, N. R., Rees, H. D., Madden, J. J., and Hersch, S. M. (1995). Identification and localization of huntingtin in brain and human lymphoblastoid cell lines with anti fusion protein antibodies. *Proc Natl Acad Sci U S A* 92, 8710-8714.
- Gutkunst, C. A., Li, S. H., Yi, H., Mulroy, J. S., Kuemmerle, S., Jones, R., Rye, D., Ferrante, R. J., Hersch, S. M., and Li, X. J. (1999). Nuclear and neuropil aggregates in Huntington's disease: relationship to neuropathology. *J Neurosci* 19, 2522-2534.
- Guyot, M. C., Hantraye, P., Dolan, R., Palfi, S., Maziere, M., and Brouillet, E. (1997). Quantifiable bradykinesia, gait abnormalities and Huntington's disease like striatal lesions in rats chronically treated with 3 nitropropionic acid. *Neuroscience* 79, 45-56.
- Hackam, A. S., Hodgson, J. G., Singaraja, R., Zhang, T. Q., Gan, L., Gutkunst, C. A., Hersch, S. M., and Hayden, M. R. (1999a). Evidence for both the nucleus and cytoplasm as subcellular sites of pathogenesis in Huntington's disease in cell culture and in transgenic mice expressing mutant huntingtin. *Phil Trans R Soc Lond B* 354, 1047-1055.
- Hackam, A. S., Singaraja, R., Wellington, C. L., Metzler, M., McCutcheon, K., Zhang, T., Kalchman, M., and Hayden, M. R. (1998). The influence of huntingtin protein size on nuclear localization and cellular toxicity. *J Cell Biol* 141, 1097-1105.
- Hackam, A. S., Singaraja, R., Zhang, T., Gan, L., and Hayden, M. R. (1999b). In vitro evidence for both the nucleus and cytoplasm as subcellular sites of pathogenesis in Huntington's disease. *Hum Mol Genet* 8, 25-33.
- Hahn-Barma, V., Deweer, B., Durr, A., Dode, C., Feingold, J., Pillon, B., Agid, Y., Brice, A., and Dubois, B. (1998). Are cognitive changes the first symptoms of Huntington's disease? A study of gene carriers. *J Neurol Neurosurg Psychiatry* 64, 172-177.
- Halliwell, B. (1992). Oxygen radicals as key mediators in neurological disease: fact or fiction? *Ann Neurol* 32, S10-15.
- Hanawalt, P. C. (1994). Transcription-coupled repair and human disease. *Science* 266, 1957-1958.
- Harper, P. S. (1991). Huntington's disease (London, W. B. Saunders).
- Harper, P. S. (1992). The epidemiology of Huntington's disease. *Hum Genet* 89, 365-376.
- Harrison, M. B., Tissot, M., and Wiley, R. G. (1996). Expression of m1 and m4 muscarinic receptor mRNA in the striatum following a selective lesion of striatonigral neurons. *Brain Res* 734, 323-326.
- Hartman, R. E., Wozniak, D. F., Nardi, A., Olney, J. W., Sartorius, L., and Holtzman, D. M. (2001). Behavioral phenotyping of GFAP-apoE3 and -apoE4 transgenic mice: apoE4 mice show profound working memory impairments in the absence of Alzheimer's-like neuropathology. *Exp Neurol* 170, 326-344.
- Hashimoto, N., Matsumoto, T., Mabe, H., Hashitani, T., and Nishino, H. (1994). Dopamine has inhibitory and accelerating effects on ischemia-induced neuronal cell damage in the rat striatum. *Brain Res Bull* 33, 281-288.
- Hasselbalch, S. G., Oberg, G., Sorensen, S. A., Andersen, A. R., Waldemar, G., Schmidt, J. F., Fenger, K., and Paulson, O. B. (1992). Reduced regional cerebral blood flow in Huntington's disease studied by SPECT. *J Neurol Neurosurg Psychiatry* 55, 1018-1023.
- Hastings, T. G., Lewis, D. A., and Zigmond, M. J. (1996). Role of oxidation in the neurotoxic effects of intrastriatal dopamine injections. *Proc Natl Acad Sci U S A* 93, 1956-1961.
- Hausladen, A., and Fridovich, I. (1994). Superoxide and peroxynitrite inactivate aconitases, but nitric oxide does not. *J Biol Chem* 269, 29405-29408.
- Hayden, M. R. (1981). Huntington's chorea (New York, Springer-Verlag).
- Hayden, M. R., Martin, W. R., Stoessl, A. J., Clark, C., Hollenberg, S., Adam, M. J., Ammann, W., Harrop, R., Rogers, J., Ruth, T., and et al. (1986). Positron emission tomography in the early diagnosis of Huntington's disease. *Neurology* 36, 888-894.
- (HDCRG), The Huntington's Disease Collaborative Research Group, (1993). A novel gene containing a trinucleotide repeat that is expanded and unstable on Huntington's disease chromosomes. *Cell* 72, 971-983.
- Hedreen, J. C., and DeLong, M. R. (1991). Organization of striatopallidal, striatonigral, and nigrostriatal projections in the macaque. *J Comp Neurol* 304, 569-595.
- Hedreen, J. C., and Folstein, S. E. (1995). Early loss of neostriatal striosome neurons in Huntington's disease. *J Neuropathol Exp Neurol* 54, 105-120.

- Henneberry, R. C. (1989). The role of neuronal energy in the neurotoxicity of excitatory amino acids. *Neurobiol Aging* 10, 611-613.
- Higgins, D. S., Jr. (2001). Chorea and its disorders. *Neurol Clin* 19, 707-722, vii.
- Hirst, M. C., Barnicoat, A., Flynn, G., Wang, Q., Daker, M., Buckle, V. J., Davies, K. E., and Bobrow, M. (1993). The identification of a third fragile site, FRAXF, in Xq27--q28 distal to both FRAXA and FRAXE. *Hum Mol Genet* 2, 197-200.
- Hodgson, J. G., Agopyan, N., Gutekunst, C. A., Leavitt, B. R., LePiane, F., Singaraja, R., Smith, D. J., Bissada, N., McCutcheon, K., Nasir, J., *et al.* (1999). A YAC mouse model for Huntington's disease with full-length mutant huntingtin, cytoplasmic toxicity, and selective striatal neurodegeneration. *Neuron* 23, 181-192.
- Holbert, S., Denghien, I., Kiechle, T., Rosenblatt, A., Wellington, C., Hayden, M. R., Margolis, R. L., Ross, C. A., Dausset, J., Ferrante, R. J., and Neri, C. (2001). The Gln-Ala repeat transcriptional activator CA150 interacts with huntingtin: neuropathologic and genetic evidence for a role in Huntington's disease pathogenesis. *Proc Natl Acad Sci U S A* 98, 1811-1816.
- Holmberg, M., Duyckaerts, C., Durr, A., Cancel, G., GourfinkelAn, I., Damier, P., Faucheux, B., Trottier, Y., Hirsch, E. C., Agid, Y., and Brice, A. (1998). Spinocerebellar ataxia type 7 (SCA7): a neurodegenerative disorder with neuronal intranuclear inclusions. *Hum Mol Genet* 7, 913-918.
- Holmes, S. E., Hearn, E. O., Ross, C. A., and Margolis, R. L. (2001a). SCA12: an unusual mutation leads to an unusual spinocerebellar ataxia. *Brain Res Bull* 56, 397-403.
- Holmes, S. E., O'Hearn, E., Rosenblatt, A., Callahan, C., Hwang, H. S., Ingersoll-Ashworth, R. G., Fleisher, A., Stevanin, G., Brice, A., Potter, N. T., *et al.* (2001b). A repeat expansion in the gene encoding junctophilin-3 is associated with Huntington disease-like 2. *Nat Genet* 29, 377-378.
- Holmes, S. E., O'Hearn, E. E., McInnis, M. G., Gorelick-Feldman, D. A., Kleiderlein, J. J., Callahan, C., Kwak, N. G., Ingersoll-Ashworth, R. G., Sherr, M., Sumner, A. J., *et al.* (1999). Expansion of a novel CAG trinucleotide repeat in the 5' region of PPP2R2B is associated with SCA12. *Nat Genet* 23, 391-392.
- Holthoff, V. A., Koeppe, R. A., Frey, K. A., Penney, J. B., Markel, D. S., Kuhl, D. E., and Young, A. B. (1993). Positron emission tomography measures of benzodiazepine receptors in Huntington's disease. *Ann Neurol* 34, 76-81.
- Hoogeveen, A. T., Willemsen, R., Meyer, N., de, R. K., Roos, R. A., van, O. G., and Galjaard, H. (1993). Characterization and localization of the Huntington disease gene product. *Hum Mol Genet* 2, 2069-2073.
- Hosfield, D. J., Frank, G., Weng, Y., Tainer, J. A., and Shen, B. (1998). Newly discovered archaeobacterial flap endonucleases show a structure-specific mechanism for DNA substrate binding and catalysis resembling human flap endonuclease-1. *J Biol Chem* 273, 27154-27161.
- Hsu, K. S., Huang, C. C., Yang, C. H., and Gean, P. W. (1995). Presynaptic D₂ dopaminergic receptors mediate inhibition of excitatory synaptic transmission in rat neostriatum. *Brain Res* 690, 264-268.
- Huang, C. C., Faber, P. W., Persichetti, F., Mittal, V., Vonsattel, J. P., MacDonald, M. E., and Gusella, J. F. (1998). Amyloid formation by mutant huntingtin: Threshold, progressivity and recruitment of normal polyglutamine proteins. *Somat Cell Mol Genet* 24, 217-233.
- Huang, Q., Zhou, D., Sapp, E., Aizawa, H., Ge, P., Bird, E. D., Vonsattel, J. P., and DiFiglia, M. (1995). Quinolinic acid-induced increases in calbindin D28k immunoreactivity in rat striatal neurons in vivo and in vitro mimic the pattern seen in Huntington's disease. *Neuroscience* 65, 397-407.
- Hunkeler, W., Mohler, H., Pieri, L., Polc, P., Bonetti, E. P., Cumin, R., Schaffner, R., and Haefely, W. (1981). Selective antagonists of benzodiazepines. *Nature* 290, 514-516.
- Hurlbert, M. S., Zhou, W. B., Wasmeier, C., Kaddis, F. G., Hutton, J. C., and Freed, C. R. (1999). Mice transgenic for an expanded CAG repeat in the Huntington's disease gene develop diabetes. *Diabetes* 48, 649-651.
- Hyttel, J. (1983). SCH 23390 - the first selective dopamine D₁ antagonist. *Eur J Pharmacol* 91, 153-154.
- Igarashi, S., Koide, R., Shimohata, T., Yamada, M., Hayashi, Y., Takano, H., Date, H., Oyake, M., Sato, T., Sato, A., *et al.* (1998). Suppression of aggregate formation and apoptosis by transglutaminase inhibitors in cells expressing truncated DRPLA protein with an expanded polyglutamine stretch. *Nat Genet* 18, 111-117.
- Imbert, G., Saudou, F., Yvert, G., Devys, D., Trottier, Y., Garnier, J. M., Weber, C., Mandel, J. L., Cancel, G., Abbas, N., *et al.* (1996). Cloning Of the Gene For Spinocerebellar Ataxia 2 Reveals a Locus With High Sensitivity to Expanded CAG/Glutamine Repeats. *Nat Genet* 14, 285-291.
- Ishiguro, H., Yamada, K., Sawada, H., Nishii, K., Ichino, N., Sawada, M., Kurosawa, Y., Matsushita, N., Kobayashi, K., Goto, J., *et al.* (2001). Age-dependent and tissue-specific CAG repeat instability occurs in mouse knock-in for a mutant Huntington's disease gene. *J Neurosci Res* 65, 289-297.
- Iyer, R. R., Pluciennik, A., Rosche, W. A., Sinden, R. R., and Wells, R. D. (2000). DNA polymerase III proofreading mutants enhance the expansion and deletion of triplet repeat sequences in *Escherichia coli*. *J Biol Chem* 275, 2174-2184.

- Jackson, G. R., Salecker, I., Dong, X. Z., Yao, X., Arnheim, N., Faber, P. W., MacDonald, M. E., and Zipursky, S. L. (1998). Polyglutamine expanded human huntingtin transgenes induce degeneration of *Drosophila* photoreceptor neurons. *Neuron* 21, 633-642.
- Jakupciak, J. P., and Wells, R. D. (1999). Genetic instabilities in (CTG.CAG) repeats occur by recombination. *J Biol Chem* 274, 23468-23479.
- Jankowski, C., Nasar, F., and Nag, D. K. (2000). Meiotic instability of CAG repeat tracts occurs by double-strand break repair in yeast. *Proc Natl Acad Sci U S A* 97, 2134-2139.
- Jason, G. W., Suchowersky, O., Pajurkova, E. M., Graham, L., Klimek, M. L., Garber, A. T., and Poirier-Heine, D. (1997). Cognitive manifestations of Huntington disease in relation to genetic structure and clinical onset. *Arch Neurol* 54, 1081-1088.
- Jaworski, A., Rosche, W. A., Gellibolian, R., Kang, S., Shimizu, M., Bowater, R. P., Sinden, R. R., and Wells, R. D. (1995). Mismatch repair in *Escherichia coli* enhances instability of (CTG)_n triplet repeats from human hereditary diseases. *Proc Natl Acad Sci U S A* 92, 11019-11023.
- Jeffreys, A. J., Tamaki, K., MacLeod, A., Monckton, D. G., Neil, D. L., and Armour, J. A. (1994). Complex gene conversion events in germline mutation at human minisatellites. *Nat Genet* 6, 136-145.
- Jenkins, B. G., Koroshetz, W. J., Beal, M. F., and Rosen, B. R. (1993). Evidence for impairment of energy metabolism in vivo in Huntington's disease using localized 1H NMR spectroscopy. *Neurology* 43, 2689-2695.
- Ji, J., Clegg, N. J., Peterson, K. R., Jackson, A. L., Laird, C. D., and Loeb, L. A. (1996). In vitro expansion of GGC:GCC repeats: identification of the preferred strand of expansion. *Nucleic Acids Res* 24, 2835-2840.
- Joseph, J. T., Richards, C. S., Anthony, D. C., Upton, M., Perez-Atayde, A. R., and Greenstein, P. (1997). Congenital myotonic dystrophy pathology and somatic mosaicism. *Neurology* 49, 1457-1460.
- Jou, Y. S., and Myers, R. M. (1995). Evidence from antibody studies that the CAG repeat in the Huntington disease gene is expressed in the protein. *Hum Mol Genet* 4, 465-469.
- Joyce, J. N., Lexow, N., Bird, E., and Winokur, A. (1988). Organization of dopamine D₁ and D₂ receptors in human striatum: receptor autoradiographic studies in Huntington's disease and schizophrenia. *Synapse* 2, 546-557.
- Joyce, J. N., and Marshall, J. F. (1987). Quantitative autoradiography of dopamine D₂ sites in rat caudate-putamen: localization to intrinsic neurons and not to neocortical afferents. *Neuroscience* 20, 773-795.
- Kahlem, P., Green, H., and Djian, P. (1998). Transglutaminase action imitates Huntington's disease: selective polymerization of Huntingtin containing expanded polyglutamine. *Mol Cell* 1, 595-601.
- Kalchman, M. A., Graham, R. K., Xia, G., Koide, H. B., Hodgson, J. G., Graham, K. C., Goldberg, Y. P., Gietz, R. D., Pickart, C. M., and Hayden, M. R. (1996). Huntingtin is ubiquitinated and interacts with a specific ubiquitin conjugating enzyme. *J Biol Chem* 271, 19385-19394.
- Kang, S., Jaworski, A., Ohshima, K., and Wells, R. D. (1995). Expansion and deletion of CTG repeats from human disease genes are determined by the direction of replication in *E. coli*. *Nat Genet* 10, 213-218.
- Kang, S., Ohshima, K., Jaworski, A., and Wells, R. D. (1996). CTG triplet repeats from the myotonic dystrophy gene are expanded in *Escherichia coli* distal to the replication origin as a single large event. *J Mol Biol* 258, 543-547.
- Karlovich, C. A., John, R. M., Ramirez, L., Stainier, D. Y. R., and Myers, R. M. (1998). Characterization of the Huntington's disease (HD) gene homolog in the zebrafish *Danio rerio*. *Gene* 217, 117-125.
- Kawaguchi, Y. (1997). Neostriatal cell subtypes and their functional roles. *Neurosci Res* 27, 1-8.
- Kawaguchi, Y., Okamoto, T., Taniwaki, M., Aizawa, M., Inoue, M., Katayama, S., Kawakami, H., Nakamura, S., Nishimura, M., Akiguchi, I., et al. (1994). CAG expansions in a novel gene for Machado-Joseph disease at chromosome 14q32.1. *Nat Genet* 8, 221-228.
- Kazantsev, A., Preisinger, E., Dranovsky, A., Goldgaber, D., and Housman, D. (1999). Insoluble detergent-resistant aggregates form between pathological and nonpathological lengths of polyglutamine in mammalian cells. *Proc Natl Acad Sci U S A* 96, 11404-11409.
- Kazantsev, A., Walker, H. A., Slepko, N., Bear, J. E., Preisinger, E., Steffan, J. S., Zhu, Y. Z., Gertler, F. B., Housman, D. E., Marsh, J. L., and Thompson, L. M. (2002). A bivalent Huntingtin binding peptide suppresses polyglutamine aggregation and pathogenesis in *Drosophila*. *Nat Genet* 30, 367-376.
- Kazemi-Esfarjani, P., and Benzer, S. (2000). Genetic suppression of polyglutamine toxicity in *Drosophila*. *Science* 287, 1837-1840.
- Kegel, K. B., Kim, M., Sapp, E., McIntyre, C., Castano, J. G., Aronin, N., and DiFiglia, M. (2000). Huntingtin expression stimulates endosomal-lysosomal activity, endosome tubulation, and autophagy. *J Neurosci* 20, 7268-7278.
- Kelly, M. A., Rubinstein, M., Phillips, T. J., Lessov, C. N., Burkhart-Kasch, S., Zhang, G., Bunzow, J. R., Fang, Y., Gerhardt, G. A., Grandy, D. K., and Low, M. J. (1998). Locomotor activity in D₂

- dopamine receptor-deficient mice is determined by gene dosage, genetic background, and developmental adaptations. *J Neurosci* 18, 3470-3479.
- Kim, E., Cho, K. O., Rothschild, A., and Sheng, M. (1996). Heteromultimerization and NMDA receptor-clustering activity of Chapsyn-110, a member of the PSD-95 family of proteins. *Neuron* 17, 103-113.
- Kim, M., Lee, H. S., LaForet, G., McIntyre, C., Martin, E. J., Chang, P., Kim, T. W., Williams, M., Reddy, P. H., Tagle, D., *et al.* (1999). Mutant huntingtin expression in clonal striatal cells: dissociation of inclusion formation and neuronal survival by caspase inhibition. *J Neurosci* 19, 964-973.
- Kirkwood, S. C., Siemers, E., Stout, J. C., Hodes, M. E., Conneally, P. M., Christian, J. C., and Foroud, T. (1999). Longitudinal cognitive and motor changes among presymptomatic Huntington disease gene carriers. *Arch Neurol* 56, 563-568.
- Kirkwood, S. C., Su, J. L., Conneally, P. M., and Foroud, T. (2001). Progression of Symptoms in the Early and Middle Stages of Huntington Disease. *Arch Neurol* 58, 273-278.
- Kita, H. (1996). Glutamatergic and GABAergic postsynaptic responses of striatal spiny neurons to intrastriatal and cortical stimulation recorded in slice preparations. *Neuroscience* 70, 925-940.
- Klawans, H. L., Jr. (1970). A pharmacologic analysis of Huntington's chorea. *Eur Neurol* 4, 148-163.
- Klawans, H. L., Stein, R. W., Tanner, C. M., and Goetz, C. G. (1982). A pure parkinsonian syndrome following acute carbon monoxide intoxication. *Arch Neurol* 39, 302-304.
- Klement, I. A., Skinner, P. J., Kaytor, M. D., Yi, H., Hersch, S. M., Clark, H. B., Zoghbi, H. Y., and Orr, H. T. (1998). Ataxin 1 nuclear localization and aggregation: Role in polyglutamine induced disease in SCA1 transgenic mice. *Cell* 95, 41-53.
- Knight, S. J., Flannery, A. V., Hirst, M. C., Campbell, L., Christodoulou, Z., Phelps, S. R., Pointon, J., Middleton, P. H., Barnicoat, A., Pembrey, M. E., and *et al.* (1993). Trinucleotide repeat amplification and hypermethylation of a CpG island in FRAXE mental retardation. *Cell* 74, 127-134.
- Koefoed, P., Hasholt, L., Fenger, K., Nielsen, J. E., Eiberg, H., Buschard, K., and Sorensen, S. A. (1998). Mitotic and meiotic instability of the CAG trinucleotide repeat in spinocerebellar ataxia type 1. *Hum Genet* 103, 564-569.
- Koide, R., Ikeuchi, T., Onodera, O., Tanaka, H., Igarashi, S., Endo, K., Takahashi, H., Kondo, R., Ishikawa, A., Hayashi, T., and *et al.* (1994). Unstable expansion of CAG repeat in hereditary dentatorubral-pallidolusian atrophy (DRPLA). *Nat Genet* 6, 9-13.
- Kolodner, R. D., and Marsischky, G. T. (1999). Eukaryotic DNA mismatch repair. *Curr Opin Genet Dev* 9, 89-96.
- Koob, M. D., Moseley, M. L., Schut, L. J., Benzow, K. A., Bird, T. D., Day, J. W., and Ranum, L. P. W. (1999). An untranslated CTG expansion causes a novel form of spinocerebellar ataxia (SCA8). *Nat Genet* 21, 379-384.
- Koroshetz, W. J., Jenkins, B. G., Rosen, B. R., and Beal, M. F. (1997). Energy metabolism defects in Huntington's disease and effects of coenzyme Q10. *Ann Neurol* 41, 160-165.
- Kosinski, C. M., Cha, J. H., Young, A. B., Persichetti, F., MacDonald, M., Gusella, J. F., Penney Jb, Jr., and Standaert, D. G. (1997). Huntingtin immunoreactivity in the rat neostriatum: Differential accumulation in projection and interneurons. *Exp Neurol* 144, 239-247.
- Kovtun, I. V., and McMurray, C. T. (2001). Trinucleotide expansion in haploid germ cells by gap repair. *Nat Genet* 27, 407-411.
- Kowall, N. W., Ferrante, R. J., Beal, M. F., Richardson, E. P., Jr., Sofroniew, M. V., Cuello, A. C., and Martin, J. B. (1987). Neuropeptide Y, somatostatin, and reduced nicotinamide adenine dinucleotide phosphate diaphorase in the human striatum: a combined immunocytochemical and enzyme histochemical study. *Neuroscience* 20, 817-828.
- Kremer, B., Almqvist, E., Theilmann, J., Spence, N., Telenius, H., Goldberg, Y. P., and Hayden, M. R. (1995). Sex-dependent mechanisms for expansions and contractions of the CAG repeat on affected Huntington disease chromosomes. *Am J Hum Genet* 57, 343-350.
- Kroutil, L. C., and Kunkel, T. A. (1999). Deletion errors generated during replication of CAG repeats. *Nucleic Acids Res* 27, 3481-3486.
- Kubota, Y., and Kawaguchi, Y. (1993). Spatial distributions of chemically identified intrinsic neurons in relation to patch and matrix compartments of rat neostriatum. *J Comp Neurol* 332, 499-513.
- Kulagina, N. V., Zigmond, M. J., and Michael, A. C. (2001). Glutamate regulates the spontaneous and evoked release of dopamine in the rat striatum. *Neuroscience* 102, 121-128.
- Kunig, G., Leenders, K. L., Sanchez-Pernaute, R., Antonini, A., Vontobel, P., Verhagen, A., and Gunther, I. (2000). Benzodiazepine receptor binding in Huntington's disease: [11C]flumazenil uptake measured using positron emission tomography. *Ann Neurol* 47, 644-648.
- Kuwert, T., Lange, H. W., Boecker, H., Titz, H., Herzog, H., Aulich, A., Wang, B. C., Nayak, U., and Feinendegen, L. E. (1993). Striatal glucose consumption in chorea-free subjects at risk of Huntington's disease. *J Neurol* 241, 31-36.

- Kuwert, T., Lange, H. W., Langen, K. J., Herzog, H., Aulich, A., and Feinendegen, L. E. (1990). Cortical and subcortical glucose consumption measured by PET in patients with Huntington's disease. *Brain* 113, 1405-1423.
- La Spada, A. R., Paulson, H. L., and Fischbeck, K. H. (1994). Trinucleotide repeat expansion in neurological disease. *Ann Neurol* 36, 814-822.
- La Spada, A. R., Roling, D. B., Harding, A. E., Warner, C. L., Spiegel, R., Hausmanowa-Petrusewicz, I., Yee, W. C., and Fischbeck, K. H. (1992). Meiotic stability and genotype-phenotype correlation of the trinucleotide repeat in X-linked spinal and bulbar muscular atrophy. *Nat Genet* 2, 301-304.
- La Spada, A. R., Wilson, E. M., Lubahn, D. B., Harding, A. E., and Fischbeck, K. H. (1991). Androgen receptor gene mutations in X-linked spinal and bulbar muscular atrophy. *Nature* 352, 77-79.
- Laccone, F., and Christian, W. (2000). A recurrent expansion of a maternal allele with 36 CAG repeats causes Huntington disease in two sisters. *Am J Hum Genet* 66, 1145-1148.
- Lalonde, R. (1987a). Motor abnormalities in staggerer mutant mice. *Exp Brain Res* 68, 417-420.
- Lalonde, R. (1987b). Motor abnormalities in weaver mutant mice. *Exp Brain Res* 65, 479-481.
- Landwehrmeyer, G. B., McNeil, S. M., Dure, L. S. t., Ge, P., Aizawa, H., Huang, Q., Ambrose, C. M., Duyao, M. P., Bird, E. D., Bonilla, E., and et al. (1995a). Huntington's disease gene: regional and cellular expression in brain of normal and affected individuals. *Ann Neurol* 37, 218-230.
- Landwehrmeyer, G. B., Standaert, D. G., Testa, C. M., Penney, J. B., Jr., and Young, A. B. (1995b). NMDA receptor subunit mRNA expression by projection neurons and interneurons in rat striatum. *J Neurosci* 15, 5297-5307.
- Lavedan, C., Hofmann-Radvanyi, H., Shelbourne, P., Rabes, J. P., Duros, C., Savoy, D., Dehaupas, I., Luce, S., Johnson, K., and Junien, C. (1993). Myotonic dystrophy: size- and sex-dependent dynamics of CTG meiotic instability, and somatic mosaicism. *Am J Hum Genet* 52, 875-883.
- Lawrence, A. D., Hodges, J. R., Rosser, A. E., Kershaw, A., ffrench-Constant, C., Rubinsztein, D. C., Robbins, T. W., and Sahakian, B. J. (1998a). Evidence for specific cognitive deficits in preclinical Huntington's disease. *Brain* 121, 1329-1341.
- Lawrence, A. D., Sahakian, B. J., Hodges, J. R., Rosser, A. E., Langes, K. W., and Robbins, T. W. (1996). Executive and mnemonic functions in early Huntington's disease. *Brain* 119, 1633-1645.
- Lawrence, A. D., Weeks, R. A., Brooks, D. J., Andrews, T. C., Watkins, L. H. A., Harding, A. E., Robbins, T. W., and Sahakian, B. J. (1998b). The relationship between striatal dopamine receptor binding and cognitive performance in Huntington's disease. *Brain* 121, 1343-1355.
- Leavitt, B. R., Guttman, J. A., Hodgson, J. G., Kimel, G. H., Singaraja, R., Vogl, A. W., and Hayden, M. R. (2001). Wild-type huntingtin reduces the cellular toxicity of mutant huntingtin *in vivo*. *Am J Hum Genet* 68, 313-324.
- Ledent, C., Vaugeois, J. M., Schiffmann, S. N., Pedrazzini, T., El Yacoubi, M., Vanderhaeghen, J. J., Costentin, J., Heath, J. K., Vassart, G., and Parmentier, M. (1997). Aggressiveness, hypoalgesia and high blood pressure in mice lacking the adenosine A2a receptor. *Nature* 388, 674-678.
- Leeflang, E. P., Tavare, S., Marjoram, P., Neal, C. O., Srinidhi, J., MacFarlane, H., MacDonald, M. E., Gusella, J. F., de Young, M., Wexler, N. S., and Arnheim, N. (1999). Analysis of germline mutation spectra at the Huntington's disease locus supports a mitotic mutation mechanism. *Hum Mol Genet* 8, 173-183.
- Leeflang, E. P., Zhang, L., Tavare, S., Hubert, R., Srinidhi, J., MacDonald, M. E., Myers, R. H., De Young, M., Wexler, N. S., Gusella, J. F., and Arnheim, N. (1995). Single sperm analysis of the trinucleotide repeats in the Huntington's disease gene: Quantification of the mutation frequency spectrum. *Hum Mol Genet* 4, 1519-1526.
- Lees, G. J. (1991). Inhibition of sodium-potassium-ATPase: a potentially ubiquitous mechanism contributing to central nervous system neuropathology. *Brain Res Brain Res Rev* 16, 283-300.
- Levine, M. S., Klapstein, G. J., Koppel, A., Gruen, E., Cepeda, C., Vargas, M. E., Jokel, E. S., Carpenter, E. M., Zanjani, H., Hurst, R. S., et al. (1999). Enhanced sensitivity to N-methyl-D-aspartate receptor activation in transgenic and knockin mouse models of Huntington's disease. *J Neurosci Res* 58, 515-532.
- Levine, M. S., Li, Z., Cepeda, C., Cromwell, H. C., and Altemus, K. L. (1996). Neuromodulatory actions of dopamine on synaptically-evoked neostriatal responses in slices. *Synapse* 24, 65-78.
- Li, H., Li, S. H., Cheng, A. L., Mangiarini, L., Bates, G. P., and Li, X. J. (1999a). Ultrastructural localization and progressive formation of neuropil aggregates in Huntington's disease transgenic mice. *Hum Mol Genet* 8, 1227-1236.
- Li, H., Li, S. H., Johnston, H., Shelbourne, P. F., and Li, X. J. (2000). Amino-terminal fragments of mutant huntingtin show selective accumulation in striatal neurons and synaptic toxicity. *Nat Genet* 25, 385-389.
- Li, H., Li, S. H., Yu, Z. X., Shelbourne, P., and Li, X. J. (2001). Huntingtin aggregate-associated axonal degeneration is an early pathological event in Huntington's disease mice. *J Neurosci* 21, 8473-8481.

- Li, I., Nakagomi, Y., Kobayashi, Y., Merry, D. E., Tanaka, F., Doyu, M., Mitsuma, T., Hashizume, Y., Fischbeck, K. H., and Sobue, G. (1998a). Nonneural nuclear inclusions of androgen receptor protein in spinal and bulbar muscular atrophy. *Am J Pathol* 153, 695-701.
- Li, M., Miwa, S., Kobayashi, Y., Merry, D. E., Yamamoto, M., Tanaka, F., Doyu, M., Hashizume, Y., Fischbeck, K. H., and Sobue, G. (1998b). Nuclear inclusions of the androgen receptor protein in spinal and bulbar muscular atrophy. *Ann Neurol* 44, 249-254.
- Li, S. H., Cheng, A. L., Zhou, H., Lam, S., Rao, M., Li, H., and Li, X. J. (2002). Interaction of Huntington disease protein with transcriptional activator Sp1. *Mol Cell Biol* 22, 1277-1287.
- Li, S. H., Gutekunst, C. A., Hersch, S. M., and Li, X. J. (1998c). Interaction of Huntingtin associated protein with dynactin P150(Glued). *J Neurosci* 18, 1261-1269.
- Li, S. H., and Li, X. J. (1998). Aggregation of N-terminal huntingtin is dependent on the length of its glutamine repeats. *Hum Mol Genet* 7, 777-782.
- Li, S. H., Schilling, G., Young, W. d., Li, X. J., Margolis, R. L., Stine, O. C., Wagster, M. V., Abbott, M. H., Franz, M. L., Ranen, N. G., and et, a. l. (1993). Huntington's disease gene (IT15) is widely expressed in human and rat tissues. *Neuron* 11, 985-993.
- Li, X. J., Li, S. H., Sharp, A. H., Nucifora, F. C., Schilling, G., Lanahan, A., Worley, P., Snyder, S. H., and Ross, C. A. (1995). A Huntingtin Associated Protein Enriched In Brain With Implications For Pathology. *Nature* 378, 398-402.
- Li, Z., Karlovich, C. A., Fish, M. P., Scott, M. P., and Myers, R. M. (1999b). A putative *Drosophila* homolog of the Huntington's disease gene. *Hum Mol Genet* 8, 1807-1815.
- Lin, B., Nasir, J., MacDonald, H., Hutchinson, G., Graham, R. K., Rommens, J. M., and Hayden, M. R. (1994). Sequence of the murine Huntington disease gene: evidence for conservation, and polymorphism in a triplet (CCG) repeat alternate splicing. *Hum Mol Genet* 3, 85-92.
- Lin, B., Rommens, J. M., Graham, R. K., Kalchman, M., MacDonald, H., Nasir, J., Delaney, A., Goldberg, Y. P., and Hayden, M. R. (1993). Differential 3' polyadenylation of the Huntington disease gene results in two mRNA species with variable tissue expression. *Hum Mol Genet* 2, 1541-1545.
- Lin, C. H., Tallaksen-Greene, S., Chien, W. M., Cearley, J. A., Jackson, W. S., Crouse, A. B., Ren, S., Li, X. J., Albin, R. L., and Detloff, P. J. (2001). Neurological abnormalities in a knock-in mouse model of Huntington's disease. *Hum Mol Genet* 10, 137-144.
- Lindahl, T., Karran, P., and Wood, R. D. (1997). DNA excision repair pathways. *Curr Opin Genet Dev* 7, 158-169.
- Lione, L. A., Carter, R. J., Hunt, M. J., Bates, G. P., Morton, A. J., and Dunnett, S. B. (1999). Selective discrimination learning impairments in mice expressing the human Huntington's disease mutation. *J Neurosci* 19, 10428-10437.
- Lipkin, S. M., Wang, V., Jacoby, R., Banerjee-Basu, S., Baxevanis, A. D., Lynch, H. T., Elliott, R. M., and Collins, F. S. (2000). MLH3: a DNA mismatch repair gene associated with mammalian microsatellite instability. *Nat Genet* 24, 27-35.
- Liquori, C. L., Ricker, K., Moseley, M. L., Jacobsen, J. F., Kress, W., Naylor, S. L., Day, J. W., and Ranum, L. P. (2001). Myotonic dystrophy type 2 caused by a CCTG expansion in intron 1 of ZNF9. *Science* 293, 864-867.
- Ludolph, A. C., He, F., Spencer, P. S., Hammerstad, J., and Sabri, M. (1991). 3-Nitropropionic acid-exogenous animal neurotoxin and possible human striatal toxin. *Can J Neurol Sci* 18, 492-498.
- Lunkes, A., and Mandel, J. L. (1998). A cellular model that recapitulates major pathogenic steps of Huntington's disease. *Hum Mol Genet* 7, 1355-1361.
- Lupski, J. R. (1998). Genomic disorders: structural features of the genome can lead to DNA rearrangements and human disease traits. *Trends Genet* 14, 417-422.
- Luthi-Carter, R., Strand, A., Peters, N. L., Solano, S. M., Hollingsworth, Z. R., Menon, A. S., Frey, A. S., Spektor, B. S., Penney, E. B., Schilling, G., et al. (2000). Decreased expression of striatal signaling genes in a mouse model of Huntington's disease. *Hum Mol Genet* 9, 1259-1271.
- Maat-Schieman, M. L., Dorsman, J. C., Smoor, M. A., Siesling, S., Van Duinen, S. G., Verschuuren, J. J., den Dunnen, J. T., Van Ommen, G. J., and Roos, R. A. (1999). Distribution of inclusions in neuronal nuclei and dystrophic neurites in Huntington disease brain. *J Neuropathol Exp Neurol* 58, 129-137.
- MacDonald, M. E., Barnes, G., Srinidhi, J., Duyao, M. P., Ambrose, C. M., Myers, R. H., Gray, J., Conneally, P. M., Young, A., Penney, J., and et al. (1993). Gametic but not somatic instability of CAG repeat length in Huntington's disease. *J Med Genet* 30, 982-986.
- Malcon, C., Achaval, M., Komlos, F., Partata, W., Sauressig, M., Ramirez, G., and Souza, D. O. (1997). GMP protects against quinolinic acid induced loss of NADPH diaphorase positive cells in the rat striatum. *Neurosci Lett* 225, 145-148.
- Mangiarini, L., Sathasivam, K., Mahal, A., Mott, R., Seller, M., and Bates, G. P. (1997). Instability of highly expanded CAG repeats in mice transgenic for the Huntington's disease mutation. *Nat Genet* 15, 197-200.

- Mangiarini, L., Sathasivam, K., Seller, M., Cozens, B., Harper, A., Hetherington, C., Lawton, M., Trotter, Y., Lehrach, H., Davies, S. W., and Bates, G. P. (1996). Exon 1 of the HD gene with an expanded CAG repeat is sufficient to cause a progressive neurological phenotype in transgenic mice. *Cell* 87, 493-506.
- Manley, K., Pugh, J., and Messer, A. (1998). Instability of the CAG repeat in an immortalized fibroblast cell culture from Huntington's disease (HD) transgenic mice. *Brain Res* 809, P412.
- Manley, K., Shirley, T. L., Flaherty, L., and Messer, A. (1999). Msh2 deficiency prevents in vivo somatic instability of the CAG repeat in Huntington disease transgenic mice. *Nat Genet* 23, 471-473.
- Mansour, A., Thompson, R. C., Akil, H., and Watson, S. J. (1993). Delta opioid receptor mRNA distribution in the brain: comparison to delta receptor binding and proenkephalin mRNA. *J Chem Neuroanat* 6, 351-362.
- Mantamadiotis, T., Lemberger, T., Bleckmann, S. C., Kern, H., Kretz, O., Martin Villalba, A., Tronche, F., Kellendonk, C., Gau, D., Kapfhammer, J., et al. (2002). Disruption of CREB function in brain leads to neurodegeneration. *Nat Genet* 31, 47-54.
- Maragos, W. F., Jakel, R. J., Pang, Z., and Geddes, J. W. (1998). 6 hydroxydopamine injections into the nigrostriatal pathway attenuate striatal malonate and 9 nitropropionic acid lesions. *Exp Neurol* 154, 637-644.
- Marder, K., Zhao, H., Myers, R. H., Cudkowicz, M., Kayson, E., Kiebertz, K., Orme, C., Paulsen, J., Penney, J. B., Jr., Siemers, E., and Shoulson, I. (2000). Rate of functional decline in Huntington's disease. Huntington Study Group. *Neurology* 54, 452-458.
- Marsh, J. L., Walker, H., Theisen, H., Zhu, Y. Z., Fielder, T., Purcell, J., and Thompson, L. M. (2000). Expanded polyglutamine peptides alone are intrinsically cytotoxic and cause neurodegeneration in *Drosophila*. *Hum Mol Genet* 9, 13-25.
- Martin, J. B., and Gusella, J. F. (1986). Huntington's disease. Pathogenesis and management. *N Engl J Med* 315, 1267-1276.
- Martindale, D., Hackam, A., Wieczorek, A., Ellerby, L., Wellington, C., McCutcheon, K., Singaraja, R., KazemiEsfarjani, P., Devon, R., Kim, S. U., et al. (1998). Length of huntingtin and its polyglutamine tract influences localization and frequency of intracellular aggregates. *Nat Genet* 18, 150-154.
- Martinez-Fong, D., Rosales, M. G., Gongora-Alfaro, J. L., Hernandez, S., and Aceves, J. (1992). NMDA receptor mediates dopamine release in the striatum of unanesthetized rats as measured by brain microdialysis. *Brain Res* 595, 309-315.
- Martinou, J. C., Dubois-Dauphin, M., Staple, J. K., Rodriguez, I., Frankowski, H., Missotten, M., Albertini, P., Talabot, D., Catsicas, S., Pietra, C., and et al. (1994). Overexpression of BCL-2 in transgenic mice protects neurons from naturally occurring cell death and experimental ischemia. *Neuron* 13, 1017-1030.
- Maruyama, H., Nakamura, S., Matsuyama, Z., Sakai, T., Doyu, M., Sobue, G., Seto, M., Tsujihata, M., Oh-i, T., Nishio, T., and et al. (1995). Molecular features of the CAG repeats and clinical manifestation of Machado-Joseph disease. *Hum Mol Genet* 4, 807-812.
- Matsuura, T., Yamagata, T., Burgess, D. L., Rasmussen, A., Grewal, R. P., Watase, K., Khajavi, M., McCall, A. E., Davis, C. F., Zu, L., et al. (2000). Large expansion of the ATTCT pentanucleotide repeat in spinocerebellar ataxia type 10. *Nat Genet* 26, 191-194.
- Maurer, D. J., Ocallaghan, B. L., and Livingston, D. M. (1996). Orientation dependence of trinucleotide CAG repeat instability in *Saccharomyces cerevisiae*. *Mol Cell Biol* 16, 6617-6622.
- Mazziotta, J. C., Phelps, M. E., Pahl, J. J., Huang, S. C., Baxter, L. R., Riege, W. H., Hoffman, J. M., Kuhl, D. E., Lanto, A. B., Wapenski, J. A., and et al. (1987). Reduced cerebral glucose metabolism in asymptomatic subjects at risk for Huntington's disease. *N Engl J Med* 316, 357-362.
- McBean, G. J., and Roberts, P. J. (1984). Chronic infusion of L-glutamate causes neurotoxicity in rat striatum. *Brain Res* 290, 372-375.
- McCabe, R. T., Olsen, R. W., Yezuita, J. P., and Wamsley, J. K. (1988). Osmotic shock: a method to eliminate endogenous gamma-aminobutyric acid and account for the influence on benzodiazepine binding affinity in autoradiographic studies. *J Pharmacol Exp Ther* 245, 342-349.
- McCampbell, A., and Fischbeck, K. H. (2001). Polyglutamine and CBP: fatal attraction? *Nat Med* 7, 528-530.
- McGeer, E. G., and McGeer, P. L. (1976). Duplication of biochemical changes of Huntington's chorea by intrastriatal injections of glutamic and kainic acids. *Nature* 263, 517-519.
- McGeer, P. L., and McGeer, E. G. (1978). Intracerebral injections of kainic acid and tetanus toxin: possible models for the signs of chorea and dystonia. *Adv Neurol* 21, 331-338.
- McGeorge, A. J., and Faull, R. L. (1989). The organization of the projection from the cerebral cortex to the striatum in the rat. *Neuroscience* 29, 503-537.
- McLaughlin, B. A., Nelson, D., Silver, I. A., Erecinska, M., and Chesselet, M. F. (1998). Methylmalonate toxicity in primary neuronal cultures. *Neuroscience* 86, 279-290.

- McNeil, S. M., Novelletto, A., Srinidhi, J., Barnes, G., Kornbluth, I., Altherr, M. R., Wasmuth, J. J., Gusella, J. F., MacDonald, M. E., and Myers, R. H. (1997). Reduced penetrance of the Huntington's disease mutation. *Hum Mol Genet* 6, 775-779.
- Meador-Woodruff, J. H., Mansour, A., Healy, D. J., Kuehn, R., Zhou, Q. Y., Bunzow, J. R., Akil, H., Civelli, O., and Watson, S. J., Jr. (1991). Comparison of the distributions of D₁ and D₂ dopamine receptor mRNAs in rat brain. *Neuropsychopharmacology* 5, 231-242.
- Mehta, A. K., and Ticku, M. K. (1999). An update on GABAA receptors. *Brain Res Brain Res Rev* 29, 196-217.
- Menalled, L., Zanjani, H., MacKenzie, L., Koppel, A., Carpenter, E., Zeitlin, S., and Chesselet, M. F. (2000). Decrease in striatal enkephalin mRNA in mouse models of Huntington's disease. *Exp Neurol* 162, 328-342.
- Mende-Mueller, L. M., Toneff, T., Hwang, S. R., Chesselet, M. F., and Hook, V. Y. (2001). Tissue-specific proteolysis of Huntingtin (htt) in human brain: evidence of enhanced levels of N- and C-terminal htt fragments in Huntington's disease striatum. *J Neurosci* 21, 1830-1837.
- Metsis, M., Brunkhorst, A., and Neuman, T. (2001). Cell-type-specific expression of the TFIID component TAF(II)135 in the nervous system. *Exp Cell Res* 269, 214-221.
- Migaud, M., Charlesworth, P., Dempster, M., Webster, L. C., Watabe, A. M., Makhinson, M., He, Y., Ramsay, M. F., Morris, R. G., Morrison, J. H., et al. (1998). Enhanced long-term potentiation and impaired learning in mice with mutant postsynaptic density-95 protein. *Nature* 396, 433-439.
- Miller, B., Sarantis, M., Traynelis, S. F., and Attwell, D. (1992). Potentiation of NMDA receptor currents by arachidonic acid. *Nature* 355, 722-725.
- Miret, J. J., Pessoa-Brandao, L., and Lahue, R. S. (1997). Instability of CAG and CTG trinucleotide repeats in *Saccharomyces cerevisiae*. *Mol Cell Biol* 17, 3382-3387.
- Mitchell, I. J., Cooper, A. J., and Griffiths, M. R. (1999). The selective vulnerability of striatopallidal neurons. *Prog Neurobiol* 59, 691-719.
- Moberg, P. J., Pearlson, G. D., Speedie, L. J., Lipsey, J. R., Strauss, M. E., and Folstein, S. E. (1987). Olfactory recognition: differential impairments in early and late Huntington's and Alzheimer's diseases. *J Clin Exp Neuropsychol* 9, 650-664.
- Modrich, P., and Lahue, R. (1996). Mismatch repair in replication fidelity, genetic recombination, and cancer biology. *Annu Rev Biochem* 65, 101-133.
- Mogenson, G. J., Jones, D. L., and Yim, C. Y. (1980). From motivation to action: functional interface between the limbic system and the motor system. *Prog Neurobiol* 14, 69-97.
- Monckton, D. G., Coolbaugh, M. I., Ashizawa, K. T., Siciliano, M. J., and Caskey, C. T. (1997). Hypermutable myotonic dystrophy CTG repeats in transgenic mice. *Nat Genet* 15, 193-196.
- Monckton, D. G., Wong, L. J., Ashizawa, T., and Caskey, C. T. (1995). Somatic mosaicism, germline expansions, germline reversions and intergenerational reductions in myotonic dystrophy males: small pool PCR analyses. *Hum Mol Genet* 4, 1-8.
- Moore, H., Greenwell, P. W., Liu, C. P., Arnheim, N., and Petes, T. D. (1999). Triplet repeats form secondary structures that escape DNA repair in yeast. *Proc Natl Acad Sci U S A* 96, 1504-1509.
- Morag, A. S., Saveson, C. J., and Lovett, S. T. (1999). Expansion of DNA repeats in *Escherichia coli*: Effects of recombination and replication functions. *J Mol Biol* 289, 21-27.
- Morris, R. (1984). Developments of a water-maze procedure for studying spatial learning in the rat. *J Neurosci Methods* 11, 47-60.
- Murphy, K. P., Carter, R. J., Lione, L. A., Mangiarini, L., Mahal, A., Bates, G. P., Dunnett, S. B., and Morton, A. J. (2000). Abnormal synaptic plasticity and impaired spatial cognition in mice transgenic for exon 1 of the human Huntington's disease mutation. *J Neurosci* 20, 5115-5123.
- Muthane, U., Ramsay, K. A., Jiang, H., Jackson-Lewis, V., Donaldson, D., Fernando, S., Ferreira, M., and Przedborski, S. (1994). Differences in nigral neuron number and sensitivity to 1-methyl-4-phenyl-1,2,3,6-tetrahydropyridine in C57/bl and CD-1 mice. *Exp Neurol* 126, 195-204.
- Myers, R. H., MacDonald, M. E., Koroshetz, W. J., Duyao, M. P., Ambrose, C. M., Taylor, S. A., Barnes, G., Srinidhi, J., Lin, C. S., Whaley, W. L., and et al. (1993). De novo expansion of a (CAG)*n* repeat in sporadic Huntington's disease. *Nat Genet* 5, 168-173.
- Myers, R. H., Vonsattel, J. P., Paskevich, P. A., Kiely, D. K., Stevens, T. J., Cupples, L. A., Richardson, E. P., Jr., and Bird, E. D. (1991). Decreased neuronal and increased oligodendroglial densities in Huntington's disease caudate nucleus. *J Neuropathol Exp Neurol* 50, 729-742.
- Naarding, P., Kremer, H. P., and Zitman, F. G. (2001). Huntington's disease: a review of the literature on prevalence and treatment of neuropsychiatric phenomena. *Eur Psychiatry* 16, 439-445.
- Nagafuchi, S., Yanagisawa, H., Sato, K., Shirayama, T., Ohsaki, E., Bundo, M., Takeda, T., Tadokoro, K., Kondo, I., Murayama, N., and et al. (1994). Dentatorubral and pallidolusian atrophy expansion of an unstable CAG trinucleotide on chromosome 12p. *Nat Genet* 6, 14-18.

- Nairn, J. G., Bedi, K. S., Mayhew, T. M., and Campbell, L. F. (1989). On the number of Purkinje cells in the human cerebellum: unbiased estimates obtained by using the "fractionator". *J Comp Neurol* 290, 527-532.
- Nakamura, K., Jeong, S. Y., Uchihara, T., Anno, M., Nagashima, K., Nagashima, T., Ikeda, S., Tsuji, S., and Kanazawa, I. (2001). SCA17, a novel autosomal dominant cerebellar ataxia caused by an expanded polyglutamine in TATA-binding protein. *Hum Mol Genet* 10, 1441-1448.
- Nance, M. A., MathiasHagen, V., Breningstall, G., Wick, M. J., and McGlennen, R. C. (1999). Analysis of a very large trinucleotide repeat in a patient with juvenile Huntington's disease. *Neurology* 52, 392-394.
- Nance, M. A., and Myers, R. H. (2001). Juvenile onset Huntington's disease--clinical and research perspectives. *Ment Retard Dev Disabil Res Rev* 7, 153-157.
- Nasir, J., Floresco, S. B., O'Kusky, J. R., Diewert, V. M., Richman, J. M., Zeisler, J., Borowski, A., Marth, J. D., Phillips, A. G., and Hayden, M. R. (1995). Targeted disruption of the Huntington's disease gene results in embryonic lethality and behavioral and morphological changes in heterozygotes. *Cell* 81, 811-823.
- Nauta, H. J. (1979). A proposed conceptual reorganization of the basal ganglia and telencephalon. *Neuroscience* 4, 1875-1881.
- Nishi, M., Takeshima, H., Fukuda, K., Kato, S., and Mori, K. (1993). cDNA cloning and pharmacological characterization of an opioid receptor with high affinities for kappa-subtype-selective ligands. *FEBS Lett* 330, 77-80.
- Nishino, H., Fujimoto, I., Shimano, Y., Hida, H., Kumazaki, M., and Fukuda, A. (1996). 3-Nitropropionic acid produces striatum selective lesions accompanied by iNOS expression. *J Chem Neuroanat* 10, 209-212.
- Nucifora, F. C., Jr., Sasaki, M., Peters, M. F., Huang, H., Cooper, J. K., Yamada, M., Takahashi, H., Tsuji, S., Troncoso, J., Dawson, V. L., *et al.* (2001). Interference by huntingtin and atrophin-1 with CBP-mediated transcription leading to cellular toxicity. *Science* 291, 2423-2428.
- O'Hoy, K. L., Tsilfidis, C., Mahadevan, M. S., Neville, C. E., Barcelo, J., Hunter, A. G., and Korneluk, R. G. (1993). Reduction in size of the myotonic dystrophy trinucleotide repeat mutation during transmission. *Science* 259, 809-812.
- Ohshima, K., Kang, S., Larson, J. E., and Wells, R. D. (1996). Cloning, characterization, and properties of seven triplet repeat DNA sequences. *J Biol Chem* 271, 16773-16783.
- Ohshima, K., Montermini, L., Wells, R. D., and Pandolfo, M. (1998). Inhibitory effects of expanded GAA.TTC triplet repeats from intron I of the Friedreich ataxia gene on transcription and replication in vivo. *J Biol Chem* 273, 14588-14595.
- Ohshima, K., and Wells, R. D. (1997). Hairpin formation during DNA synthesis primer realignment in vitro in triplet repeat sequences from human hereditary disease genes. *J Biol Chem* 272, 16798-16806.
- Okusky, J. R., Nasir, J., Cicchetti, F., Parent, A., and Hayden, M. R. (1999). Neuronal degeneration in the basal ganglia and loss of pallido subthalamic synapses in mice with targeted disruption of the Huntington's disease gene. *Brain Res* 818, 468-479.
- Olsen, R. W. (1981). The GABA postsynaptic membrane receptor-ionophore complex. Site of action of convulsant and anticonvulsant drugs. *Mol Cell Biochem* 39, 261-279.
- Olsen, R. W., and Tobin, A. J. (1990). Molecular biology of GABAA receptors. *Faseb J* 4, 1469-1480.
- Ordway, J. M., Tallaksen-Greene, S., Gutekunst, C. A., Bernstein, E. M., Cearley, J. A., Wiener, H. W., Dure, L. S. t., Lindsey, R., Hersch, S. M., Jope, R. S., *et al.* (1997). Ectopically expressed CAG repeats cause intranuclear inclusions and a progressive late onset neurological phenotype in the mouse. *Cell* 91, 753-763.
- Orr, H. T., Chung, M. Y., Banfi, S., Kwiatkowski, T. J., Servadio, A., Beaudet, A. L., McCall, A. E., Duvick, L. A., Ranum, L. P., and Zoghbi, H. Y. (1993). Expansion of an unstable trinucleotide CAG repeat in spinocerebellar ataxia type 1. *Nat Genet* 4, 221-226.
- Otto, C. J., Almqvist, E., Hayden, M. R., and Andrew, S. E. (2001). The "flap" endonuclease gene FEN1 is excluded as a candidate gene implicated in the CAG repeat expansion underlying Huntington disease. *Clin Genet* 59, 122-127.
- Palfi, S., Ferrante, R. J., Brouillet, E., Beal, M. F., Dolan, R., Guyot, M. C., Peschanski, M., and Hantraye, P. (1996). Chronic 3-nitropropionic acid treatment in baboons replicates the cognitive and motor deficits of Huntington's disease. *J Neurosci* 16, 3019-3025.
- Paques, F., Leung, W. Y., and Haber, J. E. (1998). Expansions and contractions in a tandem repeat induced by double strand break repair. *Mol Cell Biol* 18, 2045-2054.
- Parent, A. (1990). Extrinsic connections of the basal ganglia. *Trends Neurosci* 13, 254-258.
- Parent, A., Bouchard, C., and Smith, Y. (1984). The striatopallidal and striatonigral projections: two distinct fiber systems in primate. *Brain Res* 303, 385-390.

- Parker, J. A., Connolly, J. B., Wellington, C., Hayden, M., Dausset, J., and Neri, C. (2001). Expanded polyglutamines in *Caenorhabditis elegans* cause axonal abnormalities and severe dysfunction of PLM mechanosensory neurons without cell death. *Proc Natl Acad Sci U S A* *98*, 13318-13323.
- Parniewski, P., Bacolla, A., Jaworski, A., and Wells, R. D. (1999). Nucleotide excision repair affects the stability of long transcribed (CTG.CAG) tracts in an orientation dependent manner in *Escherichia coli*. *Nucleic Acids Res* *27*, 616-623.
- Passani, L. A., Bedford, M. T., Faber, P. W., McGinnis, K. M., Sharp, A. H., Gusella, J. F., Vonsattel, J. P., and MacDonald, M. E. (2000). Huntingtin's WW domain partners in Huntington's disease post-mortem brain fulfill genetic criteria for direct involvement in Huntington's disease pathogenesis. *Hum Mol Genet* *9*, 2175-2182.
- Paulsen, J. S., Ready, R. E., Hamilton, J. M., Mega, M. S., and Cummings, J. L. (2001). Neuropsychiatric aspects of Huntington's disease. *J Neurol Neurosurg Psychiatry* *71*, 310-314.
- Paulson, H. L., Perez, M. K., Trotter, Y., Trojanowski, J. Q., Subramony, S. H., Das, S. S., Vig, P., Mandel, J. L., Fischbeck, K. H., and Pittman, R. N. (1997). Intranuclear inclusions of expanded polyglutamine protein in spinocerebellar ataxia type 3. *Neuron* *19*, 333-344.
- Pearson, C. E., Ewel, A., Acharya, S., Fishel, R. A., and Sinden, R. R. (1997). Human MSH2 binds to trinucleotide repeat DNA structures associated with neurodegenerative diseases. *Hum Mol Genet* *6*, 1117-1123.
- Pearson, C. E., and Sinden, R. R. (1996). Alternative Structures In Duplex DNA Formed Within the Trinucleotide Repeats Of the Myotonic Dystrophy and Fragile X Loci. *Biochemistry* *35*, 5041-5053.
- Pearson, C. E., and Sinden, R. R. (1998). Trinucleotide repeat DNA structures: dynamic mutations from dynamic DNA. *Curr Opin Struct Biol* *8*, 321-330.
- Pearson, S. J., Heathfield, K. W., and Reynolds, G. P. (1990). Pallidal GABA and chorea in Huntington's disease. *J Neural Transm Gen Sect* *81*, 241-246.
- Pellegrini-Giampietro, D. E., Gorter, J. A., Bennett, M. V., and Zukin, R. S. (1997). The GluR2 (GluR-B) hypothesis: Ca(2+)-permeable AMPA receptors in neurological disorders. *Trends Neurosci* *20*, 464-470.
- Penney, J. B., Jr., and Young, A. B. (1982). Quantitative autoradiography of neurotransmitter receptors in Huntington disease. *Neurology* *32*, 1391-1395.
- Penney, J. B., Jr., and Young, A. B. (1986). Striatal inhomogeneities and basal ganglia function. *Mov Disord* *1*, 3-15.
- Penney, J. B., Vonsattel, J. P., MacDonald, M. E., Gusella, J. F., and Myers, R. H. (1997). CAG repeat number governs the development rate of pathology in Huntington's disease. *Ann Neurol* *41*, 689-692.
- Penny, G. R., Wilson, C. J., and Kitai, S. T. (1988). Relationship of the axonal and dendritic geometry of spiny projection neurons to the compartmental organization of the neostriatum. *J Comp Neurol* *269*, 275-289.
- Perez-Navarro, E., Canudas, A. M., Akerund, P., Alberch, J., and Arenas, E. (2000). Brain-derived neurotrophic factor, neurotrophin-3, and neurotrophin-4/5 prevent the death of striatal projection neurons in a rodent model of Huntington's disease. *J Neurochem* *75*, 2190-2199.
- Persichetti, F., Carlee, L., Faber, P. W., McNeil, S. M., Ambrose, C. M., Srinidhi, J., Anderson, M., Barnes, G. T., Gusella, J. F., and MacDonald, M. E. (1996). Differential expression of normal and mutant Huntington's disease gene alleles. *Neurobiol Dis* *3*, 183-190.
- Perutz, M. F., Johnson, T., Suzuki, M., and Finch, J. T. (1994). Glutamine repeats as polar zippers: their possible role in inherited neurodegenerative diseases. *Proc Natl Acad Sci U S A* *91*, 5355-5358.
- Peters, M. F., Nucifora, F. C., Jr., Kushi, J., Seaman, H. C., Cooper, J. K., Herring, W. J., Dawson, V. L., Dawson, T. M., and Ross, C. A. (1999). Nuclear targeting of mutant Huntingtin increases toxicity. *Mol Cell Neurosci* *14*, 121-128.
- Petersen, A., Larsen, K. E., Behr, G. G., Romero, N., Przedborski, S., Brundin, P., and Sulzer, D. (2001). Expanded CAG repeats in exon 1 of the Huntington's disease gene stimulate dopamine-mediated striatal neuron autophagy and degeneration. *Hum Mol Genet* *10*, 1243-1254.
- Petes, T. D., Greenwell, P. W., and Dominska, M. (1997). Stabilization of microsatellite sequences by variant repeats in the yeast *Saccharomyces cerevisiae*. *Genetics* *146*, 491-498.
- Petruska, J., Hartenstine, M. J., and Goodman, M. F. (1998). Analysis of strand slippage in DNA polymerase expansions of CAG/CTG triplet repeats associated with neurodegenerative disease. *J Biol Chem* *273*, 5204-5210.
- Pinborg, L. H., Videbaek, C., Hasselbalch, S. G., Sorensen, S. A., Wagner, A., Paulson, O. B., and Knudsen, G. M. (2001). Benzodiazepine receptor quantification in Huntington's disease with [(123)I]omazenil and SPECT. *J Neurol Neurosurg Psychiatry* *70*, 657-661.
- Plevry, B. J. (1991). Opioid receptors and their ligands: natural and unnatural. *Br J Anaesth* *66*, 370-380.
- Pollack, A. E. (2001). Anatomy, physiology, and pharmacology of the basal ganglia. *Neurol Clin* *19*, 523-534, v.

- Prolla, T. A., Abuin, A., and Bradley, A. (1996). DNA mismatch repair deficient mice in cancer research. *Semin Cancer Biol* 7, 241-247.
- Prolla, T. A., Pang, Q., Alani, E., Kolodner, R. D., and Liskay, R. M. (1994). MLH1, PMS1, and MSH2 interactions during the initiation of DNA mismatch repair in yeast. *Science* 265, 1091-1093.
- Pulst, S. M., Nechiporuk, A., Nechiporuk, T., Gispert, S., Chen, X. N., Lopescendes, I., Pearlman, S., Starkman, S., Orozcodiaz, G., Lunkes, A., *et al.* (1996). Moderate Expansion Of a Normally Biallelic Trinucleotide Repeat In Spinocerebellar Ataxia Type 2. *Nat Genet* 14, 269-276.
- Ranen, N. G., Stine, O. C., Abbott, M. H., Sherr, M., Codori, A. M., Franz, M. L., Chao, N. I., Chung, A. S., Pleasant, N., Callahan, C., and *et al.* (1995). Anticipation and instability of IT-15 (CAG)_n repeats in parent- offspring pairs with Huntington disease. *Am J Hum Genet* 57, 593-602.
- Ravikumar, B., Duden, R., and Rubinsztein, D. C. (2002). Aggregate-prone proteins with polyglutamine and polyalanine expansions are degraded by autophagy. *Hum Mol Genet* 11, 1107-1117.
- Rawls, S. M., McGinty, J. F., and Terrian, D. M. (1999). Presynaptic kappa-opioid and muscarinic receptors inhibit the calcium- dependent component of evoked glutamate release from striatal synaptosomes. *J Neurochem* 73, 1058-1065.
- Reddy, P. H., Williams, M., Charles, V., Garrett, L., PikeBuchanan, L., Whetsell, W. O., Miller, G., and Tagle, D. A. (1998). Behavioural abnormalities and selective neuronal loss in HD transgenic mice expressing mutated full length HD cDNA. *Nat Genet* 20, 198-202.
- Reisine, T. D., Wastek, G. J., Speth, R. C., Bird, E. D., and Yamamura, H. I. (1979). Alterations in the benzodiazepine receptor of Huntington's diseased human brain. *Brain Res* 165, 183-187.
- Reynolds, D. S., Carter, R. J., and Morton, A. J. (1998). Dopamine modulates the susceptibility of striatal neurons to 3 nitropropionic acid in the rat model of Huntington's disease. *J Neurosci* 18, 10116-10127.
- Richard, G. F., Dujon, B., and Haber, J. E. (1999). Double-strand break repair can lead to high frequencies of deletions within short CAG CTG trinucleotide repeats. *Mol Gen Genet* 261, 871-882.
- Richfield, E. K., Maguirezeiss, K. A., Vonkeman, H. E., and Voorn, P. (1995). Preferential Loss Of Preproenkephalin Versus Preprotachykinin Neurons From the Striatum Of Huntingtons Disease Patients. *Ann Neurol* 38, 852-861.
- Richfield, E. K., O'Brien, C. F., Eskin, T., and Shoulson, I. (1991). Heterogeneous dopamine receptor changes in early and late Huntington's disease. *Neurosci Lett* 132, 121-126.
- Rigamonti, D., Bauer, J. H., De-Fraja, C., Conti, L., Sipione, S., Sciorati, C., Clementi, E., Hackam, A., Hayden, M. R., Li, Y., *et al.* (2000). Wild-type huntingtin protects from apoptosis upstream of caspase-3. *J Neurosci* 20, 3705-3713.
- Rosas, H. D., Liu, A. K., Hersch, S., Glessner, M., Ferrante, R. J., Salat, D. H., van der Kouwe, A., Jenkins, B. G., Dale, A. M., and Fischl, B. (2002). Regional and progressive thinning of the cortical ribbon in Huntington's disease. *Neurology* 58, 695-701.
- Ross, C. A., Wood, J. D., Schilling, G., Peters, M. F., Nucifora, F. C., Cooper, J. K., Sharp, A. H., Margolis, R. L., and Borchelt, D. R. (1999). Polyglutamine pathogenesis. *Phil Trans R Soc Lond B* 354, 1005-1011.
- Rubinsztein, D. C., Leggo, J., Coles, R., Almqvist, E., Biancalana, V., Cassiman, J. J., Chotai, K., Connarty, M., Craufurd, D., Curtis, A., *et al.* (1996). Phenotypic Characterization Of Individuals With 30 40 CAG Repeats In the Huntington Disease (Hd) Gene Reveals Hd Cases With 36 Repeats and Apparently Normal Elderly Individuals With 36 39 Repeats. *Am J Hum Genet* 59, 16-22.
- Saint-Cyr, J. A., Taylor, A. E., and Nicholson, K. (1995). Behavior and the basal ganglia. *Adv Neurol* 65, 1-28.
- Samadashwily, G. M., Raca, G., and Mirkin, S. M. (1997). Trinucleotide repeats affect DNA replication in vivo. *Nat Genet* 17, 298-304.
- Sanberg, P. R., Calderon, S. F., Giordano, M., Tew, J. M., and Norman, A. B. (1989). The quinolinic acid model of Huntington's disease: locomotor abnormalities. *Exp Neurol* 105, 45-53.
- Sancar, A. (1999). Excision repair invades the territory of mismatch repair. *Nat Genet* 21, 247-249.
- Sanhueza, J., Valdes, J., Campos, R., Garrido, A., and Valenzuela, A. (1992). Changes in the xanthine dehydrogenase/xanthine oxidase ratio in the rat kidney subjected to ischemia-reperfusion stress: preventive effect of some flavonoids. *Res Commun Chem Pathol Pharmacol* 78, 211-218.
- Sanpei, K., Takano, H., Igarashi, S., Sato, T., Oyake, M., Sasaki, H., Wakisaka, A., Tashiro, K., Ishida, Y., Ikeuchi, T., *et al.* (1996). Identification Of the Spinocerebellar Ataxia Type 2 Gene Using a Direct Identification Of Repeat Expansion and Cloning Technique, Direct. *Nat Genet* 14, 277-284.
- Sapp, E., Kegel, K. B., Aronin, N., Hashikawa, T., Uchiyama, Y., Tohyama, K., Bhide, P. G., Vonsattel, J. P., and DiFiglia, M. (2001). Early and progressive accumulation of reactive microglia in the Huntington disease brain. *J Neuropathol Exp Neurol* 60, 161-172.
- Sapp, E., Schwarz, C., Chase, K., Bhide, P. G., Young, A. B., Penney, J., Vonsattel, J. P., Aronin, N., and DiFiglia, M. (1997). Huntingtin localization in brains of normal and Huntington's disease patients. *Ann Neurol* 42, 604-612.

- Sarkar, P. S., Chang, H. C., Boudi, F. B., and Reddy, S. (1998). CTG repeats show bimodal amplification in *E. coli*. *Cell* 95, 531-540.
- Sato, I., Kim, Y., Himi, T., and Murota, S. (1995). Induction of calcium-independent nitric oxide synthase activity in cultured cerebellar granule neurons. *Neurosci Lett* 184, 145-148.
- Sattler, R., Xiong, Z., Lu, W. Y., Hafner, M., MacDonald, J. F., and Tymianski, M. (1999). Specific coupling of NMDA receptor activation to nitric oxide neurotoxicity by PSD-95 protein. *Science* 284, 1845-1848.
- Saudou, F., Finkbeiner, S., Devys, D., and Greenberg, M. E. (1998). Huntingtin acts in the nucleus to induce apoptosis but death does not correlate with the formation of intranuclear inclusions. *Cell* 95, 55-66.
- Savasta, M., Dubois, A., and Scatton, B. (1986). Autoradiographic localization of D₁ dopamine receptors in the rat brain with [³H]SCH 23390. *Brain Res* 375, 291-301.
- Sax, D. S., Powsner, R., Kim, A., Tilak, S., Bhatia, R., Cupples, L. A., and Myers, R. H. (1996). Evidence of cortical metabolic dysfunction in early Huntington's disease by single photon emission computed tomography. *Mov Dis* 11, 671-677.
- Schauwecker, P. E., and Steward, O. (1997). Genetic determinants of susceptibility to excitotoxic cell death: implications for gene targeting approaches. *Proc Natl Acad Sci U S A* 94, 4103-4108.
- Scherzinger, E., Lurz, R., Turmaine, M., Mangiarini, L., Hollenbach, B., Hasenbank, R., Bates, G. P., Davies, S. W., Lehrach, H., and Wanker, E. E. (1997). Huntingtin encoded polyglutamine expansions form amyloid like protein aggregates *in vitro* and *in vivo*. *Cell* 90, 549-558.
- Schilling, G., Becher, M. W., Sharp, A. H., Jinnah, H. A., Duan, K., Kotzuc, J. A., Slunt, H. H., Ratovitski, T., Cooper, J. K., Jenkins, N. A., *et al.* (1999). Intranuclear inclusions and neuritic aggregates in transgenic mice expressing a mutant N terminal fragment of huntingtin. *Hum Mol Genet* 8, 397-407.
- Schilling, G., Sharp, A. H., Loev, S. J., Wagster, M. V., Li, S. H., Stine, O. C., and Ross, C. A. (1995). Expression of the Huntington's disease (IT15) protein product in HD patients. *Hum Mol Genet* 4, 1365-1371.
- Schmidt, K. H., Abbott, C. M., and Leach, D. R. (2000). Two opposing effects of mismatch repair on CTG repeat instability in *Escherichia coli*. *Mol Microbiol* 35, 463-471.
- Schmitt, I., Bachner, D., Megow, D., Henklein, P., Hameister, H., Epplen, J. T., and Riess, O. (1995). Expression of the Huntington disease gene in rodents: cloning the rat homologue and evidence for downregulation in non-neuronal tissues during development. *Hum Mol Genet* 4, 1173-1182.
- Schulz, J. B., Henshaw, D. R., Siwek, D., Jenkins, B. G., Ferrante, R. J., Cipolloni, P. B., Kowall, N. W., Rosen, B. R., and Beal, M. F. (1995). Involvement of free radicals in excitotoxicity *in vivo*. *J Neurochem* 64, 2239-2247.
- Schulz, J. B., Matthews, R. T., Henshaw, D. R., and Beal, M. F. (1996). Neuroprotective strategies for treatment of lesions produced by mitochondrial toxins: Implications for neurodegenerative diseases. *Neuroscience* 71, 1043-1048.
- Schumacher, S., Fuchs, R. P. P., and Bichara, M. (1998). Expansion of CTG repeats from human disease genesis dependent upon replication mechanisms in *Escherichia coli*: The effect of long patch mismatch repair revisited. *J Mol Biol* 279, 1101-1110.
- Schumacher, S., Pinet, I., and Bichara, M. (2001). Modulation of transcription reveals a new mechanism of triplet repeat instability in *Escherichia coli*. *J Mol Biol* 307, 39-49.
- Schwarz, R., Creese, I., Coyle, J. T., and Snyder, S. H. (1978). Dopamine receptors localised on cerebral cortical afferents to rat corpus striatum. *Nature* 271, 766-768.
- Schweitzer, J. K., and Livingston, D. M. (1997). Destabilization of CAG trinucleotide repeat tracts by mismatch repair mutations in yeast. *Hum Mol Genet* 6, 349-355.
- Schweitzer, J. K., and Livingston, D. M. (1998). Expansions of CAG repeat tracts are frequent in a yeast mutant defective in Okazaki fragment maturation. *Hum Mol Genet* 7, 69-74.
- Sharp, A. H., Loev, S. J., Schilling, G., Li, S. H., Li, X. J., Bao, J., Wagster, M. V., Kotzuc, J. A., Steiner, J. P., Lo, A., and *et al.* (1995). Widespread expression of Huntington's disease gene (IT15) protein product. *Neuron* 14, 1065-1074.
- Sharp, A. H., and Ross, C. A. (1996). Neurobiology of Huntington's disease. *Neurobiol Dis* 3, 3-15.
- Shelbourne, P. F., Killeen, N., Hevner, R. F., Johnston, H. M., Tecott, L., Lewandoski, M., Ennis, M., Ramirez, L., Li, Z., Iannicola, C., *et al.* (1999). A Huntington's disease CAG expansion at the murine *Hdh* locus is unstable and associated with behavioural abnormalities in mice. *Hum Mol Genet* 8, 763-774.
- Shieh, P. B., Hu, S. C., Bobb, K., Timmusk, T., and Ghosh, A. (1998). Identification of a signaling pathway involved in calcium regulation of BDNF expression. *Neuron* 20, 727-740.
- Shimada, N., Sobue, G., Doyu, M., Yamamoto, K., Yasuda, T., Mukai, E., Kachi, T., and Mitsuma, T. (1995). X Linked Recessive Bulbospinal Neuronopathy Clinical Phenotypes and CAG Repeat Size In Androgen Receptor Gene. *Muscle Nerve* 18, 1378-1384.

- Sian, J., Dexter, D. T., Lees, A. J., Daniel, S., Agid, Y., Javoy-Agid, F., Jenner, P., and Marsden, C. D. (1994). Alterations in glutathione levels in Parkinson's disease and other neurodegenerative disorders affecting basal ganglia. *Ann Neurol* 36, 348-355.
- Siemers, E., Foroud, T., Bill, D. J., Sorbel, J., Norton, J. A., Jr., Hodes, M. E., Niebler, G., Conneally, P. M., and Christian, J. C. (1996). Motor changes in presymptomatic Huntington disease gene carriers. *Arch Neurol* 53, 487-492.
- Sinden, R. R. (1999). Biological implications of the DNA structures associated with disease causing triplet repeats. *Am J Hum Genet* 64, 346-353.
- Sinden, R. R., and Wells, R. D. (1992). DNA structure, mutations, and human genetic disease. *Curr Opin Biotech* 3, 612-622.
- Sittler, A., Walter, S., Wedemeyer, N., Hasenbank, R., Scherzinger, E., Eickhoff, H., Bates, G. P., Lehrach, H., and Wanker, E. E. (1998). SH3GL3 associates with the Huntingtin exon 1 protein and promotes the formation of polyglu-containing protein aggregates. *Mol Cell* 2, 427-436.
- Skinner, P. J., Koshy, B. T., Cummings, C. J., Klement, I. A., Helin, K., Servadio, A., Zoghbi, H. Y., and Orr, H. T. (1997). Ataxin-1 with an expanded glutamine tract alters nuclear matrix-associated structures. *Nature* 389, 971-974.
- Smith, Y., and Bolam, J. P. (1990). The output neurones and the dopaminergic neurones of the substantia nigra receive a GABA-containing input from the globus pallidus in the rat. *J Comp Neurol* 296, 47-64.
- Snell, R. G., MacMillan, J. C., Cheadle, J. P., Fenton, I., Lazarou, L. P., Davies, P., MacDonald, M. E., Gusella, J. F., Harper, P. S., and Shaw, D. J. (1993). Relationship between trinucleotide repeat expansion and phenotypic variation in Huntington's disease. *Nat Genet* 4, 393-397.
- Somogyi, P., and Smith, A. D. (1979). Projection of neostriatal spiny neurons to the substantia nigra. Application of a combined Golgi-staining and horseradish peroxidase transport procedure at both light and electron microscopic levels. *Brain Res* 178, 3-15.
- Spiegel, R., La Spada, A. R., Kress, W., Fischbeck, K. H., and Schmid, W. (1996). Somatic stability of the expanded CAG trinucleotide repeat in X-linked spinal and bulbar muscular atrophy. *Hum Mutat* 8, 32-37.
- Spina, M. B., and Cohen, G. (1989). Dopamine turnover and glutathione oxidation: implications for Parkinson disease. *Proc Natl Acad Sci U S A* 86, 1398-1400.
- Spiro, C., Pelletier, R., Rolfsmeier, M. L., Dixon, M. J., Lahue, R. S., Gupta, G., Park, M. S., Chen, X., Mariappan, S. V., and McMurray, C. T. (1999). Inhibition of FEN-1 processing by DNA secondary structure at trinucleotide repeats. *Mol Cell* 4, 1079-1085.
- Stevanin, G., Camuzat, A., Holmes, S. E., Julien, C., Sahloul, R., Dode, C., Hahn-Barma, V., Ross, C. A., Margolis, R. L., Durr, A., and Brice, A. (2002). CAG/CTG repeat expansions at the Huntington's disease-like 2 locus are rare in Huntington's disease patients. *Neurology* 58, 965-967.
- Stoof, J. C., and Keibadian, J. W. (1981). Opposing roles for D₁ and D₂ dopamine receptors in efflux of cyclic AMP from rat neostriatum. *Nature* 294, 366-368.
- Storey, E., and Beal, M. F. (1993). Neurochemical substrates of rigidity and chorea in Huntington's disease. *Brain* 116, 1201-1222.
- Strong, T. V., Tagle, D. A., Valdes, J. M., Elmer, L. W., Boehm, K., Swaroop, M., Kaatz, K. W., Collins, F. S., and Albin, R. L. (1993). Widespread expression of the human and rat Huntington's disease gene in brain and nonneural tissues. *Nat Genet* 5, 259-265.
- Sucher, N. J., Awobuluyi, M., Choi, Y. B., and Lipton, S. A. (1996). NMDA receptors: from genes to channels. *Trends Pharmacol Sci* 17, 348-355.
- Sun, Y., Savanenin, A., Reddy, P. H., and Liu, Y. F. (2001). Polyglutamine-expanded huntingtin promotes sensitization of N-methyl-D- aspartate receptors via post-synaptic density 95. *J Biol Chem* 276, 24713-24718.
- Sur, C., Fresu, L., Howell, O., McKernan, R. M., and Atack, J. R. (1999). Autoradiographic localization of alpha5 subunit-containing GABAA receptors in rat brain. *Brain Res* 822, 265-270.
- Surmeier, D. J., Song, W. J., and Yan, Z. (1996). Coordinated expression of dopamine receptors in neostriatal medium spiny neurons. *J Neurosci* 16, 6579-6591.
- Svingos, A. L., Clarke, C. L., and Pickel, V. M. (1998). Cellular sites for activation of delta-opioid receptors in the rat nucleus accumbens shell: relationship with Met5-enkephalin. *J Neurosci* 18, 1923-1933.
- Tabrizi, S. J., Cleeter, M. W., Xuereb, J., Taanman, J. W., Cooper, J. M., and Schapira, A. H. (1999). Biochemical abnormalities and excitotoxicity in Huntington's disease brain. *Ann Neurol* 45, 25-32.
- Takano, H., Onodera, O., Takahashi, H., Igarashi, S., Yamada, M., Oyake, M., Ikeuchi, T., Koide, R., Tanaka, H., Iwabuchi, K., and Tsuji, S. (1996). Somatic mosaicism of expanded CAG repeats in brains of patients with dentatorubral-pallidolusian atrophy: cellular population-dependent dynamics of mitotic instability. *Am J Hum Genet* 58, 1212-1222.
- Tallaksen-Greene, S. J., and Albin, R. L. (1996). Splice variants of glutamate receptor subunits 2 and 3 in striatal projection neurons. *Neuroscience* 75, 1057-1064.

- Tanaka, F., Sobue, G., Doyu, M., Ito, Y., Yamamoto, M., Shimada, N., Yamamoto, K., Riku, S., Hshizume, Y., and Mitsuma, T. (1996). Differential pattern in tissue-specific somatic mosaicism of expanded CAG trinucleotide repeats in dentatorubral-pallidoluysian atrophy, Machado-Joseph disease, and X-linked recessive spinal and bulbar muscular atrophy. *J Neurol Sci* 135, 43-50.
- Tao, X., Finkbeiner, S., Arnold, D. B., Shaywitz, A. J., and Greenberg, M. E. (1998). Ca²⁺ influx regulates BDNF transcription by a CREB family transcription factor-dependent mechanism. *Neuron* 20, 709-726.
- Taylor-Robinson, S. D., Weeks, R. A., Bryant, D. J., Sargentoni, J., Marcus, C. D., Harding, A. E., and Brooks, D. J. (1996). Proton magnetic resonance spectroscopy in Huntington's disease: evidence in favour of the glutamate excitotoxic theory. *Mov Disord* 11, 167-173.
- Telenius, H., Almqvist, E., Kremer, B., Spence, N., Squitieri, F., Nichol, K., Grandell, U., Starr, E., Benjamin, C., Castaldo, I., and et al. (1995). Somatic mosaicism in sperm is associated with intergenerational (CAG)_n changes in Huntington disease. *Hum Mol Genet* 4, 189-195.
- Telenius, H., Kremer, B., Goldberg, Y. P., Theilmann, J., Andrew, S. E., Zeisler, J., Adam, S., Greenberg, C., Ives, E. J., Clarke, L. A., and et al. (1994). Somatic and gonadal mosaicism of the Huntington disease gene CAG repeat in brain and sperm. *Nat Genet* 6, 409-414.
- Telenius, H., Kremer, H. P., Theilmann, J., Andrew, S. E., Almqvist, E., Anvret, M., Greenberg, C., Greenberg, J., Lucotte, G., Squitieri, F., and et, a. l. (1993). Molecular analysis of juvenile Huntington disease: the major influence on (CAG)_n repeat length is the sex of the affected parent. *Hum Mol Genet* 2, 1535-1540.
- Tezuka, T., Umemori, H., Akiyama, T., Nakanishi, S., and Yamamoto, T. (1999). PSD-95 promotes Fyn-mediated tyrosine phosphorylation of the N-methyl-D- aspartate receptor subunit NR2A. *Proc Natl Acad Sci U S A* 96, 435-440.
- Tishkoff, D. X., Filosi, N., Gaida, G. M., and Kolodner, R. D. (1997). A novel mutation avoidance mechanism dependent on *S. cerevisiae* RAD27 is distinct from DNA mismatch repair. *Cell* 88, 253-263.
- Tomer, G., Buermeier, A. B., Nguyen, M. M., and Liskay, R. M. (2002). Contribution of human mlh1 and pms2 ATPase activities to DNA mismatch repair. *J Biol Chem* 277, 21801-21809.
- Trettel, F., Rigamonti, D., Hilditch-Maguire, P., Wheeler, V. C., Sharp, A. H., Persichetti, F., Cattaneo, E., and MacDonald, M. E. (2000). Dominant phenotypes produced by the HD mutation in STHdh(Q111) striatal cells. *Hum Mol Genet* 9, 2799-2809.
- Trifiletti, R. R., Snowman, A. M., Whitehouse, P. J., Marcus, K. A., and Snyder, S. H. (1987). Huntington's disease: increased number and altered regulation of benzodiazepine receptor complexes in frontal cerebral cortex. *Neurology* 37, 916-922.
- Trottier, Y., Biancalana, V., and Mandel, J. L. (1994). Instability of CAG repeats in Huntington's disease: relation to parental transmission and age of onset. *J Med Genet* 31, 377-382.
- Trottier, Y., Devys, D., Imbert, G., Saudou, F., An, I., Lutz, Y., Weber, C., Agid, Y., Hirsch, E. C., and Mandel, J. L. (1995). Cellular localization of the Huntington's disease protein and discrimination of the normal and mutated form. *Nat Genet* 10, 104-110.
- Tukamoto, T., Nukina, N., Ide, K., and Kanazawa, I. (1997). Huntington's disease gene product, huntingtin, associates with microtubules *in vitro*. *Brain Res Mol Brain Res* 51, 8-14.
- Turjanski, N., Weeks, R., Dolan, R., Harding, A. E., and Brooks, D. J. (1995). Striatal D₁ and D₂ receptor binding in patients with Huntington's disease and other choreas. A PET study. *Brain* 118, 689-696.
- Uitti, R. J., Rajput, A. H., Ashenurst, E. M., and Rozdilsky, B. (1985). Cyanide-induced parkinsonism: a clinicopathologic report. *Neurology* 35, 921-925.
- Usdin, M. T., Shelbourne, P. F., Myers, R. M., and Madison, D. V. (1999). Impaired synaptic plasticity in mice carrying the Huntington's disease mutation. *Hum Mol Genet* 8, 839-846.
- van den Broek, W. J., Nelen, M. R., Wansink, D. G., Coerwinkel, M. M., te Riele, H., Groenen, P. J., and Wieringa, B. (2002). Somatic expansion behaviour of the (CTG)_n repeat in myotonic dystrophy knock-in mice is differentially affected by Msh3 and Msh6 mismatch- repair proteins. *Hum Mol Genet* 11, 191-198.
- Varani, K., Rigamonti, D., Sipione, S., Camurri, A., Borea, P. A., Cattabeni, F., Abbracchio, M. P., and Cattaneo, E. (2001). Aberrant amplification of A(2A) receptor signaling in striatal cells expressing mutant huntingtin. *Faseb J* 15, 1245-1247.
- Velier, J., Kim, M., Schwarz, C., Kim, T. W., Sapp, E., Chase, K., Aronin, N., and DiFiglia, M. (1998). Wild-type and mutant huntingtins function in vesicle trafficking in the secretory and endocytic pathways. *Exp Neurol* 152, 34-40.
- Verkerk, A. J., Pieretti, M., Sutcliffe, J. S., Fu, Y. H., Kuhl, D. P., Pizzuti, A., Reiner, O., Richards, S., Victoria, M. F., Zhang, F. P., and et, a. l. (1991). Identification of a gene (FMR-1) containing a CGG repeat coincident with a breakpoint cluster region exhibiting length variation in fragile X syndrome. *Cell* 65, 905-914.

- Vonsattel, J. P., Myers, R. H., Stevens, T. J., Ferrante, R. J., Bird, E. D., and Richardson, E. P., Jr. (1985). Neuropathological classification of Huntington's disease. *J Neuropathol Exp Neurol* 44, 559-577.
- Vonsattel, J. P. G., and DiFiglia, M. (1998). Huntington disease. *J Neuropathol Exp Neurol* 57, 369-384.
- Vuillaume, I., Vermersch, P., Destee, A., Petit, H., and Sablonniere, B. (1998). Genetic polymorphisms adjacent to the CAG repeat influence clinical features at onset in Huntington's disease. *J Neurol Neurosurg Psychiatry* 64, 758-762.
- Waelter, S., Scherzinger, E., Hasenbank, R., Nordhoff, E., Lurz, R., Goehler, H., Gauss, C., Sathasivam, K., Bates, G. P., Lehrach, H., and Wanker, E. E. (2001). The huntingtin interacting protein HIP1 is a clathrin and alpha-adaptin-binding protein involved in receptor-mediated endocytosis. *Hum Mol Genet* 10, 1807-1817.
- Walker, F. O., Young, A. B., Penney, J. B., Dovorini-Zis, K., and Shoulson, I. (1984). Benzodiazepine and GABA receptors in early Huntington's disease. *Neurology* 34, 1237-1240.
- Wang, J. B., Imai, Y., Eppler, C. M., Gregor, P., Spivak, C. E., and Uhl, G. R. (1993). mu opiate receptor: cDNA cloning and expression. *Proc Natl Acad Sci U S A* 90, 10230-10234.
- Wang, Y. H., Amirhaeri, S., Kang, S., Wells, R. D., and Griffith, J. D. (1994). Preferential nucleosome assembly at DNA triplet repeats from the myotonic dystrophy gene. *Science* 265, 669-671.
- Wanker, E. E., Rovira, C., Scherzinger, E., Hasenbank, R., Walter, S., Tait, D., Colicelli, J., and Lehrach, H. (1997). HIP I: A huntingtin interacting protein isolated by the yeast two hybrid system. *Hum Mol Genet* 6, 487-495.
- Weeks, R. A., Cunningham, V. J., Piccini, P., Waters, S., Harding, A. E., and Brooks, D. J. (1997). 11C-diprenorphine binding in Huntington's disease: a comparison of region of interest analysis with statistical parametric mapping. *J Cereb Blood Flow Metab* 17, 943-949.
- Weeks, R. A., Piccini, P., Harding, A. E., and Brooks, D. J. (1996). Striatal D₁ and D₂ dopamine receptor loss in asymptomatic mutation carriers of Huntington's disease. *Ann Neurol* 40, 49-54.
- Weiss, J. H., and Sensi, S. L. (2000). Ca²⁺-Zn²⁺ permeable AMPA or kainate receptors: possible key factors in selective neurodegeneration. *Trends Neurosci* 23, 365-371.
- Wellington, C. L., Ellerby, L. M., Hackam, A. S., Margolis, R. L., Trifiro, M. A., Singaraja, R., McCutcheon, K., Salvesen, G. S., Propp, S. S., Bromm, M., *et al.* (1998). Caspase cleavage of gene products associated with triplet expansion disorders generates truncated fragments containing the polyglutamine tract. *J Biol Chem* 273, 9158-9167.
- Wells, R. D. (1996). Molecular basis of genetic instability of triplet repeats. *J Biol Chem* 271, 2875-2878.
- Wells, R. D., Parniewski, P., Pluciennik, A., Bacolla, A., Gellibolian, R., and Jaworski, A. (1998). Small slipped register genetic instabilities in *Escherichia coli* in triplet repeat sequences associated with hereditary neurological diseases. *J Biol Chem* 273, 19532-19541.
- Wexler, N. S., Young, A. B., Tanzi, R. E., Travers, H., Starosta-Rubinstein, S., Penney, J. B., Snodgrass, S. R., Shoulson, I., Gomez, F., Ramos Arroyo, M. A., and *et al.* (1987). Homozygotes for Huntington's disease. *Nature* 326, 194-197.
- Wheeler, V. C., Auerbach, W., White, J. K., Srinidhi, J., Auerbach, A., Ryan, A., Duyao, M. P., Vrbanac, V., Weaver, M., Gusella, J. F., *et al.* (1999). Length-dependent gametic CAG repeat instability in the Huntington's disease knock-in mouse. *Hum Mol Genet* 8, 115-122.
- Wheeler, V. C., Gutekunst, C. A., Vrbanac, V., Lebel, L. A., Schilling, G., Hersch, S., Friedlander, R. M., Gusella, J. F., Vonsattel, J. P., Borchelt, D. R., and MacDonald, M. E. (2002). Early phenotypes that presage late-onset neurodegenerative disease allow testing of modifiers in Hdh CAG knock-in mice. *Hum Mol Genet* 11, 633-640.
- Wheeler, V. C., White, J. K., Gutekunst, C. A., Vrbanac, V., Weaver, M., Li, X. J., Li, S. H., Yi, H., Vonsattel, J. P., Gusella, J. F., *et al.* (2000). Long glutamine tracts cause nuclear localization of a novel form of huntingtin in medium spiny striatal neurons in HdhQ92 and HdhQ111 knock-in mice. *Hum Mol Genet* 9, 503-513.
- Whetsell, W. O., Jr., Allen, G. S., and Tulipan, N. B. (1989). Alteration of kainic acid and quinolinic acid toxicity by neostriatal transplants in vitro. *Neurosci Lett* 96, 18-22.
- White, J. K., Auerbach, W., Duyao, M. P., Vonsattel, J. P., Gusella, J. F., Joyner, A. L., and MacDonald, M. E. (1997). Huntingtin is required for neurogenesis and is not impaired by the Huntington's disease CAG expansion. *Nat Genet* 17, 404-410.
- White, P. J., Borts, R. H., and Hirst, M. C. (1999). Stability of the human fragile X (CGG)(n) triplet repeat array in *Saccharomyces cerevisiae* deficient in aspects of DNA metabolism. *Mol Cell Biol* 19, 5675-5684.
- Wierdl, M., Greene, C. N., Datta, A., Jinks-Robertson, S., and Petes, T. D. (1996). Destabilization of simple repetitive DNA sequences by transcription in yeast. *Genetics* 143, 713-721.
- Wood, R. D. (1996). DNA repair in eukaryotes. *Annu Rev Biochem* 65, 135-167.
- Wozniak, D. F., Brosnan-Watters, G., Nardi, A., McEwen, M., Corso, T. D., Olney, J. W., and Fix, A. S. (1996). MK-801 neurotoxicity in male mice: histologic effects and chronic impairment in spatial learning. *Brain Res* 707, 165-179.

- Xia, X. G., Schmidt, N., Teismann, P., Ferger, B., and Schulz, J. B. (2001). Dopamine mediates striatal malonate toxicity via dopamine transporter- dependent generation of reactive oxygen species and D₂ but not D₁ receptor activation. *J Neurochem* 79, 63-70.
- Yamamoto, A., Lucas, J. J., and Hen, R. (2000). Reversal of neuropathology and motor dysfunction in a conditional model of Huntington's disease. *Cell* 101, 57-66.
- Yang, W. (2000). Structure and function of mismatch repair proteins. *Mutat Res* 460, 245-256.
- Yazawa, I., Nukina, N., Hashida, H., Goto, J., Yamada, M., and Kanazawa, I. (1995). Abnormal gene product identified in hereditary dentatorubral- pallidolusian atrophy (DRPLA) brain. *Nat Genet* 10, 99-103.
- Young, A. B., Greenamyre, J. T., Hollingsworth, Z., Albin, R., D'Amato, C., Shoulson, I., and Penney, J. B. (1988). NMDA receptor losses in putamen from patients with Huntington's disease. *Science* 241, 981-983.
- Young, A. B., Penney, J. B., Starosta-Rubinstein, S., Markel, D. S., Berent, S., Giordani, B., Ehrenkafer, R., Jewett, D., and Hichwa, R. (1986). PET scan investigations of Huntington's disease: cerebral metabolic correlates of neurological features and functional decline. *Ann Neurol* 20, 296-303.
- Young, W. S., 3rd, and Kuhar, M. J. (1979). A new method for receptor autoradiography: [3H]opioid receptors in rat brain. *Brain Res* 179, 255-270.
- Zeitlin, S., Liu, J. P., Chapman, D. L., Papaioannou, V. E., and Efstratiadis, A. (1995). Increased apoptosis and early embryonic lethality in mice nullizygous for the Huntington's disease gene homologue. *Nat Genet* 11, 155-163.
- Zeron, M. M., Hansson, O., Chen, N., Wellington, C. L., Leavitt, B. R., Brundin, P., Hayden, M. R., and Raymond, L. A. (2002). Increased sensitivity to N-methyl-D-aspartate receptor-mediated excitotoxicity in a mouse model of Huntington's disease. *Neuron* 33, 849-860.
- Zhang, Y., Monckton, D. G., Siciliano, M. J., Connor, T. H., and Meistrich, M. L. (2002). Age and insertion site dependence of repeat number instability of a human DM1 transgene in individual mouse sperm. *Hum Mol Genet* 11, 791-798.
- Zhuchenko, O., Bailey, J., Bonnen, P., Ashizawa, T., Stockton, D. W., Amos, C., Dobyns, W. B., Subramony, S. H., Zoghbi, H. Y., and Lee, C. C. (1997). Autosomal dominant cerebellar ataxia (SCA6) associated with small polyglutamine expansions in the alpha 1A-voltage-dependent calcium channel. *Nat Genet* 15, 62-69.
- Zimmer, J., and Geneser, F. A. (1987). Difference in monoamine oxidase B activity between C57 black and albino NMRI mouse strains may explain differential effects of the neurotoxin MPTP. *Neurosci Lett* 78, 253-258.
- Zuccato, C., Ciammola, A., Rigamonti, D., Leavitt, B. R., Goffredo, D., Conti, L., MacDonald, M. E., Friedlander, R. M., Silani, V., Hayden, M. R., *et al.* (2001). Loss of huntingtin-mediated BDNF gene transcription in Huntington's disease. *Science* 293, 493-498.
- Zuhlke, C., Riess, O., Bockel, B., Lange, H., and Thies, U. (1993). Mitotic stability and meiotic variability of the (CAG)_n repeat in the Huntington disease gene. *Hum Mol Genet* 2, 2063-2067.